AUTOMATED DETECTION OF TREATMENT RESPONSES WITH CARDIAC POSITRON TOMOGRAPHY

by:

ROBERT ANTHONY DEKEMP, M.Sc.

A Thesis

Submitted to the School of Graduate Studies

in Partial Fulfilment of the Requirements

for the Degree

Doctor of Philosophy

McMaster University

DOCTOR OF PHILOSOPHY (1995) McMASTER UNIVERSITY
(Electrical and Computer Engineering) Hamilton, Ontario

TITLE: Automated Detection of Treatment Responses with Cardiac Positron Tomography

AUTHOR: Robert Anthony deKemp, M.Sc. (McMaster University)

SUPERVISOR: Dr. C. Nahmias

NUMBER OF PAGES: xi, 209

AUTOMATED DETECTION OF TREATMENT RESPONSES WITH CARDIAC POSITRON TOMOGRAPHY

ABSTRACT

The physiology of the muscle of the heart (myocardium) can be studied regionally in the living body using positron tomographic techniques. Compounds are labelled with a positron emitting isotope, administered into the circulation, and their distribution in the body is measured with a positron tomograph. This enables the rates of myocardial blood flow and substrate metabolism to be measured regionally in the myocardium of the left ventricle. The accuracy and precision of these measurements are estimated to range from 2% to 15% in a given individual. Much of this variability is due to normal changes in physiological state, or to measurement noise associated with counting statistics. However, additional variability is associated with manual processing, which typically involves specification of the left ventricular myocardium of interest using an interactive visual display. An automated technique of analysis can remove this source of variance, and enable an unbiased evaluation of changes in response to the treatment of heart disease. Results can then be compared objectively between population samples or in single subjects studied under different treatment conditions. By performing appropriate statistical comparisons, a large volume of data is compressed into a form which can be interpreted in an efficient manner.

An automated analysis technique is developed to remove the variability associated with manual processing. Reduction of the measurement variability increases the statistical power to detect physiological changes in the myocardium in different states of health and disease. The position and angular orientation of the left ventricle is determined directly from the measured dataset, so that the regional measurements can be analysed and presented in a standard format. The time course of radioactivity is determined for several hundred volume elements within the left ventricular myocardium,

and for a blood region positioned in the ventricular cavity. Depending on the labelled compound and study protocol, various measures of myocardial physiology are computed from these two basic measurements. A technique is developed to compare treatment changes in physiology between *population samples*, by segmenting equivalent functional tissue regions from the left ventricular myocardium of the sample subjects. A method is also developed to evaluate the statistical significance of changes in *single subjects*, which may be useful to determine individual clinical responses to treatments. Comprehensive quality assurance outputs are generated, and are used to verify the analysis of all cardiac studies.

The performance of the method was determined using cardiac phantom and human data. The position and angular orientation of the left ventricle were determined to within 2±2 mm and 3±3 degrees of the true values respectively. The detection of treatment changes in a population sample was demonstrated using measurements of myocardial blood flow with ^{13}N-labelled ammonia. An increase in blood flow to diseased (ischemic) myocardium in response to nitroglycerin was demonstrated using a quantitative automated approach: a highly significant ($p=0.01$) difference of 16 ml/min/dg (20% of normal) was detected in a sample group of 14 subjects. The performance of the single subject analysis was verified by measuring the rate at which significant changes occured by chance, which was equal to the theoretical false positive rate. In an individual from the population sample, a significant increase ($p=0.001$) in myocardial blood flow of approximately 30% was detected in a region of known ischemia, in response to treatment with nitroglycerin. The statistical tools developed in this work can also be used to determine other sources of measurement variability. Reduction of these effects will increase further the power of positron tomography to evaluate objectively the clinical effects and mechanisms of action of cardiac treatments in health and disease.

ACKNOWLEDGEMENTS

I would like to thank my mentor and friend Claude Nahmias: my appreciation for your direction and understanding can not be fully expressed.

Thanks to my wife Susie who has been with me throughout my return to student life. Your endless patience and support will not be forgotten.

Thanks also to my committee: Dr. Coates, Dr. Capson, and especially to Dr. Garnett who was a role model for many scientists in training.

To all my friends in the department of Nuclear Medicine and in the MIND lab at McMaster University: thank you for making my time in Hamilton truly memorable.

TABLE OF CONTENTS

LIST OF TABLES

LIST OF ILLUSTRATIONS

INTRODUCTION

Positron tomography (PET) is unique in its ability to quantitatively measure regional physiological processes in the living human body. Clinical and research imaging with PET has focused historically on the heart and the brain, and more recently on tumour detection in oncology. Positron tomography of the heart has high diagnostic accuracy for the detection of coronary artery disease, and for the evaluation of ischemic, viable heart muscle (myocardium). However, relatively little effort has been made to exploit the accuracy and precision of PET for the detection of changes resulting from the effective treatment of heart disease.

In the present work, the hypothesis is explored that treatment induced effects on myocardial physiology can be detected using an automated analysis technique. The benefit of such analysis is in improved objectivity and reproducibility over manual methods for the detection of significant changes. This may allow more accurate evaluation of new treatments for heart disease, and may provide a method to monitor treatment changes in individual patients.

A brief overview of cardiac anatomy and physiology relevant to PET is presented in Chapter 1. This is followed in Chapter 2, by a description of the physics and the radiopharmaceuticals required to perform positron tomography. Chapter 3 contains a review of the current state of the art of cardiac PET image analysis in the context of systematic and random variations. These concepts are central to the detection of statistically significant changes. A completely automated analysis method is developed in Chapter 4; this new technique enables the objective comparison of population samples under different treatments, as well as the detection of single subject changes. Two specific applications are presented in Chapter 5: the first is a drug study analysis of myocardial blood flow changes between two population samples; the second application is a single subject analysis of the effects of the same drug. A detailed discussion of the analysis is presented in Chapter 6, and the results are related to previous work published in this field.

CHAPTER 1
The Human Heart

1.1 Anatomy

Gross Anatomy

The heart is located in the middle mediastinum and is partially surrounded by the lower aspects of the lungs. It rests on top of the diaphragm, with the apex tilted anteriorly and to the left. The base of the heart is superior to the apex, where the veins and arteries of the pulmonary and systemic circulations enter and exit. The heart contains four chambers as shown in Figure 1.1 (Guyton 1992). The right atrium (RA) forms the lateral right border of the heart. Venous blood enters the right atrium of the heart from the systemic circulation (body) through the superior and inferior vena cavae. It then passes through the tricuspid valve into the right ventricle (RV). The right ventricle is the most anterior chamber and comprises most of the inferior surface of the heart. Blood is pumped through the pulmonary valve to the pulmonary circulation (lungs). Oxygenated blood returns through the pulmonary veins to the left atrium (LA) which is located posteriorly. It then passes through the mitral valve into the left ventricle (LV), which is the left most chamber and is shaped like a half ellipsoid. The medial wall of the LV is the interventricular septum which separates the left and right ventricles. Blood is pumped through the aortic valve to the entire systemic circulation. The walls of the left ventricle are 8 to 15 mm thick, two to three times greater than those of the right ventricle. The muscle of the apex is often thinner.

The mitral and tricuspid valves are the atrioventricular valves which prevent blood from flowing back into the atria during ventricular contraction (systole). The valves consist of several leaflets of fibroelastic tissue secured by cordae tendineae which in turn are connected to the papillary muscles. These muscles emanate from and are oriented parallel to the ventricular walls. The pulmonic and aortic (semilunar)

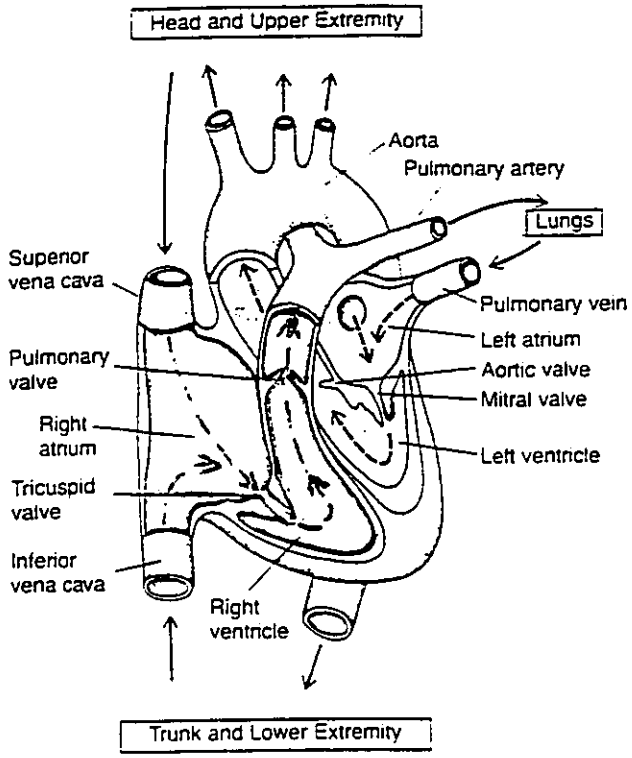

Figure 1.1. Structure of the heart viewed from the front, and the flow of blood (arrows) through the four heart chambers (Guyton 1992).

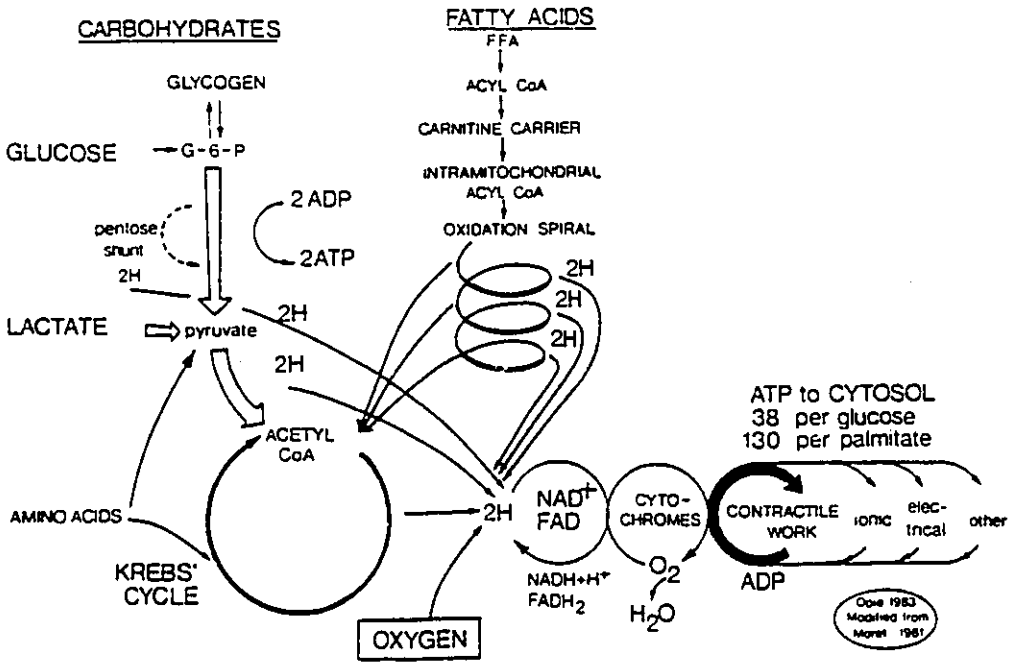

Figure 1.2. Major fuels of the heart are carbohydrates and free fatty acids. Most ATP is produced through Kreb's Cycle of oxidative metabolism, and then used for contractile work (Opie 1984).

valves are comprised of three u-shaped cusps of fibrous tissue. During ventricular relaxation (diastole) the cusps are forced together by the pressure of the blood in the arteries, thereby closing the valve. All four valves lie roughly on the (valve) plane separating the atria from the ventricles.

Blood Supply

The coronary circulation supplies blood to the muscle of the heart. The blood supply originates from the left and right coronary arteries which branch off the aorta. The left coronary artery has two main branches. The left anterior (interventricular) descending (LAD) branch runs anteriorly down from the base of the pulmonary artery, over the interventricular septum and ends on the inferior surface of the cardiac apex. The LAD artery supplies blood to the anterior aspect of the ventricles and the ventricular septum, as well as to the cardiac apex. The left circumflex (LCx) artery is the second main branch of the left coronary artery. It typically travels over the anterolateral surface and supplies the left atrial wall and the lateral left ventricle. The right coronary artery (RCA) descends from the right side of the heart to the posterior atrioventricular groove, and ends as a posterior interventricular branch. It supplies the right atrium, most of the right ventricle and the posterior aspect of the interventricular septum. The marginal branch of the RCA travels more anteriorly and supplies mostly right ventricle. There is considerable variation in coronary blood supply, as well as variable collateral circulation where many small arteries anastomose to enable blood supply from different main arteries.

The venous return from the left ventricle drains primarily into the great cardiac vein. This in turn becomes the coronary sinus on the posterior surface of the heart. The small cardiac vein receives branches from the right ventricle and drains into either the coronary sinus or the right atrium. There are other small veins which drain the anterior right atrium and ventricle directly into the cavity of the right atrium.

1.2 Myocardial Physiology

Excitation-Contraction

Cardiac muscle is composed of an interconnected lattice of striated muscle fibres. These myocardial cells are mechanically and electrically connected, causing the entire myocardium of the ventricles (and atria) to contract together as a *syncytium.* Membrane cells in the sinoatrial (SA) node rhythmically depolarize, creating the action potentials which control the periodic contraction of the atria and ventricles. The SA node is located where the superior vena cava enters the right atrium. The generated action potential innervates the atria through three internodal pathways which converge at the atrioventricular (AV) node. At this point the impulse is delayed as it passes through the bundle of His into the ventricles. This delay allows blood to pass from the contracting atria into the ventricles. The action potential is then rapidly spread down the septum and back along the ventricular walls. Contraction of the ventricles follows this path and also moves from the endocardial (inner) to the epicardial (outer) surface of the myocardium, thereby pumping blood out of the ventricular cavities.

The calcium ion (Ca^{2+}) plays a central role in the coupling of the membrane action potential with myocardial contraction. The action potential of the myocardial cell membrane is carried deep into the muscle fibre by transverse tubules which are in intimate contact with the sarcoplasmic reticulum. The sarcoplasmic reticulum is an intercellular structure containing a high concentration of Ca^{2+}. Calcium ions are released into the intracellular fluid (cytosol) by the depolarization of this internal membrane. Cytosolic calcium is needed to activate contraction of the myofibrils. By exposing active sites on the actin filaments, the bridges with the myosin filaments can act to produce contraction. When the cell membrane repolarizes, the Ca^{2+} is quickly pumped out of the cytosol and back into the sarcoplasmic reticulum, which causes the myocardial cell to stop contracting.

Ventricular Mechanics

There are four basic factors which regulate the contraction of the heart as a whole (Schlant 1986). Preload (venous return) determines the initial length of the myocardial fibres and hence the contractile force as predicted by the Frank-Starling law: as more blood enters the ventricles, the muscle fibres are stretched to accommodate the increased volume, which subsequently causes increased force of contraction. Functionally, this means that the heart pumps out all of the blood it receives. The second factor affecting cardiac function is contractility. By increasing contractility the velocity and force of contraction of the myocardium are increased, thereby emptying the ventricle more quickly. This also allows the ventricle to fill at a faster rate which increases the volume of blood that is ejected with each beat (stroke volume). The resistance to flow during contraction of the myocardium is called afterload, which is the third factor. This includes aortic impedance, arterial and peripheral vascular resistance, as well as blood viscosity and hydrostatic pressure. Afterload affects the rate and extent of systolic emptying. Heart rate is the fourth factor which affects cardiac output. When the frequency of contraction increases, more blood is pumped out and the cardiac output (stroke volume × heart rate) increases proportionately.

Autonomic Control

The rate and strength of contraction is regulated by the autonomic nervous system, which is composed of the sympathetic and parasympathetic components. The sympathetic fibres pass through the spinal cord and innervate the atria and the ventricles, the coronary arteries, and to a lesser extent the SA and the AV nodes. The parasympathetic fibres travel in the vagus nerve and innervate primarily the SA node and the AV node to regulate heart rate. Sympathetic and parasympathetic (vagal) stimulation generally have opposite effects on the heart. Normal vagal stimulation

(tone) lowers the heart rate to its resting value. When the sympathetic nervous system stimulates the heart, contractility and heart rate increase.

Cardiac output is regulated in response to changes in blood pressure, as well as blood oxygen (0_2) and carbon dioxide (CO_2) content and blood pH. Blood pressure is sensed by baroreceptors in the carotid sinus and aorta, whereas blood gases (O_2 and $C0_2$) and pH are monitored by chemoreceptors in the carotid and aortic bodies. Signals from these receptors are delivered to the vasomotor centre in the medulla of the midbrain, which controls the autonomic regulation of the heart and the peripheral blood vessels.

Nervous control of the heart is ultimately effected by the interaction of chemical compounds with the myocardial cell membrane. This interaction is often the binding of a compound with an integral membrane protein called a receptor. Receptors have binding sites for specific compounds which activate (or inactivate) a certain response within the cell. Compounds which activate the response of the receptor are called agonists, while those which inactivate the receptor are called antagonists.

Neurotransmitters are controlling compounds which are typically released at nerve endings, and are agonists of the receptors of the target cells. The neurotransmitter of the vagal system is acetylcholine, whereas the neurotransmitter of the sympathetic nervous system is norepinephrine (NE). NE can be released at the synaptic junction of a nerve and a myocardial cell, or it can be released as a circulating hormone in the blood.

In the heart there are alpha and beta *adrenergic* receptors, i.e. those which bind norepinephrine (NE), and other related compounds such as epinephrine (adrenaline). There are in turn two types of each of these receptors. Beta-1 adrenergic receptors are located primarily in the SA node, the ventricles and the AV node. They mediate myocardial contractility. Beta-2 receptors are found primarily in the lungs and liver, and to a lesser extent in the atria and the SA node. They cause dilation of the blood vessels (vasodilation). The alpha-1 receptors are post-synaptic, while the alpha-2 receptors are pre-synaptic, and both cause vasoconstriction.

The *cholinergic* receptors receive signals from the parasympathetic nervous system (binding acetylcholine). Specifically, the muscarinic receptors (binding muscarine) are associated with the vagus nerve.

1.3 Normal Metabolism

Fuels

The heart uses different fuels (metabolic substrates) depending on availability and demand. The normal fuels are carbohydrates (glucose and lactate) and lipids (free fatty acids (FFA) and triglycerides). Proteins (amino acids) and ketone bodies are not normally fuels for the heart. Most of the energy (adenosine triphosphate (ATP)) required by the myocardium is created by aerobic (oxidative) metabolism through the citric acid cycle (Kreb's cycle). Anaerobic metabolism of glucose (glycolysis) can also be used to generate ATP. The major metabolic pathways are summarized in Figure 1.2 (Opie 1984).

Under resting conditions FFA are the preferred fuel of the heart, and glycolysis is normally inhibited. When insulin levels are low, as in the fasting or diabetic state, FFA and ketone bodies comprise most of the metabolic substrates. After a high-fat meal, triglycerides and FFA are almost exclusively used, whereas after a carbohydrate meal glucose and lactate are preferred. During exercise, blood lactate levels rise and lactate becomes a fuel for the heart, with glucose and FFA.

Blood flow

The coronary circulation delivers oxygenated blood to the myocardium and removes metabolites. Under resting conditions, myocardial blood flow (MBF) is approximately 80 ml/min per 100 g of tissue. Eighty ml of blood normally contains 16 mg of oxygen, and the myocardial oxygen extraction from the blood is 50-75%. Therefore the normal myocardial oxygen consumption ($M\dot{V}O_2$) is approximately 8-12

ml/min/dg. An important clinical index of $M\dot{V}O_2$ is the heart rate × blood pressure product (RPP).

During systole the coronary vessels are markedly compressed by the contracting myocardium, thereby impeding blood flow. Consequently, the myocardium of the left ventricle receives most of its blood supply during diastole, whereas the right ventricle receives nearly equal delivery during systole and diastole. Coronary blood flow can be decreased by low diastolic pressure, and by other factors which lower the effective perfusion pressure such as narrowing (stenosis) or blockage (occlusion) of the coronary arteries.

Extracellular adenosine concentration is central to the metabolic regulation of coronary blood flow. When myocardial oxygen supply falls, energy levels decrease within the myocardial cells (ATP $\rightarrow$ ADP+P $\rightarrow$ AMP+2P) producing high concentrations of adenosine monophosphate (AMP). This compound is dephosphorylated as it leaves the cell, causing the extracellular adenosine concentration to rise. Adenosine acts as a potent vasodilator increasing myocardial blood flow and restoring oxygen supply. Blood flow is also regulated by the sympathetic nervous system through the adrenergic receptors, especially in the ventricles as described earlier.

The major factors which determine MBF are related to the demand for oxygen by the heart. These include the myocardial mass, myocardial wall tension, heart rate and contractility. Wall tension varies with pressure, radius and wall thickness of the myocardium, according to Laplace's Law. When the demand for oxygen by the heart increases, coronary blood flow increases proportionately. This increase can be a factor of five or more above the resting value, and is called the coronary reserve.

When demand exceeds supply, the myocardium is considered to be *ischemic* since the normal metabolic requirements are not met. The metabolism of fatty acids by myocardium declines and eventually ceases while glucose metabolism increases. This is simply due to the decrease in the availability of oxygen which causes anaerobic glycolysis to become one of the few sources of energy in the affected tissue. Glycolysis also produces lactate which acts as an inhibitor of this pathway, therefore the persistence of glycolytic activity depends on a critical balance between the

production and removal (by residual blood flow) of inhibitors. The amount of residual blood flow is crucial for the rate and persistence of glycolysis, and therefore is crucial to the survival of ischemic tissue. It is estimated that residual blood flow of only 15-30% of resting flow is required to sustain the life of ischemic myocardium.

1.4 Ischemic Heart Disease

Coronary Artery Disease

The most common cause of heart failure is reduced myocardial contractility of the ventricles (Guyton 1992), which is typically caused by ischemia, resulting from coronary artery disease (CAD). CAD is usually associated with a buildup of atherosclerotic plaques that progressively narrow (stenose) the arteries, and prevent adequate blood supply to the myocardium. The risk of developing atherosclerosis is highest in individuals with a known genetic predisposition, and is increased by smoking and high fat diets including cholesterol. The disease is also more common in men than in women.

Myocardial Infarction and Angina Pectoris

Atherosclerotic plaques can break through the inner layer of the coronary arteries, and facilitate formation of blood clots. A blood clot (thrombus) can either occlude the vessel directly, or break free and block a more distal artery (embolus). An acute occlusion of a coronary artery will often cause a myocardial infarction (MI). This typically results in ischemic necrosis (death) or dysfunction of myocardial tissue distal to the blockage. The dynamic changes in blood flow and cardiac work determine the extent of ischemic injury. If the area of ischemia is small, myocardial dysfunction may not be permanent. Complete recovery of contractile function is possible if collateral circulation is able to restore blood flow to the infarcted tissue. When the area of ischemia is large, cells in the centre of the region die quickly, and the

surrounding myocardium becomes dysfunctional. This causes impairment of overall cardiac function, and can result in death due to heart failure. Many individuals recover from a myocardial infarction. Over time, necrotic myocardium is replaced by fibrous scar tissue. The surrounding dysfunctional regions either recover to normal function if blood flow is restored, or they die and become scar tissue.

Ischemia can develop without the occurrence of a myocardial infarction. A common symptom of ischemia is *angina pectoris*: pain in the upper chest region, left arm and shoulder. This condition develops whenever the metabolic demands of the heart exceed the supply delivered by the coronary arteries. The effects can be transient, e.g. exercise induced, or chronic. Progressively stenosed arteries may eventually cause chronic ischemia even under resting conditions. Control of angina is effected through the use of vasodilating drugs such as nitroglycerin, or beta-adrenergic antagonists (beta-blockers) which prevent sympathetic stimulation of the heart and thus reduce myocardial oxygen consumption.

Cardiac Drugs

There are a large number of drugs used to alter cardiac function. Many work by increasing or decreasing cytosolic Ca^{2+} levels, thereby affecting the contractility of the myocardium (Schlant 1986). Contractility is increased by catecholamines such as NE acting through the beta-1 adrenergic receptors, and by digitalis compounds. Contractility is decreased by beta-blockers, calcium antagonists, and by the physiological condition of hypoxia.

Some drugs also act on the SA node and the AV node by changing conduction times, and altering the heart rate (HR) accordingly. A brief list of drugs with their physiological actions is presented in Table 1.1 (Opie 1984).

Table 1.1

Physiological Action of Selected Cardiac Drugs

Drug Class	Action	Examples
Beta receptor agonist	↑HR, ↑contractility	(Nor)Epinephrine, Dobutamine
Beta receptor antagonist	↓HR, ↓contractility	Propranolol
Calcium antagonist	↓HR, ↓contractility	Verapamil
Cholinergic antagonist	↑HR	Atropine
Vasodilators	↑HR, ↓blood pressure	Nitrates
	↓HR, ↓contractility	Adenosine
	↑HR	Dipyridamole
Digitalis Glycosides	↓HR, ↑contractility	Digitalis

Assessment and Treatment

The clinical assessment of patients with ischemic heart disease often involves many diagnostic procedures. These generally proceed from simple non-invasive procedures to more invasive measurements such as cardiac catheterization. A brief list of tests, prescribed in increasing order of invasiveness is presented in Table 1.2

Table 1.2

Diagnostic Procedures

Test	Parameter	Measurement
Initial Examination	Risk Factors	Lifestyle, Pain, Blood Pressure
Electrocardiogram (ECG)	Ischemia	Electrochemical (ST depression)
Chest X-Ray	Abnormal Anatomy	Heart size and position
Echocardiography	Contractility	Ejection Fraction (EF), Wall thickness
Exercise Capacity	$M\dot{V}O_2$	Cardiac output and oxygen extraction
Radionuclide Angiography	Contractility	Ejection Fraction, Wall motion
Radionuclide Rest-Stress	Ischemia	Perfusion defect size and persistence
Balloon Catheterization	Preload	RA pressure, Cardiac output
Coronary Angiography	CAD	Hemodynamics, EF, Stenosis

Not all tests are performed for all patients under all circumstances. For example, low risk patients may need no more than a resting ECG, while patients presenting with suspected myocardial infarction may require immediate coronary angiography to determine the appropriate course of treatment. Typical interventions may include treatment with thrombolytic drugs, coronary angioplasty (PTCA), bypass grafting surgery, or cardiac transplant. The ultimate goals of therapy are to improve cardiac function, and to reduce anginal pain caused by ischemia.

It is important to determine the extent of living (viable) tissue in ischemic areas with low blood flow, for a patient who has suffered a myocardial infarction. These regions of tissue have the best potential for improved left ventricular function after successful revascularization. For those who have no viable myocardium, such an intervention represents an unnecessary risk. Assessment of ischemic myocardium is commonly performed by rest-stress radionuclide (^{201}Tl or ^{99m}Tc-sestamibi) imaging, using single photon emission computed tomography (SPECT) (Schlant 1986). Thallium is a potassium analogue which accumulates (non-linearly) in the myocardium according to blood flow. Ischemic myocardium is identified by low flow regions (defects) present during exercise stress, which then become more uniform (redistribute) over time or after reinjection at rest. Attenuation artifacts can create apparent defects making diagnosis difficult, particularly in large-breasted women. A more accurate nuclear imaging technique called positron tomography (PET) incorporates a correction of attenuation effects. This enables quantitative measurements to be made of myocardial blood flow, and regional metabolic rates. Positron tomography is the imaging technique which offers the highest diagnostic accuracy for the evaluation of coronary artery disease (Schwaiger 1994).

CHAPTER 2
Positron Tomography

The constituent elements of organic molecules: carbon, nitrogen and oxygen can be produced in a neutron deficient state (isotope) in a particle accelerator. These proton rich isotopes then decay through positron emission. Metabolic compounds can be labelled with these isotopes, administered into the body, and subsequently *imaged* using PET techniques. This approach is very useful in the study of myocardial function and metabolic processes in vivo.

2.1 Physics

Positron Decay and Annihilation

In the process of positron emission, a proton is converted to a neutron and the excess energy and charge is emitted as a positron. The kinetic energy of this positron is subsequently lost through interactions with surrounding matter. In water (or tissue), a positron typically travels less than 2 mm before its energy decreases to thermal levels (less than 10 eV). The average distance travelled by the positron (its range) varies with the initial kinetic energy of the positron and the density of the surrounding medium. The mean positron energy and range for several isotopes used in cardiac PET are shown in Table 2.1 (Bacharach 1992).

When the positron energy reaches the thermal level, it typically combines with an electron in an annihilation reaction. This converts the rest mass of the electron and the positron to energy in the form of two 511 keV gamma photons, which travel in opposite directions (180° apart).

Table 2.1

Properties of Selected Positron Emitting Isotopes

Isotope	Half-life [min]	Mean Energy [MeV]	Mean Range [mm]
^{11}C	20.4	0.386	0.56
^{13}N	10.0	0.492	0.72
^{15}O	2.1	0.735	1.1
^{18}F	110.0	0.250	0.35
^{82}Rb	1.3	1.52	2.4

The annihilation photons interact with the surrounding matter (body tissues and detectors) in two predominant ways: photoelectric absorption and Compton scattering. The photoelectric effect occurs when a gamma photon interacts with a tightly bound electron. In this case the photon is completely absorbed and the inner orbital electron is ejected. For 511 keV photons, the linear photoelectric absorption coefficient (τ /cm) increases with the atomic number (Z) of the element as $Z^{3.5}$ (Evans 1982). An incident photon can also interact with a free electron in the surrounding medium. In this case, the incident photon transfers some of its energy to the free electron, and changes its direction of travel (is scattered). The Compton scatter coefficient (σ /cm) depends on the number of electrons available as scattering targets, and therefore increases linearly with increasing atomic number of the medium (Knoll 1989). The effective atomic number (Z) of an absorbing medium is the principal determinant of its density. Therefore, the density of the surrounding medium is the major factor governing the distribution of energy produced by positron emitting isotopes:

1. Range of positrons decreases linearly with Z,
2. Photoelectric absorption coefficient increases as $Z^{3.5}$,
3. Compton scatter coefficient increases approximately linearly with Z.

These factors affect detector design, quantification and resolution in PET.

Coincidence Detection and Image Reconstruction

It is necessary to record the position, time and energy of the annihilation photons to measure the distribution of positron emitting isotopes (Bacharach 1992). Photon detectors are typically designed to optimize one of these measurements. Several options currently exist, but by far the most commonly used is a scintillating crystal of Bismuth Germanate (BGO) coupled to photomultiplier tubes (PMTs). BGO is a very dense (Z=83) material, resulting in a high absorption coefficient. The coupled PMTs generate an output voltage proportional to the photon energy deposited in the crystal. BGO systems can not resolve the photon energy perfectly, and therefore record photons within a window of energies centered about 511 keV, e.g. 350-650 keV.

When two photons within the prescribed energy are detected by two facing detectors within a narrow time window (e.g. 10-15 ns), they are said to occur in (prompt) coincidence. If the two photons originated from a single annihilation event, and neither was Compton scattered en-route to the detectors, the recorded event (count) is called a true coincidence. A recorded true event implies that a positron decay occurred somewhere along the line of response (LOR) between the two detectors.

The true count rate measured along one LOR is ideally proportional to the line integral of the isotope concentration between the corresponding two detectors. PET is based on the measurement of line integrals along the LORs between many pairs of detectors. Detectors are typically placed in a planar (transaxial) ring, defining many LORs through a given imaging plane. The corresponding cross-sectional (tomographic) images are recovered using the methods of computed tomography. Specifically, a technique called filtered backprojection (Nahmias 1980) is often used to reconstruct tomographic images of regional count rate from the measured line integrals. When all corrections have been applied, the pixel values in the reconstructed images are linearly related to isotope concentration in the volume occupied by that pixel. Values are often expressed in counts per second per pixel (cps/pix), which can be directly converted to isotope concentration (Bq/ml). This calibration is performed by measuring a source with a known radioactive concentration, and computing the ratio of Bq/ml : cps/pix.

Most commercial scanners contain multiple (axial) rings of detectors, which measure the isotope distribution in adjacent overlapping image planes.

Corrections

It often occurs that two photons from two separate annihilation events are detected within the coincidence time interval. This is called a random or accidental coincidence. The number of random coincidences (randoms) depends on the total number of photons incident on each detector, which is referred to as the singles rate. Along any LOR the random coincidence count rate increases as the product of the singles rates of the corresponding two detectors. The randoms form a background above which the true coincidences must be measured. Correction for randoms is typically performed using a delayed coincidence time window. Any photon detected after a certain delay following an earlier photon, must have originated from a separate annihilation event, and is therefore a (delayed) random coincidence. These delayed coincidences are subtracted from the total prompt coincidences to estimate the true coincidence count rate.

When one or both annihilation photons are Compton scattered en-route to the detectors, the resulting coincidence can be recorded in the wrong LOR. This is referred to as a scattered coincidence. Scatter forms a spatially variant background which depends on the spatial distribution of the isotope and on the density and spatial distribution of the scattering medium. Although scattered photons have decreased energy, many still fall within the prescribed energy window. Therefore, energy discrimination is only effective in rejecting photons which have been scattered through a relatively large angle, e.g. 40 degrees. Scatter is traditionally reduced using interplane septa, which attenuate photons originating outside a given two dimensional (2D) imaging plane. More recently, septa are removed to permit three dimensional (3D) acquisition of coincidences in LORs which cross multiple detector rings. In this case the ratio of scattered:true coincidences increases compared to 2D acquisitions with

septa. No scatter correction technique is currently accepted for cardiac PET imaging. In the present work, all cardiac studies have been performed with septa in place.

Many photons are absorbed or scattered out of the field of view (FOV), and are never recorded in a coincidence event. This effect is called attenuation. The linear attenuation coefficient (μ) in a uniform medium is the sum of the Compton scatter coefficient and the absorption coefficient, however in most tissues Compton scatter accounts for almost all attenuation of 511 keV photons. The total linear attenuation (I/I_o) of a narrow beam of photons through a distance (x) in a uniform medium is given by Equation 2.1.

$$I/I_o = e^{-\mu x} \qquad (2.1)$$

$$\mu = \tau + \sigma \ [cm^{-1}]$$

This implies that the measured intensity is lower for structures deep inside the body, than for those near the edge. Attenuation correction is typically performed using an external source of positron emitting isotope and two additional scans: a *blank* scan performed with no object in the FOV, and a *transmission* scan performed with the subject in the FOV before the tracer is administered. The attenuation correction along each LOR is computed directly as *blank/transmission* (I_o/I), which is the inverse of the total attenuation given by Equation 2.1. Scatter must also be removed from the transmission data in order to compute accurate attenuation factors. This is typically performed by *rod windowing*, in which only coincidence counts collinear with a rotating rod source are recorded.

There is a minimum period within which only one event can be recorded by the detector and associated electronics. This is called the dead time of the system. When more than one photon strikes a detector within a time shorter than the dead time, one or more of them will not be recorded. Photons which are not counted because of this effect are referred to as dead time losses. Dead time losses below approximately 50% can be modelled accurately and corrected for, thus preserving the desired linear response of the measured count rate with isotope concentration.

The statistics of radioactive decay follow the Poisson distribution. The probability of recording n counts in an interval t is:

$$p(n) = \frac{e^{-Rt} \cdot Rt^n}{n!} \qquad (2.2)$$

where Rt (count Rate x time) is the mean number of counts, and is assumed to be small. For a given sampled count n, the mean and variance are both estimated as n. For high count rates or long measurement intervals, i.e. Rt > 20, the sampling Poisson distribution approaches a Gaussian in shape. When counts are recorded with appreciable dead time, the variance of the corrected counts increases. For example, with a non-paralyzable dead time model (Knoll 1989) the variance equals n times the dead time correction factor.

Image Resolution

Resolution is a measure of the ability of the tomograph to distinguish small objects in a reconstructed image. Object position is measured with some uncertainty, which is characterized by the point spread function (distribution) of measured counts around a small object. The full width at half maximum (FWHM) of this distribution is often used to specify the resolution of PET scanners. It is determined primarily by the size and spacing of the scintillation detectors. The range of high energy positrons can also affect resolution of the reconstructed images. Modern scanners typically have isotropic transaxial and axial resolution equal to approximately 5 mm FWHM. This relatively low resolution produces the characteristically smooth looking images associated with PET.

When a given image pixel or region includes counts from adjacent tissues with different isotope concentrations, the resulting measurement is inaccurate. This effect is called partial volume averaging, and is a direct result of finite resolution. As a general rule objects which are smaller than twice the FWHM resolution will have less than 100% recovery of the true isotope concentration. This is an important effect when imaging the 1 to 1.5 cm thickness of the myocardium of the left ventricle. In cardiac imaging, partial volume averaging also occurs as a result of myocardial wall motion

during the cardiac and respiratory cycles. This typically causes measured myocardial concentrations to be underestimated because of contributions from adjacent blood and lung tissues.

2.2 Radiopharmaceuticals

In order to study physiologic processes in vivo, metabolic compounds must be labelled with a positron emitting isotope. Small (tracer) amounts which do not affect the normal metabolism are administered into the body. The PET scanner then measures the regional distribution of isotope in a volume of interest which can include the heart. Reconstructed images reflect the spatial distribution of the tracer compound and all of its metabolites.

Tracer Compounds

The common positron emitting isotopes shown in Table 1.1 have short half-lives, and this typically necessitates the on-site location of a cyclotron for production and synthesis of the labelled compounds (radiopharmaceuticals). The need for a cyclotron can be avoided by using generator-produced radiopharmaceuticals such as ^{82}Rb, or by using longer lived tracers which can be distributed by regional distributors. There are many radiolabelled compounds used as metabolic tracers for research and clinical cardiac studies. The common clinical uses of tracers in PET are for the measurement of blood flow and glucose metabolism of the myocardium. Together, these indicate the relative health of the myocardium of the left ventricle, and can be interpreted to locate stenotic vessels and ischemic viable myocardium.

Blood Flow Tracers

Tracers of blood flow typically are classified as either particulate or diffusible indicators as shown in Table 2.2 (Schwaiger 1992). The diffusible indicators are

further distinguished between those that are temporarily trapped (extracted) by the myocardium in proportion to blood flow, and inert or freely diffusible tracers that clear from the myocardium as a function of flow.

Table 2.2

Myocardial Blood Flow Tracers

Tracer	Type	Extraction [%]
^{68}Ga-labelled albumin microspheres	Particulate	100
^{13}N-labelled ammonia	Extracted	90
^{11}C-labelled alcohols	Inert Diffusible	100
^{15}O-labelled water	Freely Diffusible	100
^{82}Rb-labelled potassium analog	Extracted	65

Particulate tracers, such as albumin microspheres labelled with ^{68}Ga or ^{11}C, are useful for measuring myocardial blood flow. The extraction fraction during a single capillary transit (single-pass) is approximately 100% which implies that the concentration measured in the tissue is directly proportional to MBF. The major drawback of this process is that the microspheres must be injected directly into the left ventricle or coronary arteries. For this reason there is limited clinical use of this technique to quantify blood flow.

The diffusible indicators represent a more practical method of quantifying MBF as they can be injected intravenously without excessive trapping in the lungs. The common tracers for blood flow, ^{13}N-labelled ammonia and ^{15}O-labeled water, are diffusible indicators and distribute in the myocardium in proportion to blood flow. ^{13}N-labelled ammonia is carried in equilibrium with the ammonium ion (NH_4^+) by the blood. At the capillaries, ammonia rapidly diffuses into the myocardial cells due to a high single-pass extraction fraction. The nitrogen is then incorporated in the synthesis of glutamine and is retained in the tissue, with complete fixation in myocardium occurring generally within two minutes of administration. Tissue retention of the ^{13}N isotope is high and only a portion of the ^{13}N leaks out of the myocardium

into the blood pool in the form of labelled amino acids. These properties result in high contrast cross-sectional images of the myocardium measured with PET. Images acquired two to three minutes after tracer administration will reflect the MBF distribution at the time of administration. Because the initial extraction fraction and tissue retention of ^{13}N are close to 100% at rest, the relation between ^{13}N tissue concentration and regional blood flow is linear. However, the extraction and retention of ^{13}N-ammonia decreases at high flow rates, causing blood flow to be underestimated. Kinetic models of ammonia uptake and metabolism can be used to obtain quantitative estimates of regional MBF at high flow rates encountered in rest-stress study protocols. A compartmental model illustrating ammonia tracer kinetics is shown in Figure 2.1B (Schwaiger 1992).

^{15}O-labelled injected water or inhaled carbon dioxide can be used to evaluate MBF with the use of a labelled blood pool tracer such as carbon monoxide to correct for blood volume. Labelled water in the blood diffuses freely across the myocardial cell membrane. A simple kinetic model is used, describing the exchange of an inert gas between blood and tissue, as shown in Figure 2.1A. The high diffusibility of water results in short residual time of the tracer in the myocardium as it equilibrates quickly between tissue and the blood pool. This causes a reduction in the contrast of the image and sophisticated analysis procedures are required to separate the myocardial (H_2O) from the blood pool (CO) activity.

There are several other tracers used to determine myocardial blood flow. Among these are ^{82}Rb and ^{62}Cu-PTSM which are extracted compounds. However, these do not have a high single-pass extraction from the blood and therefore can significantly underestimate the true regional blood flow. Compartmental models for these tracers have not been validated in humans.

Metabolic Tracers

Compounds have been developed to study pathways such as beta-oxidation of fatty acids, aerobic and anaerobic metabolism. For example, ^{11}C-acetate is used as a

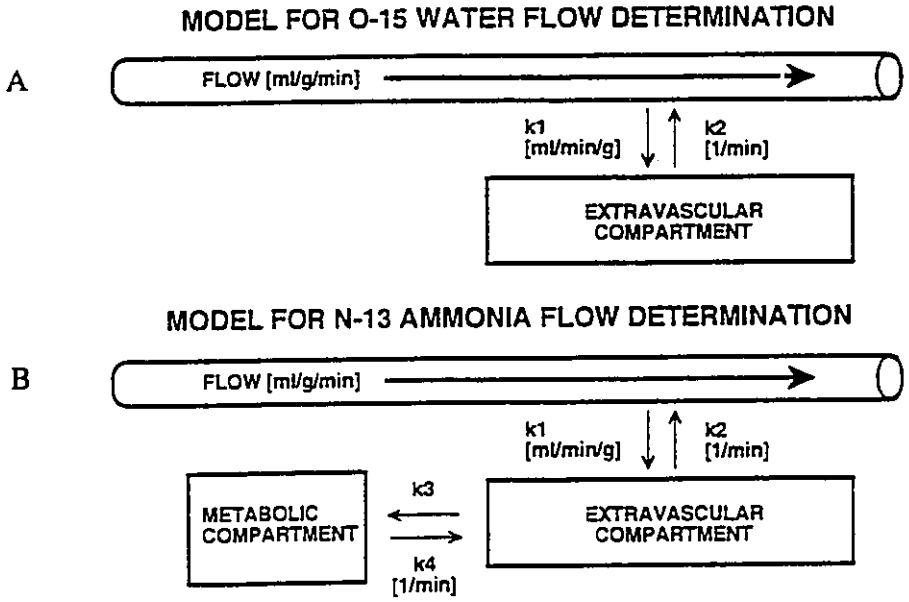

Figure 2.1. Compartmental models for ^{15}O-labelled water (A) and ^{13}N-labelled ammonia (B) blood flow. Tracer is initially taken up by the myocardial tissue (extravascular compartment). It is subsequently washed back out into the blood, or further metabolized (ammonia metabolic compartment) (Schwaiger 1992).

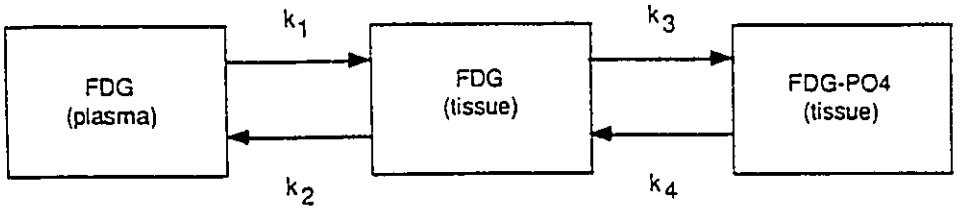

Figure 2.2. Compartmental model for ^{18}F-fluorodeoxyglucose (FDG) kinetics. FDG is initially taken up by the myocardium. It is then washed back out into the blood, or metabolically trapped by phosphorylation. Subsequent dephosphorylation (k_4) is slow (Gambhir 1989).

marker of oxidative (aerobic) metabolism. Acetate is a precursor to acetyl-CoA which is the major fuel input into Kreb's cycle of aerobic metabolism. The clearance of labelled acetate provides a measure of oxygen consumption by the myocardium. The initial uptake phase of the tracer can also be used to measure blood flow.

Unlike many other organs, the heart can use a variety of substrates to derive the required energy. The relative contribution of each substrate to metabolic activity depends on the substrate availability in plasma, the presence of certain hormones, and the cardiac work load as discussed in Chapter 1. Glucose becomes the major source of energy in ischemic tissue, therefore the quantification of glucose utilization in the myocardium is common for determining the viability of this tissue. The popular choice of tracer for measuring glucose metabolism is ^{18}F-fluorodeoxyglucose (FDG). This is an analog of the glucose molecule, in which ^{18}F is substituted for a hydrogen atom. FDG is phosphorylated after it crosses the myocardial cell membrane but is not subsequently metabolized, therefore it is essentially trapped in the myocardium. This high retention of ^{18}F by the tissue results in high contrast images of the myocardium of the left ventricle. These images can be quantified into absolute measurements of regional myocardial rates of glucose utilization in [μmol/min/dg] by using a kinetic model, if the concentration of ^{18}F is measured over time in both arterial blood and myocardium (Figure 2.2, Gambhir 1989). The metabolic rate of glucose in myocardium may provide estimates of severity of ischemia and of metabolic responses to therapeutic interventions.

Tracers have also been developed to study sympathetic nervous control of the heart. ^{18}F-dopamine is an analog of dopamine, a precursor of norepinephrine which is the neurotransmitter used in the sympathetic innervation of the heart. Meta-hydroxyephedrine can be labelled with carbon-11 (^{11}C-HED) and studied as a direct analog of NE.

2.3 Applications of Cardiac PET

The major clinical applications of PET in cardiology are the measurements of MBF and glucose metabolism to detect coronary artery disease, specifically coronary stenosis, and myocardial viability. Research applications include the detection of treatment effects resulting from drug or medical interventions.

Coronary Artery Disease

CAD is rarely identified by resting MBF measurements, therefore stress testing is generally required to increase coronary flow preferentially to normal myocardium. MBF is measured at rest and then again following an increase in blood flow induced by physical stress or a vasodilating drug such as dipyridamole. Drug induced stress is generally preferable, in order to maintain constant patient position that is required to accurately correct for attenuation. The ratio of the MBF during stress to resting flow is termed the coronary reserve, and has a typical value of 4 to 5 for normal myocardium. This ratio can decrease to just over 1 for vascular territories with significant coronary artery disease. Regions with relatively low coronary reserve indicate an attenuated response to vasodilatation, and therefore imply a stenosis in the artery supplying these regions. The extent and severity of reductions in blood flow caused by stenotic vessels can be accurately identified. Once the regions of reduced flow have been located, the viability of these tissues can be determined and the advantage of redirection of blood flow to the regions can be assessed.

Myocardial Viability

Myocardial cells which receive enough blood flow to remain alive are said to be *viable*. If there is a stenosis in a coronary artery causing a local decrease in blood flow, it is crucial to assess whether the affected tissue is viable or necrotic. After myocardial infarction, the progression from reversible ischemic injury to cell death is

a function of residual blood flow and metabolic demand. Within the area of an infarction, there tends to be the coexistence of necrotic and viable tissue, and the extent of viability also varies. The regional state of the tissue determines the risks and benefits to the patient of redirecting the blood flow to this region. After determining the existence of viable tissue in the area of an infarction with PET, an attempt can be made to reverse the effects of ischemia by restoring blood flow to the region.

The viability of the myocardium is typically determined by comparing images of MBF to those of FDG retention. Regions of normal MBF and normal FDG uptake represent normal tissue. If MBF is decreased but FDG uptake is maintained (or increased) then the tissue is considered ischemic but viable (mismatched defect), and recovery of function is expected following successful revascularization. A regional decrease in both MBF and FDG uptake (matched defect) indicates irreversible tissue necrosis with no expectation for recovery of contractile function.

PET is unique in its capacity to quantify these metabolic activities of the heart, and is essential in the evaluation of the benefits of redirecting blood flow in regions that are affected by CAD or have suffered myocardial infarction.

Treatment Effects

The primary goal during the treatment of ischemic heart disease is to maintain the viability of injured or compromised myocardium. This is accomplished by controlling the work load of the heart, and by increasing resting MBF. The effects of medical therapies are difficult to evaluate directly, and are usually deduced from indirect measurements such as exercise capacity, and reduction of anginal pain. While these are relevant measurements for increased quality of life, they are not always indicative of the underlying physiological state of the myocardium, or of the coronary arteries. There are limited methods available to monitor the progression or treatment of heart disease. Planar nuclear ventriculography is often used to measure wall motion and ejection fraction before and after revascularization. This provides important information concerning the success or failure of this treatment, based on the

mechanical function of the ventricle. However, it provides little insight to guide the course of therapy a-priori. Thallium-201 SPECT imaging is most commonly used to localize regions of ischemic myocardium which may benefit from revascularization. There are recognized deficiencies of this approach including attenuation artifacts, and less than ideal predictive accuracy.

There may be potential to directly monitor with PET, the effectiveness of medical treatment or therapy. The power of PET to detect subtle differences in myocardial physiology during treatment is not currently being exploited. Such changes resulting from treatment are typically interpreted visually, or semi-quantitatively based on techniques originally developed for interpretation of SPECT images (van Train 1986). Precise measurements can be made with PET, which maximize the statistical significance of observed changes with treatment. The state of the art in cardiac PET data analysis is reviewed in the following chapter, in the context of the detection of treatment changes.

CHAPTER 3
Review of Image Analysis in Cardiac PET

In order to detect treatment changes with statistical certainty, the precision of experimental measurements must be high relative to the magnitude of change. In cardiac studies with positron tomography, *Change magnitude* is measured in terms of myocardial isotope concentrations (or derived measures), which requires normalization for many sources of systematic variation including instrumentation effects, heart morphology and tracer delivery. *Increased precision* is achieved by lowering the error variance of the measurements. By removing unwanted systematic variations from the measurements, the error variance is reduced and is assumed to be due to random processes only. Factors such as counting noise and the normal variation of myocardial physiology can never be removed completely from the error variance.

These sources of random and systematic error are reviewed in this chapter. Current methods for the normalization of systematic effects are presented, and the factors which contribute to the random error variance are discussed. Studies which have investigated *changes* in myocardial physiology under different experimental conditions are also reviewed.

3.1 Basic Statistics

Treatment Significance

Statistical methods enable comparisons to be made between populations by examining small subsets (or samples) of those populations under different treatment conditions. In cardiac PET studies, physiological changes in response to treatment are measured as differences in local and global concentrations of tracer in the myocardium. It is necessary to evaluate the statistical significance of these differences to determine if such changes may be due to normal variation of physiology, or if the changes are

specifically due to the treatment effects. It is important to note that a statistically significant difference does not imply a physiologically significant difference or vice versa. Physiological significance must be evaluated based on the clinical effects on the subjects, which are often subjectively evaluated. For the purpose of this work conclusions are limited to statistical significance only.

Hypothesis Testing

The significance of change can be evaluated in a number of ways, but central to all is the concept of hypothesis testing. A null hypothesis (Ho) is typically proposed which states some property of a model parameter, e.g. the value of the population mean equals zero ($\mu=0$). Then statistics from the measured data are used in an attempt to disprove (reject) the null hypothesis. If it is rejected, then an alternative hypothesis is accepted which may be explicitly stated or implied from the null hypothesis. In the case of cardiac PET data, the model parameters are usually regional mean values of myocardial isotope concentration or of other derived measures of physiology.

A critical level of significance (α) is chosen with which to reject Ho. This is the probability of type I error, i.e. the false positive rate. The required test statistic is computed based on an estimate of the parameter and its standard error, e.g. the mean and standard error of the mean. If this test statistic is greater than the corresponding (α) critical value, then the null hypothesis is rejected and we claim a significant (positive) result. If the direction of change is chosen, i.e. increases or decreases, then a one-sided test is performed, otherwise a two-sided test is used. A brief summary of statistical tests is shown in Table 3.1.

An estimate of the error variance (S_e^2 or mean squared error (MSE)) is typically used in the standard error of a parameter estimate. When comparing sample means between treatment groups, the MSE is a measure of the experimental variation which occurs naturally *within* a treatment group, but separate from the effected treatment variance *between* groups. There are many factors affecting the error variance of sampled measurements of physiology with PET. The contributions of each must be

well understood, in order to select the techniques of measurement and analysis which minimize the error variance and thereby maximize the significance of the results.

Table 3.1

Standard Statistical Tests

Test	Ho	Statistic	Assumptions
Single sample	$m-\mu=0$	$Z = m-\mu / (\sigma/\sqrt{n}) \sim N(0,1)$	σ is known
Single sample	$m-\mu=0$	$T = m-\mu / (S_e/\sqrt{n}) \sim t_{n-1}$	σ is unknown
Paired samples	$d=0$	$T = d / (S_d / \sqrt{n}) \sim t_{n-1}$	$d=m_1-m_2$
Independent samples	$\mu_1-\mu_2=0$	$T = m_1-m_2 / \sqrt{((S_1^2+S_2^2)/n)} \sim t_{2n-2}$	$n=n_1=n_2$, $\sigma_1=\sigma_2$
k cond. ANOVA	$\mu_1=\mu_2=...=\mu_k$	$F = S_t^2/S_e^2 \sim F_{(k-1,n-k)}$	$\sigma_1=\sigma_2=...=\sigma_k$
	$\mu_i=\mu_j$	$T = m_i-m_j / \sqrt{(2S_e^2/n)} \sim t_{kn-k}$	F is significant
k cond. ANCOVA	$\mu_{1adj}=...=\mu_{kadj}$	$F = S_t^2/S_e^2 \sim F_{(k-1,n-k-1)}$	covariate is exact

n is the sample size
m is the sample mean
S_e is the sample standard deviation
S_t is the treatment standard deviation
k is the number of treatment conditions
μ is the population mean
σ is the population standard deviation

As shown in Table 3.1, the treatment means are the important measures to be compared, and are altered by the experimental intervention, i.e. a systematic source of variation is created by the investigator. All other sources of systematic variation make differences in the treatment means less apparent, and should be removed. The most common of these is the block effect which is present when comparing treatment means measured in different groups of subjects (blocks). In PET, this effect can be removed by using subjects as their own controls, and measuring differences relative to a baseline scan. This is generally referred to as a paired design.

Experimental Design

Any experiment which is designed to compare several treatments must satisfy two basic requirements:

1. Treatments must be repeated in several subjects to enable estimation of the sample means, as well as the between group (treatment) and within group (error) variances.
2. Treatments must be randomly assigned to the subjects in order to remove any systematic bias of the investigator, and to ensure that all measurements are independent.

The simplest type of experiment which satisfies these requirements is called the *completely randomized design.* In this case the treatment conditions are allocated randomly, and in equal number between all subjects. Each subject receives only one condition. The results are analysed using a simple one-way analysis of variance (ANOVA) as shown in Table 3.1. The variance model for the measured data (y) in subject j under treatment condition i is $y_{ij} = \mu + c_i + e_{ij}$, where μ is the grand mean, c_i are the condition means (i=1,k), and e is the error variance. If there are only two conditions e.g. baseline and treatment, then an independent t-test comparison of means is equivalent, i.e. $F=T^2$ if k=2.

In order to increase the sensitivity of the experiment, *randomized block designs* are often used. In addition to the conditions of the completely randomized design, subjects are used as their own controls i.e. each subject receives both treatment conditions, and it is assumed that there is no residual effect of the treatments which affect the later measurements. A two-way model of the variance is used, i.e. $y_{ij} = \mu + c_i + b_j + e_{ij}$ to determine if there is a block effect (b) within subjects. In the analysis of variance another systematic source of variation is removed from the estimation of the error variance, and therefore the significance of the results can be increased. It is assumed that the treatment and block effects are independent i.e. there is no interaction between the factors. This can also be checked with an ANOVA if an interaction is suspected.

A different model is needed if there is another variable x (covariate) which varies linearly with the measurements but is independent of the treatment effects. In this case the variance model is $y_{ij} = \mu + c_i + B(x_{ij} - X) + e_{ij}$, where B is the linear dependence of the measurements on the covariate x, and X is the grand mean of the covariate. The adjusted measurements are computed as:

$y_{ij}(adj) = y_{ij} - B(x_{ij} - X)$

$= \mu + c_i + e_{ij}$ which corresponds to the standard ANOVA model. This model is called a one-way analysis of covariance (ANCOVA) (Wildt 1978). Block effects can also be included, as in the two-way ANOVA layout. Where possible, confounding effects should be removed directly as part of the measurement process. Removal of confounding covariates with statistical techniques is not preferred, but it is often necessary when they can not be removed from the measurements directly.

As part of the experimental design, it is necessary to estimate both the magnitude of changes expected with a given treatment, as well as the expected precision of the measurements. If small changes are sought in the presence of relatively large noise, then a large sample size is required. Conversely, changes can be detected with a small sample size if relatively precise measurements are made. Sources of signal are then separated from noise in the measurements by selecting an appropriate statistical model. Random variations are always part of the noise signal, whereas systematic variations constitute the signal of interest (treatment effect) as well as noise from confounding effects. Therefore it is necessary to understand the sources of systematic and random variations in PET images.

3.2 Random Variations

Physiological Variation

Normal physiological variation of the variables measured with PET will always contribute to the error variance. For example, blood flow to the heart can easily change between repeated studies of a single subject in an apparent resting state.

Oxygen demand by the heart is affected by many factors including mental state which is difficult to control or assess. Every effort must be made during the course of PET studies to ensure that the complete physiological state is controlled. In this way the error variance of the measurements is minimized, and smaller changes become detectable statistically.

There are many studies which have been performed to establish ranges of normal values for certain study protocols and analysis methods. These must essentially compute variances for a set of regions covering the entire heart, based on within group variations. There are many published values for normal cardiac substrate metabolism and blood flow, measured in small samples. The results from some recent studies are summarized in Table 3.2. Typically, values are reported for a few (4 to 10) large regions of the left ventricular myocardium to decrease statistical noise, as discussed in the next section. The population sample variance ranges from 10% to 40%.

Table 3.2
Normal Values of Myocardial Blood Flow
and Substrate Metabolism in Humans

Author	Tracer	Measurement	Value	CV	N
Hutchins et al 1990	$^{13}NH_3$	rest blood flow	0.88 ml/min/g	20%	7
		stress blood flow	4.20 ml/min/g	25%	7
Lammertsma et al 1992	$C^{15}O_2$	rest blood flow	0.92 ml/min/g	15%	6
		stress blood flow	4.32 ml/min/g	20%	6
Iida et al 1988	$H_2{}^{15}O$	rest blood flow	0.95 ml/min/g	10%	7
		disease blood flow	0.63 ml/min/g	40%	8
Gropler et al 1990	$H_2{}^{15}O$	rest blood flow	0.90 ml/min/g	30%	5
	^{11}C-acetate	oxidative metabolism	0.051 /min	20%	5
	^{18}F-FDG	glycolytic flux	0.001 %ID/ml	30%	5
Kotzerke et al 1990	^{11}C-acetate	oxidative metabolism	0.057 /min	15%	10
Gambhir et al 1989	^{18}F-FDG	glycolytic flux	0.94 µmol/min/g	30%	6

%ID/ml is the percent injected dose per cc of myocardium.

Limited data is available on the reproducibility of positron tomographic measurements in a given subject. It is known that the metabolic demands on the heart

are altered by many factors, as described in Chapter 2. Therefore, estimates of myocardial blood flow and metabolism with PET can be expected to vary between repeated measurements. Relative measures of blood flow are reported to vary by as little as 5% in a given individual with repeated measurements performed at rest (Fallen 1995). The estimation of absolute MBF using the compartmental model of Hutchins et al (1990) is reported to be accurate to within 4% to 15% (Hutchins 1992). Measurement of MBF on greyhounds with the model of Iida et al (1992) was shown to be accurate to within 2% to 10%. Estimates of regional myocardial rates of glucose utilization are reported with a standard error of 3% (Gambhir 1989). It is evident that measurements with higher precision can be obtained in individuals than in the population samples reported in Table 3.2.

Counting Statistics

Coincidence counting is assumed to follow a Poisson distribution, producing uncertainty (noise) in the line integrals of activity concentration. However, the regional count rates estimated in reconstructed images are typically assumed to follow a gaussian distribution. The regional standard deviation divided by the mean (relative SD) is used as measure of image noise. For a given imaging geometry and with a low count rate, the relative SD or coefficient of variation (CV) changes inversely with the square root of the number of total counts (Carson 1993, Cherry 1993). For example, the CV decreases by a factor of 2 if either the acquisition time or the activity concentration is quadrupled. Counting noise is an important component of the error variance which can never be eliminated completely.

The variance of image regions in a uniform cylinder has been shown to depend on the trues count rate, randoms, scatter, dead time and attenuation (Carson 1993, Huesman 1984). Noise equivalent counts (NEC) are used to compare the count rate performance of different tomographs (Strother 1990). They are defined as the reduced number of true counts (T) which would produce the same SNR in images of a uniform cylinder, with no randoms (R) or scatter (S):

$$NEC = T / (1 + R/T + S/T) \quad (3.1)$$

The ratios R/T and S/T are often referred to as the randoms fraction and scatter fraction respectively.

Regional Averaging

Positron tomographs have a finite resolution which is much larger than the typical pixel size in reconstructed images. This gives PET images their characteristic smoothness. It implies that adjacent pixels are not independent and cannot be analysed as such. In many cases, pixels are grouped together into functional areas, or regions of interest (ROIs) to attempt to create independent regions and to reduce counting noise. The larger the region of tissue being investigated, the higher the number of counts recorded and the smaller is the relative variation. The variance estimated from a group of pixels in a defined ROI is not a good estimate of the uncertainty of the mean value in the region, because adjacent pixels are correlated and therefore not independent. The extent of the correlation is a function of image smoothness (Carson 1993). Regional variance decreases with increasing image smoothness, as determined by the frequency window used with the reconstruction filter or by the extent of post-reconstruction smoothing. Computation of the standard deviation of a random sample is the only true method of measuring the regional noise.

Myocardial pixels within a given region (sector) of the left ventricle are often averaged to obtain a representative value for that sector. The spatial resolution of PET will currently allow localization to within 5 mm. This produces approximately 500 independent volume elements (each 5 mm^3) in the myocardium of a left ventricle which is 8 cm long and 6 cm in diameter. This is the order of magnitude of sectors that are used in volumetric representations of the myocardium of the left ventricle.

The sectoral regions are often larger than the effective resolution of the PET scanners. This implies that conclusions are drawn about volumes of myocardium which are assumed to be homogeneous in metabolism. In general this is not true, and

estimated values will be inaccurate due to partial volume averaging of adjacent tissues. Partial volume corrections will be discussed in detail in the next section.

As an alternative to large sectors, individual pixels can be used as the basic measurement element. In this case, changes of any size, shape and location can be detected, but adjustments must be made for the pixel correlations resulting from image smoothness (Friston 1991b). With any of the above methods, when significant regional changes are found, it is typically *impossible* to know whether a large difference has occurred in a small region, or whether a larger region has undergone a small change.

Noise in Systematic Corrections

Correction for many physical factors is necessary to produce uniform and linear measurements of cardiac function. These corrections often utilize other measurements which characterize the systematic variation, e.g. attenuation and scatter corrections. It is not only important that these measured corrections be accurate, but also precise in order to minimize the error variance.

Normalization for some systematic effects may involve a degree of operator interaction. Whenever there is subjective evaluation required to perform the normalization, there is an associated error variance. Different operators will choose different parameters, and even the same operators will choose different parameters on different occasions. The sources of variation caused by these choices are not typically included in the variance model, i.e. if the analysis has been performed by one person with one estimate per condition, then the precision of the technique is not known. Inter- and intra-operator variability can be determined by having multiple operators analyse the data multiple times, and then performing an appropriate analysis of variance. This is not done routinely, but it is important to know whether any systematic bias changes from one operator to another. The goal during these stages of analysis is not to introduce more variance than that associated with the effect being corrected. Accurate automated methods of analysis can reduce or remove the variability associated with operator interactions.

The magnitude of operator variability can equal 2%-8% when computing left ventricular volumes, and is reduced to 1%-4% with automated analysis (Levy 1992). A semi-automated technique of left ventricular reorientation is reported to significantly improve the reproducibility of the estimated parameters over manual methods (He 1991). Automated methods have been used to quantify coronary flow reserve, severity of CAD and progression/regression of disease (Hicks 1989). A semi-automated quantification of the extent and severity of CAD was shown to have high sensitivity and specificity for the localization of CAD, however observer variabilities from 3%-20% remained (Laubenbacher 1993). Myocardial regions have also been defined automatically and used to obtain accurate and objective measurements of MBF (Muzik 1993). Absolute infarct mass and total left ventricular mass have been estimated semi-automatically, with operator variabilities of 5%-30% (Delbeke 1993). The degrees of operator variability presented above can be responsible for large fractions of the total error variance of positron tomographic measurements in the heart (Table 3.2). It may be the dominant source of variance when comparing repeated measurements in individuals, where many physiological and anatomical variations between subjects do not contribute to the total error variance.

3.3 Systematic Variations

Physics and Instrumentation

There are many factors related to the physics of positron tomography, which cause systematic errors in the measurement of *volumetric isotope concentrations*. These systematic variations require corrections which are performed using separate measurements, or using models of the physical processes.

Attenuation correction is typically performed by multiplying an emission scan by the ratio of a *blank/transmission* scan as described in Chapter 2. Each of these scans has its own statistical uncertainty, and therefore adds noise to the corrected emission scan according to the size and density of the absorbing media (Dahlbom

1987). In studies of the chest, the correction is especially noisy because of the large width of the chest and adjacent arms. In this case the attenuation correction can reach a factor of 50 or higher. This correction can be caiculated if the tissue boundaries and attenuation coefficients of the tissue types are known (Meikle 1993, Digby 1989). This technique has the advantage that no additional statistical noise is added to the emission data. Misalignment of the attenuation correction and emission scans is an important source of systematic variation, and this can cause serious artifacts which are difficult to detect in cardiac imaging (McCord 1992).

Scatter in emission scans forms a spatially variant background with a broad distribution. It increases the apparent isotope concentration, especially in regions of low activity which are surrounded by regions of higher concentration, e.g. in small regions of ischemic or scarred myocardium, or in the ventricular cavities of the heart after tracer uptake. No proven scatter correction is currently accepted for clinical cardiac studies. Several empirical techniques have been developed for the brain which approximate the scatter distribution, and which can approach to within 5% of the true values (Bergstrom 1983, Lercher 1994). These are not applicable to cardiac imaging because of the irregular shape and density of tissues in the chest. One theoretical method computes the distribution with Monte Carlo techniques using assumed isotope and tissue distributions (Hiltz 1994). This is very time consuming, but is useful to validate correction techniques.

Random coincidences are relatively uniform throughout the FOV, and they represent an activity background above which the emission signal (trues) must be measured (Dahlbom 1987). Randoms correction is often performed by subtracting events recorded in a delayed coincidence window. This measurement itself has some statistical uncertainty, therefore the process of randoms correction decreases the SNR of the measured trues even more than the level implied by the formula for NEC shown in Equation 3.1.

Other physical factors such as detector dead time and isotope half-life are accurately modelled and corrected, such that a linear response of measured count rate

is obtained over a known range of isotope concentrations, e.g. 0.1 to 5 μCi/cc. These corrections have a simple scaling effect on the error variance.

Activity from different tissues are blurred together due to finite resolution and motion of the heart during the cardiac and respiratory cycles. The systematic variation due to this partial volume averaging is difficult to correct. If the locations of the boundaries of the myocardium (or the relative tissue compositions) are known independently, then corrections can be made to the images themselves. One approach is to measure the blood pool proportion within the myocardium using a separate scan (Iida 1988, Lammertsma 1992), and subtract this from the regional myocardial concentration. This is feasible with certain studies, but it is not an acceptable clinical approach due to time and tracer availability constraints. It is very difficult to determine myocardial concentration at the pixel level because the pixel volumes do not contain myocardial cells exclusively. The principles of compartmental modelling can be used to include a correction for partial volume averaging in the heart; these are presented in the next section.

If cardiac gated studies are performed in which there is little motion of the myocardium in a given time interval, then simpler recovery coefficient methods can be used if the thickness of the tissue is known, or if a constant thickness is assumed (Choi 1993, Krivokapich 1989). Recovery methods are typically used with sector analyses of the left ventricle, even in static imaging protocols. Correction for recovery does not account for blood pool spillover into the myocardium. A similar coefficient is often used to correct for this effect.

Current instrumentation does not support gated acquisitions in dynamic scan protocols. Gated acquisitions may find some utility in routine clinical studies, where static imaging protocols can be replaced with gated studies to improve the effective spatial resolution (Miller 1994). In the research environment, multiple short lived tracers are often used to obtain flow and metabolic information in the same study protocol. Because the time course of uptake of the tracer provides more important information than the tracer concentration throughout the cardiac cycle, gated studies are not often performed. The result is significant partial volume averaging throughout the

cardiac cycle. As a result of these factors, under typical imaging conditions the temporal and spatial resolution of PET is not sufficient to directly measure myocardial concentration.

During dynamic scanning, the timing of the individual frames also causes systematic variation. The isotope concentration measured in a certain time interval is often assumed to represent the true value at the interval midpoint, i.e. the concentration is assumed to change linearly over the measurement interval. However, the true midpoint values will either be higher or lower than the measured concentrations depending on whether the rate of change of the concentration is decreasing or increasing respectively. This can only be removed by modelling the shape of the uptake curve and making appropriate adjustments. This effect is typically not corrected, and therefore remains present in the error variance.

The processes described above all complicate the measurement of accurate volumetric concentrations of radioactivity. Correction for these effects is the first step towards quantitative myocardial imaging.

Left Ventricular Morphology

It is possible to estimate the concentration of activity in the *myocardial tissue* of the left ventricle by correcting for systematic variations in heart morphology. It is necessary to have a standard anatomical frame of reference in order to compare corresponding regions of the myocardium in different subjects, and to compare the results from positron tomography with the results from other diagnostic tests such as coronary angiography. There are several factors which distort the regional measurements in a systematic way: myocardial thickness, shape, and orientation of the left ventricle. These variations must be removed in order to estimate regional myocardial concentration. The random variation which remains depends on the precision of the correction procedures.

The human heart sits at an oblique angle in the chest with respect to the volume dataset of transaxial tomograms measured with PET. The anatomic orientation of the

heart is specified by the long axis, which passes through the apex and the geometric center of the base of the left ventricle. In the standard SPECT tomographic format, images which are perpendicular to the long axis of the myocardium are called short axis sections. They are oriented to approximate viewing from the cardiac apex towards the base of the LV. The shape of the normal myocardium in the short axis sections is nearly circular. If the orientation and extent of the long axis are estimated for a given individual then the measured volume can be rotated and translated, and displayed in the standard short and long axis sections (ACC/AHA/SNM 1992). A large source of anatomic variability is removed by resampling the myocardium into this standard orientation.

Many different methods are used to find the orientation of the long axis of the myocardium. Typically this is performed manually by an operator using an interactive computer program. The operator must define two or three angles of the long axis, as well as the center of mass, or the apex and base of the myocardium (Laubenbacher 1993, Hicks 1989, Miller 1988). The long axis can be found semi-automatically using a linear fitting method when the approximate extent of the myocardium is known, and when good contrast images are available (He 1991). No completely automatic method has been reported to find the long axis of the heart and reorient PET (or SPECT) datasets into the standard sections.

Many techniques exist to find rotation angles and translations to *match* volume datasets in medical imaging. Surface fitting is used for multimodal registration of brain images (Pelizzari 1989), but requires accurate segmentation of brain or skull surfaces. The volume principal axes transformation is also used to register different scans from the same subject (Alpert 1990). This model assumes that the object within the volume is a rigid body, and does not account for variation in size or shape between subjects. Surface fitting and principal axes techniques are sensitive to noise in the extracted contours and to local deformations of shape (Rusinek 1993). A geometric shape such as an ellipse can be fitted on cardiac scintigrams by using the Hough transform and searching for the maximum likelihood estimate (Blockland 1987). A relaxation labelling technique is used to detect endocardial surfaces; which are subsequently used

to register cardiac SPECT and MRI images (Faber 1991a). . Most of these methods require that the surface contours be extracted from the image before the fitting process is performed. This is often not possible with noisy transmission images, or with emission images containing local uptake defects.

Several authors report a technique which maximizes the correlation coefficient between two volume datasets to compute the required offsets and rotations (Junck 1990, Bettinardi 1993, Bacharach 1993). This appears to be a powerful and flexible method for volume matching which works well even with poor contrast images. A similar approach has been reported using differences or sign changes as the similarity function to be minimized (Hoh 1993).

Circumferential profiles (sectors) are typically used to perform functional assessment of the myocardium of the left ventricle. These sectors are regional averages computed under the assumption of uniform motion and thickness of myocardium throughout the LV. There is a normal variance in geometry of the left ventricle, but under diseased conditions there can be significant changes in regional wall motion and thickness. Sectoral processing removes these systematic variations of myocardial shape. It is also assumed that the distribution of tracer (or physiological process) is constant within the radial thickness of the myocardium. Although this has been shown not to be the case in general, the resolution of PET and cardiac motion leave no other alternative.

There are many methods used to determine the sectoral values such as searching for the maximum pixel values (Miller 1988, Laubenbacher 1993, Kotzerke 1990), or the top 2% of pixels to reduce sensitivity to statistical noise (Hicks 1989). Some investigators use sectoral averages with a recovery correction for partial volume averaging assuming a constant myocardial thickness (Choi 1993). A geometric model such as an ellipse has also been used with a local threshold to determine the locations of ROIs with known contributions of blood and myocardial tissue (Muzik 1993). Many of these methods also employ heuristic rules to reduce the effects of noise or poor uptake in defective heart tissues. The accuracy of these methods is dependent on the radiopharmaceutical being used, which in turn determines the SNR of the image

dataset. It is difficult to appreciate the errors which may result from these different methods, without verification of the analysis under different imaging conditions.

Sector processing enables the isotope distribution in the entire left ventricle to be visualized. The most popular format is called a polar plot where the sectors from each short axis section are plotted as concentric rings; starting with the apex in the middle of the image and proceeding to the base in the outermost ring. This enables patterns to be seen which may be difficult to detect when looking at serial sections. This is not an equal area representation of the myocardium, since the apex receives a relatively small area, whereas the base is over-represented. An equal area projection could easily be implemented from cartographic applications by using a simple geometric model of the heart such as an ellipsoid. Models of the heart have been used for the determination of left ventricular volume (Levy 1992). Model based and ellipsoid shapes are used for perspective displays of the myocardium to combine shape and function information (Faber 1995, Laubenbacher 1993). However in this format only one side of the heart can be seen at a given time, cinematic display of multiple views can facilitate interpretation (Miller 1988).

When these systematic morphological variations have been removed, estimates of the relative distribution of *myocardial isotope concentration* can be compared between subjects with different shaped hearts in different positions within the chest.

Tracer Delivery

If the regional measurements are divided by the injected dose, then the concentrations can be expressed on a relative scale in terms of the fraction of injected dose (Hicks 1989). However, even if the same dose of tracer is administered to two subjects, the myocardial uptake may vary due to a difference in the (blood) volume of distribution of the tracer between subjects. If this is taken into account (using height and weight information) then we may expect to find similar relative fractions of isotope in the myocardium of subjects under similar metabolic conditions. These semi-

quantitative methods have the advantage that numerical values can be compared between subjects.

It is possible to transform myocardial isotope concentration into a physiological measurement by normalizing for the delivery of tracer to the myocardium. Global changes in tracer uptake are affected by the injected dose, metabolic state of the subjects, volume of distribution of the tracer, radiochemical purity of the tracer, and accuracy of the measured blood concentration over time. If there is independent information available to normalize for global uptake, then comparison of absolute or quantitative measurements can be made. When this information is not available then only relative or qualitative comparisons can be made.

Statistical Models of Global Uptake

Statistical models can be used to remove confounding effects such as global uptake, and to separate treatment effects from measurement noise. These methods are used to analyse qualitative data only, since quantitative information of global flow values are removed explicitly. These models of treatment changes are typically either additive or multiplicative. Multiplicative models are used when the ratio or product of two values represents the fundamental measurement, e.g. relative local activity equals measured concentration at each pixel divided by global concentration. Additive models are used when the difference between values is the function of interest, e.g. difference between treatment means.

It is common to analyse cardiac PET studies by comparing the relative distribution of tracer in the left ventricle to a reference database of normal subjects (Hicks 1989, Laubenbacher 1993). Isotope concentration is measured with a static scan and expressed as a percentage of maximal (or normal) concentration. A simple z-test is used to quantify regions of the heart which are greater than N standard deviations from the mean (N=1,2...). The database incorporates population variations which may or may not be present in a given individual. This multiplicative model can be used to characterize coronary artery disease and to visualize regional deviations from

normal coronary blood flow (Laubenbacher 1993). It can also be used to visualize relative changes in isotope distribution, e.g. stress/rest. However, one can not interpret these changes when the scales of measurement (presumed normal values) are different.

There are other strategies which have been developed to detect changes in sample groups under different treatment conditions. Most have been developed for the examination of brain function with *activation studies*, as this has been a major focus of PET research in the field of psychology. Change distribution analysis was first proposed for PET studies of the brain by Fox et al (1988). Different subjects' scans are normalized for anatomical variation by fitting into a standard brain atlas. This allows scans from different subjects to be combined and compared. Then foci of image differences (of fixed size and shape) are localized and assessed for significance. In this case a proportional (multiplicative) dependence of local counts (y) on global counts (x) is implied because the ratio (r_i) of local/global activity (y_{ij}/x_j) is used to compute the magnitude of changes, i.e. $y_{ij} = r_i \cdot x_j + e_{ij}$ for region i in subject j. This model implies that all regions respond proportionally to global changes, which may be true for large regions of the brain (Friston 1990). Functional changes between treatment conditions is implicitly identified as a regional change in slope (r_i) of this proportional model. Several authors have cautioned against using regional values divided by whole brain mean values in statistical comparisons. It is not clear exactly what these differences really indicate in relation to the original measurements (Ford 1986, Moeller 1987).

A more flexible model was proposed by Friston (1990) for the analysis of brain blood flow activation studies with an integral scanning protocol. This allowed for an additive component (r0) of change as well as a proportional change (r1), i.e. $y_{ij} = r0_i + r1_i \cdot x_j + e_{ij}$. Using this model the confounding effect of global flow on the measured regional values can be removed using an analysis of covariance (ANCOVA). Only the regional changes are investigated, and it is assumed that changes in global flow are not of interest. Furthermore, if it can be shown that regional changes in concentration are independent of global flow (and additive), then functional changes are represented only by shifts in the regression lines of local to global flow. When this approach is

combined with block design experiments using subjects as their own controls, a powerful method of change detection is created which is sensitive to treatment changes as small as 10%. This technique is applicable only to images which have been shown to represent some physiological variable of interest such as blood flow or substrate metabolism. The method has since been applied in a single subject paradigm using repeated measurements under baseline and stimulus conditions (Silbersweig 1993). It is this recent report which prompted the current hypothesis that similar techniques may be applicable to cardiac PET studies as well.

It is desireable to incorporate control of a confounding variable such as global flow into a statistical model which enables reporting of changes in the original measured data units. However, it is preferable if these covariates can be removed from the measurements directly. This is often possible using kinetic models which can convert regional isotope concentrations into quantitative physiological units.

Physiological Models of Global Uptake

While relative measures provide some degree of normalization, absolute methods are preferred to compare data between subjects. There are differences in heart rate, heart motion, tracer administration, and circulation which can only be accounted for by measuring the concentration of radioactivity in arterial blood and in the myocardial tissue over time. Absolute measures of physiology are obtained through kinetic or graphical modelling techniques. The time course of radioactivity of the input function (arterial blood), and response function (myocardium) are used with physiological models, to compute quantitative rate constants. These constants represent the rates of flux of the isotope, moving between different anatomic or metabolic compartments.

Tracer kinetic modelling is accomplished by measuring the radioactivity concentration in the arterial blood over time $C_a(t)$, which is also called the arterial blood (input) curve. In cardiac studies this curve can be measured from sequential (dynamic) PET images in a region in the left ventricle. This is an ideal source for the

measurement of $C_a(t)$, as the blood has a very short transit to the coronary arteries and hence to the myocardial tissue (Weinberg 1988, Iida 1992).

In addition to the blood input curve, the output curve (time course of radioactivity in a myocardial region) $C_m(t)$ is also obtained from the dynamic PET data (Hutchins 1990). The tomographic measurement of the myocardium is considered as the sum of all radioactivity in one or more biological *compartments*. These compartments represent volumes in which the concentration of a tracer material is assumed to be homogeneous. The compartments may be physical (arterial blood, intercellular fluid) or biochemical (tracer compound, labelled metabolites) in nature.

A mathematical model is formulated which describes the flux of radioactivity between the compartments, and the output of the model y(t) is defined to equal the sum of activities in all of the compartments. The values of the model parameters which produce the best fit between the measured output $C_m(t)$ and the modelled output y(t) are determined.

For any tracer, the flux of radioactivity out of a given compartment is assumed to be proportional to the concentration of isotope in the compartment. The rate of change of radioactivity $\dot{C}_i(t)$ in a given compartment i equals the total flux into minus the flux out of the compartment. Therefore, the flux between n compartments can be described mathematically with a set of linear first-order differential equations as shown in Equation 3.2.

$$\dot{C}_i(t) = \Sigma\, k_{ij}C_j(t) - \Sigma\, k_{ji}C_i(t);\ i\neq j;\ i,j=[1,n] \qquad (3.2)$$

k_{ij} is the proportional rate of flux [min^{-1}] of radioactivity into compartment i from compartment j. Under the assumption of linearity, the impulse response of the complete system I(t) is equal to the sum of the responses of all compartments to an unit impulse input into a given compartment i. Therefore, if the set of differential equations is integrated with initial conditions of $C_i(0) = 1$ and $C_j(0) = 0$; $i\neq j$ (to obtain $C_i^*(t)$; i=[1,n]), then the impulse response of the system can be written as:

$$I(t) = \Sigma\, C_i^*(t);\ i=[1,n] \qquad (3.3)$$

In order to calculate the amount of activity in the compartments for *the real input function* we convolve the impulse response I(t) with the measured blood input curve $C_a(t)$ to get a predicted output curve:

$$y(t) = C_a(t) * I(t) \tag{3.4}$$

Once the model has been chosen, i.e. the number of compartments and parameters (rate constants), then the predicted output depends on the values of the rate constants (k_{ij}). This predicted output y(t) is fitted (in a least squares sense) to the measured output $C_m(t)$, by varying the values of the rate constants k_{ij} in the model. If the model has been properly chosen to represent the biological behaviour of the tracer, then the rate constants can often be directly related to physiological parameters such as MBF.

As described earlier, partial volume averaging is caused by finite image resolution and by the motion of the heart. In addition there is always a fraction of blood perfusing a given myocardial tissue region. As a result of these factors, it is impossible to measure myocardial isotope concentration directly. There are typically three different signal sources contributing to the total measured concentration in a myocardial region. There is the activity in the myocardium which is the tissue of interest. There are the tissues on either side of the myocardium; typically these are blood on the endocardial boundary, and lung or liver on the epicardial boundary. In the septum however, the myocardium of the LV borders on the cavity of the right ventricle.

It is possible to separate two of these signal sources using a blood pool region which is measured independently from the myocardium. If an endocardial image region contains only myocardium and blood then the radioactivity in the myocardial tissue can be estimated by including the blood pool fraction (F_a) in the kinetic model (Hutchins 1992, Muzik 1993). The model of regional isotope concentration in this case is modified from Equation 3.4:

$$y(t) = F_a \cdot C_a(t) + (1-F_a) \cdot \{C_a(t) * I(t)\} \tag{3.5}$$

The blood pool fraction F_a is included in the least squares fitting procedure, and is estimated in addition to the rate constants.

A two compartment model for the uptake and metabolism of ^{13}N-labelled ammonia (Figure 2.1B) can be used with Equation 3.5 to obtain direct estimates of myocardial blood flow at rest (Hutchins 1990). The first compartment represents ammonia which has diffused into the extravascular (intercellular) space, and the second represents (retained) ammonia which has been incorporated into glutamine. In this model K_{10} represents the product of delivery and extraction of ^{13}N ammonia in [ml/min/g]. It is known that MBF can be slightly underestimated using this model because the single-pass extraction of ammonia decreases nonlinearly with increasing flow. Values of coronary reserve obtained with this method, agree closely with values assessed by invasive methods.

A single-pass model can be used to estimate *net extraction* (retention) directly from a short dynamic series of myocardial images as in Equation 3.6 (Neinaber 1991, Bellina 1990). Retention (R) equals the measured myocardial concentration at time t divided by the integral of the blood curve to that time.

$$R = C_m(t) \,/\, \int_0^t C_a(T)dT \qquad (3.6)$$

It is assumed that there is complete retention of the tracer in the myocardium over time, and no recirculation in the blood.

A graphical approach can also be taken if there is an irreversible compartment at the end of the metabolic chain (Gambhir 1989, Choi 1993). After steady-state conditions are achieved, the slope on a plot of normalized counts versus normalized time (Equation 3.7) is an estimate of retention in myocardial regions imaged with ^{13}N-labelled ammonia.

$$\frac{C_m(t)}{C_a(T)} = R \cdot \frac{\int_0^t C_a(T)dT}{C_a(T)} \qquad (3.7)$$

Functional Physiology

The quantitative and semi-quantitative measurements described in the previous sections are often presented as a distribution within the myocardium of the left ventricle. There are always different metabolic variations between subjects which affect

the uptake and distribution of the tracer. These metabolic variations may be associated with certain disease processes which occur in distinct areas of the ventricle. In this case, treatment effects can not be detected by comparing results over the whole heart. It is necessary to treat these areas as distinct groups. In this context the manner of investigating changes, no longer using anatomical locations but functional locations. Segmentation of the data is necessary to select myocardial regions from different subjects and group them together in terms of function (or disease state). Treatment changes in specific tissue types can then be evaluated, instead of simple regional changes.

Regional myocardial tissue states can be distinguished using relative indices of health or disease. For example, differences and ratios are often used in rest/stress perfusion studies to determine regions of normal or reduced coronary reserve (Laubenbacher 1993). When subjects with myocardial infarction are being studied, the regions of interest are often only the areas with low perfusion. Relative indices are used to locate regions of ischemia in FDG/flow studies, since these areas have reduced MBF but normal or increased glucose utilization. The relative indices are usually measured as a percent of diseased myocardium to normal myocardium and referred to as normalized values. Tillisch et al (1986) and Schwaiger et al (1986) defined ischemic myocardium to be a *difference* between normalized FDG and flow values, which was greater than 2 SD above the mean from a normal database (Marshall 1983). Bonow et al (1991) quantified FDG uptake relative to MBF on a five point scale, and defined ischemic myocardium as regions which have normal or increased FDG uptake and reduced blood flow. The value for normal FDG uptake in a given subject is defined from the corresponding region of maximal (normal) flow. Ratios of FDG/flow are also used to directly visualize ischemic regions of myocardium.

Treatment Changes

Objective and reproducible analysis is required to detect treatment changes in sample groups under different experimental conditions, or in single subjects over time.

There have been many reports of qualitative and quantitative measurements of physiological processes with PET, but relatively few attempts to assess the significance of treatment changes. For example, it is clinically important to determine changes in blood flow with surgical or pharmacologic treatment, exercise, disease progression etc. Changing patterns of myocardial blood flow during daily life profoundly affect clinical prognoses. Coronary reserve is measured with PET (Hutchins 1990), but not the significance of the flow differences between rest and stress. The effects of cholesterol lowering on regional blood flow has recently been reported using a semi-quantitative statistical analysis (Gould 1994). Relative values of stress/rest flows are compared to a normal database and the extent and severity of abnormal flow is quantified. Similar techniques are used to compare early to late ^{82}Rb scans, to monitor disease progression and to compare metabolic to flow data in the evaluation of viability (Hicks 1989). Normal MBF was compared to flow distal to stenoses, before and after coronary angioplasty in a group of 13 patients (Walsh 1990). Quantitative estimates of flow reserve were obtained with dipyridamole stress, and were found to increase significantly in low flow regions after revascularization. Qualitative changes in FDG uptake relative to ammonia have been evaluated in response to coronary artery bypass surgery (Tamaki 1989). Before surgery, relative FDG excess was found to predict improvement in perfusion and wall motion. Coronary reserve has been compared in patients with syndrome X (Camici 1991a), and hypertrophic cardiomyopathy (Camici 1991b). Comparisons have also been performed on patients who received cardiac transplants (Krivokapich 1991). The potential for future research in this area is almost unlimited. As new treatment procedures evolve, their efficacy to improve myocardial blood flow or function can be evaluated with PET. Automated analysis will facilitate objective and reliable detection of physiological changes in the heart.

CHAPTER 4
Automated Detection of Treatment Effects

As discussed in Chapter 3, precise measurements are essential in order to detect small changes with statistical significance. The random and systematic effects which influence the precision of positron tomographic measurements of cardiac physiology have been presented. It is evident that accurate and precise measurements can be made to within a few percent of the true values, therefore small changes in physiology resulting from the treatment of ischemic heart disease should be detectable with positron tomography. Automated methods of analysis can remove operator bias and variability, and thus reduce the error variance of the measurements and increase statistical sensitivity.

A completely automated, three dimensional analysis technique is developed in this chapter, which removes the major sources of systematic variation that occur in cardiac PET studies. These include left ventricular orientation, extent and shape. The method produces objective estimates of the regional isotope concentration in the left ventricle, and in the arterial blood. These two measurements form the basis of most qualitative and quantitative analysis of cardiac PET images. Normalization for tracer delivery and global myocardial uptake is then performed objectively, to produce relative or absolute measures of cardiac physiology. Treatment changes between samples of subjects are evaluated in functional tissue beds. Single subject changes are assessed in distinct regions over the entire left ventricular myocardium. Appropriate quality assurance outputs are generated at each stage of analysis, to verify underlying assumptions.

4.1 Reorientation

Registration with an Ellipsoid Model

A method is developed to estimated the orientation and extent of the LV long axis directly from the measured PET image volume. The orientation of the ventricle is defined by the long axis as described in Chapter 3. The extent of the LV is defined by the distance from the apex to the base, along the long axis. In terms of the transaxial images acquired by the positron tomograph, the long axis is defined by two rotation angles, and a three-dimensional coordinate origin. The myocardium of the left ventricle is approximately semi-ellipsoid in shape, therefore the reorientation parameters can be defined by the major axis of a truncated ellipsoid, whose shape is fitted to the measured activity in the LV myocardium. Objective and reproducible results are obtained because the technique is completely automatic, thereby removing any operator variability or bias.

The axial distribution p(z) of isotope in the myocardium is estimated from the total activity on the cardiac side of the transaxial image volume m(x,y,z), using Equation 4.1. The variables x and y are the pixel coordinates for a given transaxial image z. This distribution (Figure 4.1A) is thresholded at 60% of the maximum value to remove background activity superior or inferior to the left ventricle. The thresholded distribution ($p_T(z)$) is given by Equation 4.2, and is shown in Figure 4.1A as the portion of curve above the dotted line. The integer mean of $p_T(z)$ is used as the transaxial image number (az) to select from the measured volume (Equation 4.3). In Figure 4.1A, the vertical dashed line shows that transaxial image number 19 is selected out of 31 measured planes.

$$p(z) = \sum_{X}\sum_{Y} m(x,y,z) \tag{4.1}$$

$$p_T(z) = \begin{cases} p(z) & \text{if } p(z) > 0.6 \cdot \max(p(z)) \\ 0 & \text{otherwise} \end{cases} \tag{4.2}$$

$$az = \{\sum_{z} p_T(z) \cdot z\} \; / \sum_{z} p_T(z) \qquad (4.3)$$

Although a three-dimensional ellipsoid model is implied, a transaxial section at the mid-ventricular level (az) invariably has an approximately elliptical shape (Figure 4.1B). A complete ellipse is used to model the orientation and extent of the myocardium in this plane. This transaxial section is smoothed with a 12 mm FWHM gaussian filter to reduce any gross distortion of shape. The starting center coordinate (ax,ay) is estimated as the weighted average of all image pixels on the cardiac side of the image (Equation 4.4). This is done to avoid contribution from activity which may have accumulated in the left lung or liver.

$$ax = \{\sum_{X}\sum_{Y} m(x,y,az) \cdot x\} \; / \; p(az)$$
$$ay = \{\sum_{X}\sum_{Y} m(x,y,az) \cdot y\} \; / \; p(az) \qquad (4.4)$$

Initially the major and minor axis lengths of the ellipse ($2 \cdot a$, $2 \cdot b$) are set to 80 mm and 50 mm, and the starting axial angle (θ) to 55 degrees. Fifty equally spaced points on the ellipse are computed, and pixels spanning a width of 6 mm are set to a constant value to model the myocardium (Figure 4.1C). Next the correlation coefficient (Equation 4.5) between the model image (i) and the measured transaxial image (j) is maximized (MATLAB 1992) by sequentially optimizing the five ellipse parameters: ax,ay,a,b,θ in the given order. This optimization is iterated until the parameters converge or a maximum of six iterations is reached. The values of these parameters typically converge within three iterations.

$$r_{ij} = \frac{\sigma^2_{ij}}{\sqrt{\sigma^2_{ii} \cdot \sigma^2_{ij}}} \qquad (4.5)$$

A long axis section is then taken normal to the transaxial plane, and along the major axis of the fitted ellipse (Figure 4.1D). This image is smoothed with a 6 mm or 12 mm FWHM gaussian filter to remove distortions in shape as on the transaxial section, and to increase the SNR in studies with poor uptake. The shape of the

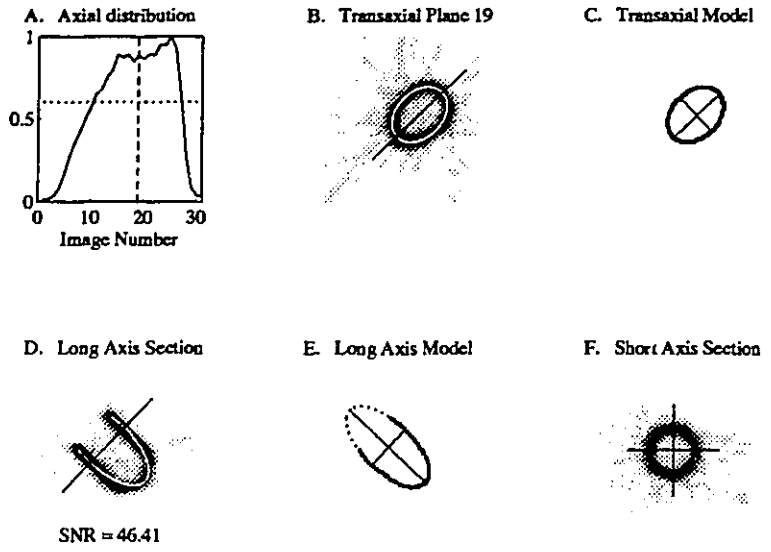

Figure 4.1. Reorientation of cardiac phantom. (A) Axial count distribution p(z). (B) Selected transaxial plane (az). (C) Fitted transaxial model. (D) Long axis section through B. (E) 2/3 ellipse long axis model. (F) Short axis section through D.

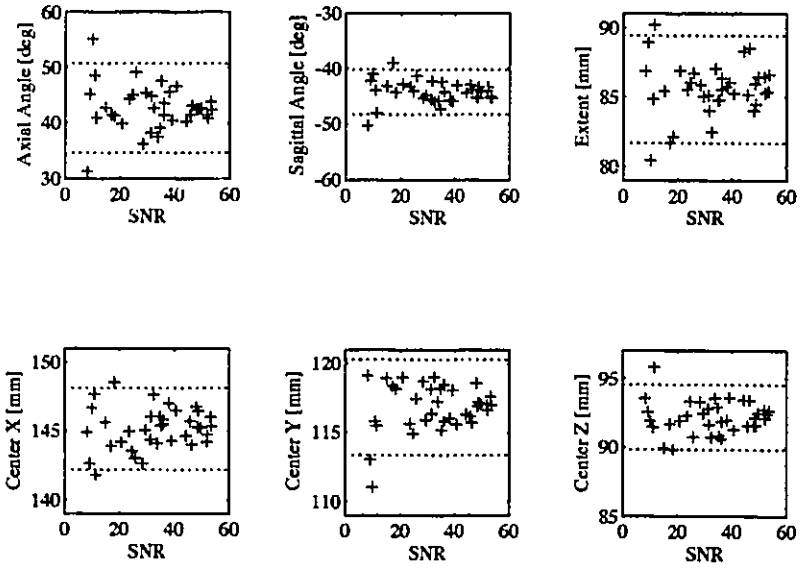

Figure 4.2. Precision of the cardiac phantom reorientation parameters. Dotted lines are shown at the mean ± 2 standard deviations.

myocardium in this image is modelled with 2/3 of an ellipse as shown in Figure 4.1E. In this case the major axis length is increased to 120 mm, which keeps the total length of the modelled myocardium at 80 mm. The starting angle (ϕ) is -25 degrees, and the starting center coordinates (lx,ly) are computed using a weighted average as in Equation 4.4. The correlation coefficient is maximized as before with one modification; the major axis of the ellipse is optimized after the last iteration to obtain the best estimate of the total extent ($4/3 \cdot a$) of the left ventricle. A short axis section taken along the minor axis of this ellipse (Figure 4.1F) shows a circular section of the myocardium in the center of the image.

Once these parameters have been found, the orientation of the long axis of the myocardium is known. The angles (θ,ϕ) are known directly, and the pixel coordinate of the center of the modelled ellipse (cx,cy,cz) can be calculated from ax,ay,lx,ly using simple trigonometry.

The signal-to-noise ratio (SNR) is used to assess image quality of the long axis section, and is related to the precision of the estimated parameters. The SNR is defined in Equation 4.6 as the mean (μ_S) divided by standard deviation (σ_S) of all pixels within the extent of the modelled ellipse on the long axis image (Figure 4.1D). It is normalized to the ratio of the myocardial mean (μ_S) divided by the ventricular blood pool mean (μ_N), to account for varying blood to myocardium contrast.

$$SNR = \mu_S/\sigma_S \cdot \mu_S/\mu_N \tag{4.6}$$

Accuracy and Precision

The only parameters needed to generate a complete short axis series are the center of the modelled ellipsoid (cx,cy,cz), the two orientation angles (θ,ϕ), and the total extent of the left ventricle. The precision and accuracy of these parameters have been evaluated using a series of 36 cardiac phantom scans (Appendix A.2). The acquisition times of these scans were varied from 10 s to 10 min in order to obtain a wide range of image SNRs. The true values of the reorientation parameters were

compared to the means of the estimated parameter values in Table 4.1. None of the true values differed significantly ($Z>1.65$, $p2<0.1$) from the estimated distribution. The true values were all within one standard deviation of the estimated means (except for the extent), which shows that the technique is accurate. The extent had a slightly higher Z-value because the ellipse is fitted to the midline of the myocardium not to the outer edge, resulting in a slight underestimation.

Table 4.1

Accuracy of Cardiac Phantom Reorientation
N=36

Parameter	True Value	Estimated Value	Z-value
Axial Angle [deg]	43.0	42.6 ± 4.03	0.10
Sagittal Angle [deg]	-44.5	-44.3 ± 2.03	0.10
Extent [mm]	80.0	77.4 ± 1.75	1.49
Apex X [mm]	193.4	91.8 ± 2.40	0.67
Apex Y [mm]	157.0	160.0 ± 3.12	0.96
Apex Z [mm]	30.0	29.6 ± 2.42	0.17

Estimated Values are means ± standard deviations

The fitted ellipses from a typical scan of the cardiac phantom are shown in Figure 4.1. Although the cylindrical phantom does not model the correct shape of the left ventricle, the ellipses are nearly perfectly superimposed on top of the transaxial and long axis sections in Figures 4.1B and 4.1D. The short axis sections are well centered as in Figure 4.1F, indicating that the axial and sagittal angles were accurately determined.

The variation of the parameters with SNR, determined from the 36 phantom studies is shown in Figure 4.2. The dotted lines are shown at the means ± two standard deviations. The variance of the axial angle estimate is higher than the sagittal angle, and both the axial and sagittal angles show increased variance when the SNR is relatively low. Similarly, the precision of the other parameters shows a slight

dependence on SNR. The graphs indicate that a SNR below 10 may be used as a quality control threshold below which the results should be verified visually by carefully examining the fitted ellipses, as well as subsequent quality assurance outputs.

The axial and sagittal angles for the phantom data are determined on average to within 4 and 2 degrees of the true values respectively. The center coordinates of the ellipsoid (cx,cy,cz) are estimated to within 2 mm. The extent estimate has a standard deviation of 1.75 mm. This corresponds to less than one half of the short axis slice thickness when 20 images are produced within the extent of the modelled myocardium.

Human Studies

The precision of the method for human data was determined using dynamic scans of FDG uptake in 6 patients with known coronary artery disease. In each patient, 6 sequential 5 min scans were reoriented using the automated method, and the means and standard deviations were computed. The fitted ellipses for the last scan of each of the 6 patients are shown in Figure 4.3. These are the highest SNR images of each patient, because contrast generally increases throughout the study. These 5 min FDG images are noisier than the 30 min images acquired in practice, and represent the lower range of image quality typically obtained with diseased hearts, where uptake is often impaired. In all cases suitable results were observed, even in the presence of marked defects and low SNR.

Table 4.2 shows the means and standard deviations of the estimated parameters for all scans in the six human studies. Phantom data from Table 4.1 is included for comparison. The SNRs observed in these patients are lower than those of the phantom studies; in general the patient SNRs are comparable to the 10 s scans of the cardiac phantom. The precision of the estimated parameters does not appear to vary systematically with SNR in the range encountered. The average axial and sagittal standard deviations are 3.3 and 1.5 degrees respectively, compared to 4 and 2 degrees for the phantom studies. The standard deviation of the center coordinate is typically

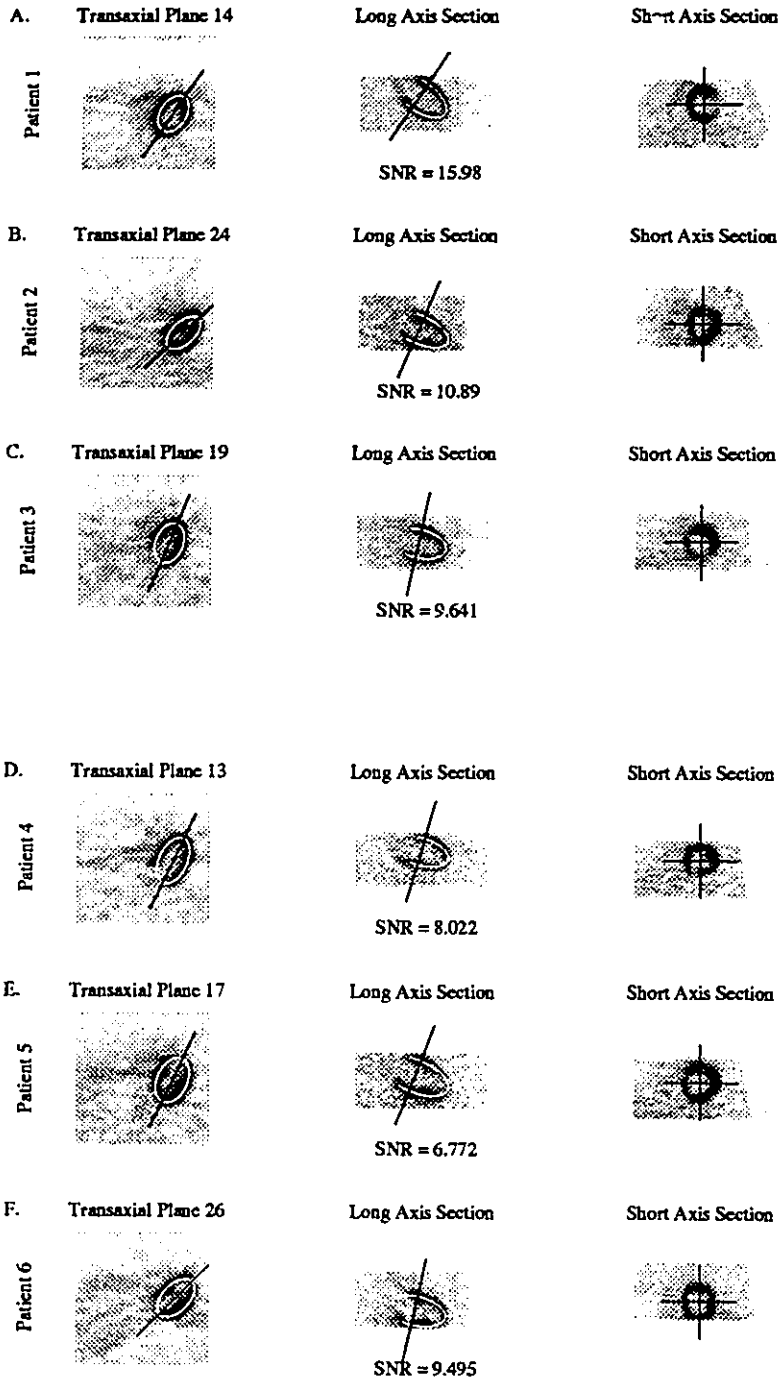

Figure 4.3. Reorientation of the last 5 min frame for each of the six patients analysed. SNR is estimated on the long axis sections.

below 2 mm, and the extent below 4 mm. The variance of the extent estimate is higher than in the phantom study because of the variation in shape at the base of the heart, i.e. there is rarely a straight and abrupt edge, as in the cardiac phantom.

Table 4.2

Precision of Automated Reorientation
N=6

Patient	SNR	Axial [degrees]	Sagittal [degrees]	Extent [mm]	CX [mm]	CY [mm]	CZ [mm]
1	13.7±1.7	54.7±1.7	-34.6±0.9	78.6±2.4	166.8±0.8	96.8±1.4	67.9±0.9
2	9.8±2.8	45.6±3.4	-22.4±2.6	82.7±2.8	185.6±1.7	96.8±0.9	43.2±1.7
3	9.1±1.4	70.5±3.7	-13.3±1.7	75.8±3.5	170.4±1.3	110.0±2.6	51.0±3.1
4	7.2±0.8	62.9±2.2	-15.5±1.3	73.2±1.8	181.7±1.1	119.3±1.3	70.1±1.1
5	7.0±1.5	61.1±7.0	-22.3±1.0	87.2±4.3	176.4±2.0	114.9±1.6	64.0±1.2
6	8.1±0.8	43.5±1.9	-14.8±1.7	80.8±2.6	181.1±1.1	119.5±1.6	38.5±2.2
Average	9.2±1.5	56.4±3.3	-20.5±1.5	79.7±2.9	* ±1.3	* ±1.6	* ±1.7
Phantom	32.8±14.1	42.6±4.0	-44.3±2.0	77.4±1.8	145.2±1.5	116.8±1.7	92.2±1.2

Values are means ± standard deviations.
*Average centre coordinate of the heart is not of interest.

Three-Dimensional Resectioning

A series of short axis sections are computed using trilinear interpolation from the original volume dataset as in Figure 4.1F. The resolution of the positron tomograph at McMaster University is isotropic at approximately 6 mm FWHM (Appendix A.1), and the raw image data is reconstructed on a 3 mm grid, which corresponds to sampling at roughly twice the Nyquist frequency. Therefore, no resolution mismatch artifacts are observed on any oblique short axis sections through the measured volume.

Twenty-two images are generated to span the estimated extent of the myocardium, and two images are appended at the apex for quality assurance, and at the base for potential definition of blood pool regions in the left atrium. The typical spacing of these sections is 4 mm, but varies according to the measured extent of the left ventricle. These images are subsequently used to compute regional myocardial activity and arterial blood curves. The short axis sections can also be rotated to normalize the orientation of the right ventricle. This is not done routinely since the variability is small, and the right ventricle is not always visible. A standard number of sections are used for all subjects. This enables studies to be compared image by image, since the volume has been normalized for long axis orientation and extent. Some variability in shape and normal regional uptake remains, and is not accounted for with this model. Variation in shape is easily removed when computing circumferential profiles of average myocardial uptake, as presented in the next section.

The resectioned short axis series from the last 5 min scan of patient 5 is shown in Figure 4.4. The first two images in the short axis series contain no data. The apex spans slices 3 to 7 and has generally decreased image intensity, consistent with the apical defect shown in Figure 4.3E. The apical images are typically well centered (as in this example) because the model is explicitly fitted through the apex, as seen on the sagittal images in Figure 4.3. This is an important result if polar plots are generated to include the cardiac apex. The body of the heart spans images 8 to 24. The last two images typically contain little or no left ventricular myocardium, as in this case. Any inaccuracy in the angles or the center coordinate typically causes the sections through the base of the heart to drift off-center. In this particular case, the fit is excellent and even the basal images are well centered. Any inaccuracy in the extent estimate, typically results from a failure to exactly define the basal plane.

The effect of inaccurate LV orientation parameters was evaluated using the images from the last frame of patient 1. This scan was resectioned with parameters calculated from the first and the fourth 5 min scans. The angles differed by 2.7 degrees axially and 2.3 degrees sagittally, while the center coordinates differed by 0.5 to 2.0 mm which represents the typical variation as shown in Table 4.2. Even with

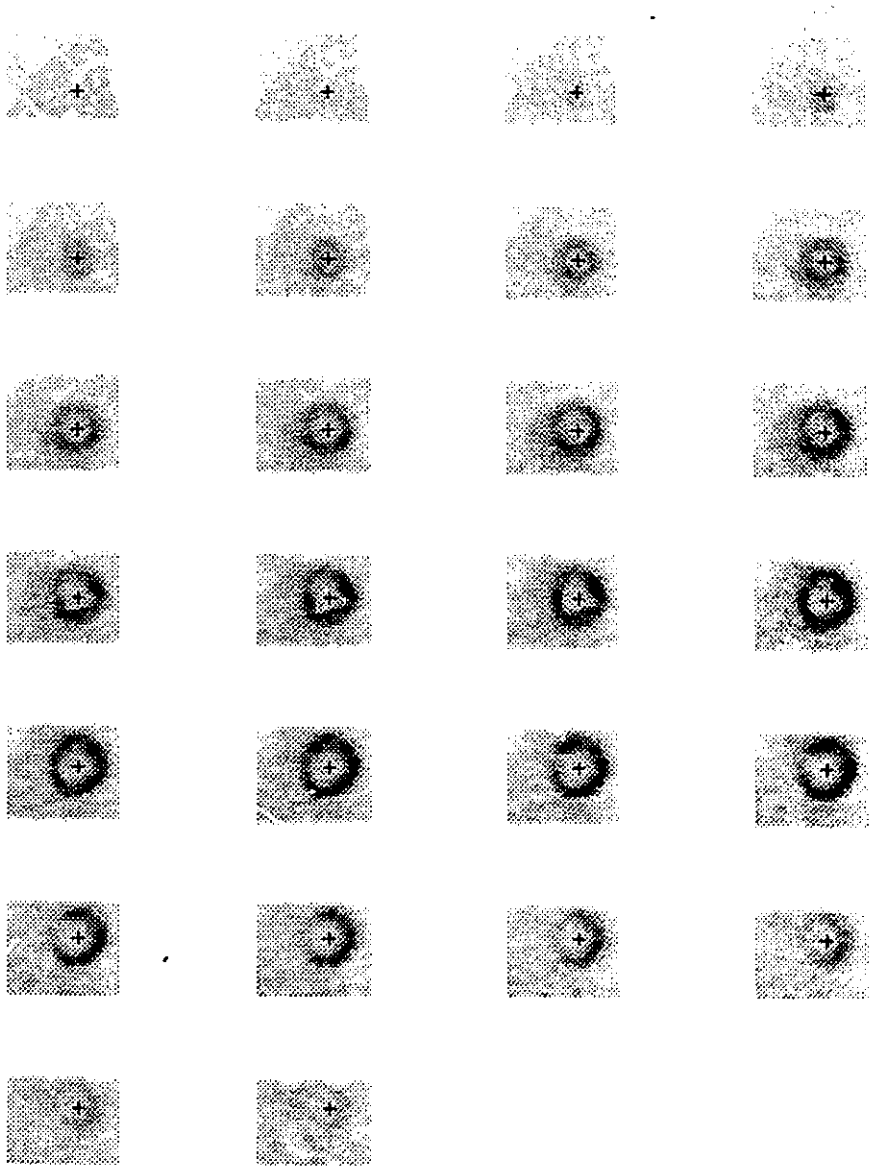

Figure 4.4. Resectioned short axis images from patient 5 who has an apical defect. All images are centred about the '+' indicating that the long axis was correctly oriented. The central 22 images span the estimated extent of the left ventricle.

these changes in the axial and sagittal angles, the results are visually indistinguishable. This demonstrates the level of precision necessary in order to achieve suitable results in the short axis sections.

4.2 Regional Analysis

Circumferential Profiles

The short axis sections are smoothed with a 5-6 mm Gaussian filter in three dimensions. This increases the SNR in studies with poor statistics. The width of this smoothing filter is smaller than the scanner resolution (Appendix A.1) and therefore does not markedly affect image resolution. *Bottlebrush sampling* of the cardiac apex is used (Laubenbacher 1993) to create 5 apex images corresponding to 20 degree wedges through the myocardium (Figure 4.5). On the 7 apical short axis sections, the wedges correspond to circular annuli of varying radius. To form the 5 apex images, the maximum pixel values are chosen across the overlapping annuli. This technique was chosen to match the *radial maximum* process used to estimate myocardial activity on the short axis sections. The 5 apex images are processed similarly to the remaining sections of the cardiac body.

All sections are resampled into polar coordinates using nearest neighbour rebinning. Pixel indices (v) of the short axis sections (S) are precomputed for all elements of the polar coordinate images (P), such that the transformation is performed with a single matrix lookup (Friston 1991a) as shown in Equation 4.7.

$$\mathbf{P} = \mathbf{S}(\mathbf{v}) \tag{4.7}$$

This transformation is very efficient and presents the sections in a format which is ideally suited to create circumferential profiles. Because the short axis sections ideally have centred myocardium, the polar coordinate images show the maximum intensity at an approximately constant radius for all angles as shown in Figure 4.6A. The radial pixel dimension is 2 mm and the angular dimension is 5 degrees in the polar images. These dimensions were chosen to create polar images with an identity pixel mapping

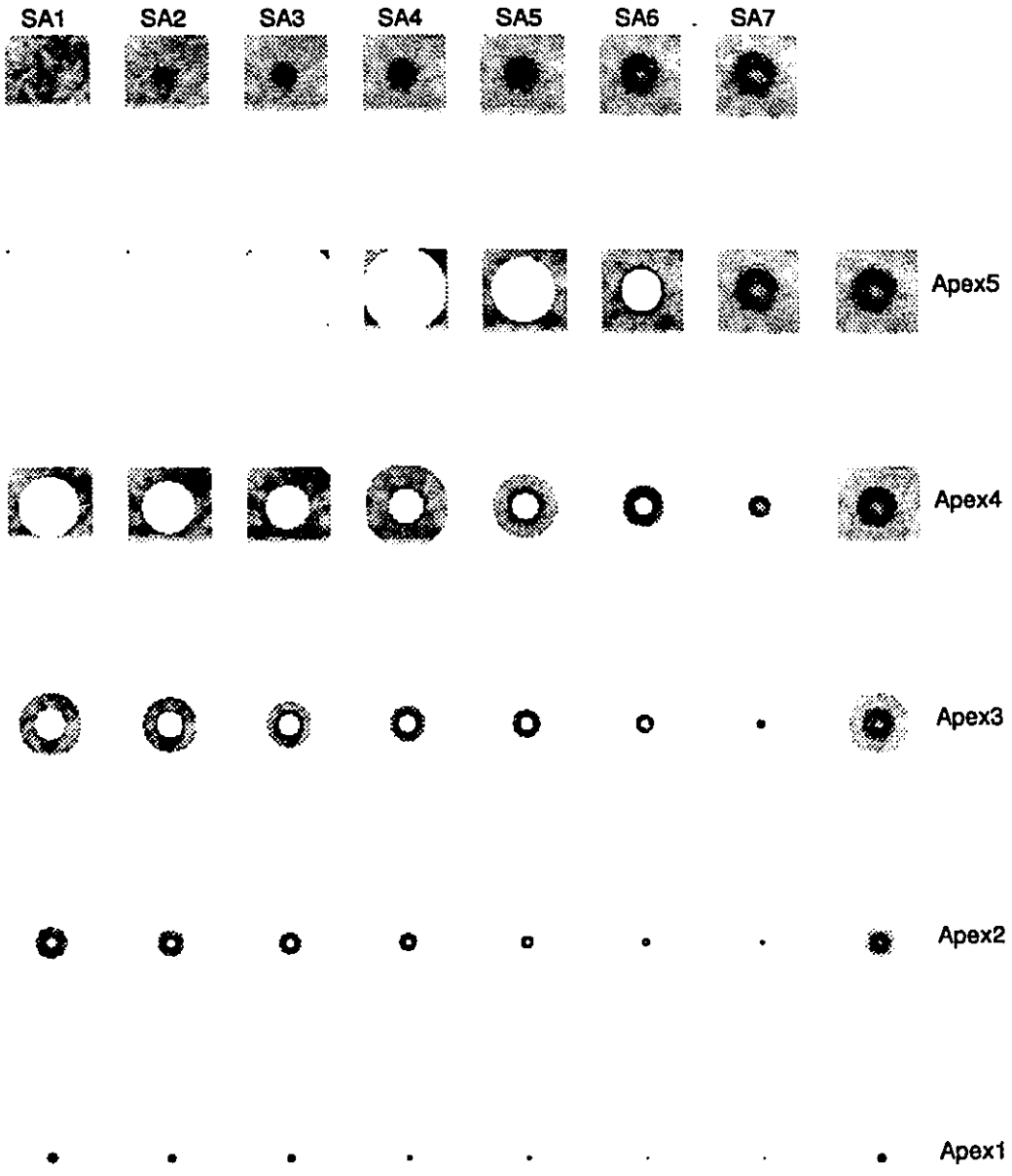

Figure 4.5. Bottlebrush sampling of the cardiac apex. Short axis sections (SA1-SA7) are divided into annuli corresponding to 20 degree wedges, and recombined to form apex images (Apex1-Apex5).

between the two formats at the expected myocardial radius of 3 cm. Regions closer than 3 cm from the centre are oversampled, while regions further than 3 cm are undersampled using this pixel mapping. A complete set of circumferential profiles consists of 36 sectors from each of 15 short axis images in the heart body, plus sectors from the 5 apex images, producing a total of 640 independently measured myocardial sectors.

On each polar coordinate image, an average radial profile is computed across all angles, excluding the posterior 90 degrees where activity in the liver may be present. The maximum point in this profile an estimate of the mean distance of the myocardium from the center of the left ventricle. A 1.5 cm range of radii surrounding the mean is searched for the maximum local average, as shown by the vertical black lines in Figure 4.6A. Average myocardial concentration is defined as the mean of 10 degree sectors across three radial pixels (6 mm). Regions are not explicitly corrected for blood pool spillover or partial volume averaging. This technique allows for some variation from the ideally circular shape of the myocardium on the short axis sections, and also compensates for slightly off-centered sections which can result from inaccurate reorientation. The mean radius, the range of radii searched, and the final radii obtained (white line), are shown on a typical polar coordinate image in Figure 4.6A, and on the original short axis section in Figure 4.6B.

The sector radii must be determined separately for scans performed with different subject positions, e.g. during separate study protocols. Radii can be estimated for each scan in a given protocol, to account for subject motion. The accuracy and precision of such estimates has not been evaluated, but is likely limited to 2 mm shifts and 2 degree rotations based on the phantom experiment results. If motion above this amount is not present (or suspected), then it is valid to apply reorientation parameters and sector radii from a high contrast FDG study (for example) to previous or subsequent noisier flow studies. In the analysis of dynamic studies, sequential frames can be averaged to obtain the best possible image of the myocardium, and then used to define the sector radii. These radii can then be used for all frames to compute regional myocardial uptake over time, assuming no subject motion occurred.

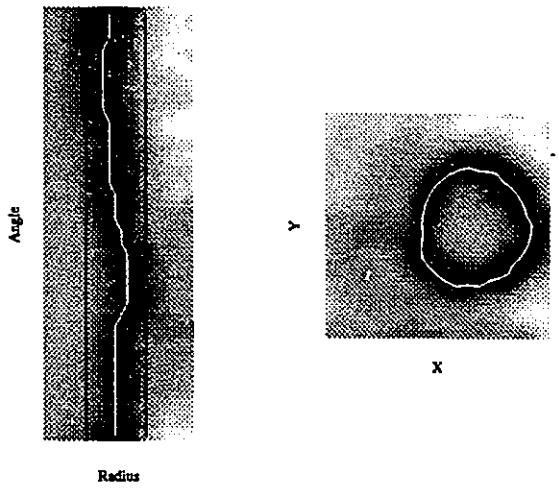

Figure 4.6. Myocardial radius estimation. (A) Polar coordinate image of a short axis section, with search limits and estimated sector radii. (B) Estimated centre of the myocardium on the original short axis section.

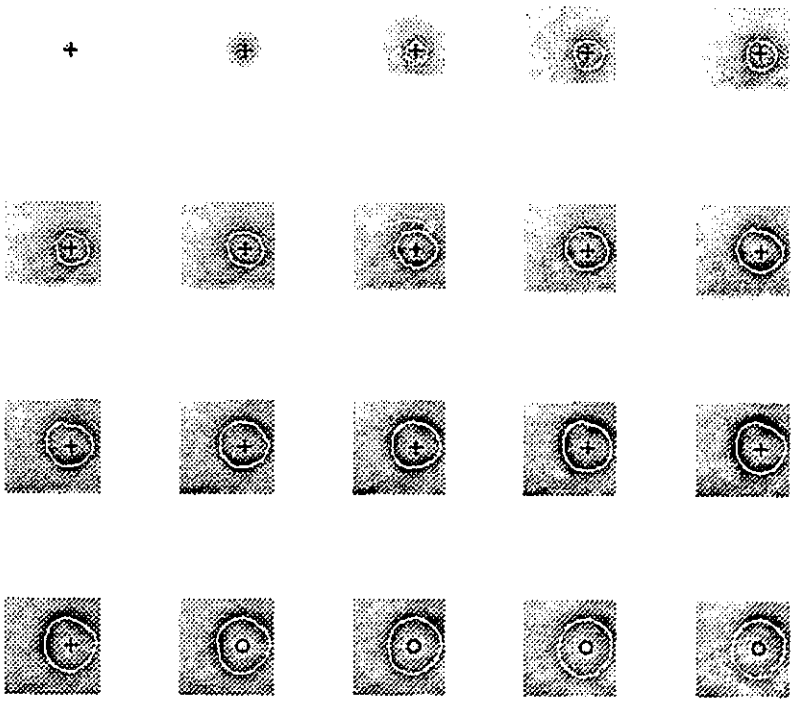

Figure 4.7. Quality assurance apex and short axis images with superimposed myocardial radii. Twenty images are used to represent the left ventricle. The long axis (+) and blood pool (o) positions are shown.

Quality Assurance of the Circumferential Profiles

In low count regions the myocardial radii can be very disjoint, and may correspond to activity in other organs such as the liver. Spurious noise in the estimated radii is removed using median filters. The radii of each section (excluding the most apical 3) are smoothed with a median filter with an angular extent of 90 degrees. The radii are also smoothed with a 5 point (2 cm) median filter along the long axis. An explicit continuity constraint is also applied to the 5 most basal images to prevent masking of inferior defects by the liver in particular: the radii on these basal images are only permitted to vary by one pixel (2 mm) between sections (4 mm spacing). This technique has been found to give smooth and accurate estimates of the position of the centre of the myocardium on typical series of 20 apex and short axis sections.

The four most basal images are typically not analysed because of excessive positional variability. In extremely noisy images, median filtering can produce a step artifact in the radius estimates, however in such cases the low SNR typically precludes any useful interpretation. The basal anterior wall, or the inferior wall and apex of the LV can be missing from the sampled image volume if the heart is mispositioned in the scanner. On the corresponding short axis images, the result is missing myocardium on the top or bottom edges, which prevents estimation of the corresponding sector averages. Missing sectors are explicitly identified, and removed from subsequent analysis. They are apparent as step discontinuities in the expected circular shape of the polar plots, e.g. Figure 5.1C

Short axis and apex images are shown in Figure 4.7 from a ^{13}N-labelled ammonia study of a subject with a basal posterolateral defect and some activity in the liver. This quality assurance (QA) output is used as a guide to interpret or verify the distribution of myocardial uptake, presented as polar plots or three dimensional (3D) views. The radii of the center of the myocardium are used to define a 3D surface on which the distribution of activity is superimposed. The regional distribution of blood flow from a patient with a large anterior and apical defect is shown in polar map form,

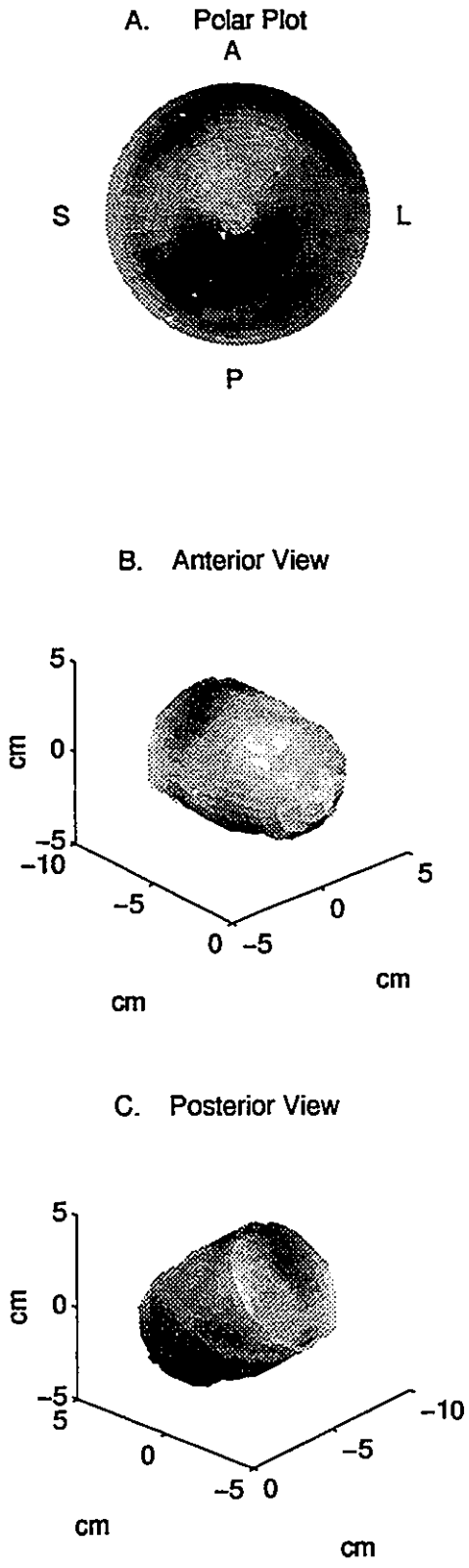

Figure 4.8. Three dimensional views of relative ammonia uptake in the left ventricle. (A) Polar plot. (B) Anterior and (C) Posterior views of relative uptake superimposed on the estimated myocardial radii of the left ventricle.

as well as anterior and posterior 3D displays in Figure 4.8. The 3D displays show the distribution of flow superimposed on the true measured shape of the LV. In the polar plot format, it is evident that the display area corresponding to the apex is severely under-represented compared to the anterior 3D view.

Arterial Blood Regions

Normalization for the delivery of tracer to the myocardium typically requires knowledge of the time course of activity in arterial blood. This blood curve is estimated automatically using regions in the left ventricle, or left atrium. Regions from the 4 basal sections are used to measure the blood input function. The regions are each 1.4 cm square, and centered within the left ventricle. The central coordinate is computed as the centroid of the points (radii) defining the center of the myocardium as shown in Figure 4.7. Alternately, the same regions can be used on 4 atrial sections outside the left ventricle, to determine which curve gives a better measure of the true input function.

A Typical LV blood curve from a dynamic ammonia scan is shown in Figure 4.9. Although well placed blood regions in the LA may have less spillover from myocardial tissue, this cavity is smaller than the LV and is therefore more prone to mispositioning errors. Because imprecision in the reorientation procedure is usually manifested as off-centre drift of the basal sections, the LV blood pool is preferred over the LA to avoid contamination by the adjacent myocardium.

4.3 Functional Analysis

Ischemic Myocardium

The detection of treatment effects can be performed using one of two spatial models: functional or volumetric. In experimental designs with multiple subjects the analysis of change is necessarily functional. Subjects have disease processes which

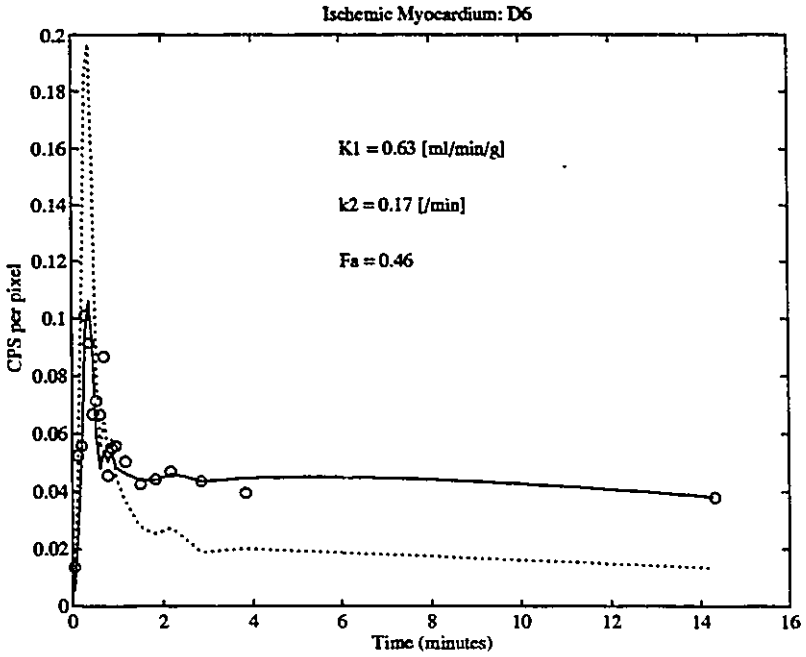

Figure 4.9. Labelled ammonia time-activity curves of LV blood (dashed), ischemic myocardium region (circles), and compartmental model fit (solid).

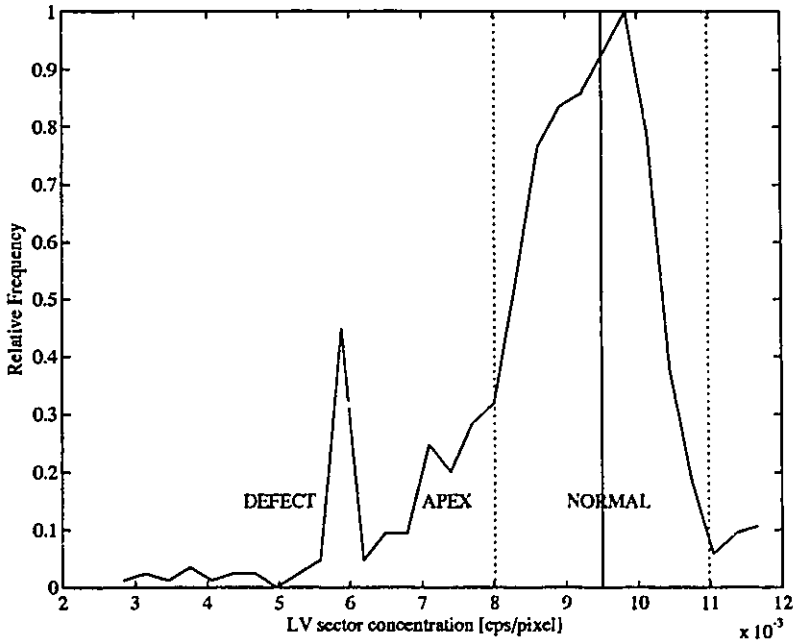

Figure 4.10. Relative distribution of polar map values. The median ± 2 SD defines the normal range. Low values are in the apex and defect regions.

vary in anatomic location and severity, therefore the myocardium must be segmented into functional subgroups such as ischemic tissue regions.

The sector data from a given scan is segmented into two classes: normal and low values. It is assumed that the median value of the distribution of activity in the LV myocardium (excluding the apex and base) is 'normal'. The median is less sensitive than the mean to outliers (defect regions) in the distribution, and accurately reflects the representative normal value. Regions which are more than two standard deviations below the normal value are considered to be 'low'. This technique has the attractive feature of incorporating the statistical noise of the estimated sectors into the segmentation, i.e. the statistical distribution is used to define regions of low uptake relative to normal. An example of the statistical distribution in the cardiac phantom with a moderate sized defect is shown in Figure 4.10. Using this method, defect regions are more accurately defined in scans with lower statistical noise.

Regions of severely ischemic tissue are identified as mismatched defects in a resting flow (ammonia) scan compared to a FDG scan. Sectors below the normal range, in the *ratio* of flow/FDG scans are classified as ischemic. Selected regions must also occupy at least 10% of one or more of the vascular territories of the coronary arteries, to be included in subsequent analysis (Laubenbacher 1993). Five overlapping vascular territories are used: three for the LAD (apical, anteroseptal, anterolateral), one for the LCx (inferolateral), and one for the RCA (inferoseptal). Ischemic blood flow is then computed as the average value from the region(s) covering the largest proportion of one vascular territory. This method attempts to find the *most ischemic* tissue, which may be apparent when blood flow scans are performed at rest. Ischemic regions are more difficult to detect using resting flow imaging compared to stress flow imaging. These stages of segmentation are shown in the QA output for 14 subjects (Appendix C.2), and are presented again in Chapter 5.

Similar methods can be used to define regions of necrotic myocardium, which show a large matched decrease in metabolism and flow. In this case ratios of flow/metabolism can not be used, because both may decrease an equal amount with tissue necrosis. Instead, low uptake regions are identified separately from each scan,

and combined logically to localize necrotic tissue. Regions of mildly or moderately reduced metabolism *and* flow compared to normal, may represent a mixture of ischemic and scar tissue (Bonow 1991).

Myocardial Blood Flow Measures

Quantitative or absolute scale measurements are preferred when comparisons must be made between groups of subjects, as described in Chapter 3. Four different regional blood flow measurement procedures were implemented to evaluate the detection of change in ischemic myocardium, as part of a drug study analysis presented in Chapter 5. These measures were used to compare two sample groups for the assessment of blood flow changes with drug treatment. ^{13}N-labelled ammonia was used as the flow tracer, with the dynamic scanning protocol described in Appendix A.3.

The sector data (circumferential profiles) are normalized for tracer delivery using different semi-quantitative and quantitative techniques. First, sector data measured in the final static frame are normalized to a percent of normal uptake by dividing by the maximum value of all sectors in the heart. Secondly, absolute tracer concentrations measured in the final frame are simply divided by the injected dose. Thirdly, the net retention (uptake) of ammonia is computed using the last frame, and dividing by the integral of the arterial blood curve over the first 2 min of the study (Neinaber 1991, Bellina 1990). This blood integral approximates the single-pass delivery of tracer to the myocardium. Lastly, myocardial blood flow (MBF) is estimated using a simplified one tissue compartment model with two rate constants as presented in Chapter 3 (Hutchins 1990). Under resting conditions, the estimated rate constants have been shown to represent MBF [ml/min/g] (K1), and relative washout [1/min^{-1}] (k2).

As a verification of the compartmental model accuracy, the rate constants from normal myocardial regions in 16 patients were measured: K1=0.79±0.18 and k2=0.15±0.06. These values agree with published values by Hutchins et al (1990) (K1=0.83±0.19 and k2=0.18±0.09), using this simplified model. This verifies that the model is functioning properly and that the arterial blood input curves and myocardial

tissue curves are accurate. The results of a typical compartment model fit, in a region of ischemia is shown in Figure 4.9. The fit is excellent, and the measured MBF (K1=0.63) is below normal as expected for ischemic tissue.

4.4 Volumetric Analysis

Regional Changes in the Left Ventricle

In contrast with functional analysis of population samples, volumetric analysis of the entire LV myocardium can be performed when monitoring changes in a single subject. As reviewed in Chapter 3, changes of smaller magnitude may be statistically detectable in individuals because many sources of intersubject variability are removed from the measurement error variance. In a given individual, every region (sector) of the myocardium can be treated as an independent measurement, allowing an exploratory search for significant changes in *any* area of the LV. The requirement for quantification of function can be relaxed in this case, if it is only the location of change which is of primary interest, not the absolute magnitude of change. For example it may be useful to know that myocardial blood flow is preferentially increased in areas of ischemia regardless of the magnitude of the change. Qualitative measures of flow can be used in this case, as well as statistical models which adjust for delivery or global uptake of tracer. This technique of volumetric analysis of the LV myocardium is developed in subsequent sections, and verified using simulations and phantom experiments. The technique is applied to subjects from a human drug trial in the next chapter.

This new technique essentially uses a modified static scan protocol. A dynamic scan (with frames of equal duration) is performed under steady state conditions to estimate both the mean and the variance of the regional isotope concentration. The regional variance estimate is then used to assess the statistical significance of changes between treatment conditions. There are three types of change which are examined. The first is difference in global uptake in the left ventricle. The second is difference

in local activity relative to the global uptake (adjusted), i.e. areas in the heart which respond differently from the norm. These areas may be associated with different states of disease such as ischemia or necrosis. Change in absolute flow is the final factor, and indicates the net result of global and local effects.

It is necessary to chose between an additive and a multiplicative model when assessing relative changes. The multiplicative model is often chosen where change is assumed to be proportional to the global mean. In this case local values are divided by the global mean to obtain relative values. If the change is assumed to be additive and independent of the global mean, then the global mean is subtracted from the local means to obtain relative values. The model chosen will affect the apparent contrast (and significance) between treatment conditions. The multiplicative model must prevail for the measured values themselves, but the additive model has been shown to be valid for regional changes (Friston 1990), and is used exclusively in this work.

It is desireable to know the sampling distribution from which the measured values are taken, in order to verify the underlying assumption of random, normally distributed error variance. Values of radioactive concentration in myocardial sectors are treated as independent measurements, and are sampled according to the dynamic scan protocol described above. Repeated measurements (samples) are made on a given subject under a baseline and a treatment condition. The significance of the differences between baseline and treatment are assessed sector by sector using two-tailed paired t-tests, producing a polar plot of t values. This polar plot is thresholded at the critical value corresponding to a particular level of significance, thereby showing all sectors which are significantly altered, i.e. p2(sector) < α-level. Because there are a large number of comparisons being made, the distribution of t values can be plotted to illustrate the treatment effect on the sampling distribution. The t values follow the t distribution under the null hypothesis of no significant changes, but form a shifted or skewed distribution in the presence of change. Values in the tails of the distribution have a low probability of occurring unless a significant change exists. The observed *number* of significantly changed sectors follows the Poisson distribution, under the null hypothesis. Therefore the significance of a given polar map is assessed as a whole

p(LVmap), by integrating the Poisson distribution over the observed number of significant sectors (Friston 1990).

Sensitivity

Simulated polar maps were created and analysed to verify the volumetric statistical analysis. Samples of N=4 were generated with a uniform activity level, and gaussian noise with standard deviation of 20% was added (Appendix A.4). Variable size and severity of defects were generated as local increases and decreases in activity. Two-tailed t-tests were used to detect the local increases or decreases, using α=0.001. On the thresholded t-map significantly increased sectors are black, decreases are white, and regions of no change are shown in grey. The sector with the most significant *local* difference is circled on both the thresholded t-map and the adjusted difference map, as shown in Figure 4.11. The absolute and adjusted differences are reported for this *local* sector. Sensitivity is defined here as the ability to accurately identify the most significantly changed local sector in the known defect region. These results are reported in Table 4.3.

The Poisson distribution of the number of significant sectors was verified using the data from condition 1 where there was no focal change. Observed and expected frequencies were compared with the chi-squared statistic (Appendix B.1), and no significant difference was found (p=0.45). This verifies the accuracy of the technique used to assess the significance of the polar map as a whole p(LVmap).

One additional test was performed using condition 4. A simulation was performed with the significance threshold set to p<0.01 instead of p<0.001. Focal detectability was identical, global detectability was increased from 0.04 to 0.06 as expected, and mean p(LVmap) was decreased slightly to 0.006. Therefore the technique is relatively insensitive to changes in significance threshold between these values.

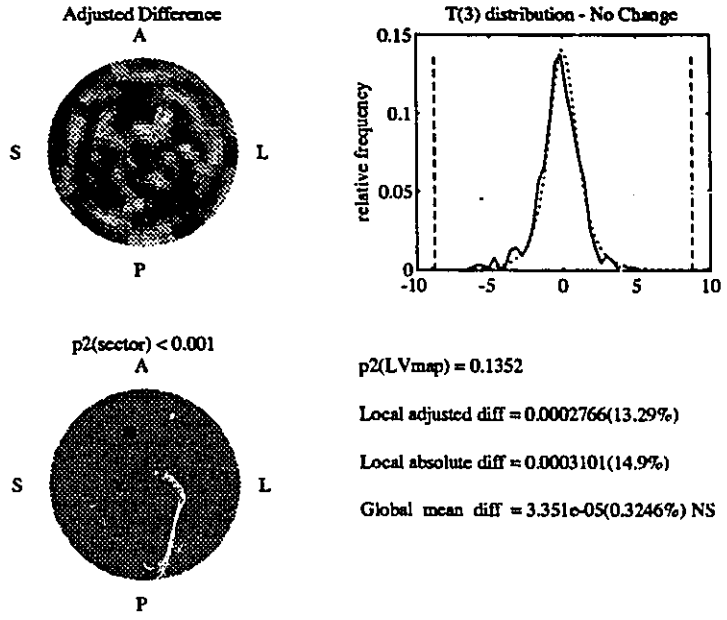

Figure 4.11. Cardiac phantom results: no change from baseline to treatment. (A) Adjusted differences and (C) significantly changed sectors. (B) Expected and observed t-distributions. (D) LV map significance, local (circled) and global differences.

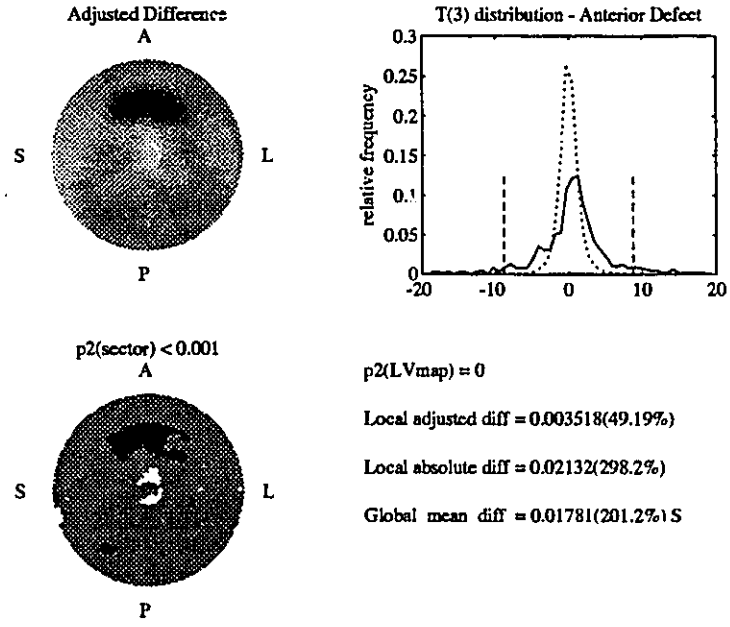

Figure 4.12. Cardiac phantom results processed with 10 mm smoothing. Uniform minus Anterior defect differences are cleary shown and highly significant. Significant differences in the apex are false-positives.

Table 4.3

Simulated Polar Map Sensitivity
20% noise, N=50

Condition	Size	Level of Change Local	Global	Sensitivity Local	Global	Significance p(LVmap)
1	no change	0%	0%	-	-	0.74
2	small	+40%	+1%	0.32	0.00	0.17
3	small	-40%	-1%	0.34	0.00	0.16
4	small	+80%	+2%	0.78	0.04	0.01
5	small	-80%	-2%	0.76	0.00	0.01
6	moderate	+40%	+4%	0.60	0.12	0.04
7	moderate	-40%	-4%	0.68	0.12	0.02
8	moderate	+80%	+8%	0.90	0.52	$<1x10^{-7}$
9	moderate	-80%	-8%	0.88	0.46	$<1x10^{-9}$
10	large	+40%	+9%	0.62	0.50	0.004
11	large	-40%	-9%	0.62	0.52	0.007
12	large	+80%	+18%	0.82	1.00	$<1x10^{-20}$
13	large	-80%	-18%	0.86	1.00	$<1x10^{-20}$

The variance of gaussian noise was decreased to simulate the effect of smoothing the images before computing the sector averages. A focal decrease of 40% was created for a small sized area. The results are compared to those with the original noise levels in Table 4.4. The same size and magnitude of change is much more significant when measured with lower noise. The estimated error variance decreases, and causes the significance of the t-tests to increase. Therefore, sensitivity increases dramatically from approximately 30% to 90% for a small focal change measured with 20% noise versus 5% noise. Sensitivity to a 10% difference with 5% noise, is approximately equal to a 40% difference in the presence of 20% noise, as expected.

These simulation studies demonstrate the sensitivity of the method to detect changes of various magnitude and size in the presence of noise. Local changes were often evident as a group of significant pixels, which did not necessarily include the

sector with the *maximum* significance. These changes were not detected automatically, but would easily be identified visually. Therefore sensitivity can be increased with visual interpretation of the t-maps. The mean value of significance p(LVmap) is a conservative measure, since most of the values were below the mean. The distribution of p(LVmap) was skewed towards lower values, e.g. in condition 11, the mean p(LVmap)=0.007 whereas the median p(LVmap)<$5x10^{-6}$.

Table 4.4

Simulated Effects of Smoothing
N=50

Noise	Size	Level of Change		Sensitivity		Significance
		Focal	Global	Focal	Global	p(LVmap)
20%	small	-40%	-1%	0.34	0.00	0.16
5%	small	-10%	-0.25%	0.30	0.00	0.21
5%	small	-40%	-1%	0.88	0.06	$<1x10^{-11}$

Specificity

In order to determine if the technique is specific to real changes in activity distribution within the left ventricle, two samples (N=4) from a cardiac phantom scan performed with an anterior defect were compared (Appendix A.2). There was no difference in the activity distribution between the two samples, therefore a significant change was not expected, i.e. the null hypothesis was true. This test was also performed to verify that data acquired with the tomograph had the same statistical properties as the simulated data, i.e. random & independent sector measurements, and normally distributed error variance. These assumptions were verified because the sectors of the observed t-map followed the t distribution under the null hypothesis (Figure 4.11). The observed and expected t-distributions agree closely, and only two

sectors are significantly changed. The method is expected to produce (on average) 0.64 significantly altered sectors by chance on any given polar plot, with α=0.001. This is close to the number detected, resulting in a p(LVmap) = 0.13 which is not significant.

No change in global concentration is observed (as expected), and the local significant sector difference is 0.0003 (15%) cps/pixel. The average count rate observed in this cardiac phantom experiment is 0.01 cps/pixel, which is lower than that observed (0.05 cps/pixel) in typical ^{13}N-labelled ammonia studies (Appendix A.3). This analysis was also performed on data which was smoothed with a 10 mm gaussian filter before the sector averages were computed. The estimated p(LVmap)=0.47 was increased since only 1 sector was significantly changed. The mean activity concentration remained the same (0.01 cps/pixel), whereas the estimated error variance decreased from 5% to 2.5%. It is also important to note that smoothing did not change the underlying (Student's t) sampling distribution, since the serial measurements of the sector concentrations were still independent. Smoothing produces results similar to those presented in Table 4.4; decreasing noise and thereby increasing the magnitude of focal change relative to the error variance (noise).

Regional measurements with low noise are obtained when a large number of counts are recorded; either during high count rate studies or using long counting intervals. The signal to noise ratio can also be increased after data acquisition by smoothing the reconstructed images, with a resultant loss in resolution. In neither the smoothed (10 mm) nor the unsmoothed (5 mm) case is any significant change in global or local concentration detected. This indicates that the technique should be very specific, since no significant change was detected when none was present.

When the anterior defect phantom scans are compared with uniform activity cardiac phantom scans (Appendix A.2), there is a significant increase (uniform-defect) detected in the region of the defect. The null hypothesis of no change is rejected with p(LVmap)=0, and a large number of sectors (4 x 6 = 16 mm x 26 mm) are significantly changed in the region of the cardiac insert. There was a significant global increase of 200%, and an absolute local increase of 300% as shown in Figure 4.12. The adjusted local increase was approximately 50% and occurred near the edge of the

insert. Larger relative increases were found at the centre of the insert, but did not reach the same level of statistical significance.

The number of sectors which are significantly increased, corresponds to a slightly smaller area than the actual size of the defect (20 mm x 30 mm). This is due to the finite resolution of the reconstructed and resectioned images, coupled with the significance level chosen (α=0.001). If a larger α-level was chosen then this region size would increase. The smallest significant difference was 7.0%, and may represent the minimum magnitude of change that is detectable at this significance level, and with this image noise level. The mean increase in the whole defect region was approximately a factor of 2, as the count rate in the anterior defect was approximately 35% of that in the surrounding sectors. It is known that there was no activity in the defect therefore this apparent activity is due to the finite image resolution in the short axis sections. When smoothing is used to increase the signal to noise ratio, the magnitude of the measured differences will be underestimated in small regions.

Smoothing also increased the statistical significance of small differences in the bottlebrush sampling at the apex of the cardiac phantom. Slightly different ellipse fits in the two scans caused a misregistration of the two datasets, resulting in changes in the apparent concentration in some apical sectors. These changes were statistically significant because the variance of the phantom data was very low. Such differences are not anticipated in the analysis of human data for two reasons: the first is that the variance of sector data in the human apex is much higher than in the cardiac phantom; the second reason is that the shape of the human LV myocardium more closely matches the shape of the elliptical model (Figures 4.1 and 4.3) and is therefore less susceptible to apical misregistration. In the comparison of the human studies presented in Chapter 5, no significant apical differences were observed.

The measured statistical distribution can be shifted by the global adjustment, in the presence of differences with a large spatial extent. The measured distribution is basically centred on the theoretical distribution and then tested for outliers. A large number of significantly increased sectors would shift the body of the distribution down. The net result for the phantom data shown in Figure 4.12 is a conservative test of real

increases and a liberal test of decreases, i.e. fewer significant increases detected and more significant decreases. In light of these findings a conservative interpretation of p(LVmap) is required when large regions of myocardium are increased or decreased.

If specific regions of the LV myocardium are identified a-priori then significant differences in those areas can be reported at the α-level used for the comparison. An example of this type of result is demonstrated in the next chapter, where a region of ischemic myocardium is identified a-priori.

For quality assurance, the radii of the myocardial sector regions should always be verified on the short axis sections as shown in Figure 4.7. The additional QA outputs illustrated in Figures 4.11 and 4.12 must also be used to determine which sectors are likely real changes; if regional artifacts are apparent on the adjusted difference map, then significant changes identified in those regions are likely not real. Furthermore, a small value of p(LVmap) does not necessarily imply that the treatment *caused* a significant effect, because isolated sectors may also change significantly with normal physiological variation. Focal regions which comprise a large number of contiguous sectors, and located in the body of the heart are the most likely to represent real changes. However, this method does not assess the significance of focal differences as such.

4.5 Data Reduction

Automated analysis serves an important function in data volume reduction as well as in objective interpretation. The image data from a single static frame requires approximately 1 Mb of disk storage. This represents 31 transaxial images measured with the positron tomograph. These images are typically resampled along the left ventricular long axis into 10 to 20 short axis sections, on average requiring 0.5 Mb per frame. Visual analysis is performed on these short axis series, if knowledge of the relative distribution of tracer is sufficient for diagnosis. Interactive visualization is typically used in this format, as vertical and horizontal long axis sections can be generated and displayed quickly on many computer workstations.

The entire distribution in the left ventricle can be visualized if measurements are averaged across the myocardial thickness to create circumferential profiles (sectors). These sectors can be displayed as concentric rings in a polar plot, which is a massive data reduction down to less than 5 Kb. This averaging is justified in SPECT and in PET because the effective resolution of these instruments is not currently sufficient to distinguish endocardial from epicardial function.

A typical dynamic series of images produced with ^{13}N-labelled ammonia may consist of 20 frames taken over a period of 10-20 min. Each of these frames can be processed into myocardial sectors, and presented as a time series. This data is not typically interpreted visually because dynamic imaging is performed to obtain some quantitative measure of cardiac function using a mathematical model which describes the tracer metabolism over time. In this case there is also a temporal reduction in data volume. 20 frames of data are essentially compressed into a few parametric frames which represent different myocardial tissue characteristics such as blood flow, relative washout, retention etc. These parametric images can be volume based (transaxial or short axis images), but are not routinely created as the data processing required is significant. It is more common to create parametric images in the form of polar plots, which require parameter estimation of only a few hundred sectors, as opposed to perhaps a hundred thousand image pixels.

If there are certain functional tissues which are of interest then it is not necessary to parameterize the function of the entire ventricle, but only a few sectors such those which are ischemic. In many cases ischemic tissues are located in a specific area of the ventricle and may be analysed using a single centred region. The function may be summarized by only a few values of the specific parameters of interest. In studies comparing samples of subjects in different treatment groups, such a functional analysis must be used. It is common for the scans from each patient to be summarized by a single parameter value, or by the difference between values in subsequent (treatment) scans. The final and ultimate data compression is performed when representative measurements (or differences) from sample groups are compared

using a statistical test to compute a single value of the significance of the desired treatment effect.

Table 4.5

Data Volume Compression

Study Design	Transaxial Images [Mb]	Short Axis Images [Mb]	Polar Plots [Kb]	Functional Regions [b]	Functional Parameters [b]	Treatment Changes [b]	Treatment Significance [b]
Treatments	TFS	TFS/10	TFS	TFS	TS	S	1
Subjects	FS	FS/10	FS	FS	S	1	
Frames	F	F/10	F	F	1		

T - number of treatments (scans) per subject
S - number of subjects
F - number of frames per scan

The stages of data compression are summarized in Table 4.5; they do not necessarily occur in the given order, but are presented for consistency. For example a functional polar plot may be generated from the polar plots of a dynamic scan with F frames which would require 1 Kb, as opposed to the 1 byte required for a single (regional) functional parameter shown in Table 4.5.

In an experimental design comparing two treatments with 10 subjects per sample and imaged using 20 frame dynamic series, the compression of data that is required to assess the significance of the treatment change in a functional tissue region is indeed massive. 400 Mb of image data is compressed into a single number representing an estimate of statistical significance. An analysis of such a study is presented in the next chapter. Two samples of subjects are compared to evaluate the effect of a vasodilating drug upon myocardial blood flow.

CHAPTER 5
Analysis of a Drug Treatment Study

The techniques of automated cardiac analysis developed in the previous chapter are applied for the evaluation of the treatment effect of a vasodilating drug. Treatment changes are first demonstrated in a specific functional tissue type (ischemic myocardium), by comparing two samples of subjects under placebo and drug conditions. Several common measures of MBF are computed to determine which is the most sensitive to change. Treatment effects are then evaluated in an exploratory analysis of the entire left ventricle, using single subjects scanned under baseline and drug (or baseline and placebo) conditions. At each stage, appropriate quality assurance outputs are generated to verify the analysis procedure.

5.1 Functional Analysis

Population Drug Study

Data were analysed from 14 patients in a drug study which evaluated the effect of topical nitroglycerin on myocardial blood flow at rest (Fallen 1995). Subjects all had at least one coronary artery with a minimum 50% stenosis diameter as determined with coronary angiography. All demonstrated chronic stable angina responsive to sublingual nitroglycerin. The experimental design was a double blind placebo-control study. It was hypothesized that nitroglycerin would increase flow to ischemic tissue, thereby relieving anginal pain. As part of the present analysis, it was also hypothesized that a quantitative analysis of MBF would have reduced error variance compared to semi-quantitative measurements and provide a sensitive assessment of blood flow changes with the drug treatment.

Three scans were performed on each subject under resting conditions. In brief, ^{13}N-labelled ammonia was used as a qualitative and quantitative tracer to measure MBF,

while FDG was used as a qualitative marker of exogenous glucose utilization. First a *baseline* blood flow scan was performed, followed by drug or placebo administration and a second *treatment* flow scan. An FDG scan was then performed to evaluate the relative distribution of glucose utilization. The ratio of baseline ammonia and FDG scans was used to define regions of ischemia as described in Chapter 4. Detailed scan protocols are given in Appendix A.3.

Data Analysis and Quality Assurance

The automated functional analysis was performed as described in Chapter 4 to evaluate perfusion changes during treatment; this method determines the magnitude and statistical significance of blood flow changes in ischemic myocardium. Comprehensive quality assurance (QA) outputs are produced to verify the analysis.

The orientation and extent of the long axis of the left ventricle was determined using the FDG images because these typically had a higher SNR than the ammonia images. The LV angles and extent parameters were subsequently applied to the ammonia images in order to determine the centre coordinate only. This was intended to account for different LV positions between the ammonia scans. The last (20 min) frame of the ammonia dynamic scan was used to determine the position of the left ventricle, and also to define the myocardial radii. Sector radii were estimated separately for the FDG study, and for the two ammonia studies. These parameters were then used for all time points in the respective studies, to compute regional myocardial uptake. Quality assurance outputs, with which the accuracy of the reorientation parameters (as in Figure 4.1) and the myocardial radii (as in Figure 4.7) were verified, are shown in Appendix C.2 for the three scans in all subjects.

Typical output for a given subject is shown in Figure 5.1. The polar maps of the three scans, the derived ratio maps, the segmented ischemic regions, and the LV blood curves are all automatically determined. The top row (A-C) presents the polar maps of the final frame of each scan in the study. Note that there is missing data in

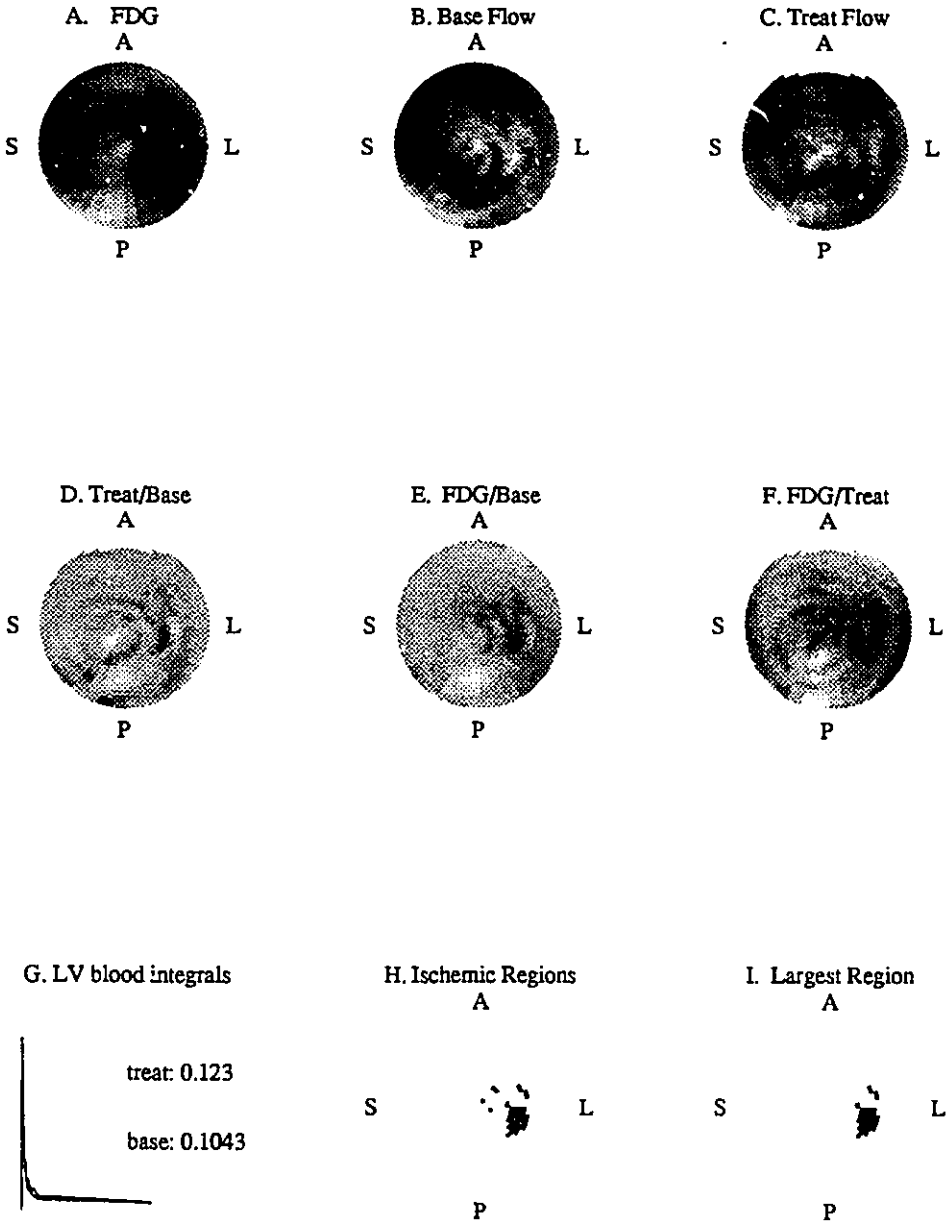

Figure 5.1. Quality assurance polar maps. (A) FDG (B) Baseline flow (C) Treatment flow (D) Flow ratio (E) Baseline ischemia (F) Treatment ischemia (G) Ammonia blood curves and integrals (H) Ischemic regions (I) Largest ischemic region.

the treatment flow map, because the anterior wall was truncated slightly at the base of the heart in this scan.

The second row (D-F) shows ratios of these static measurements. The ratio polar maps are used to visualize the relative differences between the three scans. The ratio of FDG to baseline flow sectors is an index of ischemic myocardium, as shown by the relatively dark areas in Figure 5.1E (FDG/Base). Excellent qualitative agreement can be seen between this ischemic index map (E) and the treatment/baseline flow ratio shown in (D). The dark areas in the distal lateral wall of both of these polar maps coincide almost exactly, and represent highly ischemic myocardium which received a large increase in blood flow with the vasodilating drug. The ratio of FDG to treatment flow (FDG/treat) shown in (F) is more globally uniform after the drug is administered, indicating less severe ischemia.

The inverse of the ischemic index map is used as a predictor to localize expected changes in treatment blood flow compared to baseline. Sectors with a low ratio of flow/FDG relative to normal are assumed to correspond to the most ischemic myocardium, as described in Chapter 4. To calculate the difference in ischemic flow before and after treatment, the ischemic index map is first thresholded at the assumed normal value, producing the segmented ischemic sectors shown in (H). Then the largest region is selected from a single vascular territory as shown in (I). LV blood curves and the respective 2 min integrals, from the baseline and treatment ammonia scans are shown in (G).

The selected ischemic regions, the treatment/baseline flow ratio maps, and the measured ammonia blood curves (and integrals) for all 14 subjects are shown in Figure 5.2. A positive predicted effect can be seen visually in some subjects who received the drug, e.g. D5 and D6, but a false positive may be identified in P3 who did not receive the drug. In some scans, no ischemic regions were segmented because of excessive noise in the ischemic index map, or because they did not cover the minimum of 10% of a given vascular territory.

Detection of a treatment difference is very sensitive to misregistration of the baseline and treatment scans. If the left ventricles from the two scans are not sampled

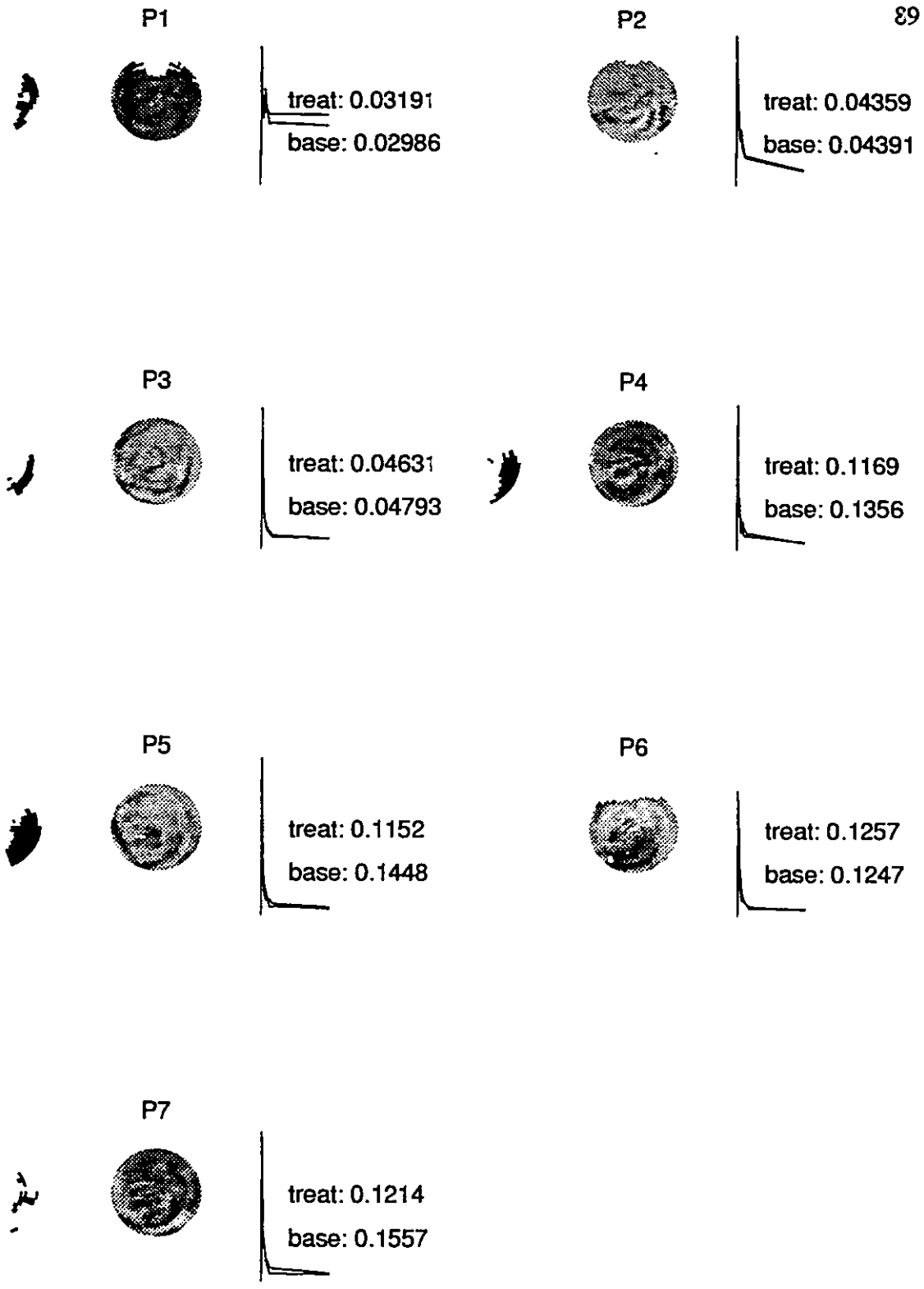

Figure 5.2a. Quality assurance summary of drug study analysis: subjects in **placebo condition**. Ischemic regions (black), treatment/baseline ratio map, ammonia blood curves and integrals are shown for all subjects.

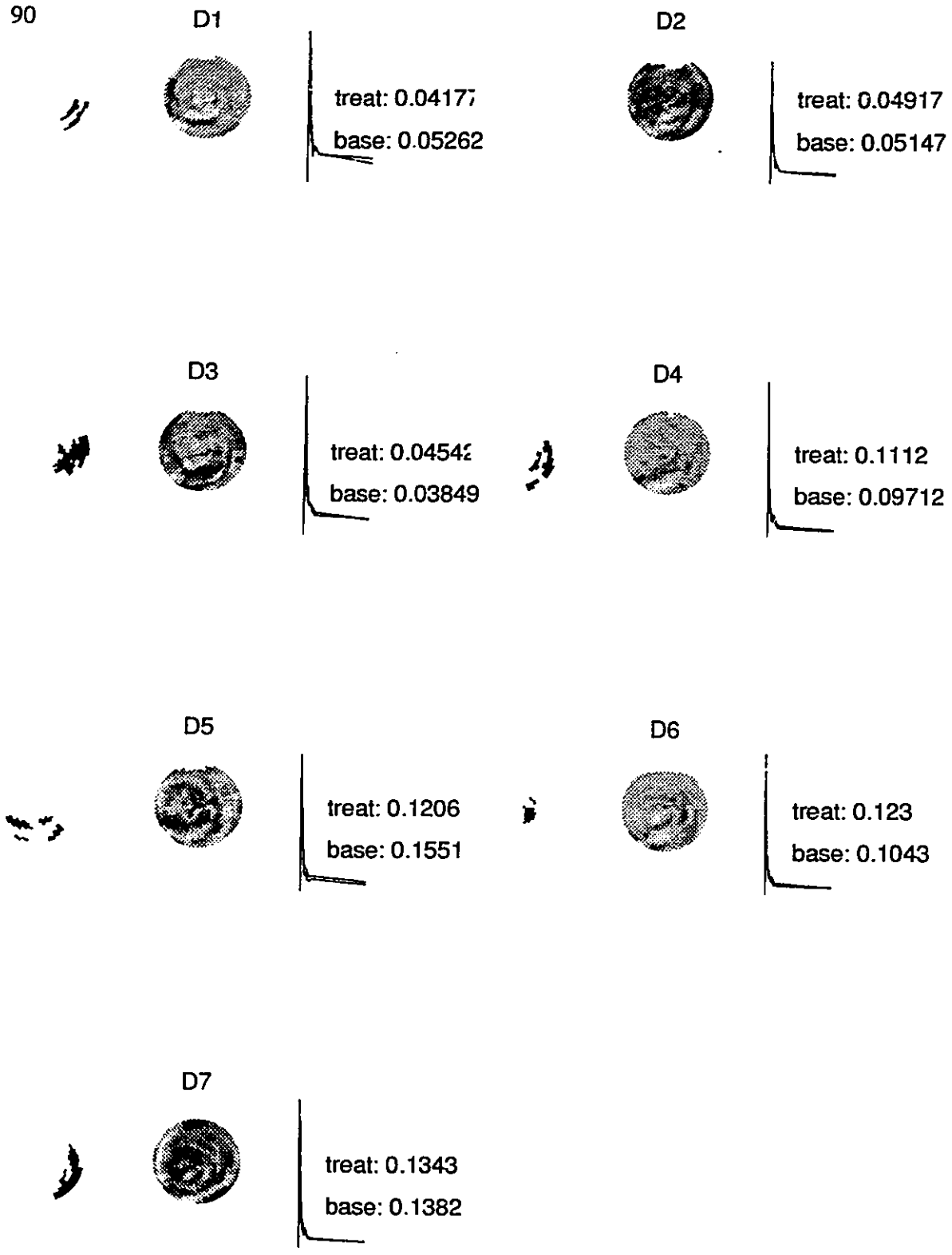

Figure 5.2b. Quality assurance summary of drug study analysis: subjects in **drug condition**. Ischemic regions (black), treatment/baseline ratio map, ammonia blood curves and integrals are shown for all subjects.

identically, then the computed sector differences will not be accurate. Misregistration is typically apparent as a half ring or full ring artifact near the outer edge (basal sectors) of the ratio polar plot. This is indicative of changing orientation or position of the estimated long axis. Use of the FDG angles and extents to estimate the LV position on the ammonia scans minimized the occurrence of such ring artifacts. The agreement between the baseline and treatment ammonia scans is apparent in the ratio polar maps shown in Figure 5.2, i.e. there are no visible dark or light rings around the treatment/baseline ratio maps.

The regions of ischemic myocardium shown in Figure 5.2 do not systematically include the outer edges of the polar maps, where misregistration artifacts are most likely to appear. The appropriate selection of the ischemic regions are verified using the QA outputs as in Figure 5.1 for all subjects (Appendix C.2). This evidence supports the conclusion that registration between the FDG and baseline flow scans was satisfactory.

Treatment Changes

To demonstrate the power of an automated and quantitative analysis of MBF, several methods of normalization for tracer delivery are computed, as described in Chapter 4. Briefly, the percent of maximum uptake and fraction of injected dose are evaluated as two qualitative indicators of blood flow. The net retention of ammonia is used as a semi-quantitative measure. Lastly, a quantitative two compartment tracer kinetic model was used, which solved for two rate constants (K1,k2) and a blood pool fraction (F_a). K1 is an accurate estimate of regional myocardial perfusion at rest (Hutchins 1990).

Differences from baseline to treatment are shown in Table 5.1, while all measured values are listed in Appendix C.1. The placebo and drug groups were first analysed separately. Paired t-tests were used to assess whether changes in ischemic flows were significantly different from zero. The difference between drug and placebo

conditions was then assessed with a two-sample t-test. A p-value of less than 0.05 was considered statistically significant.

Table 5.1

Ischemic Differences in Blood Flow
(Treatment-Baseline)

Subject	Dose Norm [cps/Ci]	Max Norm [%]	Blood Norm [1/min]	Kinetic Model [ml/min/g]
P1	0.054	0.025	-0.026	0.005
P2	*	*	*	*
P3	0.225	0.063	0.066	-0.066
P4	0.033	0.020	0.061	-0.052
P5	-0.327	0.035	-0.039	-0.052
P6	*	*	*	*
P7	-0.106	0.094	0.076	0.009
Pmean	-0.024	0.047	0.028	-0.031
p2<0.05	**no**	**yes**	**no**	**no**
D1	0.116	0.071	0.133	0.301
D2	*	*	*	*
D3	0.051	0.055	-0.032	0.054
D4	0.595	0.124	0.047	0.056
D5	0.980	0.171	0.013	0.178
D6	0.934	0.144	0.057	0.173
D7	-0.283	0.006	-0.020	0.037
Dmean	0.40	0.095	0.053	0.133
p2<0.05	**no**	**yes**	**no**	**yes**
Drug-Placebo	0.424	0.048	0.025	0.164
p2<0.05	**no**	**no**	**no**	**yes**
p2-value	0.12	0.14	0.88	0.01

*No ischemic region found

All of the above analyses were performed with sector data from the identical ischemic myocardial regions. Both the qualitative and semi-quantitative methods use

the last frame of the ammonia uptake scans normalized by some measure of the amount of tracer delivered to the myocardium, to compute a measure of MBF. ^{13}N-labelled ammonia is assumed to accumulate in the myocardium in proportion to blood flow. Although it is known that the net extraction of ammonia from blood is limited at high flow rates, this assumption is still likely valid at the low flow rates encountered at rest.

The simplest qualitative normalization is division by the injected dose, which is subject to timing and procedural variations during intravenous injection. This method produces a 17 fold increase from baseline to treatment flow, but the data have such a high error variance that this difference is not statistically significant.

The maximum sector concentration has a more direct relation with the ischemic region concentration, as both are measured during the same time frame. One may expect the distribution of flow throughout the LV to become more uniform with the drug compared with placebo, i.e. that flow in the ischemic region will be closer to the maximal (normal) flow under the drug condition. Indeed this seems to be the case; there was a 9.5% increase in *relative flow* with the drug, however there was also a 4.7% increase with placebo. This method of analysis produced a significant positive bias, because both increases were significantly different from zero. There was however, no significant difference in the drug minus placebo effect.

Division by the integral of the LV blood curve has been shown to provide a useful measure of MBF (Bellina 1990, Neinaber 1991). The values of net retention in Table 5.1 show a similar pattern to those of relative flow above. The increase in the treatment-baseline difference is approximately twofold higher with the drug compared with placebo. However, in this case the added noise in the measurement of the blood curve integral increases the error variance, causing neither change to reach statistically significance.

The kinetic model uses the time course of activity from both ischemic myocardium and LV blood to estimate MBF. With this model blood flow is measured by the delivery and initial extraction from arterial blood, compared with the previous methods which use later time points only, as an indicator of MBF. This technique is

expected to be the most accurate and indeed shows a statistically significant change with the drug, and no change with placebo. Furthermore, there is a significant difference (p2=0.01) of about 16 ml/min/dg between placebo and drug conditions.

These results indicate the requirement for quantitative analysis of cardiac PET data. Clinically significant changes may be small in magnitude and difficult to detect statistically. This is particularly true in this study where ischemic regions and blood flow changes were identified at rest. Use of the segmentation technique developed in Chapter 4 is justified by the apparent positive predictive effect of MBF changes in the chosen ischemic regions. It may be that the drug *only* increased blood flow to the *most* ischemic tissue. The effect of nitroglycerin on blood flow to the ischemic myocardium appears to be mild at best. Otherwise, large effects would have been detected even by the simpler qualitative normalization methods. These other MBF measures utilize additional measurements which increase the error variance, without increasing the magnitude of the treatment effect. This is evidenced by the low statistical significance of the difference between the drug and placebo treatment conditions. Only the quantitative kinetic analysis was able to discriminate between the treatment conditions.

Automated methods produce objective and consistent results, and are necessary to obtain reliable interpretations of experimental data. The techniques developed and applied here have enabled an objective comparison of MBF normalization methods, and a reliable analysis of the treatment effect in a typical drug study. It is apparent from Table 5.1 that the effect was more pronounced in some subjects than in others. It would be desireable to monitor the changes in blood flow in these individuals, and relate these changes to clinical indicators such as relief of anginal pain.

5.2 Volumetric Analysis

Ischemic heart disease typically affects specific regions of myocardium which are distal to a stenosis or occlusion. Therefore diseased myocardium tends to be localised in focused areas deficient in blood flow. It is desirable to monitor focal

changes in blood flow and to correlate these changes with clinical changes resulting from disease progression or disease treatments. A sector by sector assessment of changes in myocardial activity can be made if measurement samples are taken under different treatment conditions, using the volumetric technique developed in Chapter 4. The fundamental element of this method is to measure both the mean value and the variation about the mean, independently in all sectors of the left ventricle. This technique is shown to localize statistically significant changes in myocardial blood flow for individual patients.

Data Analysis and Quality Assurance

Two subjects from the drug study presented in the previous section, were reanalysed using this single subject volumetric paradigm. One subject received the nitroglycerin drug, and the other received placebo. It was hypothesized that the former would have increased blood flow in the ischemic regions, and the latter will show no significant changes.

Sample frames (N=4) were taken from the dynamic ammonia scans under baseline and treatment conditions for both subjects. These frames were 20 s in duration and started 1 min after intravenous injection of ^{13}N-labelled ammonia. It would have been preferable to wait 2 to 3 min after injection for steady state to be achieved, however the earlier samples were the only 4 equal duration frames available in the acquisition protocol used for this particular study. In the two subjects analysed, the time course of activity in the blood pool was assessed visually (Appendix C.2), and had nearly reached steady state levels after the first minute. The mean activity levels in the left ventricle were also stable over the four frames as shown in Table 5.2; the deviations from the means ranged from 1% to 3%. Both subjects received the same dose of tracer for baseline and treatment scans, as shown by the similar mean activity concentrations. It is emphasized that these measurements were separate from the respective final frames of the ammonia scans, that were used to identify the ischemic regions in the functional analysis of the previous section.

Table 5.2

Mean LV Activity During Dynamic Scanning
N=4

Subject	Condition	Mean Activity [cps]
P4	Baseline	0.0577 ± 0.0006
	Placebo	0.0581 ± 0.0012
D6	Baseline	0.0378 ± 0.0010
	Drug	0.0399 ± 0.0013

For a given subject, the polar maps (LV sector data) are compared sector by sector using the method developed in Chapter 4. Briefly, the global mean of all sectors in each sample (N=4) is computed and subtracted from the raw sector data. Then these adjusted samples (baseline and treatment) are compared using paired t-tests. The output of the analysis includes both the adjusted difference polar map, and the associated t-value polar map which has been thresholded at the chosen significance level (α). Expected and observed t-distributions are shown to verify the assumptions required for paired t-testing. Summary statistics are shown which include the global difference, the maximum local difference, and the significance of the thresholded t-map as a whole p(LVmap).

Both of the subjects' volumetric analyses were performed with 5 mm and 10 mm smoothing of the short axis sections. As demonstrated by the phantom experiments in Chapter 4, moderate smoothing has the effect of focusing changes into smaller regions with lower apparent contrast. The net result is generally more significant sectors and lower p-values. An α-level of 0.01 was used as the threshold for statistical significance.

Quality assurance of the volumetric analysis begins as with the functional analysis presented at the start of this chapter. The accuracy of the reorientation and the myocardial radii are verified with the associated QA outputs (Figures 4.3 and 4.7).

Processing artifacts such as misregistration of baseline and treatment scans and subject motion can cause apparent significant changes (false positives) in the LV polar map. Misregistration can occur if the orientation, extent and position of the long axis are not accurately identified, or if the estimated myocardial radii are different in the baseline and treatment scans. Sectors at the base of the heart (near the outer edge of the polar map) are more susceptible to such artifacts because of the increased variability of the reorientation and sectoral averaging in these regions. The polar map showing the difference between baseline and placebo scans (Figure 5.3A) can be used to detect the presence of such artifacts. Significantly altered sectors near such artifacts, or near regions of missing data could be false-positives, and should not be reported.

Treatment Changes

The subject who received placebo (P4) showed nine significantly changed sectors when analysed with 5 mm smoothing. This was not a significant result with p(LVmap)=0.20. In the most significantly altered sector there was a decrease of 30%, and the difference of 0.7% in global activity was not significant. These results agree with those obtained in the cardiac phantom (Figure 4.11), and confirm that the method is specific to real changes, since no significant change was detected when none was induced by treatment.

When processed with 10 mm smoothing, this subject demonstrated a large number of significantly changed sectors, as shown in Figure 5.3. These changes were almost all decreases from the baseline to the treatment condition, principally in the distal posterolateral wall. This area of the myocardium appears to be adjacent to the region of relative ischemia shown in Figure 5.2 (P4). The most significant change occurred in a sector in the basal septum, and was a decrease of only 6%. The two regions of increased flow were in normal myocardium, whereas two adjacent sectors with decreased flow were detected in the ischemic tissue region. The statistical t-distribution appears more broad with smoothing. This is either due to *equal* increases

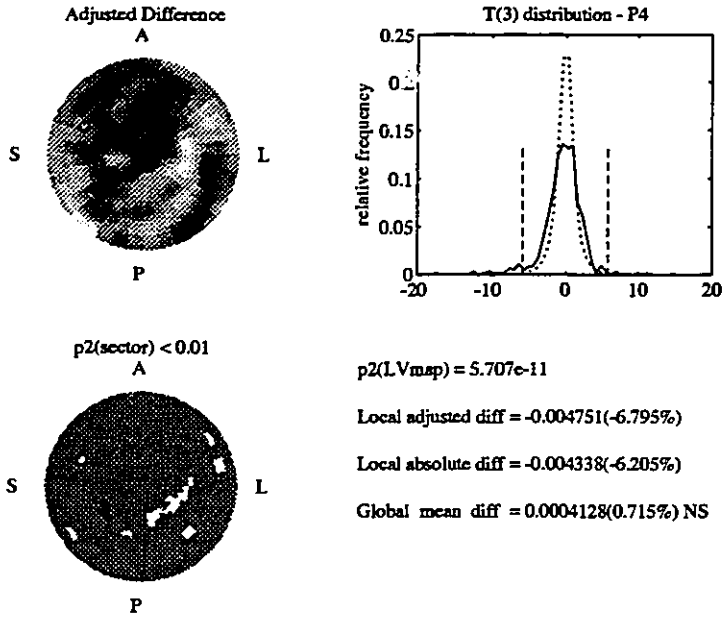

Figure 5.3. Single subject results with Placebo. (A) Placebo-Baseline Flow. (B) Expected and observed t-distribution. (C) Significantly changed sectors. (D) LV map significance, local and global differences.

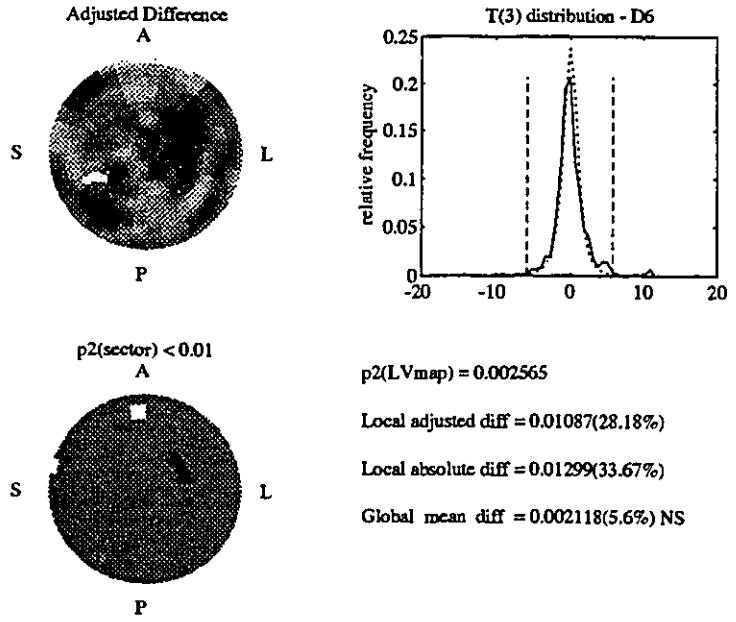

Figure 5.4. Single subject results with Drug. (A) Treatment-Baseline flow. (B) Expected and observed t-distribution. (C) Significantly changed sectors. (D) LV map significance, local and global differences.

and decreases in uptake, or it is a result of added variance in the data from sources other than counting statistics alone.

The result from this placebo analysis is interpreted as a small decrease in flow over a moderate sized region of the distal posterolateral wall, which can be seen visually in the polar map of the adjusted difference. The result of smoothing appears to be different in this study than in the uniform cardiac phantom, since decreases in blood flow were detected when none was induced. It is likely that these detected decreases are real, i.e. that some normal physiological variation in blood flow occurs which is detectable with this technique. In general, 10 mm smoothing increases the SNR over 5 mm smoothing and enhances the significance of changes which are present in the data. It is important to note that there were *no increases* in blood flow detected in the ischemic region of this subject who received placebo.

The subject who received the vasodilating drug (D6) showed seven significantly changed sectors when processed with 5 mm smoothing, which was not a significant result with p(LVmap)=0.46. The most significant sector had a decrease of 20%, at the anterior base of the LV. The basal anterior portion of the heart was not imaged in the treatment scan as seen by the missing anterior sectors in Figure 5.4. The significantly decreased uptake in this region is likely a processing artifact near this missing data. Four of the seven significant sectors were adjacent and in a region of relative ischemia, as shown in Figure 5.2 (D6).

The effects of 10 mm smoothing were again to enhance the patterns of change. Similar areas of the LV were significantly changed, but with enlarged extent and decreased p(LVmap) (p2=0.0026), as shown in Figure 5.4. The locations of detected change were the same; a decrease in the anterior base (artifact), and an increase in the distal lateral wall in a region of ischemic myocardium. The maximum (local) sector significance corresponded to a distal lateral wall increase of 34% in the ischemic region. There is excellent agreement between the theoretical and measured t-distribution, validating the underlying assumptions of random, independent measurements and normal error variance. The global change of 5.7% was not

significant at the α=0.01 level, and is similar to the value obtained with 5 mm smoothing.

The accuracy of the estimated local change magnitude and position can be assessed qualitatively by examining the polar map of the adjusted difference between baseline and treatment. The local sector is identified by the circle on the thresholded significance map, and the adjusted difference map. If the difference map is smooth in the region identified, then the estimate is expected to be accurate and precise, i.e. the difference magnitude will not be sensitive to small changes in position. The significantly decreased sectors are also in a smooth region of the change map, but are suspiciously close to the missing anterior sectors, and should be interpreted conservatively.

The extent of the increased flow to the lateral wall can also be probed by raising the significance threshold, as shown in Figure 5.5. The location of altered sectors is the similar, but the region of increased (ischemic) flow extends anteriorly and posteriorly towards the centre of the known ischemic region. This positive result becomes more highly significant with $p(LVmap)<5x10^{-6}$, although this p-value is artificially lowered by the inclusion of the decreased sectors at the base of the LV. The smaller p-value obtained with a raised significance threshold indicates that there are more sectors of the LV (than expected) which received small increase in flow, than received a larger increase in flow.

This study demonstrates a focal increase in uptake (blood flow) of approximately 30% induced by a vasodilating drug, in a region known to be ischemic. This ischemic region was assessed independently using the ratio of FDG/ammonia polar maps from static scans. This effect is evident visually in Figure 5.2 (D6), but is shown to be a statistically significant result as well. This result is specific to a single subject, and was obtained using only 80 s of dynamic data in each of two conditions.

Significant results have been found using both a functional and a volumetric analysis of a typical drug study, using the methods developed in Chapter 4. More highly significant changes are detected with the qualitative volumetric analysis, than with the quantitative functional analysis of population samples. Smaller magnitude

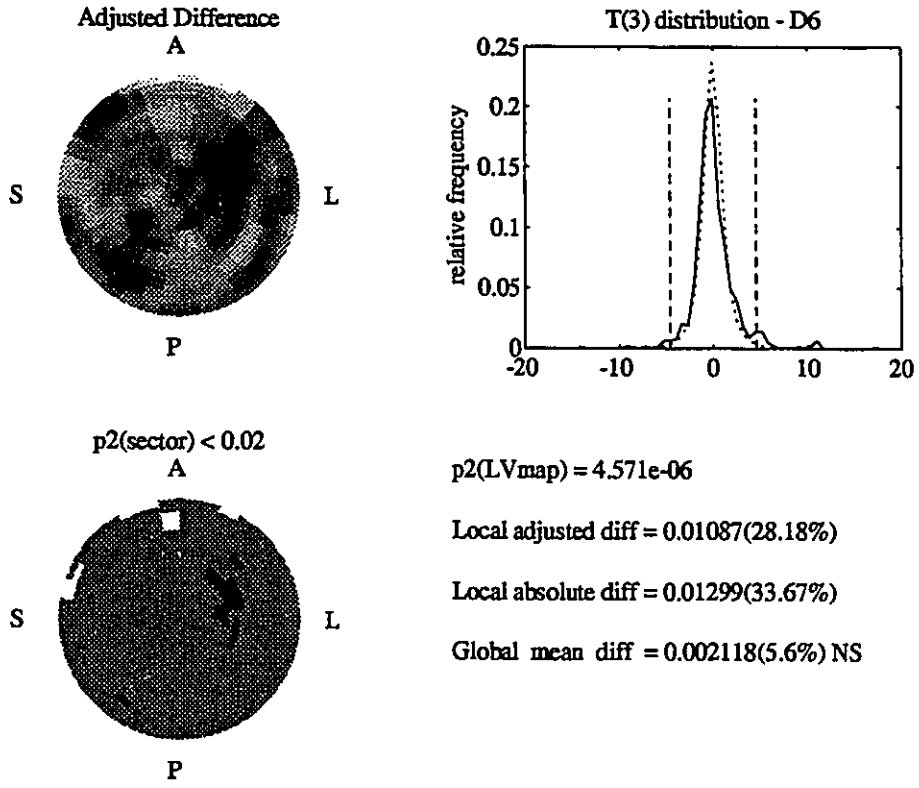

Figure 5.5. Single subject results with Drug. The extent of the region of change is increased compared to Figure 5.4 by raising the significance threshold from 0.01 to 0.02.

changes appear significant using the single subject (volumetric) paradigm, because there are fewer components of the error variance. Lower error variance produces changes with higher statistical significance. This may indicate that the discriminating power of PET is not being fully utilized. Even smaller changes may be detectable using quantitative measurements of blood flow with this single subject experimental design.

CHAPTER 6
Discussion of the Automated Analyses

Techniques of automated analysis have been developed in the present work to enable the objective detection of treatment changes in cardiac physiology as measured by positron tomography. Parameters defining the position and angular orientation of the left ventricle have been estimated directly from the measured transaxial tomograms of FDG and ^{13}N-labelled ammonia uptake. These parameters are used to resection the measured image volume, and thus present the distribution of uptake in the left ventricle in the standard format. The accuracy and precision of the estimated parameters have been verified using a cardiac phantom as an approximation of the normal left ventricular shape and uptake distribution. Sensitivity to deviations from this ideal were investigated using FDG studies from patients with significant coronary artery disease.

The automated analysis of the drug study presented in Chapter 5 provided a further validation that the reorientation techniques are applicable to a general population of patients with coronary artery disease. The results of this analysis also provided evidence that small changes in myocardial blood flow can be detected using quantitative measurements of flow, in ischemic tissue regions identified at rest. Significant regional differences in relative blood flow were also detected and verified using the single subject analysis introduced in Chapter 4.

In this chapter, the results of the automated analyses developed in this work are discussed and compared to results from other manual or semi-automated techniques reported in the literature. Recommendations for future work in the detection of treatment responses with cardiac positron tomography, are discussed at the end of the chapter.

6.1 Reorientation

Accuracy and Precision

The accuracy and precision of the reorientation parameters (Figure 4.2) is shown to be excellent for the cardiac phantom; which has a uniform distribution of activity and regular shape. The effects of shape and uptake variations as well as ventricular blood pool activity can be subjectively evaluated using the SNR of Equation 4.6. Deviation of the ventricular shape from the elliptical model increases the variance of the pixels within the modelled myocardium, and therefore decreases the SNR. Uptake defects also decrease the SNR for the same reason, whereas blood pool activity in the ventricular chamber decreases contrast and therefore decreases the SNR. Ventricular motion during the cardiac cycle tends to decrease the measured myocardial concentration, but the effect on SNR was not explicitly determined in this work.

The reorientation parameters are insensitive to changes in left ventricular shape and to FDG uptake defects caused by heart disease, as shown in Table 4.2 and Figure 4.3. Patient 1 has a lateral defect which is visualized on the short axis section of Figure 4.3A. There is no distortion of shape either on the transaxial or the long axis images resulting in the excellent ellipse fits. The SNR equals 16, which is the highest value of the 6 patients analysed. The left ventricle in the studies of patients 2 and 6 may have been truncated inferiorly (Figures 4.3B,F). This does not appear to cause any error on the long axis fits, because the short axis sections are still well centered. Similar performance is obtained for the study of patient 4, whose left ventricle was truncated at the superior aspect (Figure 4.3D). Patient 3 has a large inferior defect as well as absent septal uptake at the cardiac base. Even with this large uptake defect, the parameter values are still precisely defined, and the short axis sections appear to be properly centered. There is a large distortion of shape on the superior aspect transaxial images of this patient. This does not affect the results since a mid-ventricular section is used to find the axial angle (Figure 4.3C). A moderate apical defect in FDG uptake is present in patient 5 (Figure 4.3E). Again, this does not

increase the variance of the extent estimate of the myocardium; even though there is no fixed end point to fit the ellipse on the long axis section, the technique still performs well because enough shape information is present. This patient also has a severe septal defect, which could cause an underestimation of the extent of the LV if the long axis section is taken too far on the septal side. However this implies a very poor fit on the transaxial image which is not observed in any of these studies. The increased extent variance observed in this patient is not due to the apical uptake defect as might be expected. There is a gross distortion of shape, combined with an anterior defect on the superior and mid-ventricular transaxial images. This caused an underestimation of the axial angle from the (noisy) first 5 min scan, which subsequently caused an underestimation of the extent on the long axis section.

The low SNR in these patient studies is due to the low overall uptake in the diseased state, and the short 5 min scan time. Nevertheless, the variation in the parameter values is comparable to those of the phantom study, where the average SNR is higher, there is no motion and no variation in shape or activity distribution. For a given human study, precision can be estimated using the measured SNR and phantom results of Figure 4.2.

Ellipsoid Model of the Left Ventricle

The three dimensional model of the myocardium implies that the expected axial distribution is unimodal; which is true if there is no significant uptake in the lungs or liver. This is a valid assumption for FDG studies, because the left ventricle normally accumulates this tracer at a higher rate per unit volume than any of the neighboring tissues, and therefore has a higher isotope concentration (Bq/cc) than any of the surrounding tissues. When the technique is used for ^{13}N-labelled ammonia studies, this assumption may be invalid; the axial distribution can be bimodal if there is significant uptake in the lungs or liver. In this case Equations 4.1 to 4.3 are modified to select an appropriate transaxial image. Equation 4.1 is divided by the square root of the total counts in the left half of each image, to remove a second peak corresponding to the

liver. Initial experience with images using tracers other than FDG, including ^{13}N-ammonia, ^{18}F-dopamine and ^{11}C-acetate indicates that this modified equation is generally applicable.

The long axis section of the left ventricle is modelled as 2/3 of an ellipse. This value was selected because it produced the highest correlation coefficient (Equation 4.5) for several normal FDG studies. This proportion has not been established as the optimum value for the whole population, but a semi-ellipse is likely too small, judging from Figure 4.3A for example. The basal narrowing may be due to decreased ventricular motion in the valve plane.

Variation in shape of the left ventricle is an important factor affecting the precision of the automatic reorientation. It was observed that the superior aspect transaxial sections often have more distortion in shape than mid-ventricular sections. It is important not to use superior aspect images to determine the axial angle, even though the left ventricle in these sections appears elliptical in normal subjects. In severely diseased hearts, this effect is minimized by using Equations 4.1 to 4.3 to select the appropriate (FDG) transaxial image. In addition, transaxial smoothing reduces the effect of distortions by making the shape more elliptical, thereby improving the precision of the fit. The extent of the smoothing filter used on the long axis sections is smaller than the effective resolution of these images, given the blurring effect caused by the motion of the heart during the cardiac cycle. Therefore, the noise is preferentially attenuated and the SNR increases. The smoothing filter extents of 12 mm FWHM (transaxial) and 6 mm FWHM (long axis) were chosen somewhat arbitrarily. These values are not necessarily optimal, however more transaxial smoothing seems to be necessary to reduce distortions of left ventricular shape. There is less variation is shape observed on the long axis sections, except on the inferior aspect of the cardiac base. This again supports the choice of the ellipsoid model to determine the long axis angle and extent.

Uptake defects do not have a large influence on the accuracy or precision of the reorientation parameters using the ellipsoid model of the LV myocardium. As long as there is enough shape information defined by the myocardium, an ellipsoid model

can be fitted. The precision of the axial angle is larger than the sagittal angle (Figure 4.2) because the eccentricity of the ellipse is smaller on the transaxial images than on the long axis images. When the images are noisy, angles can be determined more precisely with a more elliptical shape. On the long axis images, the endpoints of the basal LV myocardium also serve to orient the truncated elliptical model (Figure 4.1E).

Quality Assurance Outputs

There are two stages of quality assurance output which are generated to verify the automated reorientation and regional analysis. The first stage is during the determination of the long axis of the left ventricle. Long and short axis sections are displayed, and the SNR is estimated. The distortion from normal ventricular shape can be visualized from the transaxial and long axis sections. The angular accuracy can be assessed from the short axis section which should be well centered. The SNR provides a measure of confidence with which to assess this procedure. The SNRs of all the drug study scans are tabulated in Appendix C.1. The average SNR of the FDG scans was 9.9±2.9 (n=14), versus 7.9±2.6 for the ammonia studies (n=28). It was found that FDG studies with a SNR below a value of approximately 5 were not visually interpretable. One such scan was still included in the automated drug study analysis of Chapter 5: FDG SNR(P6) = 3.4.

The second stage of QA output is used to verify the accurate estimation of isotope concentrations in the myocardium and in the cavity (arterial blood) of the LV. The spatial and temporal resolution of PET is not sufficient to quantify the activity in the myocardium routinely. Therefore, the maximum count density is used to estimate the regional myocardial activity, which assumes *uniform* thickness and motion of the myocardium. This method is coupled with a shape continuity constraint (section 4.2) to estimate activity in low count regions (uptake defects) where the maximum myocardial activity is not measurable above background levels. This search strategy is not trivial, and is therefore verified with suitable QA output (Figure 4.7). The positions (radii) of the maximum activity regions are superimposed on the short axis

sections of the myocardium. This verifies that the regions correspond to the centre of the myocardium and not to liver tissue adjacent to an inferior uptake defect, for example. If an inaccuracy is observed then the invalid data may be removed, or the positions of the regions altered manually. In the drug study analysis of the 28 ammonia scans in diseased hearts presented in Chapter 5, no serious positional errors were observed.

The position and extent of the left ventricular blood pool region is verified on the same short axis sections used for QA of the myocardial regions (Figure 4.7). A central region at the base of the left ventricle is easily positioned, because the extent of the heart is known from the reorientation, and the position of the myocardium has been identified on the standard set of short axis sections. Blood regions defined in this manner were of excellent quality (Figure 4.9) with a single high peak, often followed by a small secondary peak, and a smooth decrease to a low background level. Arterial blood regions in the left atrium were of lower quality because of spillover from myocardial tissue around the smaller atrial cavity.

Three Dimensional Registration

The automated technique developed in Chapter 4 uses the image correlation coefficient (Equation 4.5) as a measure of similarity between the ellipsoid model and the measured myocardial isotope concentration. Bettinardi et al (1993) used the correlation coefficient to register repeated transmission images of the chest from the same subject. They reported average coordinate and angular errors of 2.5 mm and 1 degree respectively. Bacharach et al (1993) used a similar technique and reported errors of 1 mm and 1.5 degrees. Hoh et al (1993) evaluated two similarity measures (other than the correlation coefficient) used to register cardiac ammonia studies from the same subject, and reported average errors below 1±1 mm and 1±1 degree. These methods also worked well for studies with low count rate and simulated uptake defects. This confirms the findings from the patient studies in Chapter 4; that registration using the volume correlation coefficient is insensitive to SNR. Rusinek et al (1993)

compared surface fitting (Pellizarri 1989) with the principal axis technique (Alpert 1990) for volume registration of multimodal brain scans from the same subject. This group found the average error for both techniques to be 1 to 2 mm under ideal conditions. Local deformations of shape were found to increase the registration error. This was confirmed in the present study where the average precision for the axial angle was larger than for the sagittal angle because of greater deviation in shape from the elliptical model.

In summary, the automated method of registration developed in Chapter 4 achieves results comparable to methods reported previously, which have focused on the registration of image volumes from the *same* subject. The registration of measured cardiac studies with an ellipsoid model as developed in the present work is inherently a more difficult problem because the two datasets being matched are known *not* to be identical. A model based approach has also been used to detect the epicardial and endocardial surfaces of the myocardium on SPECT and MRI short axis sections (Faber 1991a,1991b,1995). Surface coordinates were registered to within an average of 2.7 mm, *after* the transaxial images had been resectioned into the standard short axis views. The advantage of the method developed in Chapter 4 is that the intensity data is used directly, without the need for surface detection prior to registration. The results shown in Table 4.2 show that comparable coordinate errors of 1 to 2 mm are still obtained, with larger angular errors of 3.3 degrees in the transaxial plane only. This indicates that the shape of the left ventricle can be accurately modelled with a three dimensional ellipsoid, and its orientation and extent can be determined directly from a measured volume dataset.

The reproducibility of manual identification of the long axis angles was evaluated by He et al (1991). This group reported that the interoperator variability decreased from approximately 3.4±5.9 degrees to 0.6±2.7 degrees when using a semi-automated technique, which still required manual selection of an appropriate transaxial section, as well as the apical and basal limits of the LV myocardium. The technique developed in Chapter 4 is totally automated and has an average angular variability of 0.0±2.4 degrees.

Three dimensional analysis is necessary to visualize regional metabolic processes accurately in the myocardium of the left ventricle. Hicks et al (1989) used a semi-automated analysis with a polar map display of ^{82}Rb and ^{13}N-labelled ammonia uptake to visualize changes between pairs of studies on a given patient. This was used to look for changes between rest and stress, perfusion and metabolic studies, early and late ^{82}Rb images to assess myocardial viability. Laubenbacher et al (1993) also used a semi-automated 3-D analysis procedure to correlate regional perfusion with angiographically determined stenosis diameter in coronary artery disease. Both of these methods required some operator intervention to reorient and/or resection the images of the LV myocardium before the regional analysis was performed, and were therefore subject to intraoperator and interoperator variabilities. The technique developed in the present work being totally automated, removes these components from the error variance.

6.2 Population Study

Ischemic Indices

The hypothesis tested in the drug study analysis of Chapter 5, was that blood flow to ischemic myocardium is altered by nitroglycerin. Therefore it was necessary to verify that the regions chosen were in fact ischemic and corresponded to regions of increased flow with drug treatment. Graphical QA output was generated, consisting of polar plots showing the largest ischemic regions and the relative flow change (treatment/baseline). The degree to which these maps corresponded represented the positive predicted effect (Figure 5.2).

An index of ischemia was used to identify regions with predicted blood flow changes due to treatment. Viable myocardium which is moderately to severely ischemic can be detected at rest by perfusion/metabolic imaging with PET. The subjects in the drug study all had moderate to severe CAD, with stenosis greater than 50% of at least one coronary artery. In many cases the estimated extent of ischemic

myocardium was small, and in three cases was absent. This is due in part to the low SNR of many of the ammonia and FDG studies. The segmentation of myocardial sectors into normal and low classes, accounts for variations in SNR by varying the threshold according to the sampling statistics as described in Chapter 4 (Figure 4.10). A very noisy study will have a large variance of *normal* uptake, which makes it less likely to find *low* values greater than 2 SD below the normal value. The FDG study of subject P6 had the lowest SNR of all the FDG studies. No ischemic region is identified in this subject, possibly because of the large variance of the segmented normal sectors. The two other studies with absent ischemic areas had suitable SNRs. Subject D2 had high SNRs on the FDG (12.9) and ammonia (6.2, 9.6) images. The baseline ammonia and FDG distributions were very well matched, and demonstrated no regions of marked ischemia. The subject P2 had a high FDG SNR (12.3) and average ammonia SNRs (7.6, 6.8). There was a large area with a small relative degree of ischemia, which was visually apparent on the QA output (Appendix C.2), however the magnitude of ischemia in this subject was not outside the estimated normal range.

The automated analysis developed in Chapter 4 tends to locate small regions of relatively severe ischemia. This differs from other techniques reported which typically classify tissue as ischemic (viable), normal or scar. Camici et al (1986) identified ischemic tissue regions as reductions in flow relative to baseline, induced by exercise. This technique was not appropriate for the drug study analysis of Chapter 5, because all flow measurements were made at rest. Other groups use differences or ratios of metabolic and flow images, thresholded at presumed normal values (Bonow 1991, Tillisch 1986). However, these normal values are determined either using a database of normal subjects, or from a maximum (presumed normal) flow region. Use of a normal database requires several assumptions which are not appropriate for the detection of treatment changes; these will be discussed in the next section. The use of a reference flow image to establish normal FDG values is very useful clinically. Initial observations from data used in the drug study analysis showed that this method generally increased the size of the ischemic regions, and reduced the statistical significance of the semi-quantitative flow measures presented in Table 5.1. This may

indicate that large areas of ischemic but viable myocardium were present in most subjects, but the drug only produced a significant flow increase in the most severely ischemic regions.

Quantitative Analysis of MBF

Results from the drug study analysis in Chapter 5 showed that small differences in myocardial blood flow are detectable under resting conditions, using an automated and quantitative analysis. The semi-quantitative measures of MBF examined in this study all had increased error variance relative to the magnitude of changes detected (Table 5.1), resulting in the low statistical significance of drug-placebo differences. These measures were not able to account for variations in tracer delivery and uptake, resulting in significant measurement noise. The noise was reduced with the quantitative compartmental analysis, which used the time course of radioactivity in the left ventricular arterial blood and in ischemic myocardium.

The results from the automated analysis of the drug study are in agreement with a semi-quantitative analysis of the same study by Fallen et al (1995). These authors used the net retention of ammonia in ischemic myocardium relative to normal myocardium (percent maximum) as a blood flow index. A significant increase over baseline was found in ischemic myocardium with the drug ($p<0.05$), compared to no significant difference with placebo. The automated analysis presented in Chapter 5 found no changes at all in ischemic myocardium using absolute net retention as a measure of blood flow. Also, a significant positive bias was found for both placebo and drug conditions using percent maximum uptake as a blood flow measure. However with the automated compartmental analysis, there was a significant increase in blood flow over baseline, detected in the drug condition. There was also a significant difference between placebo and drug conditions detected with this analysis (Table 5.1); a small difference in K1 of only 16 ml/min/dg between placebo and drug conditions was significant at the $\alpha=0.01$ level. In addition to providing quantitative accuracy, the compartmental analysis of MBF is also more precise.

The use of quantitative flow analysis is supported by the findings of Krivokapich et al (1989) with ^{13}N-labelled ammonia. This group reported a low sensitivity of net retention measurements to the expected increase in MBF induced by exercise. This is due partly to decreased retention at high flow rates, but measurements of net retention also seem to suffer from a relatively large error variance. They reported an increase in net retention of 0.33 /min (1.31±0.35 - 0.98±0.2, n=12; $p2<0.01$) from resting to peak exercise flow. However with a quantitative compartmental analysis, the difference was 0.65 ml/min/g (1.35±0.22 - 0.7±0.17, n=12; $p2<0.00001$), which was much more highly significant.

The precision of graphical analysis (Gambhir 1989, Choi 1993) for the detection of significant treatment changes in MBF has not been specifically reported. This technique may reduce the error variance compared to semi-quantitative methods, because the time course of activity is used from both the arterial blood and from myocardial tissue.

Treatment Changes

Several other studies have been performed to detect changes in myocardial physiology under different treatment conditions. The results of these studies indicate that significant changes in MBF can be detected between groups which have an anatomically diffuse physiological response to treatment. Changes are more difficult to detect when the disease state varies over the extent of the LV. In this case, segmentation of functional tissue types is required to quantify changes with respect to the myocardial tissue of interest. In many of the studies, the statistical significance of change in the given tissue of interest is not reported.

Camici et al (1991b) measured coronary reserve under dipyridamole stress in patients with hypertrophic cardiomyopathy. They compared the hypertrophied septum with the non-hypertrophied LV free wall, and found significant differences in resting and stress MBF, as well as reduced coronary reserve compared to normals. This study is unique in the PET literature in that the regions of disease are also anatomically

distinct. This condition may enable an exploratory analysis of treatment responses with multiple subjects (analogous to the single subject analysis in the present work), because regional segmentation of specific tissue types is not required to compare results between subjects.

Preliminary results have been reported on the effects of adrenergic tone on blood flow in women with syndrome X (Camici 1991a). This disease process is widespread throughout the heart, and does not require tissue type segmentation to compare results between subjects. Significantly increased MBF is reported by this group using stress flow imaging, in subjects with alpha-1 blocker treatment. In this study statistical significance is properly assessed, and a significant treatment effect is reported using a stress-to-rest ratio of coronary reserve.

The response of MBF to exercise in cardiac transplant patients has been compared to that in normal volunteers by Krivokapich et al (1991). Anatomic regions can be compared between samples, again because the entire heart in each of the two groups is considered to be different. This group reported no difference in MBF at peak exercise, and a significant difference in the exercise-to-rest ratio between the two groups.

Measurement of coronary reserve is the most common test of differences in blood flow (Hutchins 1990, Krivokapich 1989). In healthy subjects, large increases in MBF are typically reported with relatively low variance. In this case, statistical significance is assumed to be obvious and the specific level is not assessed. However in subjects with coronary artery disease, the increases are often small and may not be statistically significant. Therefore in regions where there is poor uptake and corresponding poor image quality, it may not be possible to evaluate coronary reserve. It is necessary to attach a level of certainty to these measured changes, as performed by the single subject analysis developed in the present work.

Coronary reserve distal to a stenosis was evaluated relative to normal myocardium by Goldstein et al (1987), who found that changes in perfusion reserve correlated highly with changes in stenosis area after PTCA. Myocardial regions were

selected manually, but an automated segmentation of the desired tissues could have been used to remove operator variabilities, as performed in the present work.

Size and severity of coronary reserve abnormalities (above a threshold compared to normal) have been used to quantify changes induced by cholesterol lowering treatment (Gould 1994). This analysis was performed using an objective automated technique with good clinical utility. However, no direct assessment was made of the statistical significance of the stress-induced perfusion defects. Semi-quantitative normalizations of MBF were performed to combine results from different subjects. The power of such comparisons may be improved by quantitative analysis of regional flow differences and by analysing functional tissue types as a group, as demonstrated by the results of the drug study analysis performed in the present work. It may also be possible to quantitatively monitor the effects of such treatments on a patient by patient basis. Hicks et al (1989) used a visual comparison of serial flow images in single subjects, to assess the progression or regression of disease, and myocardial viability. However, no statistical comparisons were made, i.e. it was assumed that there was practically no variation in the measurements.

Walsh et al (1990) compared qualitative and quantitative measures of MBF before and after angioplasty, and demonstrated restoration of uniform blood flow after treatment. Before angioplasty, significant differences were found between regions proximal (normal) versus distal (low flow) to a stenosis. After successful angioplasty, these differences were no longer significant. Region selection was performed manually, and the treatment effect was not specifically tested in the sample, nor in individuals.

Changes in myocardial perfusion and oxidative metabolism after thrombolytic therapy were assessed quantitatively by Henes et al (1990). Jeopardized zones of myocardium were again selected manually from ^{11}C-acetate images, early after myocardial infarction. This group found no significant differences in perfusion early after thrombolysis, but did report a significant difference in oxidative metabolism between jeopardized and normal regions. The treatment effect was assessed using a relative (percent normal) index, and showed an increase in oxidative metabolism in jeopardized regions after therapy. However, absolute differences were not assessed and

the reported increase actually resulted from a highly significant ($p2<0.01$) decrease in the normal regions. Single subject changes are also shown without any statistical analysis.

There is a trend in many of these studies examining the treatment of ischemic heart disease to report changes using relative measurements which produce significant results, but which are not of primary interest; few answer the most important question: "Was there a specific treatment effect on the measured variables?". A tabular presentation of results is often omitted, precluding independent statistical analysis. These issues were addressed in the analysis of the drug study presented in Chapter 5, comparing baseline with treatment blood flow under placebo and drug conditions. An objective measure of ischemia was used to segment functional tissue regions of the left ventricle, which was necessary to compare results between multiple subjects.

6.3 Single Subject Studies

Normal Databases

It is common to compare a single subject's scan to a normal database. This is essentially a z-test of the hypothesis that a given subject has normal distribution of function in the myocardium. Blood flow distributions measured during pharmacologic stress show gross abnormalities in blood flow compared to a normal database, which can be correlated with CAD location and severity (Laubenbacher 1993). Blackout displays can be used to visualize and quantify the extent and severity of CAD (Hicks 1989). This visual display is also used to monitor the progression/regression of disease in single subjects; static scans are acquired and absolute and relative ratios displayed to localize regions of change. This technique has good localizing power, but is not able to assess the significance of change in a single subject. The techniques reported by Hicks et al (1989) and by Laubenbacher et al (1993) are shown to work well for PET data with high SNR, however there is no description of the effect of noise on the performance of these methods. Comparing studies to a normal database assumes

minimal regional variance in the measured sector data. In effect, all sectors are assumed to be measured with a uniform error variance which is identically equal to zero. This is clearly impossible in practice, as there is always some measurement uncertainty caused by counting statistics. In the extreme, a very noisy study can not provide diagnostic information without first smoothing to increase the SNR. For example, the blackout display of Hicks et al (1989) generated from a low count ^{82}Rb study, would have many small regions fall outside of the normal uptake range. Furthermore, the error variance is known to vary with the regional mean activity. It is important to incorporate this regional variation of the measured data when performing statistical analysis. The most sensitive way is to do this sector by sector, and to include only pure measurement error with little or no physiological variation, as in the single subject analysis developed in Chapter 4.

The significance of changes resulting from the treatment of heart disease should not be assessed using normal databases. Blood flow under treatment may *not* be very different from the normal range, but may be *very* different from a baseline scan in the same individual. Conversely, baseline and treatment scans may both be different from normal, but not significantly different from each other. Groups of subjects must be studied under different treatment conditions and compared directly, in order to assess a given treatment. Alternatively, subjects can be used as their own controls and studied under both conditions. This is preferable if it is practically feasible, because observed changes typically have greater statistical significance using a paired design.

The single subject (volumetric) analysis developed in the present work differs fundamentally from those previously published. Two independent samples are taken under physiologically steady-state conditions, and compared sector by sector using paired t-tests. In a clinical setting, uptake is often severely compromised in diseased hearts resulting in very noisy, low count, low SNR studies; this can preclude effective visual interpretation. The automated method improves the SNR with smoothing, localizes significant changes, and generates graphical and numerical QA outputs which allow the investigator or clinician to view and verify the results easily.

Single subject changes were reported by Fallen et al (1995), comparing 20 min static ammonia images, normalized by the blood curve integral. Two polar maps were presented: one before and one after drug treatment, showing an obvious regional increase in blood flow. Intuitively this represents a highly significant result, yet no statistical significance was reported for this specific case. The single subject analysis presented in Chapter 5, automatically identified a similar region of increased flow using independent scans of 80 s total duration. The analysis also provided some information about the approximate extent of the ischemic region, and most importantly estimated the statistical significance of the treatment effect.

Statistical Models of Change

The statistical model of the single-subject analysis developed in this work attempts to locate regions of the LV which respond (to treatment) differently from the mean. The basic requirement of the model is to measure both the mean and the variance of some physiological variable (such as MBF) under two different conditions, and then to perform regional statistical comparisons between these two measurements. The single subject analysis in Chapter 5 was performed to demonstrate an application of this method; a significant regional increase in ammonia uptake was detected in response to a vasodilating drug in an area of the ventricle known to be ischemic. This type of volumetric comparison of regional measures of left ventricular blood flow or metabolism has not been reported previously.

When using the single subject (volumetric) model developed in Chapter 4, measurements made over the whole left ventricle are assumed to equal the sum of the mean global response plus the local differences relative to the mean. Similarly, the differences between baseline and treatment conditions are assumed to equal the sum of global and local differences. It is probable that differences in global uptake during treatment can mask local differences. Therefore, the measurements are adjusted for the global mean under each condition, such that local differences become more apparent.

Local differences are presented in the original measured units as well as in percent increases over the baseline scan, as shown in Figure 5.5.

The single subject analysis presented in section 5.2 demonstrated how global and local differences are used to characterize changes in MBF as measured with ^{13}N-labelled ammonia. Global uptake of ^{13}N-labelled ammonia is indicative of the overall metabolic demands made on the heart; increase in global flow is seen with exercise or with pharmacologic stress. Apparent changes in global flow can also be caused by inaccurate normalization for the injected dose. Ammonia uptake varies in proportion to the injected dose at rest, and should be adjusted accordingly before a single subject analysis. Detected differences in global uptake (representing flow, concentration, etc.) are only meaningful if both measurements are made on the same scale. In the two subjects analysed in section 5.2, equal doses of ^{13}N-labelled ammonia were administered to each subject therefore no significant difference in global uptake was observed between treatment conditions.

Local uptake can vary independently from the global mean. Myocardial tissues in different states of health or disease, respond differently to treatments. For example, it may be desirable to increase blood flow to ischemic myocardium preferentially, compared to normal or scar tissue. In order to localize such preferential differences, the global treatment effects are first removed by the single subject analysis. This can be done using either an additive or a multiplicative model, i.e. subtract or divide by the respective global mean. An additive model is suitable for this adjustment procedure, as well as for the identification of local changes which are independent of global change (Friston 1990). The additive model developed in Chapter 4 has equal sensitivity for local increases and decreases, and it enables the interpretation of changes on the original measured scale. The additive model tends to identify local regions with a large adjusted *difference* from baseline to treatment, as opposed to those with a large change in *ratio*. Table 6.1 compares the magnitude of changes detected using an additive versus a multiplicative model. The units of the numerical values are arbitrary, but may represent MBF for example. A baseline measurement is set arbitrarily to a global value of 100, with a local decrease (defect) of 50. Then different treatments

(T1-T4) are administered, which are evaluated based on the resulting global and local changes. A large uniform increase in all sectors (T1) would not produce a detected local difference using the additive model (0%). However this seems physiologically unlikely, and only a relatively small deviation from uniformity is required to detect a local difference (T2): such a near-uniform increase is detected equally using an additive or multiplicative model (30% or 35%). On the other hand, a near-proportional increase (T4) may cause a local difference to be masked with a multiplicative model (15%), but is detected much more easily using an additive model (130%).

Table 6.1

Additive versus Multiplicative Adjustments
for the Detection of Local Differences

	Global (Normal)	Local (Defect)	Additive D-N	Multiplicative D/N	Treatment Response
Baseline (B)	100	50	-50	0.5	
Treatment 1 (T1)	200	150	-50	0.75	uniform
difference (T1-B)			0 (0%)*	0.25 (50%)	increase
Treatment 2 (T2)	200	135	-65	0.68	near-uniform
difference (T2-B)			-15 (30%)	0.18 (35%)	increase
Treatment 3 (T3)	200	100	-100	0.5	proportional
difference (T3-B)			-50 (100%)	0.0 (0%)*	increase
Treatment 4 (T4)	200	85	-115	0.43	near-proportional
difference (T4-B)			-65 (130%)	-0.07 (-15%)	increase

*local differences of zero are not detected.

Local changes can be detected equally well with an additive or a multiplicative model in the absence of global change. However, changes are easily interpreted on the original (absolute) scale of measurement, with the traditional (additive) methods of adjustment and statistical testing. Local differences are more easily perceived on a visual display if the magnitude of change is large compared to baseline. An additive

model generally preserves larger local differences when there is a difference in the global mean, as shown by the percent increases over baseline in Table 6.1. An explicit choice between models must be made when there is significant global change between treatment conditions, such as measuring coronary flow reserve. Ideally, the healthy heart should respond to stress with a uniform increase in MBF over a uniform resting distribution. Local departure from this ideal is best shown using a paired design additive model. Note that it is implicitly assumed that the variances of paired measurements are equal. This must be verified if the single subject technique is applied to measurements of coronary reserve, as variance may increase with the mean number of counts.

The concept of local and global differences is similar to the display of absolute and relative uptake by Hicks et al (1989). However in their analyses, multiplicative models are used exclusively, e.g. local uptake is presented as a percent of maximal uptake; relative and absolute ratios are used to evaluate coronary flow reserve with ^{82}Rb and ^{13}N-labelled ammonia. The magnitude of absolute differences is lost using this method, and the significance of change between treatment conditions is not assessed. Instead subjective visual comparisons are made of the polar map distributions and associated statistics.

In certain scanning protocols there may also be global variation within samples. In such cases, a combination of additive and multiplicative models may be appropriate, as with the ANCOVA analysis of brain activation studies (Friston 1990, Silbersweig 1993). With this model, the multiplicative effect of global uptake is removed with linear regression, and the additive treatment effect is assessed using adjusted means, analogous to the single subject method developed in Chapter 4. It is emphasized that multiple subjects can not generally be used to detect treatment changes in the myocardium with the ANCOVA technique of Friston et al (1990), because functionally equivalent tissues are typically not in the same anatomic locations. If large functional tissue regions are selected, e.g. ischemic myocardium, then the assumption of independence of local and global changes is likely violated. In addition, when two or

more of the predictors are correlated, e.g. blocks, covariate, or treatments, ANCOVA (Wildt 1978) can fail algebraically, producing inaccurate results without warning.

Spatial Models of Change

A volumetric model is useful for exploratory analyses of change in the entire left ventricle, in contrast with the region of interest based approach necessary to test differences in functional tissue groups. With the volumetric single subject analysis developed in the present work, isotope concentrations, or derived parameters, are measured in volume elements (sectors) which are approximately 5 mm^3. Then, differences are assessed based on sample statistics under baseline and treatment conditions. Friston et al (1990) have previously used a similar approach to analyse brain activation studies. They used the image pixel as the basic spatial unit of measurement. In the single subject analysis developed in Chapter 4, it was shown that smoothing increases the magnitude of changes relative to the error variance. SNR increases because the noise is reduced to a greater degree than the change magnitude (signal). Smoothing does not markedly affect the sampling distribution of the sectors when no change is present. It does tend to redistribute the sector t-values into larger focal regions when there are changes present. The end result is that local changes become statistically significant over a larger area, thereby decreasing p(LVmap). This finding is in agreement with those of Friston et al (1990).

When a large number of independent comparisons are made, a certain number of significant results are expected by chance. This number equals the α-level times the total number of comparisons; for example when 640 sectors of the LV are compared at an α-level of 0.01, 6.4 sectors are expected to change significantly by chance. The p(LVmap) value represents the probability of finding a given number of significant sectors (or greater) by chance (Friston 1990). If all the comparisons are independent, then a Bonferonni correction can be made to the α-level to account for multiple comparisons. When this correction is used, then individual significant sectors can be reported, otherwise only the LVmap as a whole can be reported. However, it

is known that the individual sectors are not independent, and therefore a Bonferonni correction is too severe. This is intuitively apparent in the smooth appearance of the polar maps. In fact, a smoothness dependent correction of the α-level is required to properly test individual foci of significant change (Friston 1991b). Bonferonni corrections were not used in this study, therefore results should only be reported for the LVmap as a whole. If an anatomic location is identified a-priori, e.g. an ischemic region, then individual significant sectors or foci of change in those areas can be reported at the chosen α-level.

6.4 Future Applications

Reorientation Methods

The automated method of analysis has been applied to FDG and ^{13}N-labelled ammonia scanning protocols under steady state conditions. Differences were assessed between resting flow studies, measured on the same (qualitative) scale in single subjects, and measured on an absolute (quantitative) scale in multiple subjects. High SNR images of FDG uptake were used to determine initial reorientation parameters. Significant results have been obtained without any operator intervention, using analysis tools specifically designed for this experimental design, i.e. placebo-control evaluation of drug-induced MBF changes to ischemic tissue. These tools are directly applicable to studies with the same design, but may be made more generally applicable with several enhancements.

There are many tracers available to study myocardial blood flow and metabolism. FDG typically produces images with higher contrast and SNR than other tracers. If no FDG study is available to compute the reorientation angles and extent of the LV (as described in section 5.1), it may be desireable to average several adjacent slices in order to obtain suitable transaxial and long axis sections. Compensation for low SNRs may be achieved by averaging several midventricular transaxial images, instead of simply selecting one image (Equation 4.3) for the

estimation of the transaxial LV orientation. Similar averaging of long axis sections may prove useful to reduce the noise sensitivity of the automated LV reorientation.

Tracers other than FDG may not produce a unimodal axial distribution of counts which is implied by the use of Equation 4.3 to select the initial midventricular image for reorientation. Modifications have been made in Equations 4.1 to 4.3 in order to compensate for tracer uptake in the lungs and liver. This technique appears to be generally applicable, but has not been formally tested for different tracers.

The sensitivity to inaccurate reorientation has not been established for the single subject analysis. Methods were chosen to minimize ring artifacts around the polar maps, which typically resulted from misregistration. Large errors in LV orientation and position cause a misregistration of baseline and treatment scans, and may cause apparent significant differences (false positives). False positives were observed in the apical region of the cardiac phantom (Figure 4.12); these resulted from a poor fit of the elliptical model to the cylindrical shape of the phantom. This increases the false positive rate over that expected by chance, and thereby falsely lowers the p(LVmap) value. This effect may be more pronounced at the base of the heart, where angular and extent registration errors are typically manifested. The precision of the method should be established for a low SNR tracer, and the effects on the single subject analysis should be characterized.

Samples of N=4 were chosen for the single subject comparisons of blood flow based on the scanning protocol used to perform the original drug study. This frame rate and total scanning time are likely not optimal for the detection of significant differences. For a given total scanning time under steady state metabolic conditions, there is a frame rate which will minimize the standard error of the measurements, and thereby maximize the significance of any differences. Initial observations indicate that the regional variance in myocardial sectors does *not* increase in proportion to the total measured counts (frame time), as predicted by Poisson statistics. Practically, this means that more highly significant results may be obtained by using a larger number of short frames within a given total scanning time.

Single Subject Protocols

The single subject analysis can be applied to any imaging protocol where the following three requirements are satisfied. First, measurements under baseline and treatment conditions must be on the same scale, which can be qualitative or quantitative. Second, paired design measurements are assumed to be sampled from distributions with equal variance. The paired t-test is relatively insensitive to moderate deviations from this assumption, therefore changes in rest to stress blood flow may still be analysed with this technique. Third, samples must be taken under steady state conditions in order to estimate both the mean and variance of the measurements.

With these basic assumptions stated, several applications may be feasible. Stress-to-rest comparisons as mentioned above, may require quantitative measurements because of the non-linear retention of some tracers at high flow rates. Metabolism to flow differences may be used as an objective marker of ischemia; extent and severity of ischemia could then be assessed as with CAD (Laubenbacher 1993), but without the need for a normal database. It may be possible to use estimated parameters in a single subject analysis if variance estimates are also available, for example kinetic rate constant estimates of MBF with associated error variances (Landaw 1984). Comparisons could then be made between parametric or functional images (polar maps) before and after treatment, if associated error variance images (polar maps) are also estimated.

It may be possible to use the single subject analysis method to monitor the individual progression or treatment of disease, as a diagnostic or preventative tool. It will be important to correlate treatment changes with clinical indices which are directly related to the patient's prognosis. This is the most important indication of a treatment's ultimate usefulness. To prove that single subject analysis is relevant in clinical practice, it will be necessary to demonstrate that physiological changes induced by treatment can be correlated with the changes measured by PET.

Population Studies

There are two important differences between the single subject analysis of MBF and that of population samples. The first difference is in the assumption that there is no variation in global uptake within a given single subject sample, whereas global uptake can obviously vary in a population sample composed of several subjects. The second difference is that functional tissue regions must often be segmented to combine results from multiple subjects used in population samples. This may be necessary to test a hypothesis specific to that type of tissue, e.g. ischemic myocardium. The drug study analysed in this work is an example of one such experimental design.

Differences in measurements of the entire LV myocardium can be compared between subjects if the treatment affects the heart as a whole and specific tissue types are not targeted. In this case it may seem appropriate to use ANCOVA to adjust local values for inter-subject variations in global uptake. However in this case, differences in the global means would be of primary interest, not the local differences from the global mean as in the single subject analysis. Therefore, a sector by sector analysis of the LV would not be necessary, but only an ANOVA of block (subject) and treatment effects. The power of the single subject analysis arises from paired design, and the ability to adjust for global differences to localize significant regional differences. This localizing power is not available in most population sample studies because the locations of regional differences typically vary between subjects.

Standard methods of tissue type segmentation will enable automated and objective evaluation of treatment responses in functional tissues of interest. The ischemic index used in the present work segments one such tissue type, representing severely ischemic myocardium. Accepted methods of selecting normal, mildly ischemic, hibernating, stunned, or necrotic myocardial regions, will enable standardized evaluation of treatment effects in a clinical setting.

SPECT Imaging

Quantitative SPECT provided the historical origin for normal database comparisons in PET (van Train 1986). SPECT measurements are not made on a quantitative scale, and can suffer from attenuation artifact. To overcome this difficulty, secondary measures are quantified such as the location and extent of ventricular uptake which is different from normal. The automated methods of analysis developed in this work are generally applicable to SPECT imaging as well as PET, particularly the detection of single subject changes. Using a subject as his/her own control, the detection of relative baseline to treatment changes is possible even on the qualitative scale of measurement used in SPECT. It would be necessary to perform repeated measurements to estimate regional means and variances; then local differences in regional uptake could be detected relative to the mean uptake in the LV.

Visual analysis is used extensively in SPECT, and in some instances may be as sensitive as an automated analysis for the detection of treatment changes. No direct comparison has been made between a manual analysis and the automated analysis developed in this work. Certainly, an automated detection of the LV orientation would reduce the error variance in some measurements of LV function with SPECT as well.

CONCLUSION

Regional changes in left ventricular blood flow resulting from the treatment of heart disease have been detected using an automated quantitative analysis of positron tomographic data. The orientation of the left ventricle is estimated directly from the measured transaxial tomograms without any manual interaction, thereby removing operator variability and bias. An ellipsoid model is fitted to the pattern of regional tracer uptake in the left ventricular myocardium; this technique produces accurate and precise estimates of the reorientation parameters, even using patient scans which have marked uptake defects of FDG or ^{13}N-labelled ammonia. Transaxial tomograms are automatically resectioned into standard short axis images which are used for quality assurance and for the estimation of arterial blood and regional myocardial isotope concentrations.

Severely ischemic myocardium is detected at rest using an automated analysis of the ratio of FDG to ammonia uptake. Significant changes in myocardial blood flow in response to drug treatment were detected in these ischemic regions using a quantitative tracer kinetic analysis of population samples. Significant regional changes were also detected in individuals, using a statistical comparison of a baseline scan of ^{13}N-labelled ammonia uptake to a scan performed after treatment with a vasodilating drug. This single subject analysis is based on an additive model of local and global changes, and demonstrated increased uptake in a region of ventricular myocardium known to be ischemic. Additional research will determine the full potential of the single subject analysis developed in this work. The technique may help to utilize more fully the sensitivity of positron tomography to detect changes in cardiac physiology which result from the treatment of heart disease.

APPENDIX A
Experimental Methods

A.1 Data Acquisition

Positron tomography was performed using the ECAT 953/31 (Siemens/CTI, Knoxville TN) at McMaster University. This scanner has a spatial resolution of approximately 5.5 mm FWHM in all three dimensions. A total of 31 transaxial tomograms are produced within the axial field of view of 10.4 cm. All images were reconstructed using a Hann window of the ramp filter with a cutoff frequency of 0.5 cycles/pixel. The entire chest cavity was centered in each 128×128 image matrix with a pixel size of 2 mm (zoom=2). Blank and transmission measurements were acquired using ring source of $^{68}Ge/^{68}Ga$. Attenuation correction was performed using the ratio of blank to transmission scans acquired on the same day.

A.2 Phantom Studies

Reorientation Precision and Accuracy (hpten%)

A cardiac phantom (Data Spectrum Corp, Chapel Hill, N.C.) was inserted inside a 20 cm diameter water filled cylinder, which was approximately 30 cm in length. The phantom contained a 1 cm thick and 8.0 cm long myocardial chamber which was oriented at approximately 45 degrees in the axial plane and -45 degrees sagittally. The myocardial chamber was filled with approximately 1.5 μCi/ml of ^{18}F in solution, and the inner chamber was filled with water. A series of 6 identical dynamic scans was performed. The acquisition times of the frames were 600,300,100,60,30 and 10 sec, producing a total of 36 frames in total. The activities at the start of the scans were 1.5,1.25,1.0,0.75,0.5 and 0.25 μCi/ml. A 1 hour transmission scan (2 million counts per plane) was used for attenuation correction of all frames.

This data was used to determine the precision of the reorientation with varying SNR. Means (and standard deviations) of the parameter values were calculated for the 36 phantom studies. Accuracy of the parameters (angles, extent, and apical endpoint) was determined by comparing the estimated with the true values using a two-tailed z-test. True values were determined with an interactive three dimensional resectioning system developed in this laboratory. The apex of the left ventricle was used instead of the center coordinate because it is the point on the long axis which is the easiest to identify visually. The true extent of the phantom was measured directly.

Uniform Uptake Cardiac Phantom (hpnorm)

The myocardium compartment of the cardiac phantom was loaded with approximately 1 μCi/ml of ^{18}F in solution. No defects were inserted, therefore uniform concentration was expected in all myocardial sectors. Three dynamic scans were performed: 20 frames x 1 min, 10 frames x 2 min, 5 frames x 4 min. Attenuation correction was performed with a 1 hour transmission scan. Two samples (N=4) of one minute frames were compared to assess the specificity of the volumetric analysis. One minute frames were used to compare with images of the phantom with an anterior defect inserted.

Anterior Defect Cardiac Phantom (hpant)

The myocardium compartment of the cardiac phantom was loaded with approximately 1 μCi/ml of ^{18}F in solution. A solid defect was inserted on the anterior wall. A dynamic scan was performed with the following frame rates: 24 x 15 sec, 12 x 30 sec, 6 x 60 sec, 3 x 120 s. The interplane septa were removed during this scan, the lower energy discriminator was set to 350 keV, and a rotating rod source was used for transmission measurement. One minute frames were compared with the uniform uptake phantom.

A.3 Human Studies

Reorientation

Dynamic scans were analysed from ^{18}F-fluorodeoxyglucose (FDG) studies of 6 patients. Six sequential 5 min scans were obtained 30 to 60 min after injection of 10 to 15 mCi (370 to 540 MBq) of FDG. 30 min transmission scans were used for attenuation correction and had a minimum of 2 million counts per plane. The subject sample was taken from patients with previous myocardial infarction. These cases were selected to evaluate the sensitivity to defects in myocardial uptake and variation in shape of the left ventricle. Locations of the infarct were determined with radionuclide wall motion studies and angiography. Patients 4 and 5 had anterior infarcts and the other patients' infarcts were all inferior. These studies were used to assess the precision of the reorientation procedure.

Normal MBF values

Regions of maximal blood flow were selected manually from the ^{13}N-labelled ammonia scans of 16 patients, separate from those used in the drug study. These regions were approximately 10 mm thick x 20 mm in length, and were assumed to represent regions of normal MBF. Arterial blood curves were obtained manually from small regions near the base of the LV. The two-compartment model of Hutchins et al (1990) was used to estimate K1 [ml/min/g], and k2 [1/min]. The results are tabulated below.

Subject	K1	k2
1	1.00	0.15
2	0.95	0.12
3	0.62	0.09
4	0.72	0.26
5	0.74	0.08
6	0.55	0.22
7	0.80	0.17

8	0.64	0.15
9	1.06	0.18
10	0.87	0.25
11	1.06	0.13
12	0.66	0.18
13	0.69	0.10
14	0.55	0.06
15	1.02	0.11
16	0.73	0.22
mean	0.79	0.15
SD	0.18	0.06

Drug Study Protocol

All patients had at least one coronary artery stenosis of more than 50% lumen diameter, and previous diagnostic evidence of myocardial ischemia. Patients with conditions including acute myocardial infarction, cardiomyopathy, nitrate intolerance or diabetes mellitus were excluded from the study. All cardiac medications were discontinued 48 hours before the start of the study. Transmission scans were performed for 30 min. Baseline dynamic imaging was initiated during intravenous injection of 12 to 15 mCi (440 to 540 MBq) of ^{13}N-labelled ammonia, under resting conditions. The dynamic frame rates were: 12 x 5 sec, 4 x 20 sec, 2 x 60 sec, 1 x 20 min. Half the patients then received Nitro-Dur precordial skin patch (0.4 mg/hr), and half received placebo. Two hours later, they received 50 g of glucose drink (Trutol) to stimulate uptake of FDG. One hour later, a second transmission scan was performed, followed by another 'treatment' dynamic ammonia scan, again under resting conditions. Patients were then injected with 8 to 10 mCi (300 to 370 MBq) of FDG, followed by a 30 min static scan, 45 min later. FDG and baseline ammonia scans were used to identify regions of ischemia, as described in Chapter 4.

Since these patients were resting at the time of the scan, MBF was assumed to be in the normal range, i.e. below 2 ml/min/g. Under these conditions the extraction fraction is assumed to equal 100%. The metabolism of trapped glutamine into glutamate is very slow compared to the length of the scan under normal flow rates

(Hutchins 1990), therefore a second tissue compartment was not included in the compartmental model. Any effective glutamine metabolism (k3) is absorbed into the value of k2. The parameter F_v was included to estimate the regional blood pool fraction which includes both blood pool spillover and intercellular ^{13}N-labelled ammonia. The model parameters (K1,k2,F_v) were estimated by minimizing the residual sum of squares between the measured and modelled myocardial time-activity curves, weighted by the scan time of each frame. The minimization was implemented using the simplex method (MATLAB 1992).

A.4 Simulations

Simulated polar maps were created and analysed to verify the single subject statistical analysis. Samples of N=4 were generated with a mean sector value equal to 5, and an additive gaussian noise model with standard deviation of 1 (20% noise). Variable sized defects of increased or decreased values were introduced to determine the levels of detectability in the presence of noise. Several configurations were tested to mimic expected changes in blood flow at rest. Small (16 sectors) moderate (64 sectors) and large (144 sectors) focal increases and decreases in local activity were generated at 2 levels each (±2,±4 SD), plus a baseline test with no changes for a total of 13 conditions. Because the mean value is set to 5, changes of 2 and 4 standard deviations correspond to absolute changes of 40 and 80 percent respectively. The significance of change in the global value is also reported, e.g. a moderate sized increase of 4 standard deviations will increase the global mean from 5 to 5.4. A two-tailed t-value corresponding to $p<0.001$ was used to test the sector data for significant change. Detectability (sensitivity) of the focal change, global change and significance of the LV polar map as whole p(LVmap) are reported from the average of 50 datasets per condition.

APPENDIX B

Statistical Analysis

B.1 Poisson Distribution of Significant Sectors

The false positive rate for finding significant sectors by chance is tested using the Chi-squared statistic. The mean significance from 50 trials was p(LVmap)=0.74 as reported in Table 4.3. The sample mean and variance of the *number* of significant sectors are 0.56 and 0.58 respectively. The mean number is not significantly different (t_{49}=0.8;p2=0.6) from the number expected (0.001×640=0.64). The expected and observed number of significant pixels are compared using 3 bins:

N	Obs	Exp
0	28	28.56
1	18	16.00
>=2	4	5.44
total	50	50.00

The χ_1^2 value is 0.64 which has one-tailed significance of p=0.45. The null hypothesis is rejected that the data do not follow the Poisson distribution. This verifies that the number of observed significant sectors follows the Poisson distribution under the null hypothesis, i.e. that p(LVmap) is an accurate measure of the statistical significance of the thresholded t-value polar map.

B.2 Treatment Effect t-tests

Statistical tests of Drug versus Placebo conditions were performed using Microsoft EXCEL. Two-tailed significances were reported in Table 5.1 assuming unequal variances.

K1 differences

Placebo	Drug
0.005	0.301
-0.066	0.054
-0.052	0.056
-0.052	0.178
0.009	0.173
	0.037

t-Test: Two-Sample Assuming Equal Variances

	Variable 1	Variable 2
Mean	-0.0312	0.133167
Variance	0.001251	0.010647
Observations	5	6
Pooled Variance	0.006471	
Hypothesized Mean Difference	0	
df	9	
t	-3.37441	
P(T<=t) one-tail	0.0041	
t Critical one-tail	1.833114	
P(T<=t) two-tail	0.008199	
t Critical two-tail	2.262159	

t-Test: Two-Sample Assuming Unequal Variances

	Variable 1	Variable 2
Mean	-0.0312	0.133167
Variance	0.001251	0.010647
Observations	5	6
Pearson Correlation	#N/A	
Pooled Variance	0.006471	
df	6.351239	
t	-3.65292	
P(T<=t) one-tail	0.005335	
t Critical one-tail	1.943181	
P(T<=t) two-tail	0.010669	
t Critical two-tail	2.446914	

Blood Norm (net retention) comparisons

Placebo	Drug
-0.026	0.133
0.066	-0.032
0.061	0.047
-0.039	0.013
0.076	0.057
	-0.02

t-Test: Two-Sample Assuming Unequal Variances

	Variable 1	Variable 2
Mean	0.0276	0.033
Variance	0.00306	0.003641
Observations	5	6
Pearson Correlation	#N/A	
Pooled Variance	0.006471	
df	8.88032	
t	-0.15467	
P(T<=t) one-tail	0.440456	
t Critical one-tail	1.859548	
P(T<=t) two-tail	0.880913	
t Critical two-tail	2.306006	

Max Norm Comparisons

Placebo	Drug
0.025	0.071
0.063	0.055
0.02	0.124
0.035	0.171
0.094	0.144
	0.006

t-Test: Two-Sample Assuming Unequal Variances

	Variable 1	Variable 2
Mean	0.0474	0.095167
Variance	0.000955	0.003823
Observations	5	6
Pearson Correlation	#N/A	
Pooled Variance	0.006471	
df	7.594595	
t	-1.65978	
P(T<=t) one-tail	0.070459	
t Critical one-tail	1.894578	
P(T<=t) two-tail	0.140918	
t Critical two-tail	2.364623	

Dose Norm Comparisons

Placebo	Drug
0.054	0.116
0.225	0.051
0.033	0.595
-0.327	0.98
-0.106	0.934
	-0.283

t-Test: Two-Sample Assuming Unequal Variances

	Variable 1	Variable 2
Mean	-0.0242	0.398833
Variance	0.042467	0.265704
Observations	5	6
Pearson Correlation	#N/A	
Pooled Variance	0.006471	
df	6.789657	
t	-1.84141	
P(T<=t) one-tail	0.057576	
t Critical one-tail	1.943181	
P(T<=t) two-tail	0.115153	
t Critical two-tail	2.446914	

APPENDIX C

Drug Study Results

C.1 MBF Measures in Ischemic Regions

Subject	Scan	SNR	Dose	IschMyo	Blood	MaxMyo	K1	k2
P1	FDG	8.2	14.2					
dr06	BF	5.5	15.0	0.0239	0.0299	0.0413	1.37	0.82
	TF	9.6	15.0	0.0247	0.0319	0.0410	1.37	0.94
P2	FDG	12.3	12.6					
ga07	BF	7.6	15.0	**	0.0439	0.0244		
	TF	6.8	15.0	**	0.0436	0.0236		
P3	FDG	11.8	12.3					
ho09	BF	7.3	12.0	0.0109	0.0479	0.0170	0.53	0.22
	TF	8.3	12.0	0.0136	0.0463	0.0193	0.46	0.21
P4	FDG	12.5	11.9					
so14	BF	9.1	15.0	0.0482	0.1356	0.0857	0.70	0.16
	TF	8.0	15.0	0.0487	0.1169	0.0836	0.65	0.17
P5	FDG	7.3	12.7					
ku16	BF	7.5	13.5	0.0411	0.1448	0.0662	0.49	0.16
	TF	8.3	10.4	0.0282	0.1152	0.0431	0.43	0.13
P6	FDG	3.4	10.3					
ma18	BF	2.2	13.0	**	0.1247	0.0682		
	TF	3.2	13.0	**	0.1257	0.0791		
P7	FDG	12.8	10.5					
pa20	BF	13.1	14.0	0.0489	0.1557	0.0722	0.50	0.07
	TF	11.2	14.0	0.0474	0.1214	0.0615	0.51	0.10
D1	FDG	6.8	13.4					
br05	BF	5.0	13.5	0.0193	0.0526	0.0383	0.73	0.27
	TF	3.8	13.5	0.0209	0.0418	0.0363	1.03	0.28
D2	FDG	12.9	13.6					
ha08	BF	6.2	15.0	**	0.0515	0.0261		
	TF	9.6	15.0	**	0.4917	0.0259		
D3	FDG	10.8	12.3					
le10	BF	11.2	12.0	0.0114	0.0385	0.0254	0.36	0.17
	TF	10.3	12.0	0.0120	0.0454	0.0238	0.42	0.23
D4	FDG	8.9	13.1					
sm13	BF	10.1	15.0	0.0254	0.0971	0.0548	0.38	0.20
	TF	6.4	15.0	0.0344	0.1112	0.0584	0.43	0.15

D5	FDG	12.7	11.5					
mo15	BF	12.1	15.0	0.0386	0.1551	0.0643	0.42	0.17
	TF	9.7	13.0	0.0462	0.1206	0.0600	0.60	0.16
D6	FDG	10.7	10.9					
fo17	BF	5.7	12.5	0.0263	0.1043	0.0537	0.37	0.18
	TF	6.8	12.5	0.0380	0.1230	0.0599	0.54	0.17
D7	FDG	7.4	10.4					
ko19	BF	8.1	14.0	0.0432	0.1382	0.0800	0.42	0.16
	TF	8.0	14.0	0.0392	0.1343	0.0718	0.46	0.14

Subject - P1-P7 (placebo group), D1-D7 (drug group)
FDG - ^{18}F-labelled fluorodeoxyglucose static scan
BF - Baseline ^{13}N-labelled ammonia static scan
TF - Treatment ^{13}N-labelled ammonia static scan (drug or placebo)
Dose - Injected dose of tracer [mCi]
Blood - Blood curve integral from ammonia dynamic scans [1/min]
IschMyo - Ischemic myocardial sector activity in final frame [cps/pixel]
** - No ischemic region detected
MaxMyo - Maximum myocardial sector activity in final frame [cps/pixel]
K1,k2,Fa - Compartmental model parameters of ^{13}N-ammonia kinetics

C.2 Quality Assurance Outputs

Four stages of QA output are provided to verify the analysis of the 14 dynamic FDG and ^{13}N-labelled ammonia studies from the drug study analysed in Chapter 5:

1. Segmentation of ischemic regions, LV blood curves, and visualization of treatment/baseline changes, as in Figure 5.1.

2. Short axis resectioning and identification of the LV myocardial radii:

   TOP: **FDG**
   MID: **BASELINE AMMONIA**
   BOT: **TREATMENT AMMONIA**

3. Results of compartmental modelling of ischemic tissue regions (K1, k2, Fa):

   TOP: **BASELINE AMMONIA**
   BOT: **TREATMENT AMMONIA**

   There were no ischemic tissue regions found for subjects P2, P6, D2.

4. Accuracy of the reorientation parameters:

   TOP: **FDG**
   MID: **BASELINE AMMONIA**
   BOT: **TREATMENT AMMONIA**

Quality Assurance: Subject Drug 1 (D1)

A. FDG

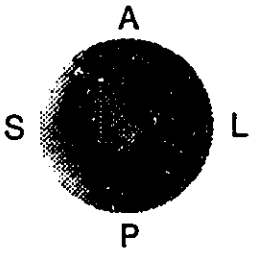

B. Base Flow

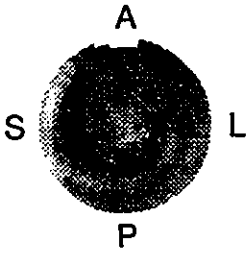

C. Treat Flow

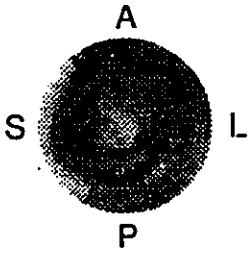

D. Treat/Base

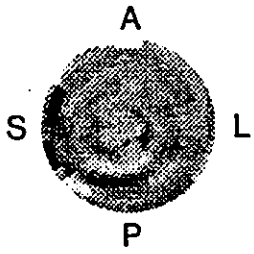

E. FDG/Base

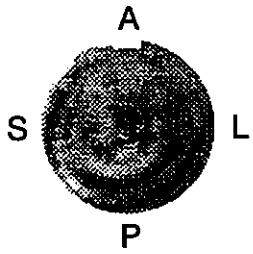

F. FDG/Treat

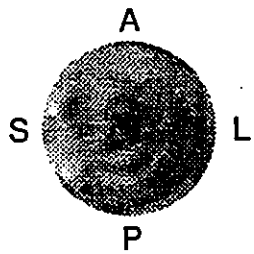

G. LV blood integrals

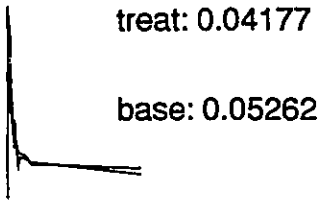

H. Ischemic Regions

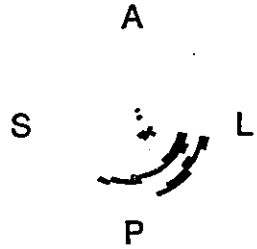

I. Largest Region

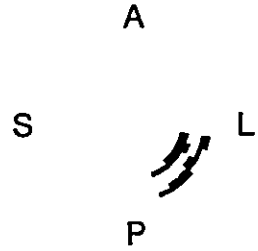

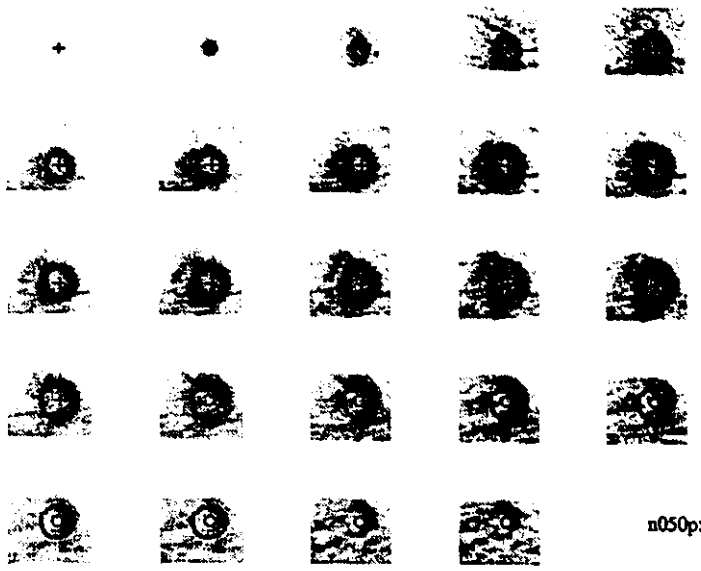

n050pxxf00

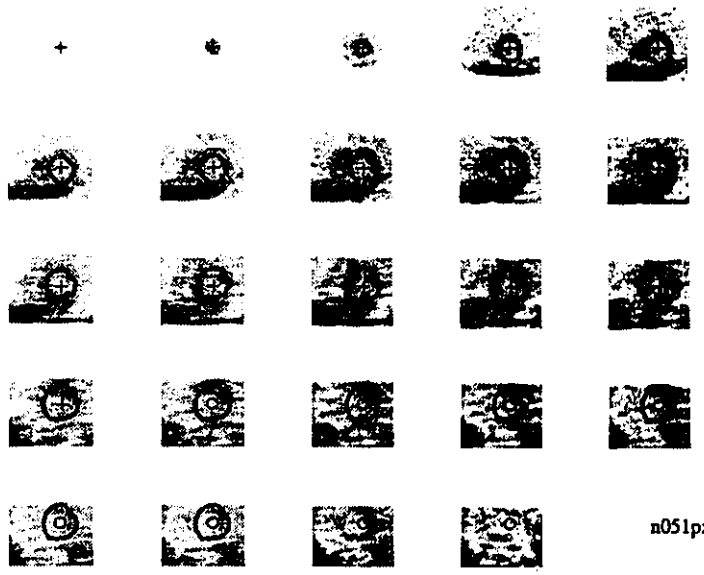

n051pxxf00

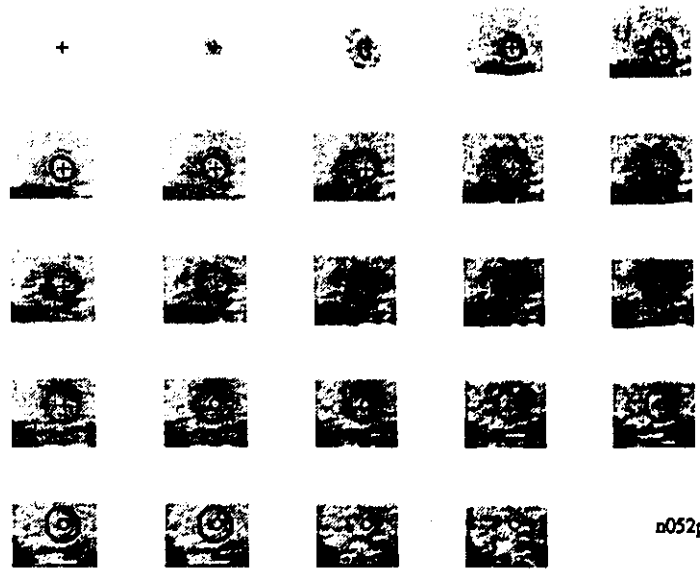

n052pxxf00

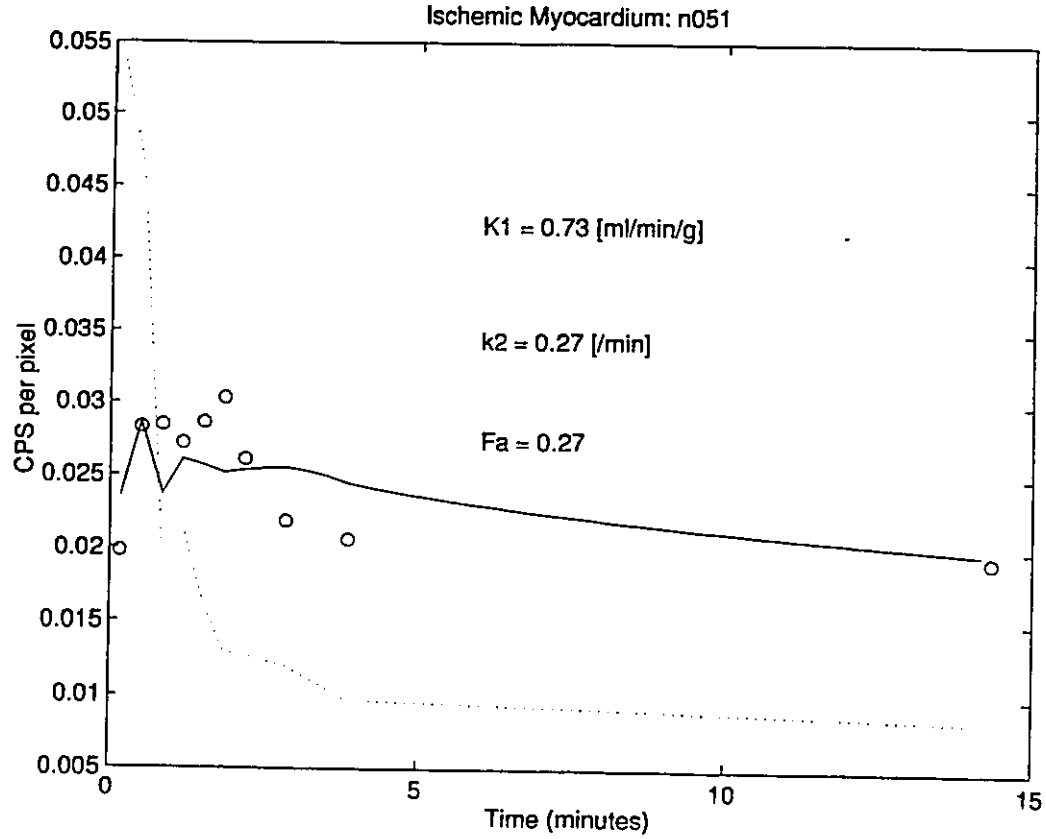
Ischemic Myocardium: n051
K1 = 0.73 [ml/min/g]
k2 = 0.27 [/min]
Fa = 0.27
CPS per pixel
Time (minutes)
0.055
0.05
0.045
0.04
0.035
0.03
0.025
0.02
0.015
0.01
0.005
0
5
10
15

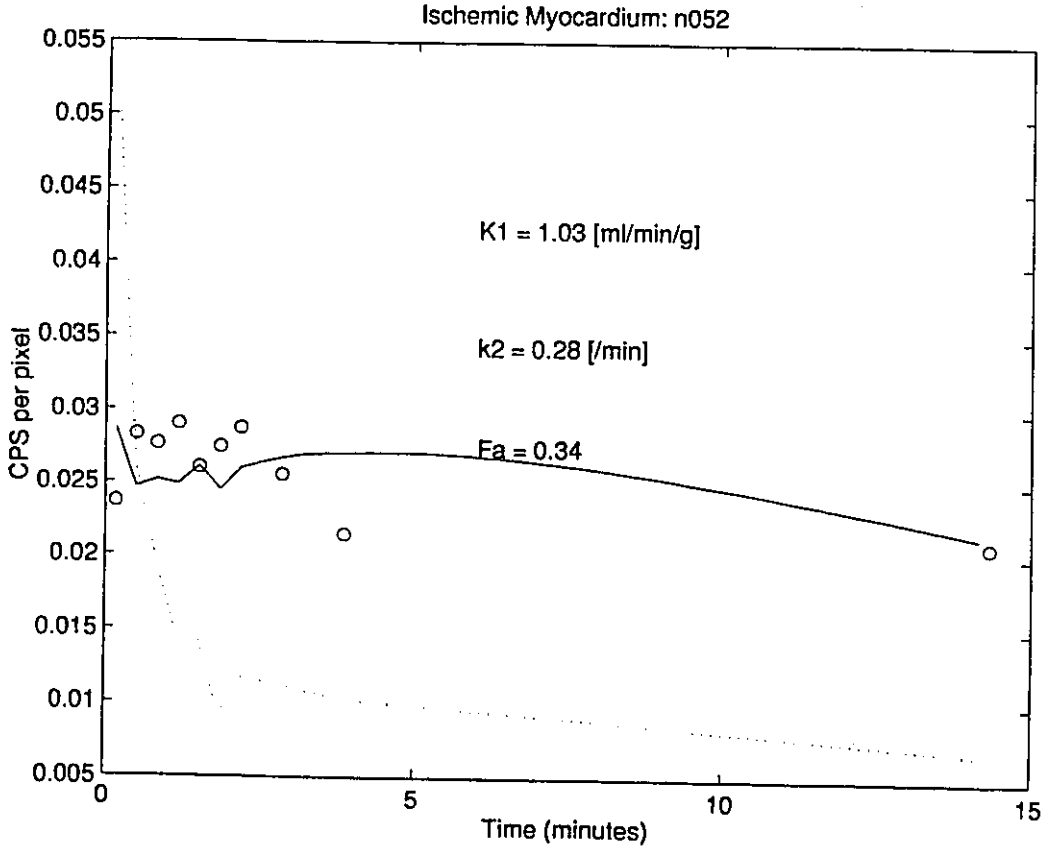
Ischemic Myocardium: n052
K1 = 1.03 [ml/min/g]
k2 = 0.28 [/min]
Fa = 0.34
CPS per pixel
Time (minutes)
0.055
0.05
0.045
0.04
0.035
0.03
0.025
0.02
0.015
0.01
0.005
0
5
10
15

Axial distribution

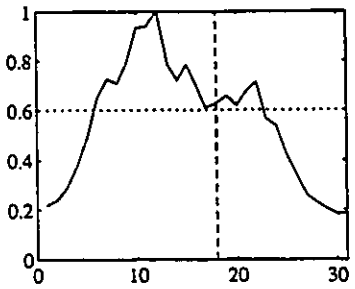

Transaxial Plane 18

Long Axis Section

Short Axis Section

Axial distribution

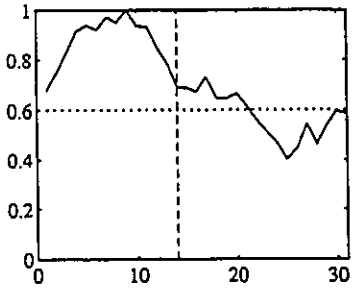

Transaxial Plane 14

Long Axis Section

Short Axis Section

Axial distribution

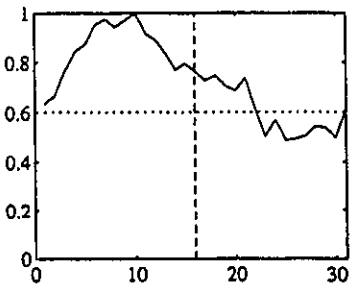

Transaxial Plane 16

Long Axis Section

Short Axis Section

Quality Assurance: Subject Placebo 1 (P1)

A. FDG

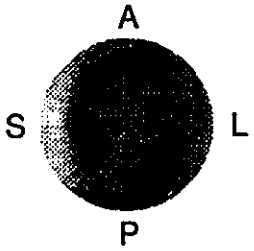

B. Base Flow

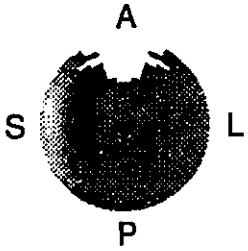

C. Treat Flow

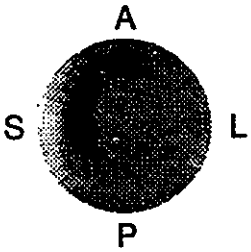

D. Treat/Base

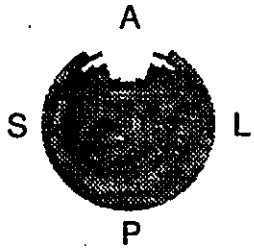

E. FDG/Base

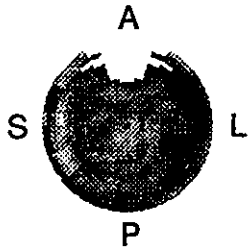

F. FDG/Treat

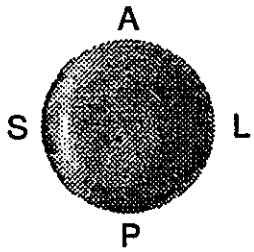

G. LV blood integrals

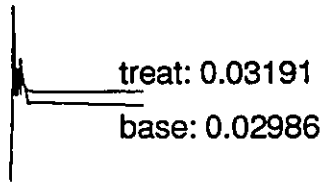

H. Ischemic Regions

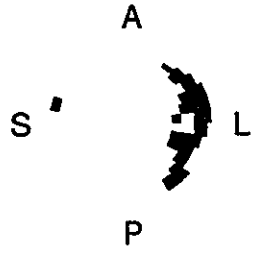

I. Largest Region

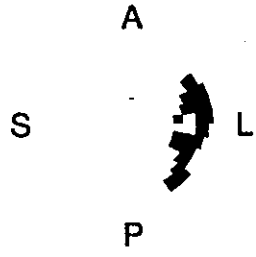

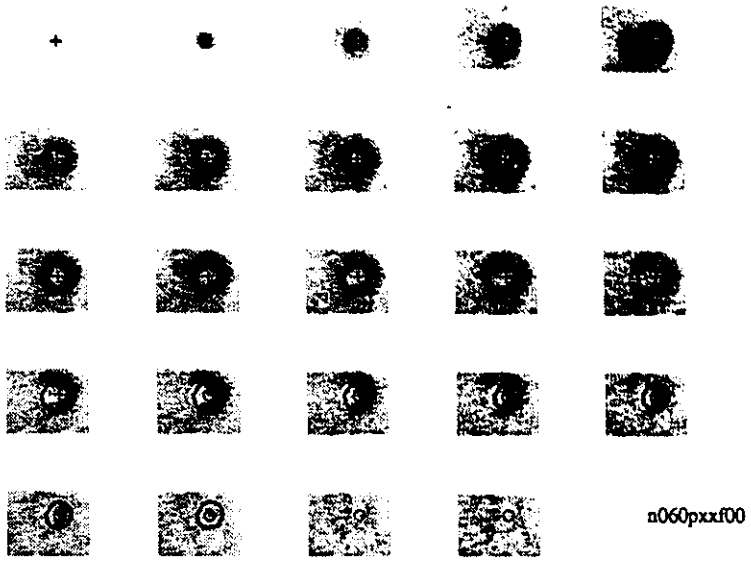
n060pxxf00

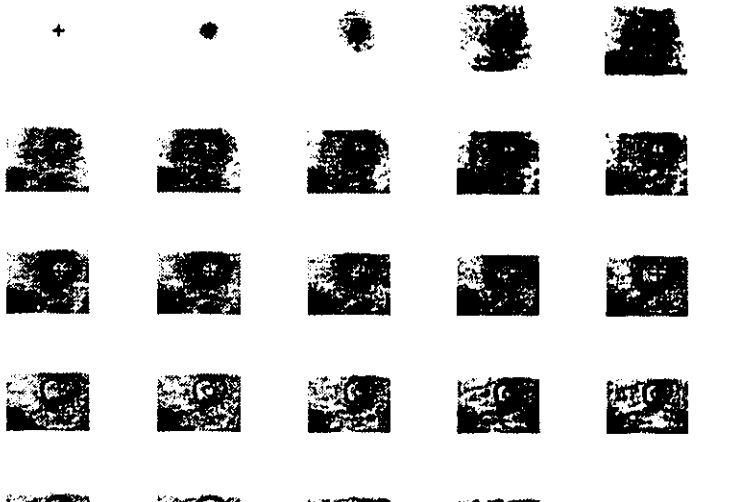
n061pxxf00

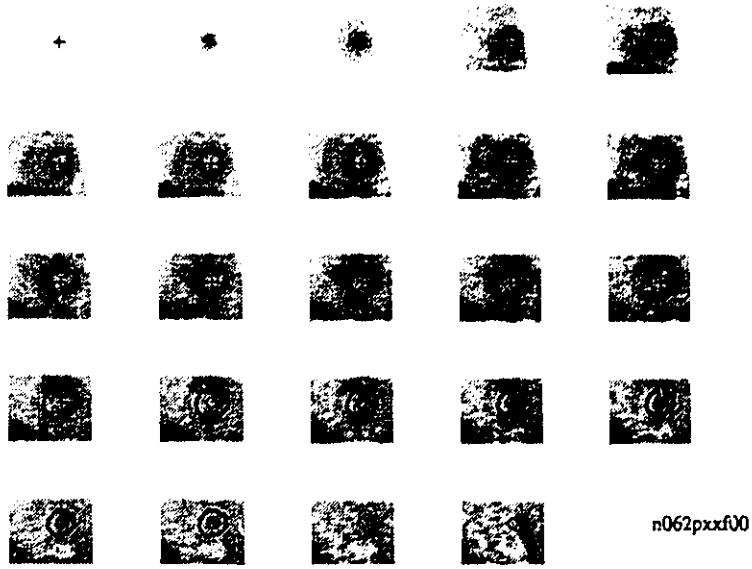
n062pxxf00

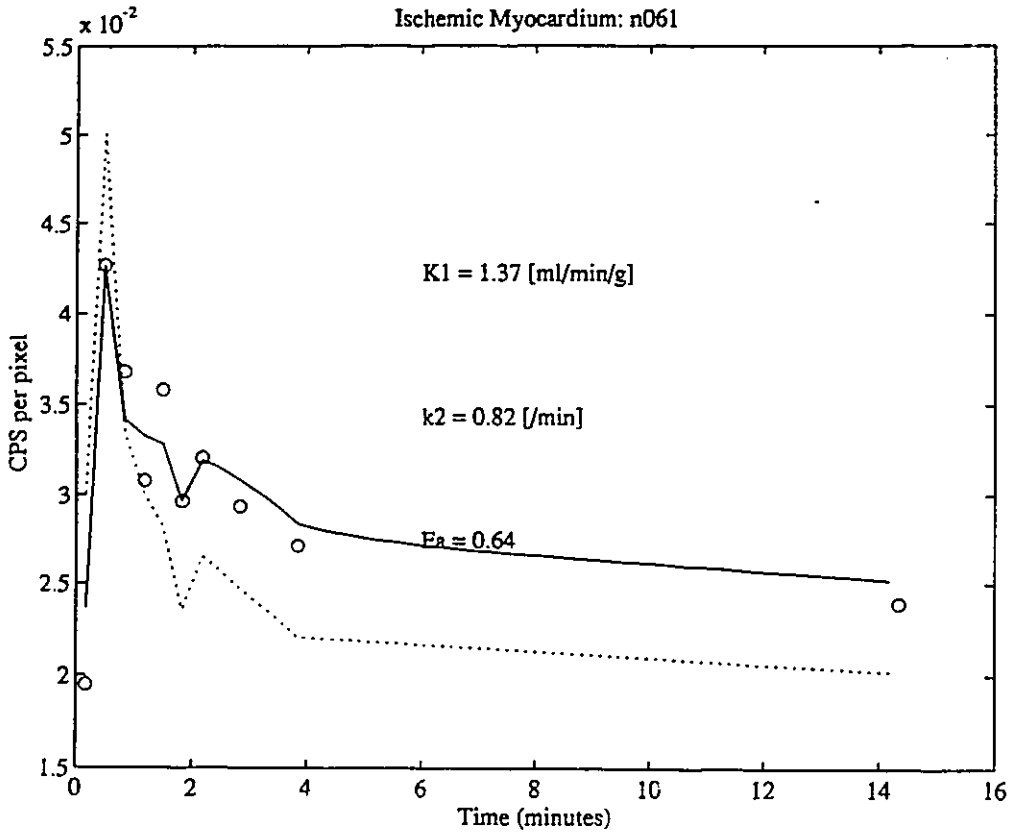
Ischemic Myocardium: n061
x 10^-2
CPS per pixel
K1 = 1.37 [ml/min/g]
k2 = 0.82 [/min]
Fa = 0.64
Time (minutes)

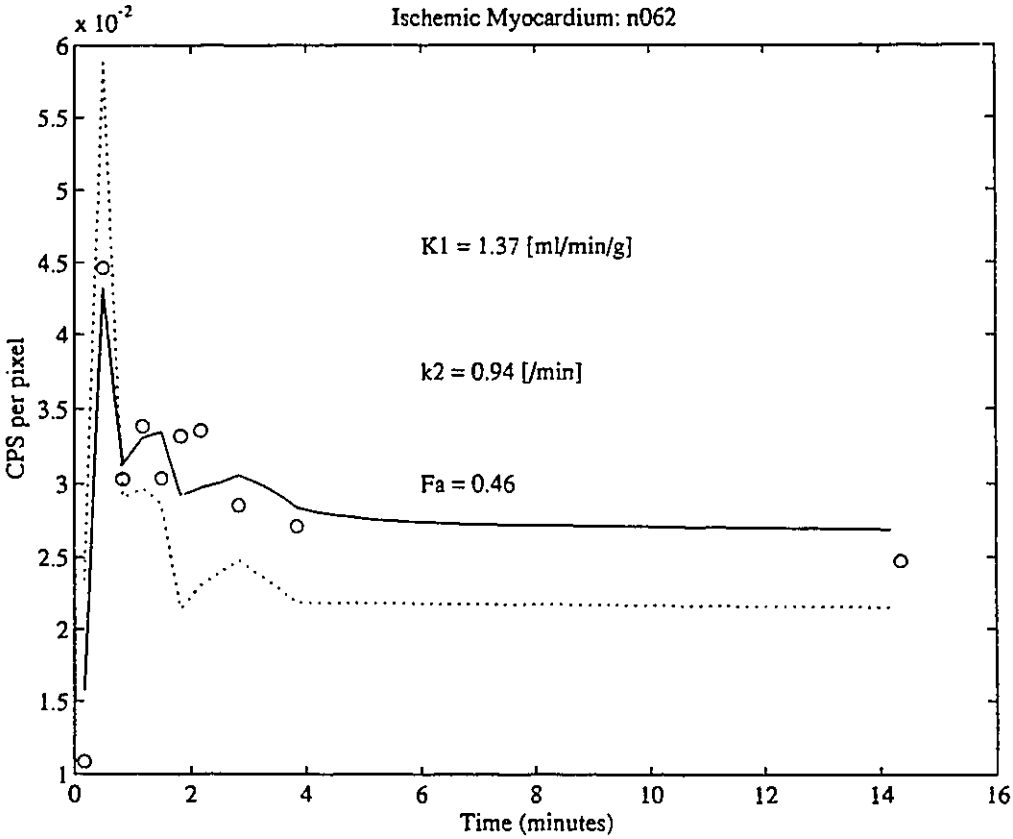
Ischemic Myocardium: n062
x 10^-2
CPS per pixel
K1 = 1.37 [ml/min/g]
k2 = 0.94 [/min]
Fa = 0.46
Time (minutes)

Axial distribution

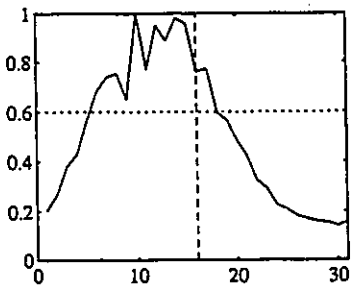

Transaxial Plane 16

Long Axis Section

Short Axis Section

Axial distribution

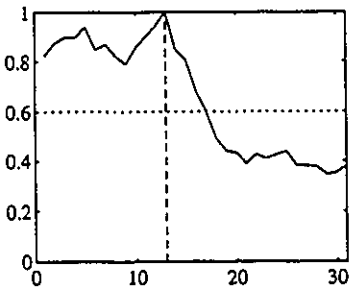

Transaxial Plane 13

Long Axis Section

Short Axis Section

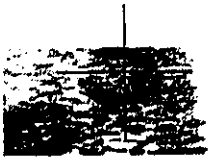

Axial distribution

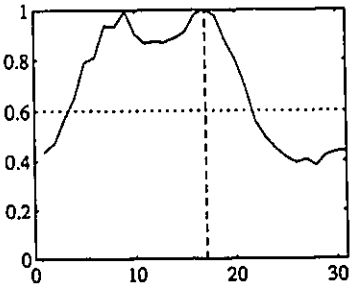

Transaxial Plane 17

Long Axis Section

Short Axis Section

Quality Assurance: Subject Placebo 2 (P2)

A. FDG

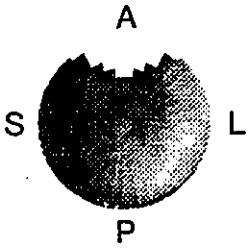

B. Base Flow

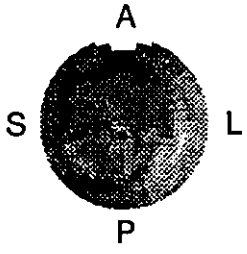

C. Treat Flow

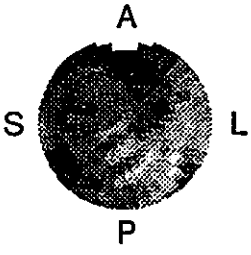

D. Treat/Base

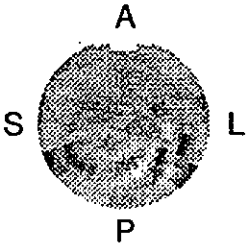

E. FDG/Base

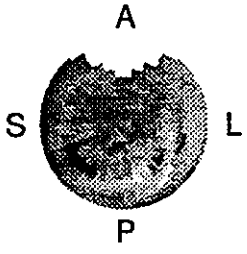

F. FDG/Treat

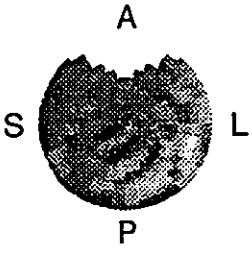

G. LV blood integrals

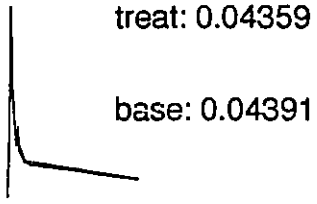

H. Ischemic Regions

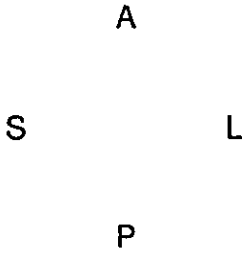

I. Largest Region

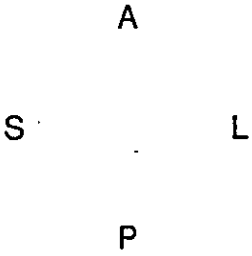

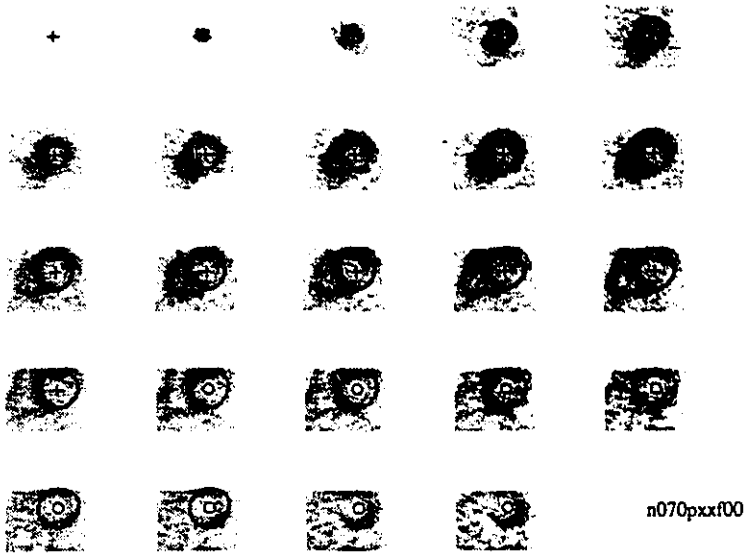

n070pxxf00

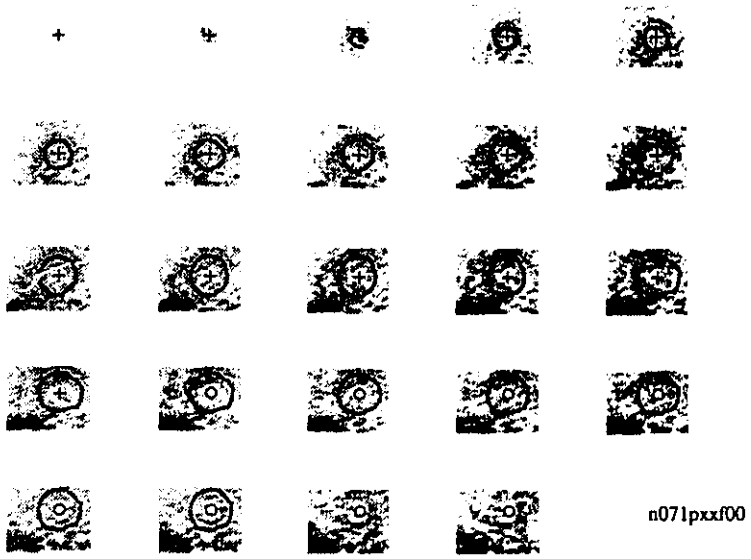

n071pxxf00

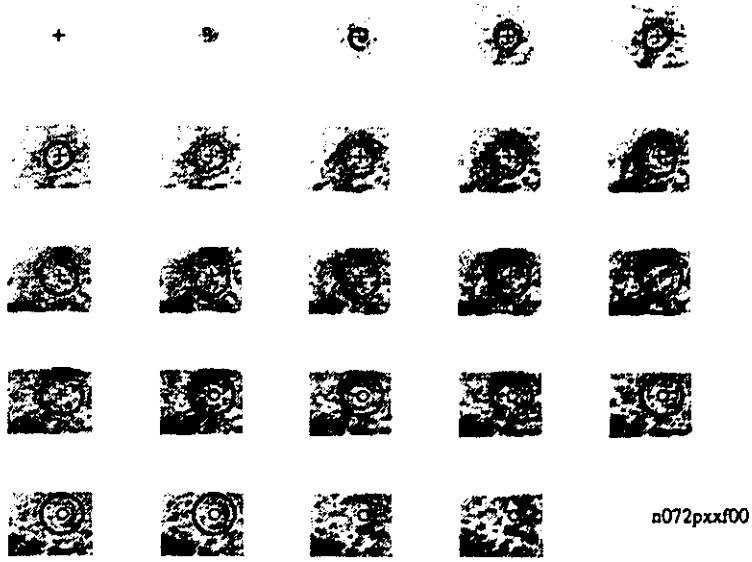

n072pxxf00

Axial distribution

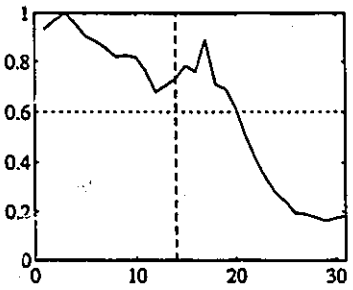

Transaxial Plane 14

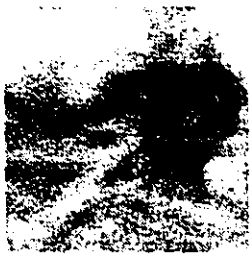

Long Axis Section

Short Axis Section

Axial distribution

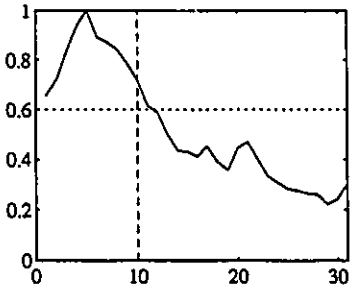

Transaxial Plane 10

Long Axis Section

Short Axis Section

Axial distribution

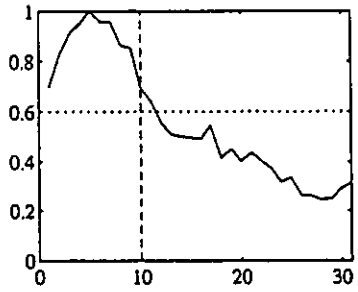

Transaxial Plane 10

Long Axis Section

Short Axis Section

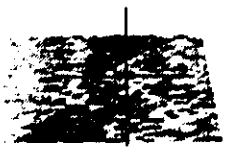

SNR = 6.789

Quality Assurance: Subject Drug 2 (D2)

A. FDG

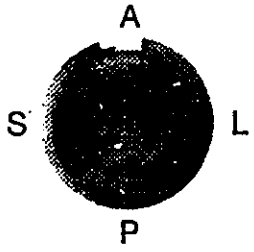

B. Base Flow

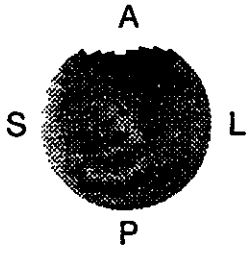

C. Treat Flow

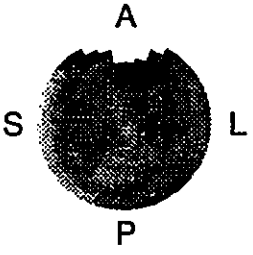

D. Treat/Base

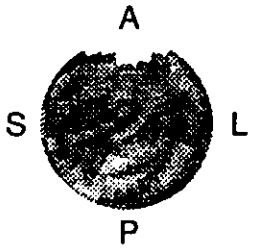

E. FDG/Base

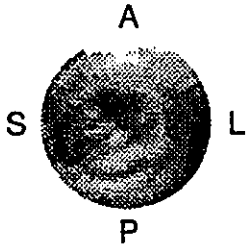

F. FDG/Treat

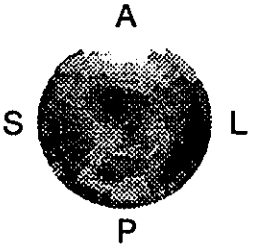

G. LV blood integrals

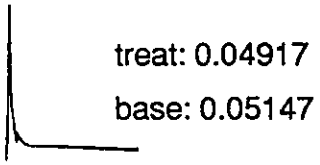

H. Ischemic Regions

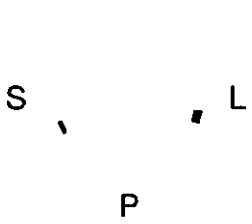

I. Largest Region

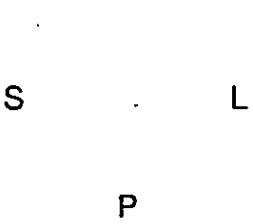

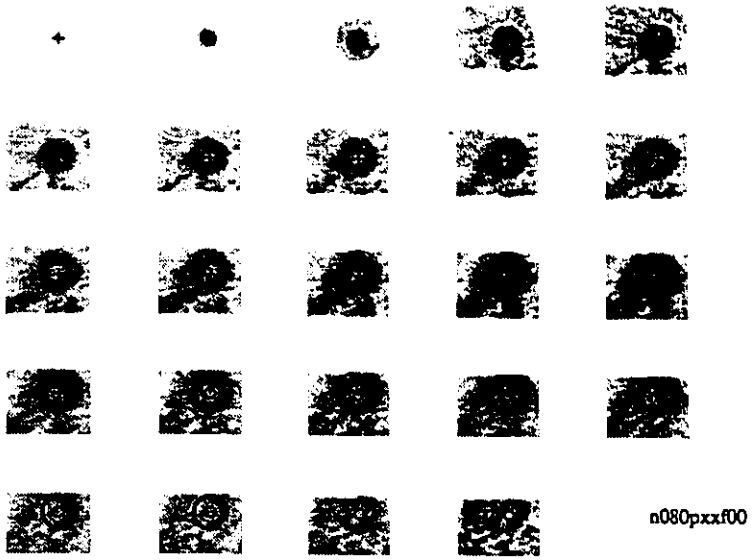

n080pxxf00

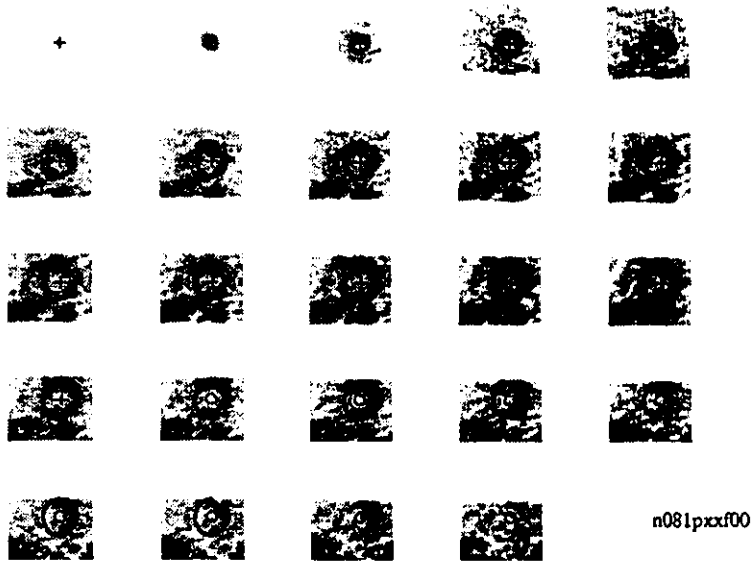

n081pxxf00

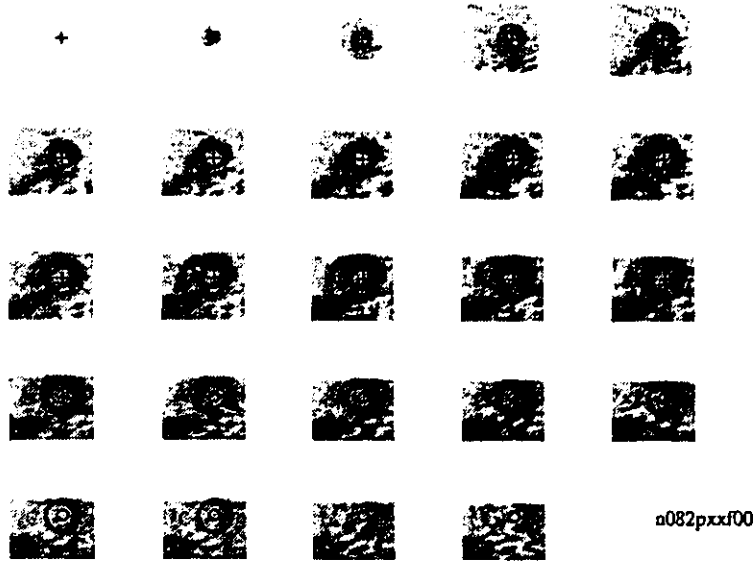

n082pxxf00

Axial distribution

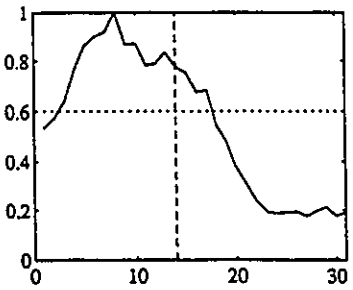

Transaxial Plane 14

Long Axis Section

Short Axis Section

Axial distribution

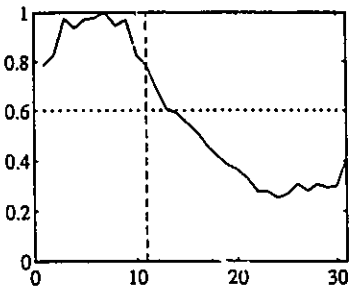

Transaxial Plane 11

Long Axis Section

Short Axis Section

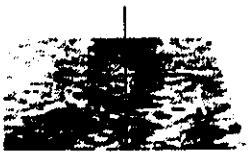

Axial distribution

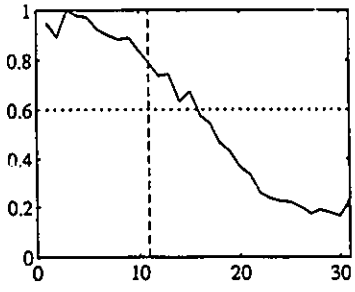

Transaxial Plane 11

Long Axis Section

Short Axis Section

Quality Assurance: Subject Placebo 3 (P3)

A. FDG

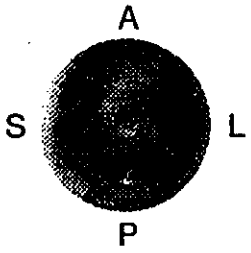

B. Base Flow

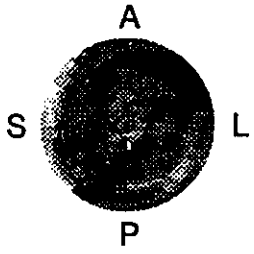

C. Treat Flow

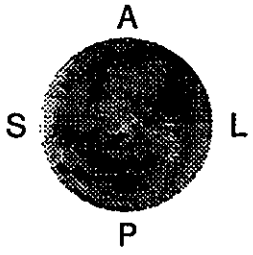

D. Treat/Base

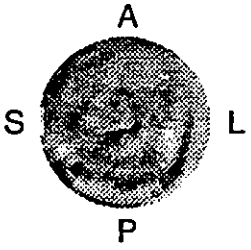

E. FDG/Base

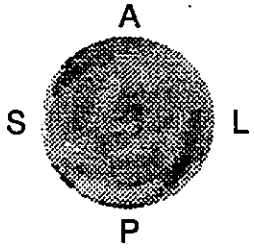

F. FDG/Treat

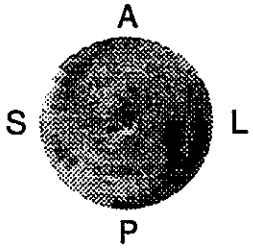

G. LV blood integrals

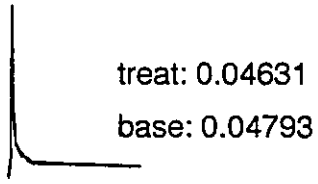

H. Ischemic Regions

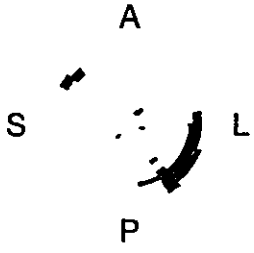

I. Largest Region

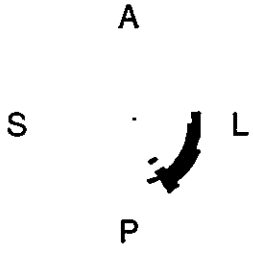

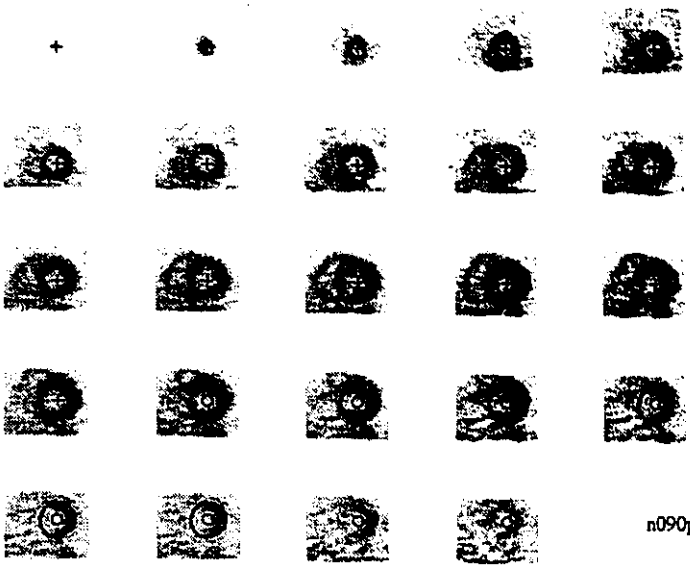

n090pxxf00

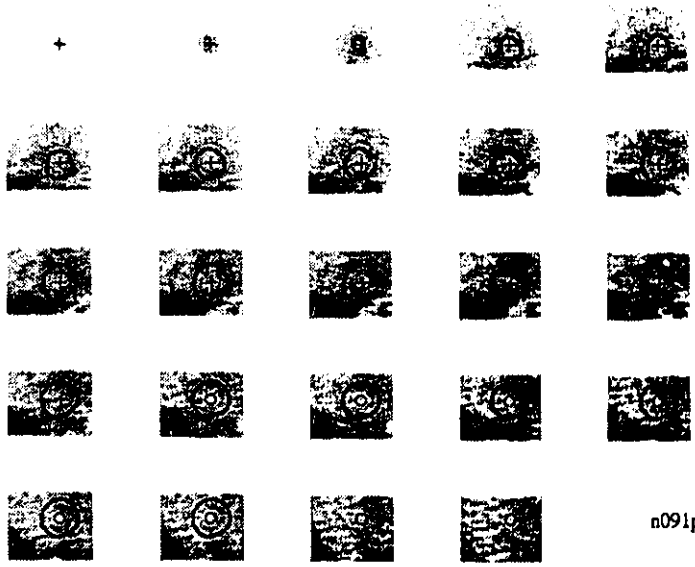

n091pxxf00

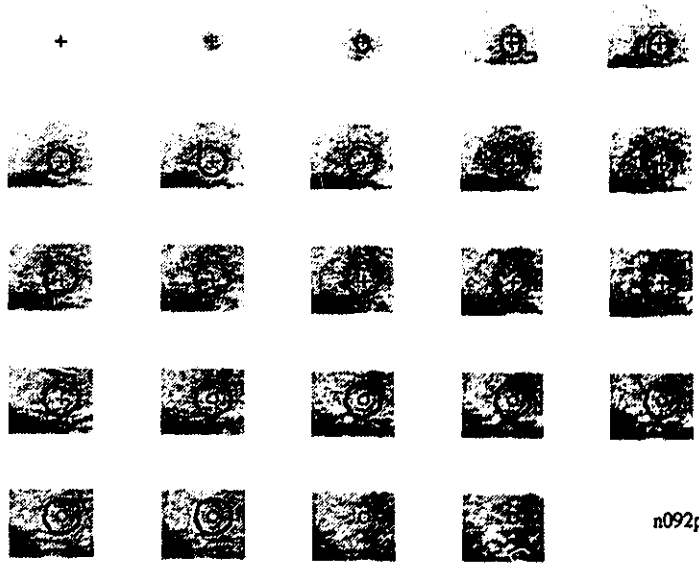

n092pxxf00

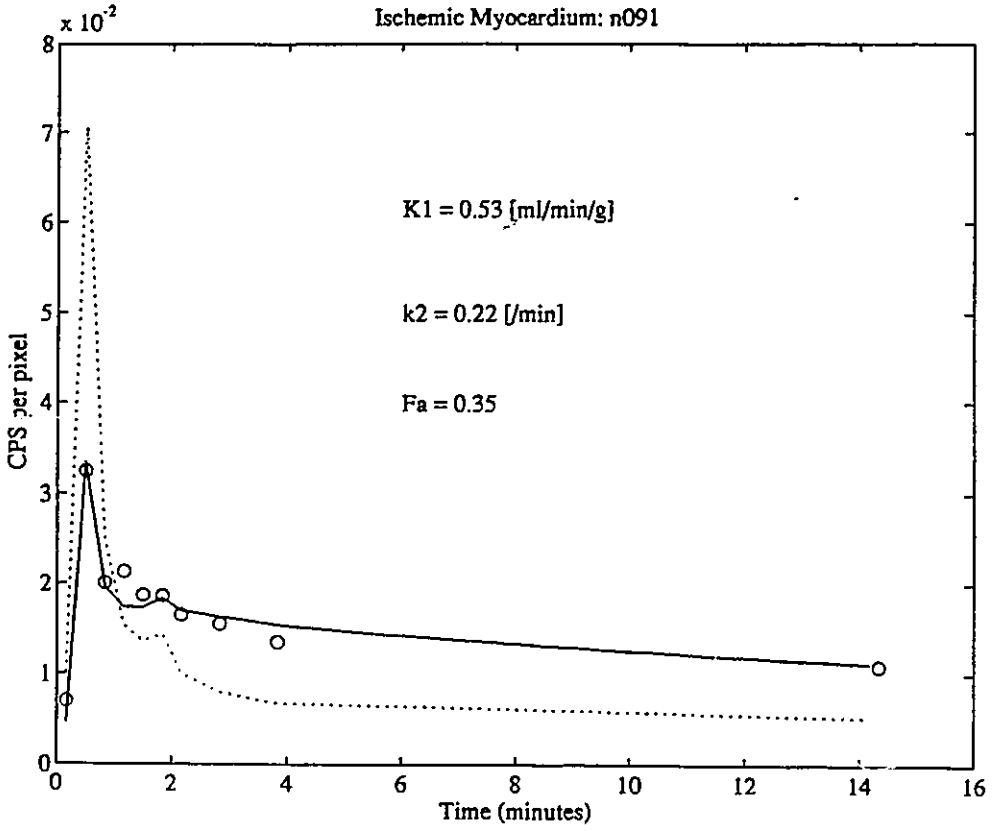
Ischemic Myocardium: n091
x 10^-2
CPS per pixel
K1 = 0.53 [ml/min/g]
k2 = 0.22 [/min]
Fa = 0.35
Time (minutes)

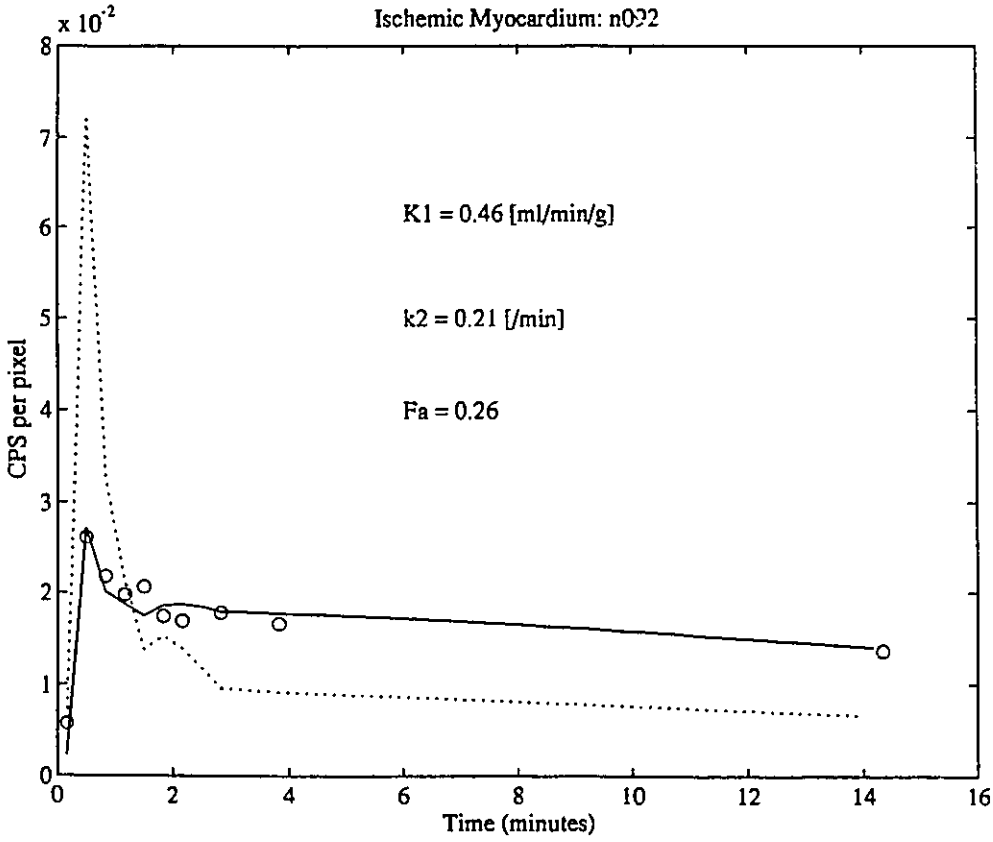
Ischemic Myocardium: n092
x 10^-2
CPS per pixel
K1 = 0.46 [ml/min/g]
k2 = 0.21 [/min]
Fa = 0.26
Time (minutes)

Axial distribution

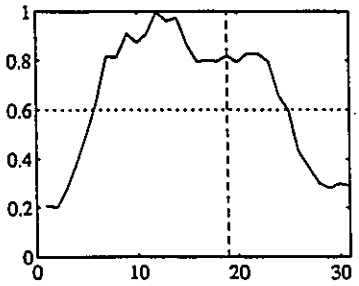

Transaxial Plane 19

Long Axis Section

Short Axis Section

Axial distribution

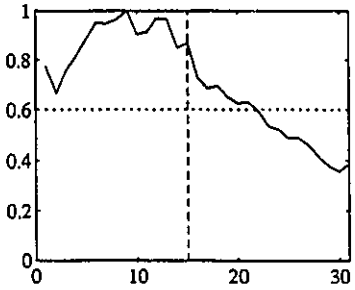

Transaxial Plane 15

Long Axis Section

Short Axis Section

Axial distribution

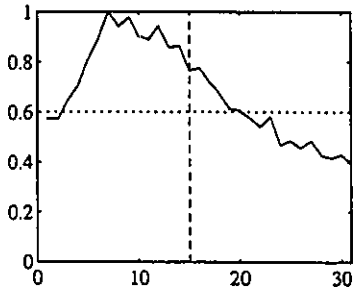

Transaxial Plane 15

Long Axis Section

Short Axis Section

Quality Assurance: Subject Drug 3 (D3)

A. FDG

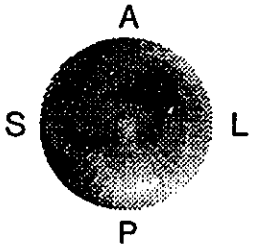

B. Base Flow

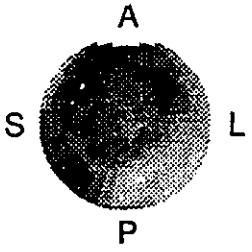

C. Treat Flow

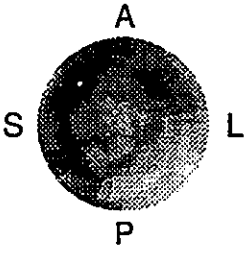

D. Treat/Base

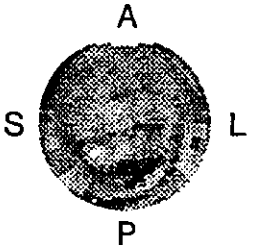

E. FDG/Base

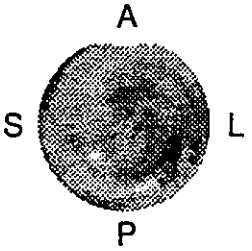

F. FDG/Treat

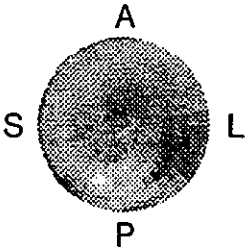

G. LV blood integrals

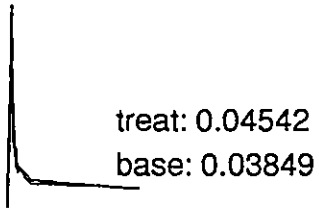

H. Ischemic Regions

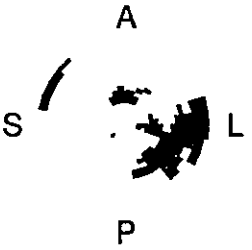

I. Largest Region

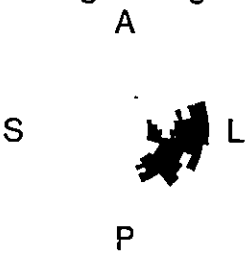

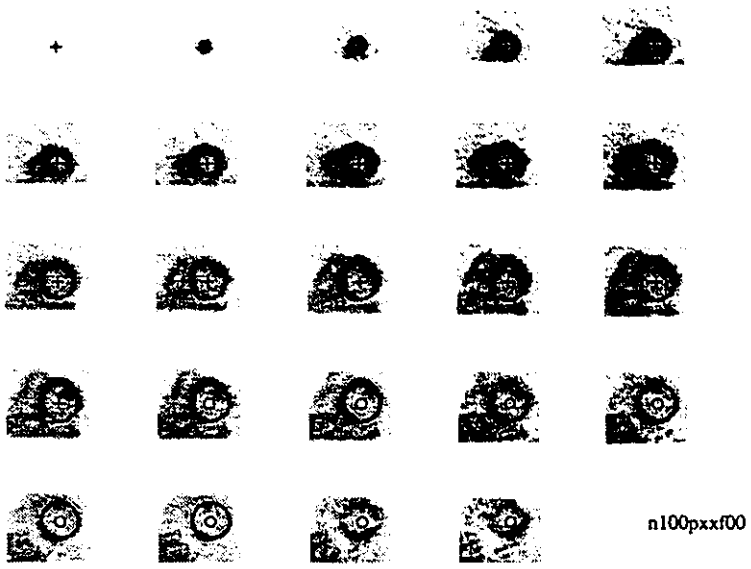
n100pxxf00
n101pxxf00
n102pxxf00

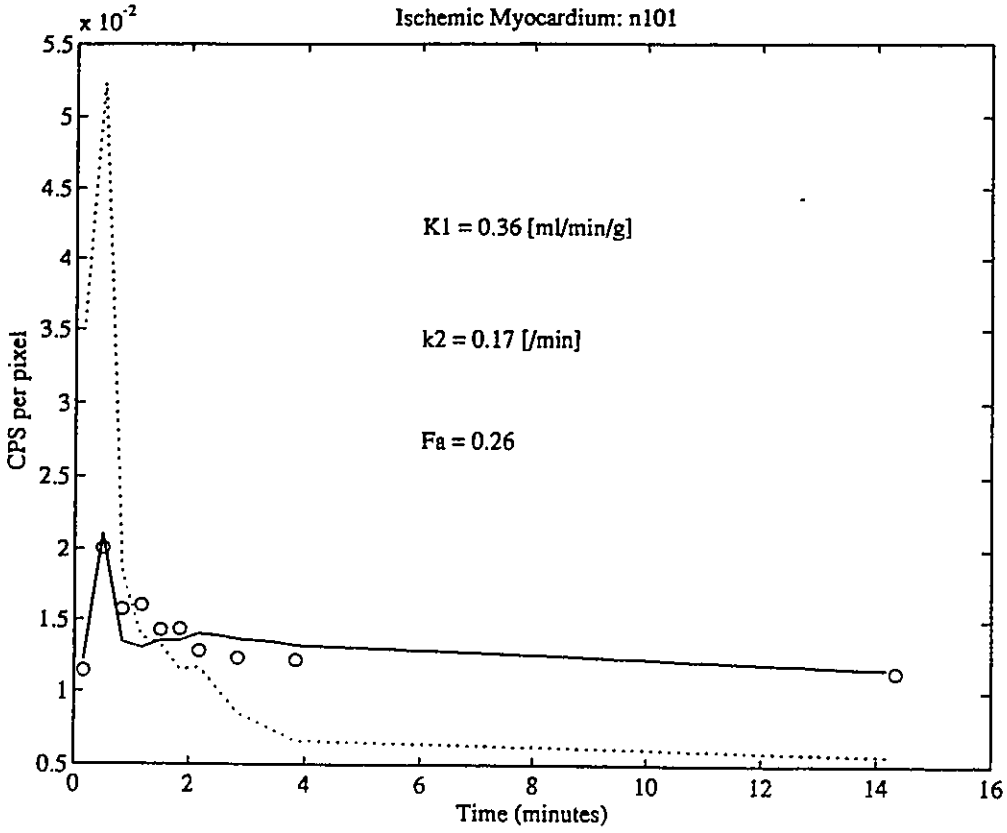
Ischemic Myocardium: n101
x 10^-2
CPS per pixel
Time (minutes)
K1 = 0.36 [ml/min/g]
k2 = 0.17 [/min]
Fa = 0.26

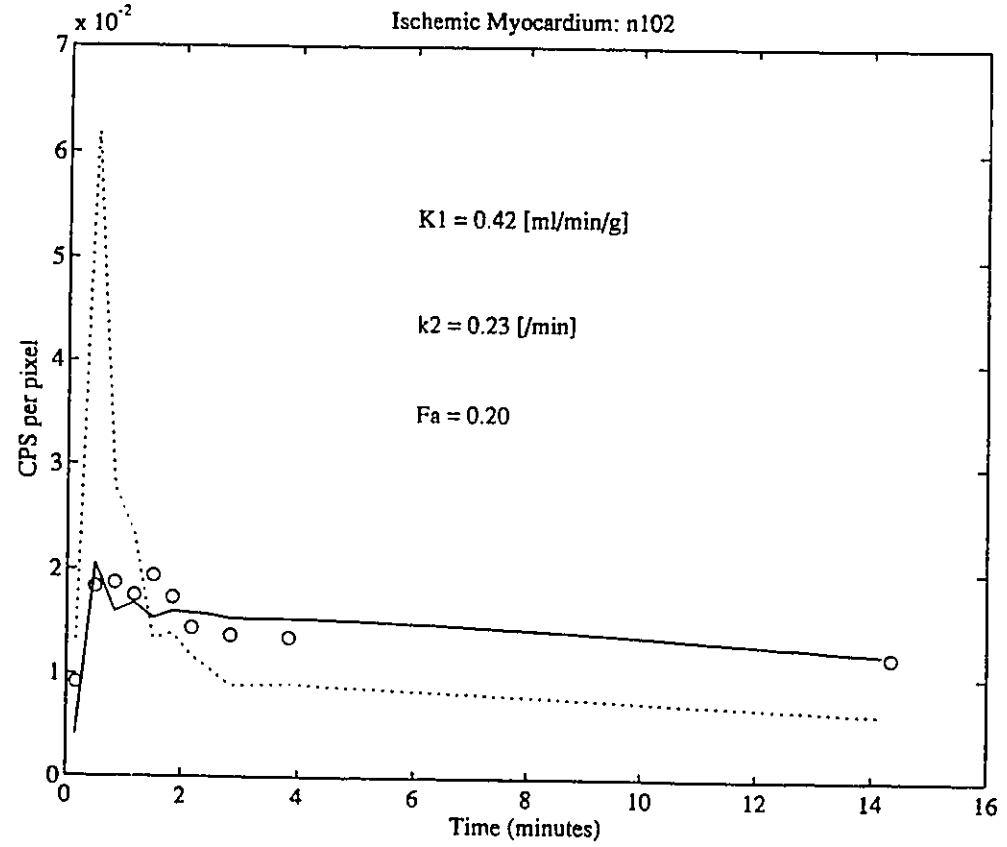
Ischemic Myocardium: n102
x 10^-2
CPS per pixel
Time (minutes)
K1 = 0.42 [ml/min/g]
k2 = 0.23 [/min]
Fa = 0.20

Axial distribution

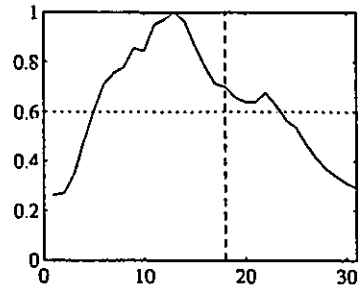

Transaxial Plane 18

Long Axis Section

Short Axis Section

Axial distribution

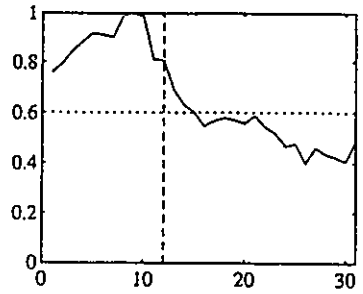

Transaxial Plane 12

Long Axis Section

Short Axis Section

Axial distribution

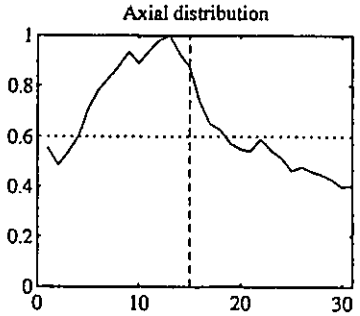

Transaxial Plane 15

Long Axis Section

Short Axis Section

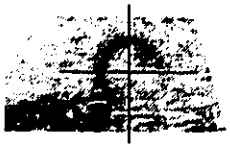

Quality Assurance: Subject Drug 4 (D4)

A. FDG

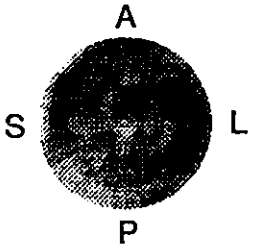

B. Base Flow

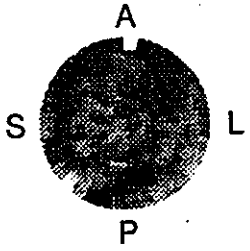

C. Treat Flow

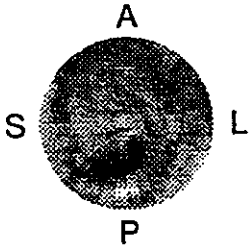

D. Treat/Base

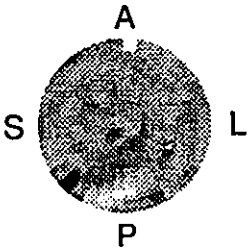

E. FDG/Base

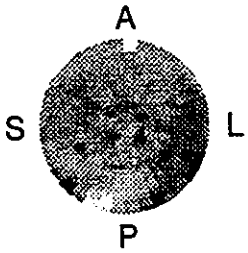

F. FDG/Treat

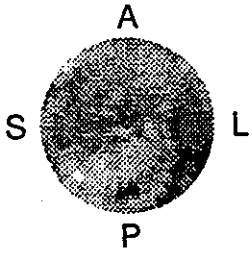

G. LV blood integrals

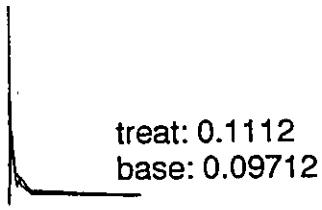

H. Ischemic Regions

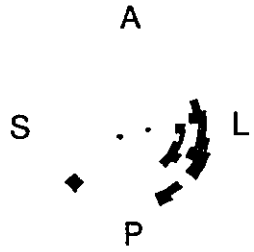

I. Largest Region

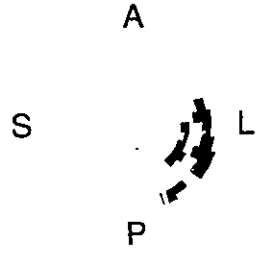

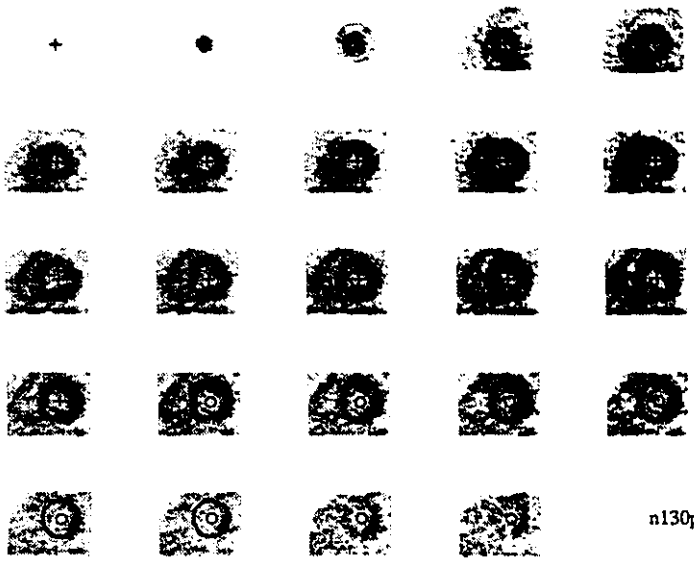

n130pxxf00

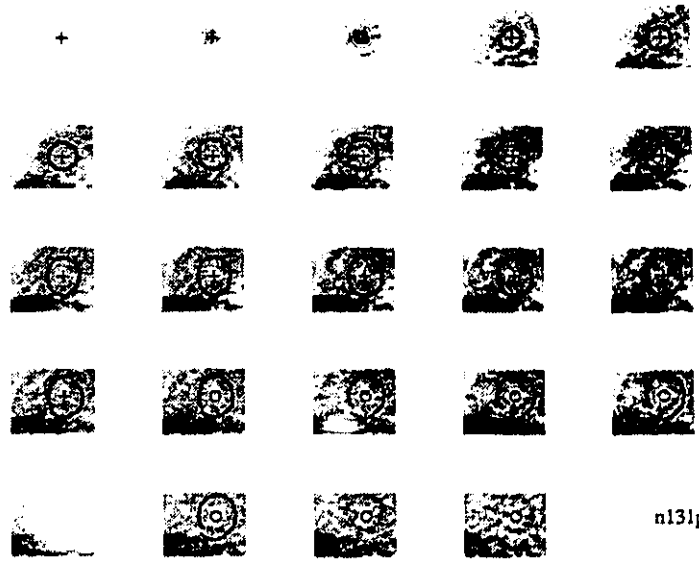

n131pxxf00

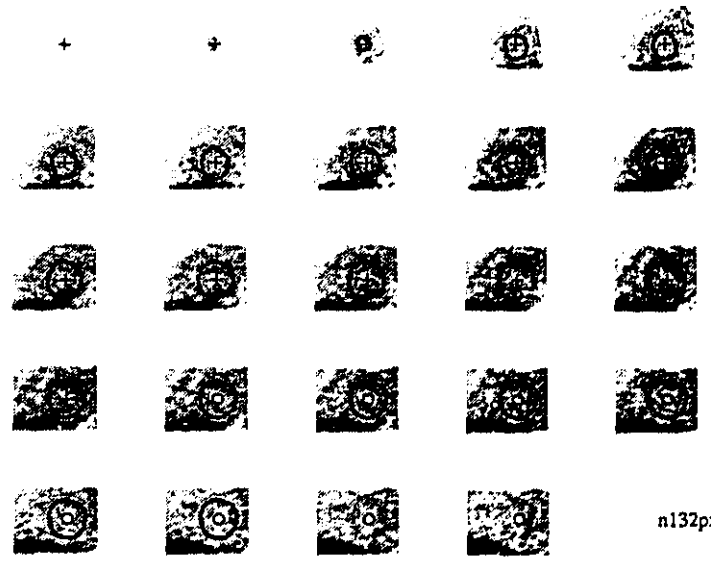

n132pxxf00

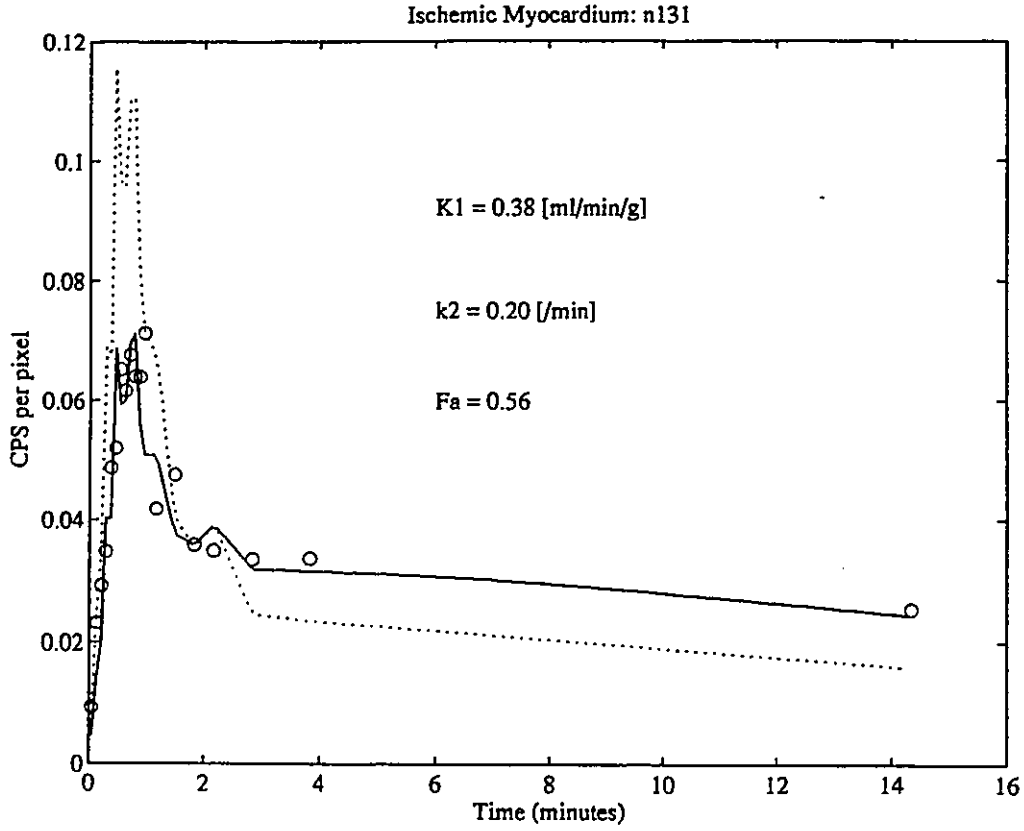
Ischemic Myocardium: n131
K1 = 0.38 [ml/min/g]
k2 = 0.20 [/min]
Fa = 0.56
CPS per pixel
Time (minutes)
0.12
0.1
0.08
0.06
0.04
0.02
0
0
2
4
6
8
10
12
14
16

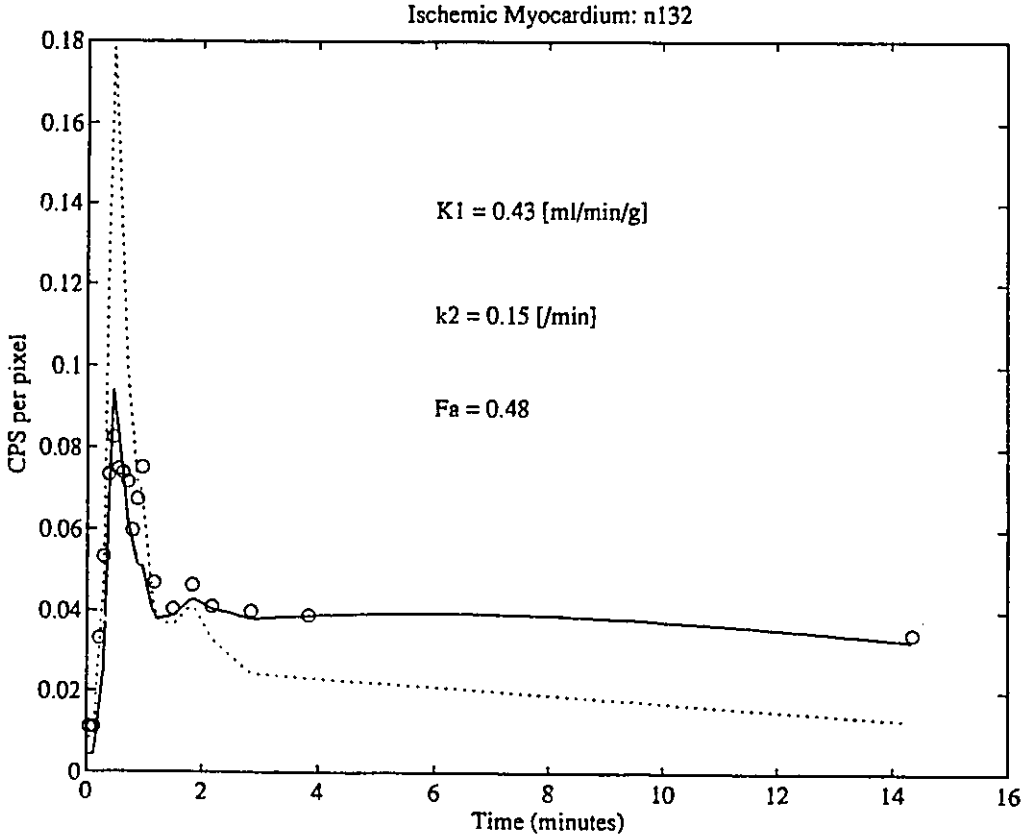
Ischemic Myocardium: n132
K1 = 0.43 [ml/min/g]
k2 = 0.15 [/min]
Fa = 0.48
CPS per pixel
Time (minutes)
0.18
0.16
0.14
0.12
0.1
0.08
0.06
0.04
0.02
0
0
2
4
6
8
10
12
14
16

Axial distribution

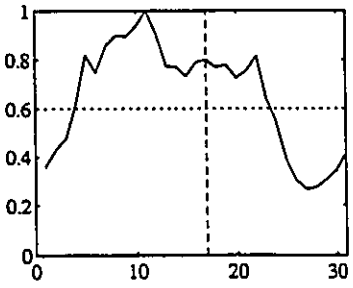

Transaxial Plane 17

Long Axis Section

Short Axis Section

Axial distribution

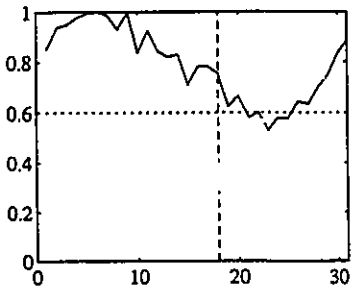

Transaxial Plane 18

Long Axis Section

Short Axis Section

Axial distribution

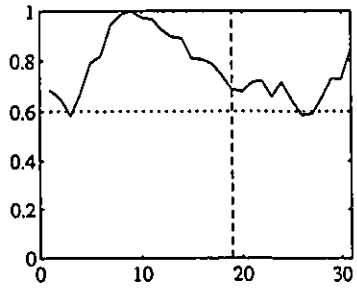

Transaxial Plane 19

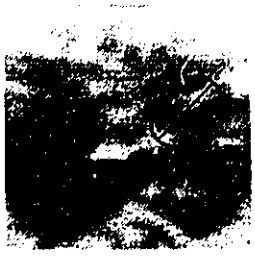

Long Axis Section

Short Axis Section

Quality Assurance: Subject Placebo 4 (P4)

A. FDG

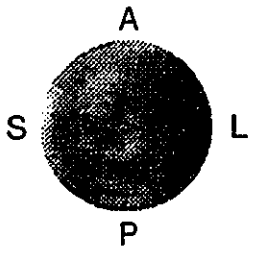

B. Base Flow

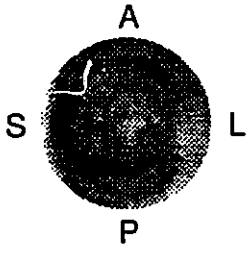

C. Treat Flow

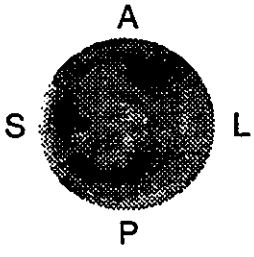

D. Treat/Base

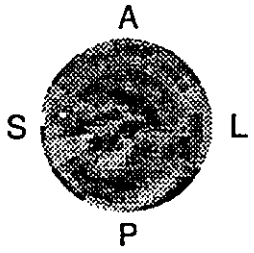

E. FDG/Base

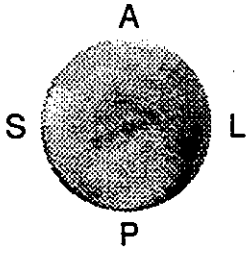

F. FDG/Treat

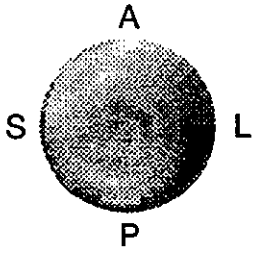

G. LV blood integrals

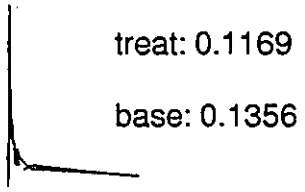

H. Ischemic Regions

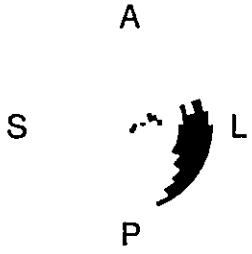

I. Largest Region

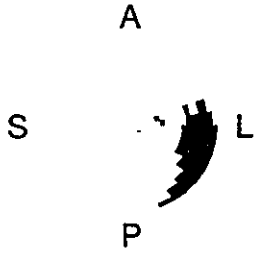

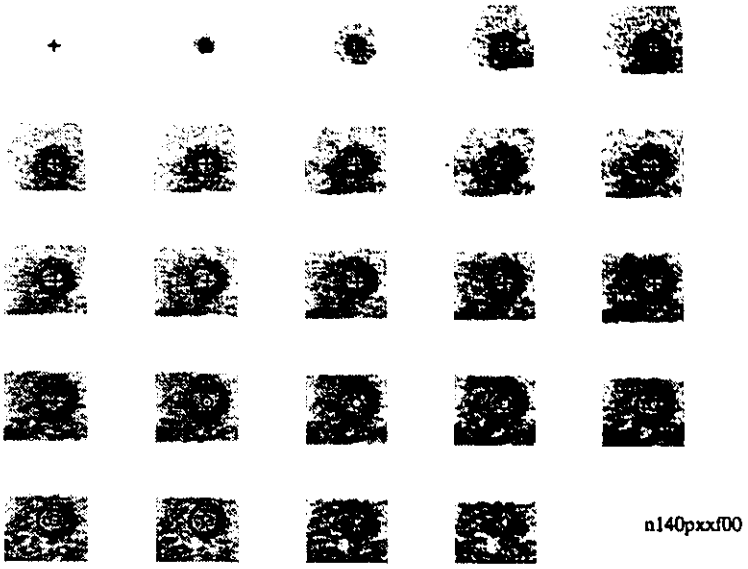

n140pxxf00

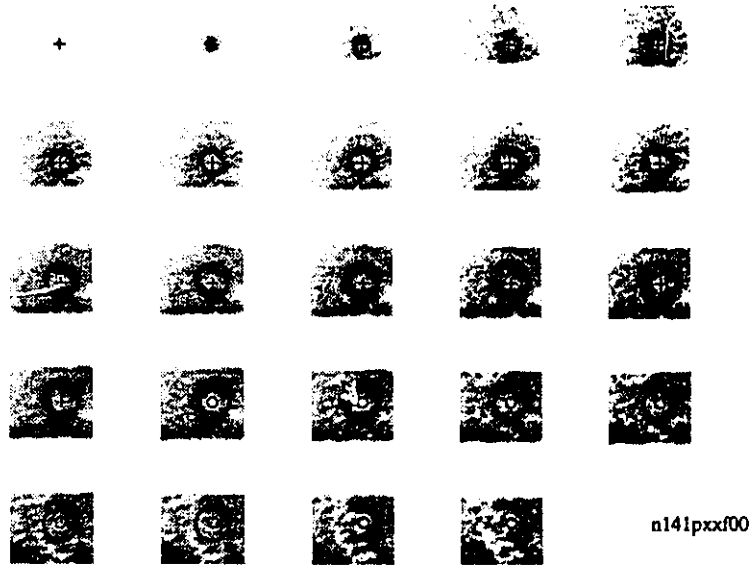

n141pxxf00

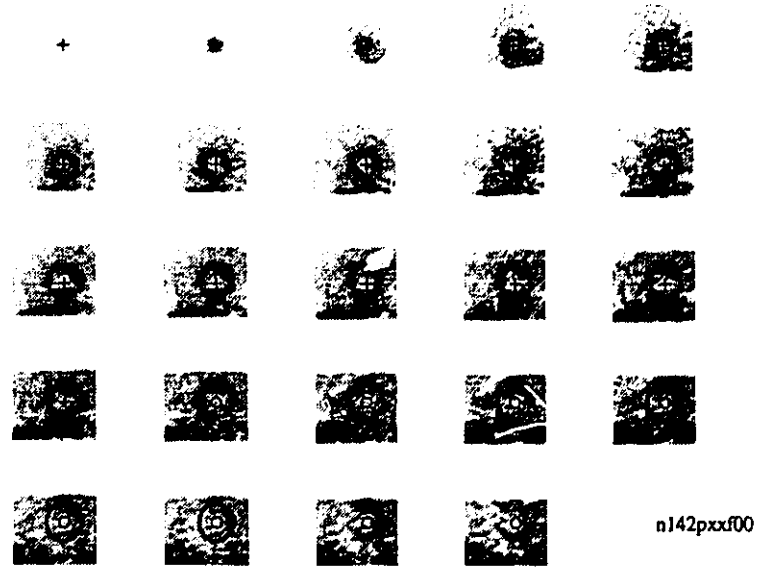

n142pxxf00

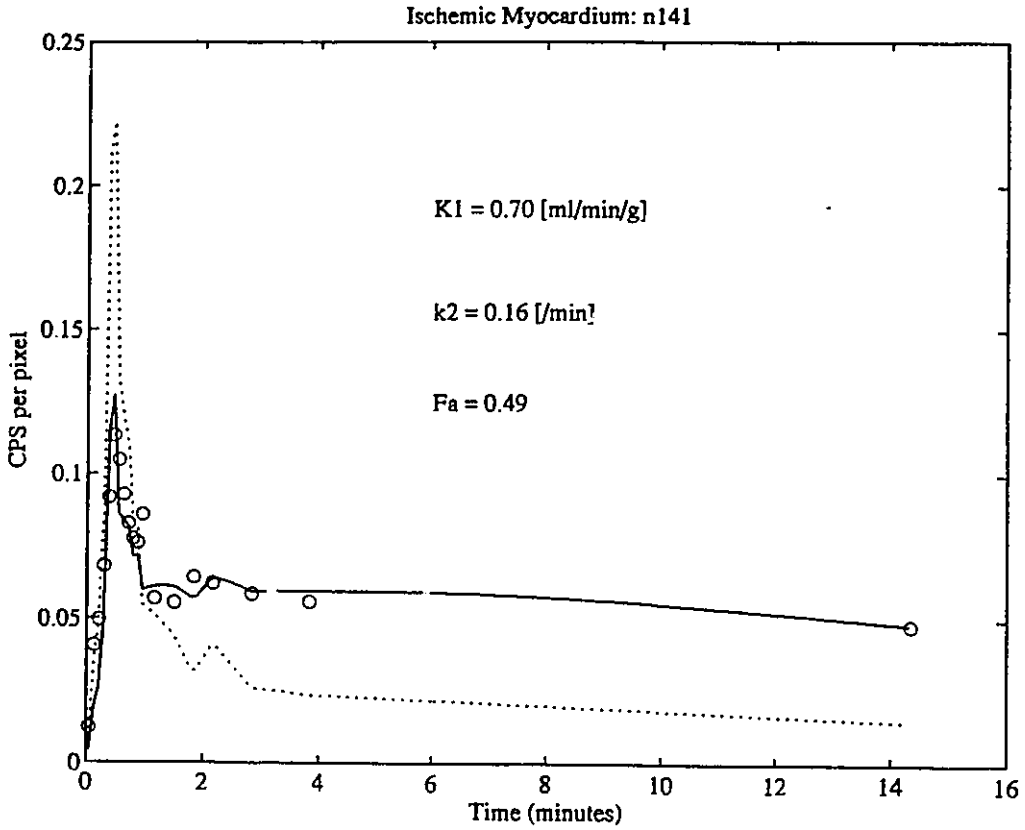
Ischemic Myocardium: n141
K1 = 0.70 [ml/min/g]
k2 = 0.16 [/min]
Fa = 0.49
CPS per pixel
Time (minutes)
0.25
0.2
0.15
0.1
0.05
0
0
2
4
6
8
10
12
14
16

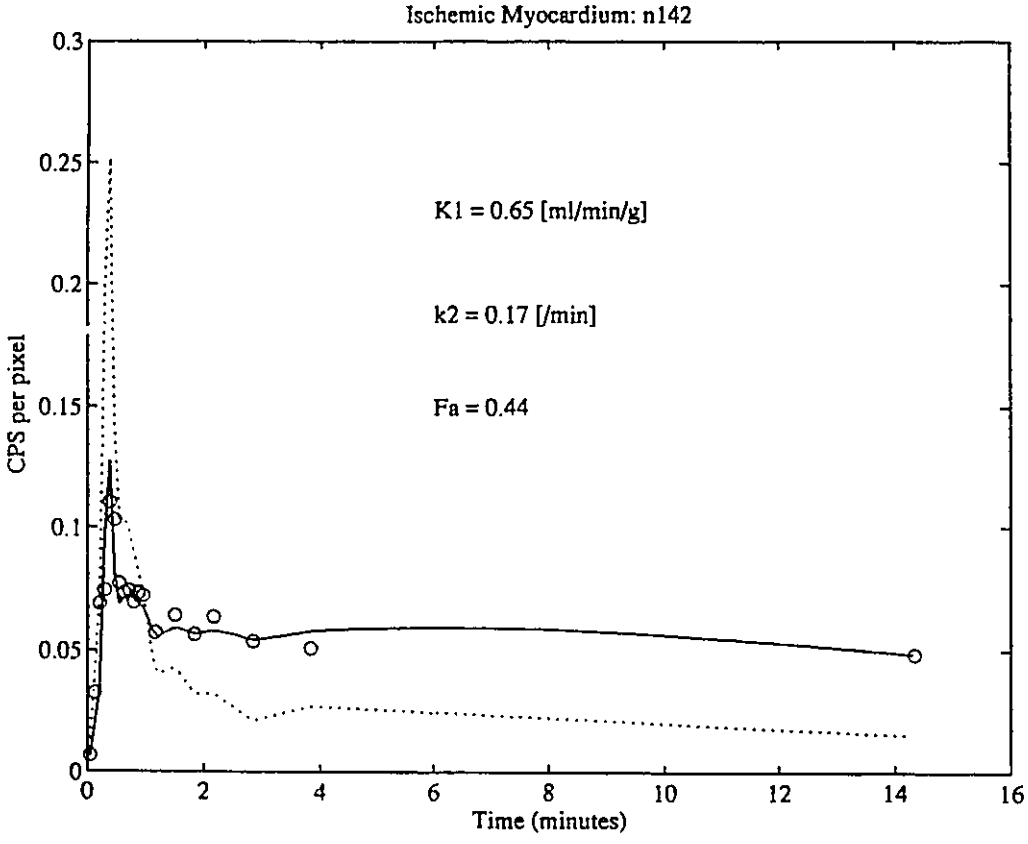
Ischemic Myocardium: n142
K1 = 0.65 [ml/min/g]
k2 = 0.17 [/min]
Fa = 0.44
CPS per pixel
Time (minutes)
0.3
0.25
0.2
0.15
0.1
0.05
0
0
2
4
6
8
10
12
14
16

Axial distribution

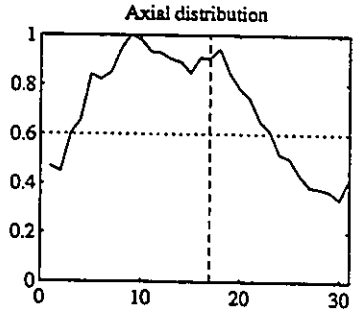

Transaxial Plane 17

Long Axis Section

Short Axis Section

Axial distribution

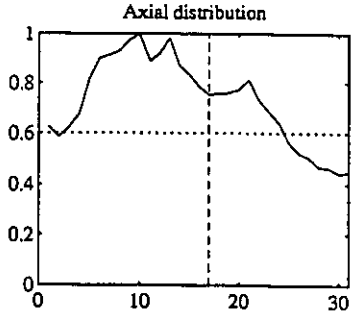

Transaxial Plane 17

Long Axis Section

Short Axis Section

Axial distribution

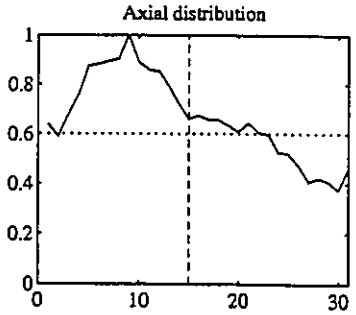

Transaxial Plane 15

Long Axis Section

Short Axis Section

Quality Assurance: Subject Drug 5 (D5)

A. FDG

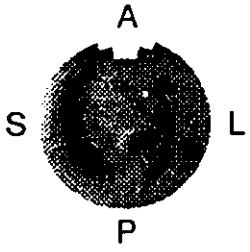

B. Base Flow

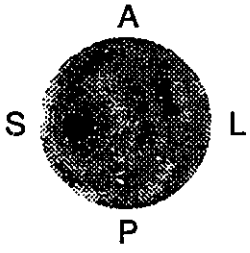

C. Treat Flow

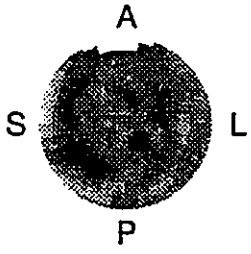

D. Treat/Base

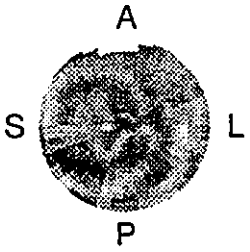

E. FDG/Base

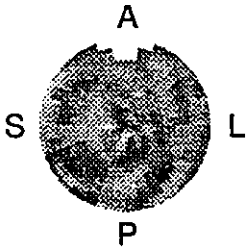

F. FDG/Treat

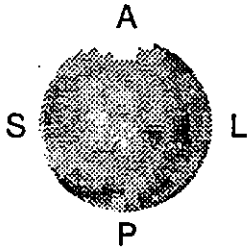

G. LV blood integrals

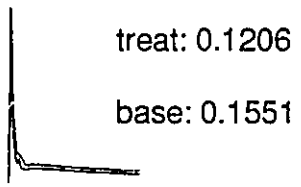

H. Ischemic Regions

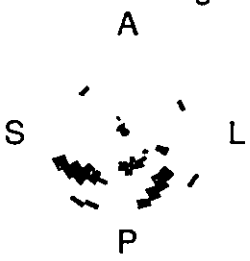

I. Largest Region

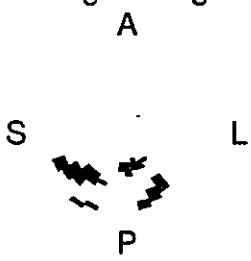

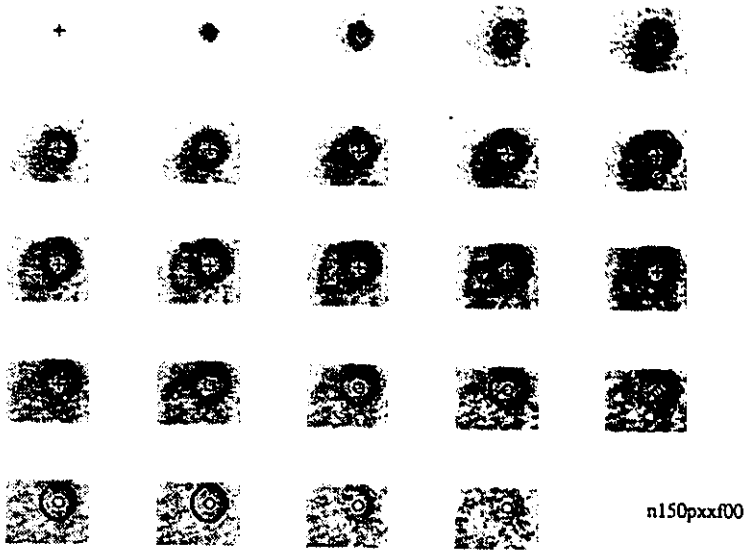
n150pxxf00

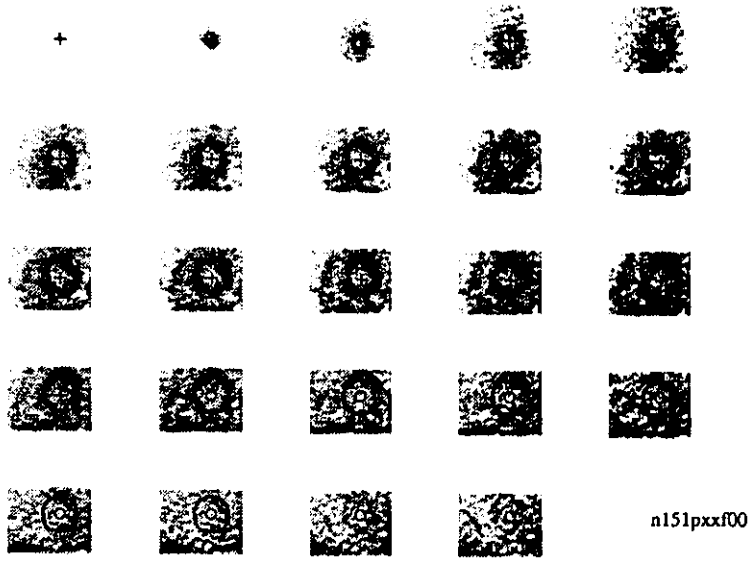
n151pxxf00

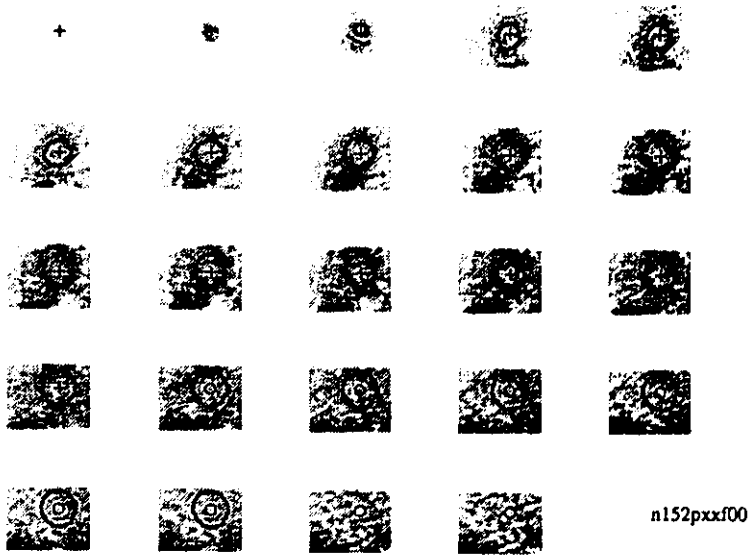
n152pxxf00

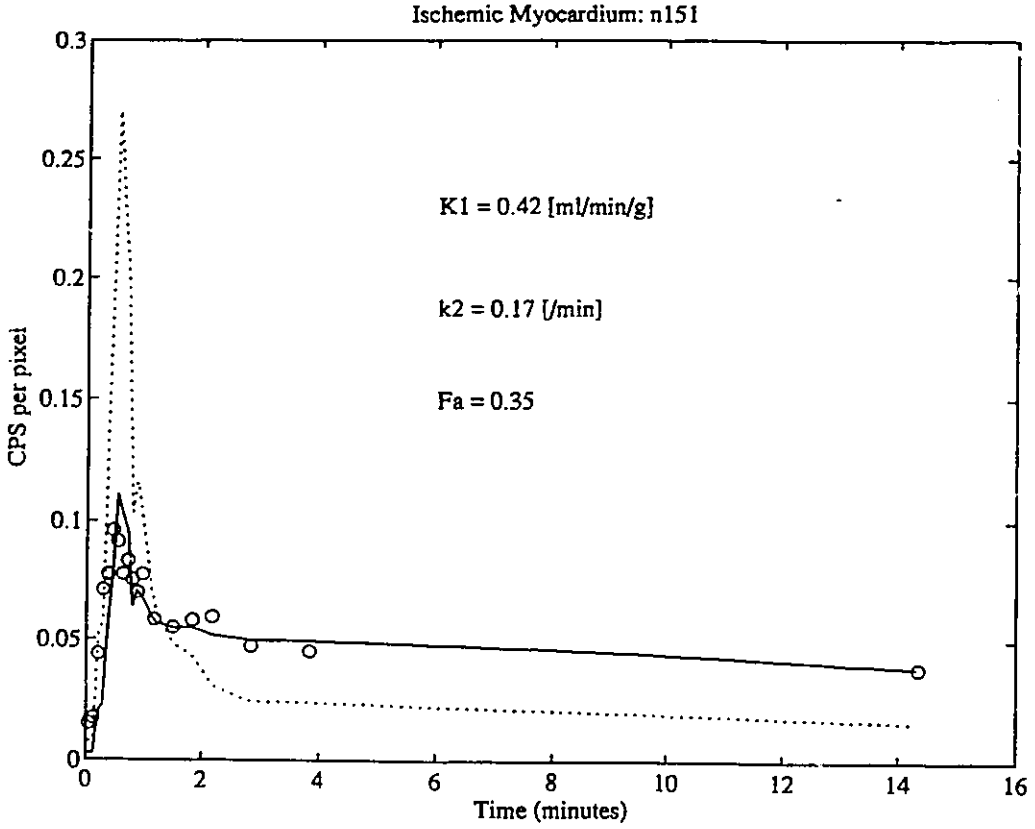
Ischemic Myocardium: n151
K1 = 0.42 [ml/min/g]
k2 = 0.17 [/min]
Fa = 0.35
CPS per pixel
Time (minutes)
0.3
0.25
0.2
0.15
0.1
0.05
0
0
2
4
6
8
10
12
14
16

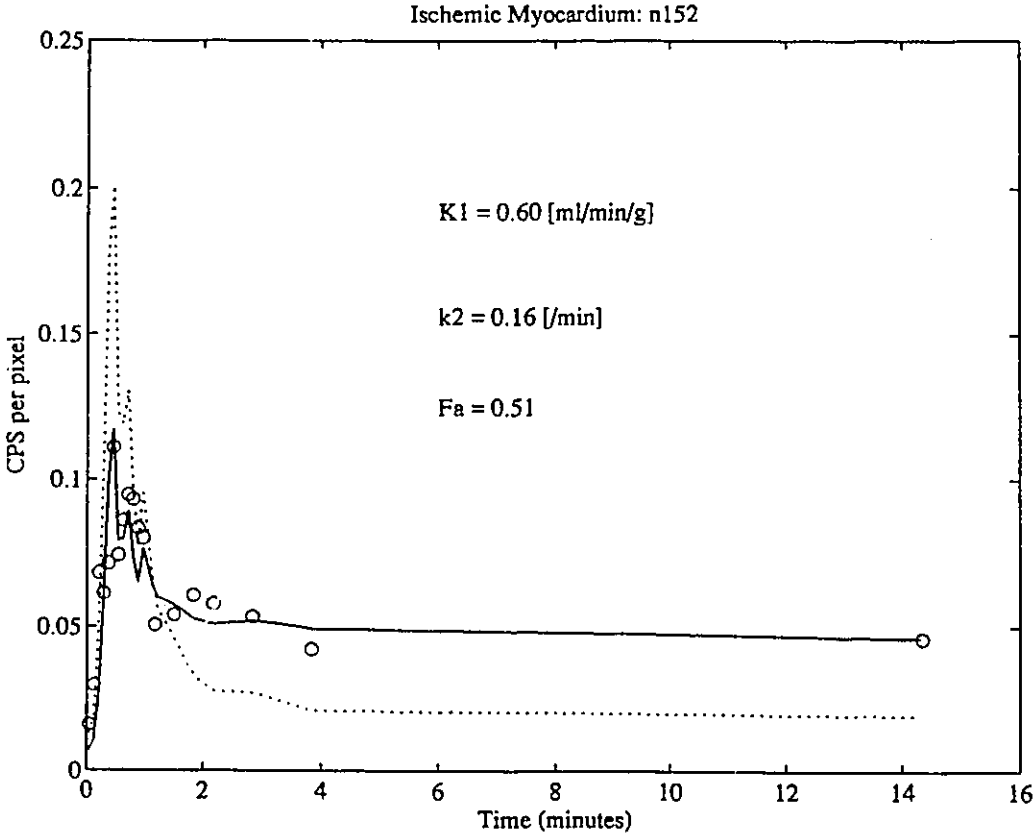
Ischemic Myocardium: n152
K1 = 0.60 [ml/min/g]
k2 = 0.16 [/min]
Fa = 0.51
CPS per pixel
Time (minutes)
0.25
0.2
0.15
0.1
0.05
0
0
2
4
6
8
10
12
14
16

Axial distribution

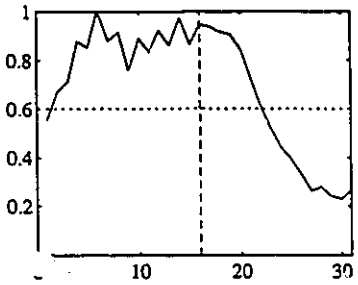

Transaxial Plane 16

Long Axis Section

Short Axis Section

Axial distribution

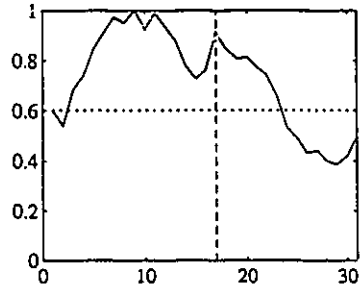

Transaxial Plane 17

Long Axis Section

Short Axis Section

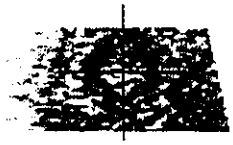

Axial distribution

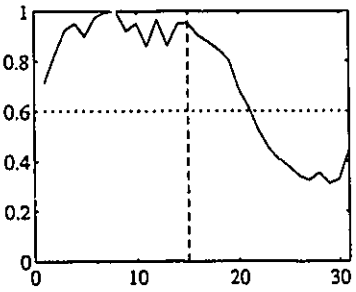

Transaxial Plane 15

Long Axis Section

Short Axis Section

Quality Assurance: Subject Placebo 5 (P5)

A. FDG

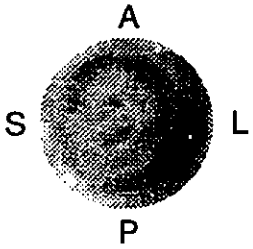

B. Base Flow

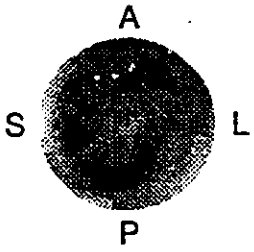

C. Treat Flow

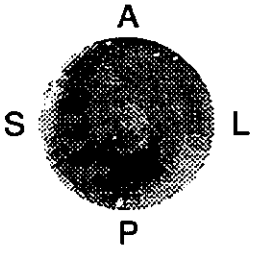

D. Treat/Base

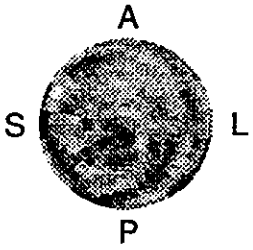

E. FDG/Base

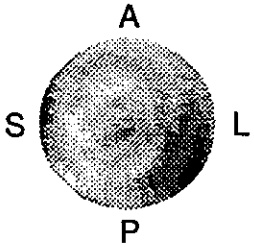

F. FDG/Treat

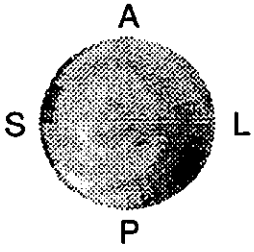

G. LV blood integrals

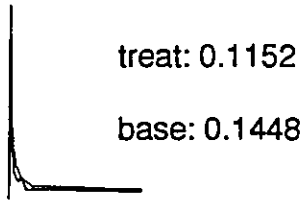

H. Ischemic Regions

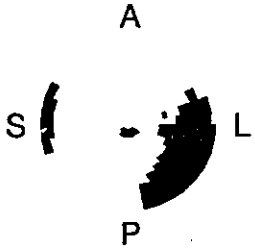

I. Largest Region

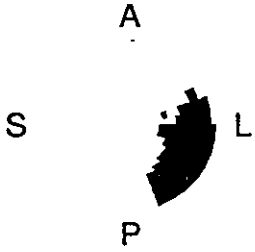

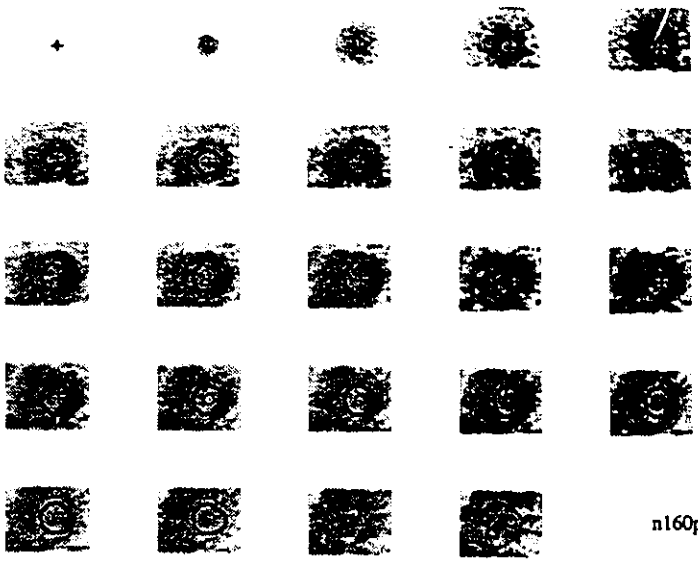

n160pxxf00

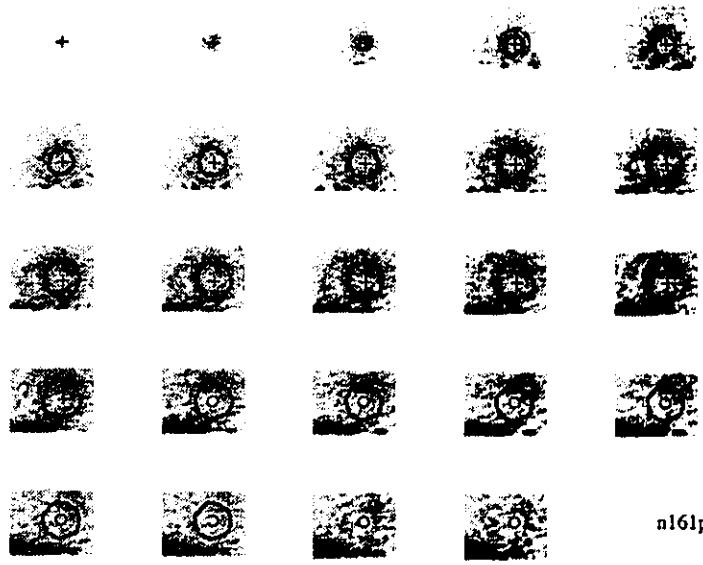

n161pxxf00

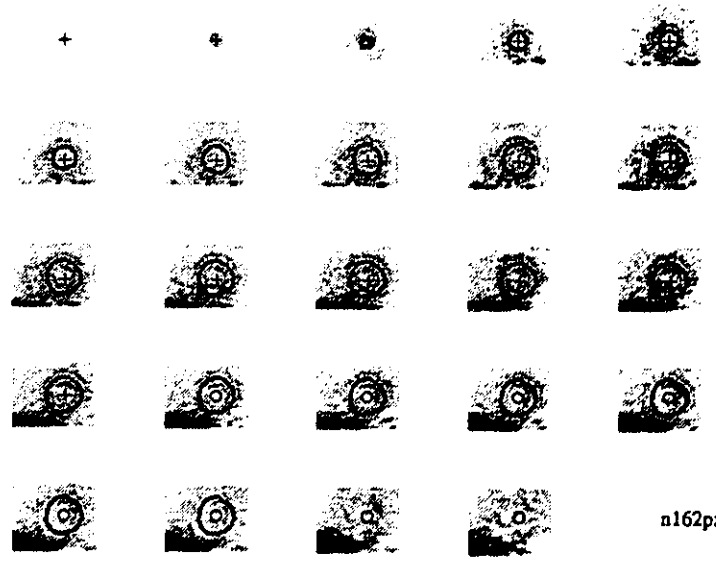

n162pxxf00

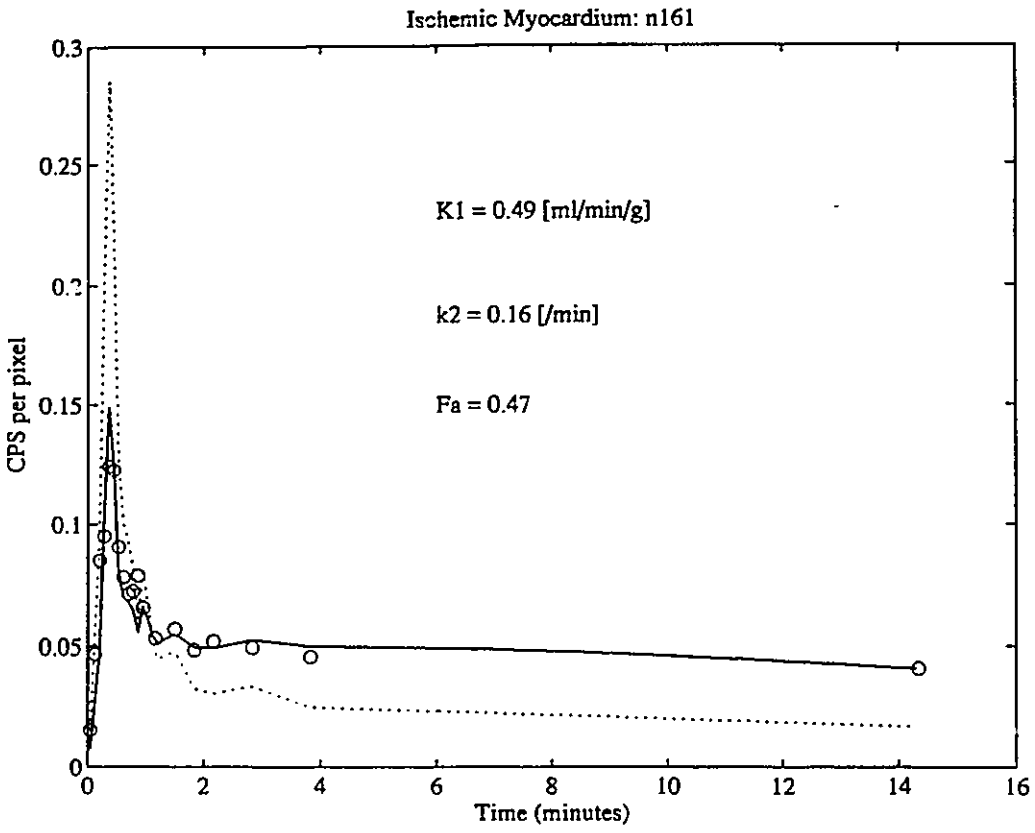
Ischemic Myocardium: n161
K1 = 0.49 [ml/min/g]
k2 = 0.16 [/min]
Fa = 0.47
CPS per pixel
Time (minutes)
0.3
0.25
0.2
0.15
0.1
0.05
0
0
2
4
6
8
10
12
14
16

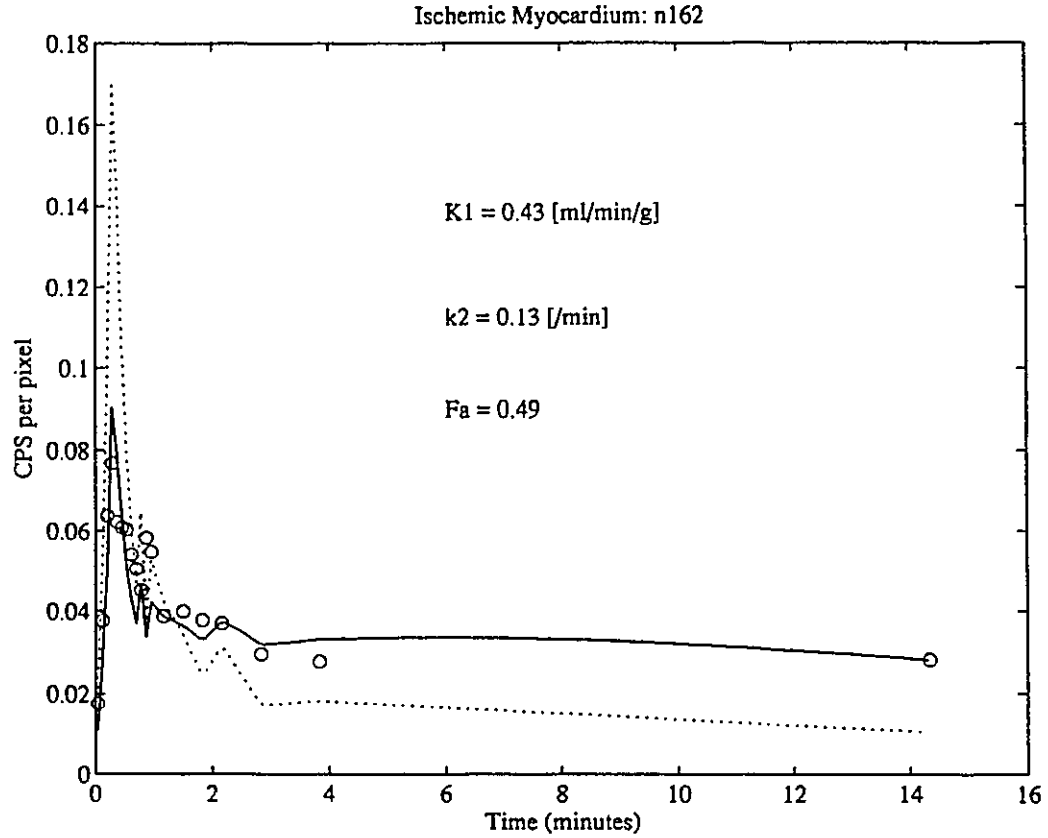
Ischemic Myocardium: n162
K1 = 0.43 [ml/min/g]
k2 = 0.13 [/min]
Fa = 0.49
CPS per pixel
Time (minutes)
0.18
0.16
0.14
0.12
0.1
0.08
0.06
0.04
0.02
0
0
2
4
6
8
10
12
14
16

Axial distribution

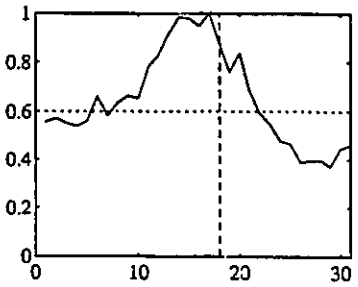

Transaxial Plane 18

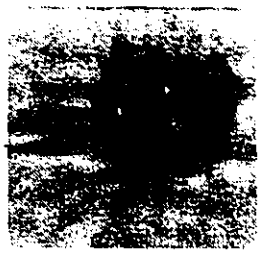

Long Axis Section

Short Axis Section

Axial distribution

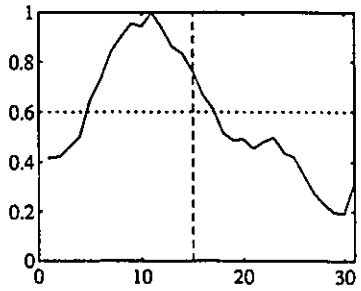

Transaxial Plane 15

Long Axis Section

Short Axis Section

Axial distribution

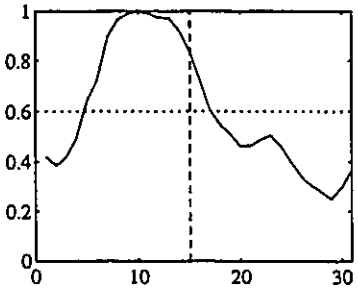

Transaxial Plane 15

Long Axis Section

Short Axis Section

Quality Assurance: Subject Drug 6 (D6)

A. FDG

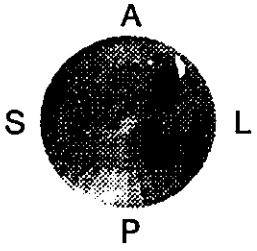

B. Base Flow

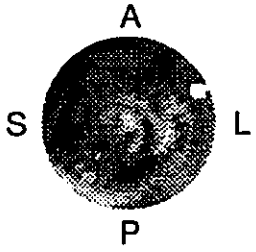

C. Treat Flow

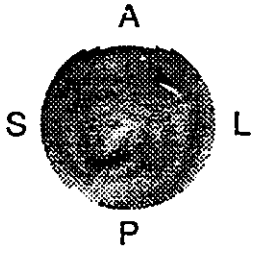

D. Treat/Base

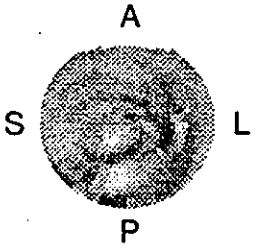

E. FDG/Base

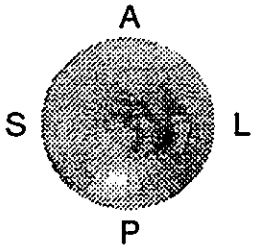

F. FDG/Treat

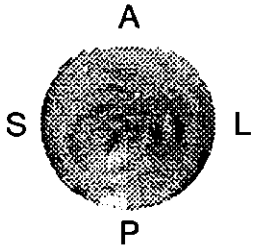

G. LV blood integrals

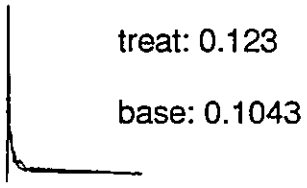

H. Ischemic Regions

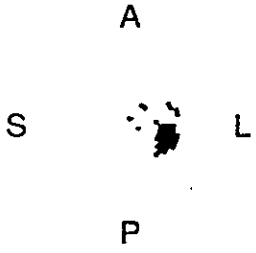

I. Largest Region

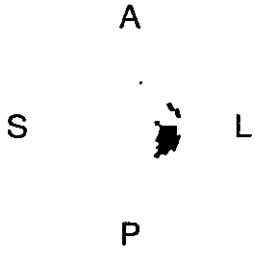

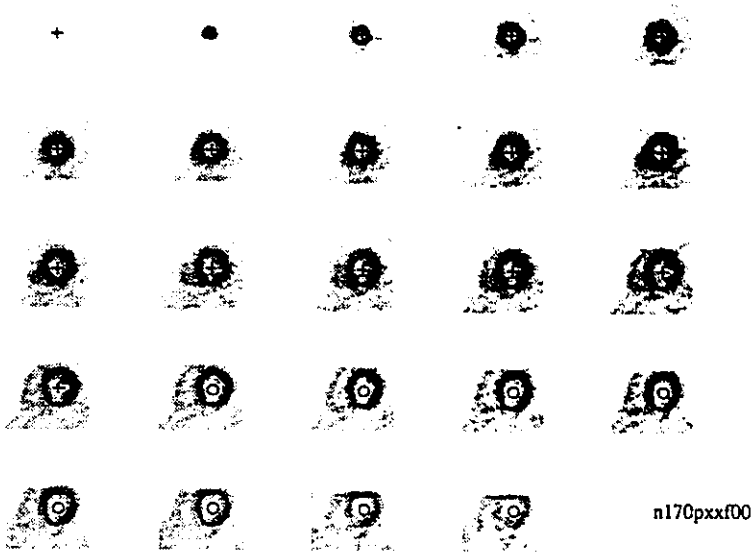

n170pxxf00

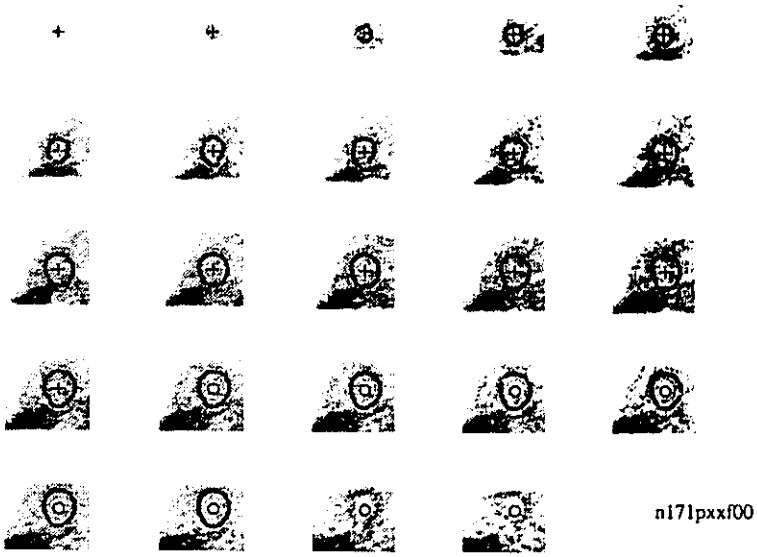

n171pxxf00

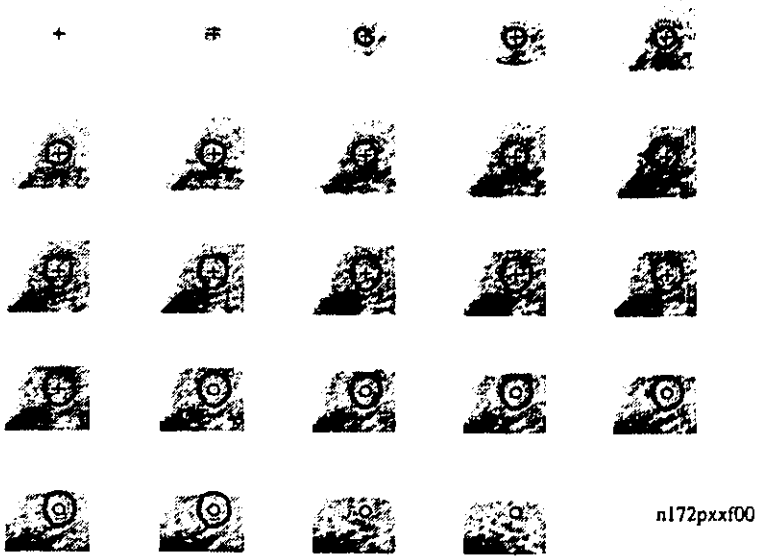

n172pxxf00

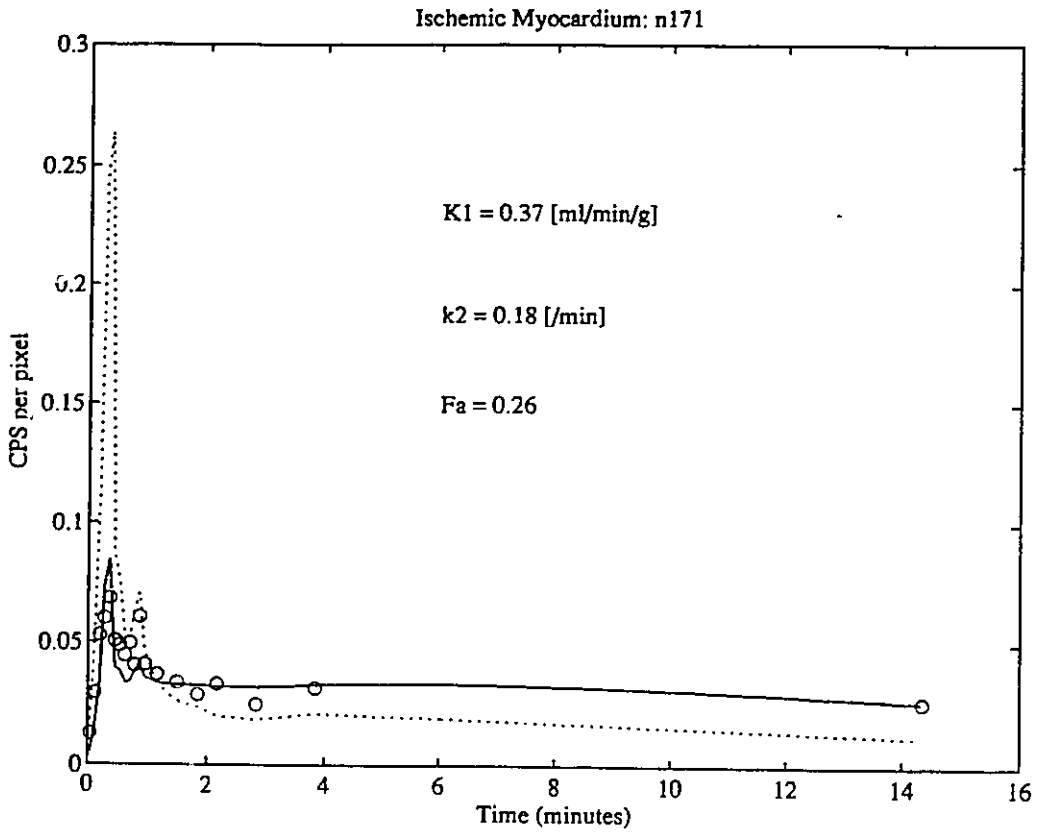
Ischemic Myocardium: n171
K1 = 0.37 [ml/min/g]
k2 = 0.18 [/min]
Fa = 0.26
CPS per pixel
Time (minutes)
0.3
0.25
0.2
0.15
0.1
0.05
0
0
2
4
6
8
10
12
14
16

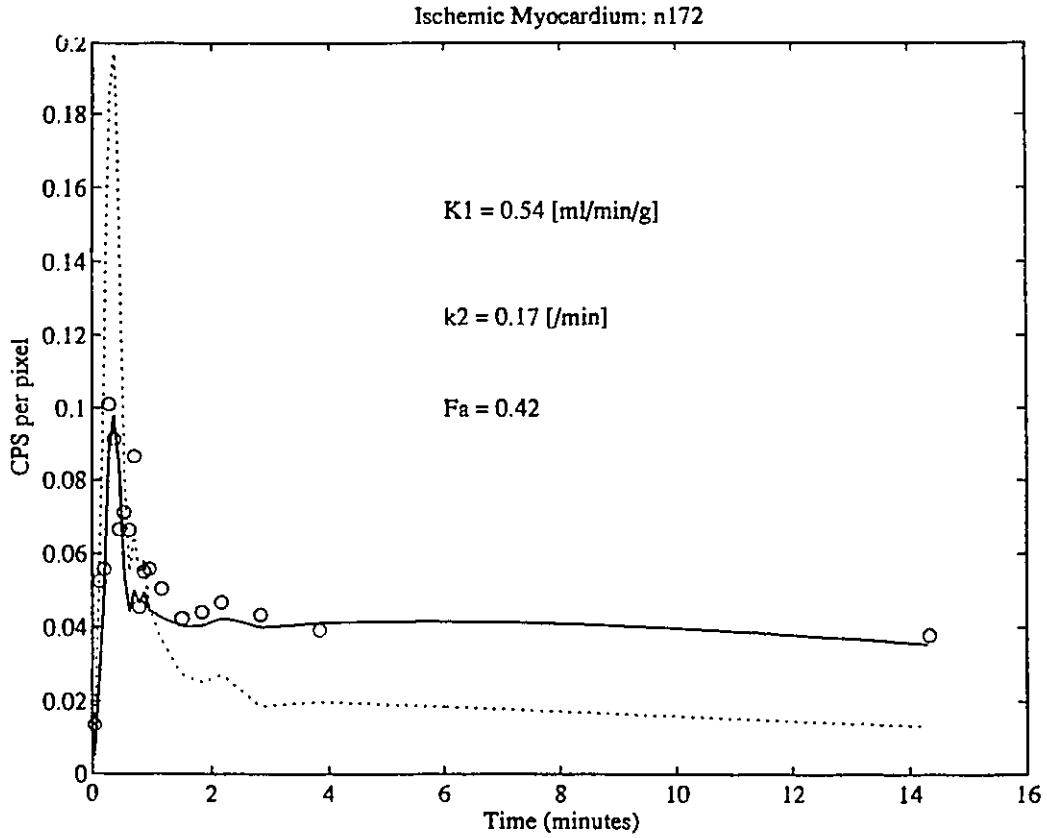
Ischemic Myocardium: n172
K1 = 0.54 [ml/min/g]
k2 = 0.17 [/min]
Fa = 0.42
CPS per pixel
Time (minutes)
0.2
0.18
0.16
0.14
0.12
0.1
0.08
0.06
0.04
0.02
0
0
2
4
6
8
10
12
14
16

Axial distribution

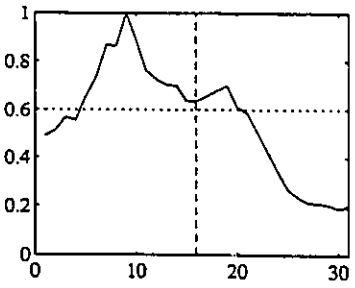

Transaxial Plane 16

Long Axis Section

Short Axis Section

Axial distribution

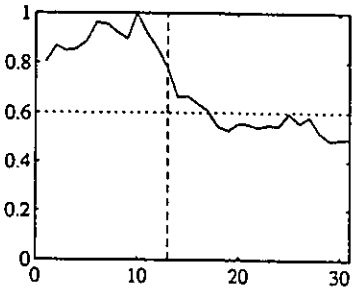

Transaxial Plane 13

Long Axis Section

Short Axis Section

Axial distribution

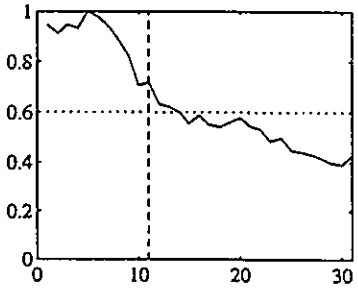

Transaxial Plane 11

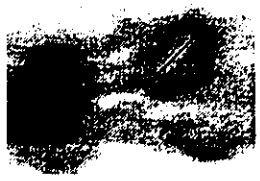

Long Axis Section

Short Axis Section

Quality Assurance: Subject Placebo 6 (P6)

A. FDG

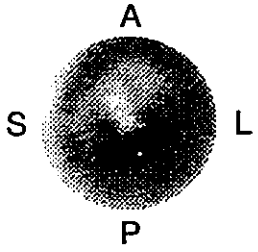

B. Base Flow

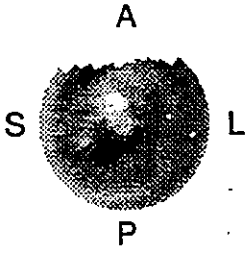

C. Treat Flow

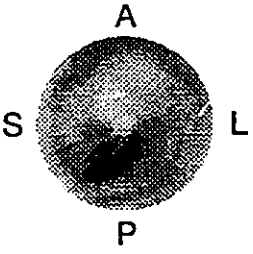

D. Treat/Base

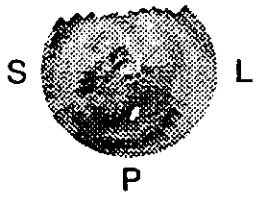

E. FDG/Base

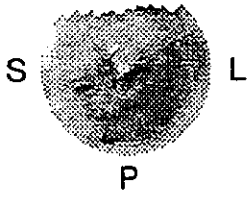

F. FDG/Treat

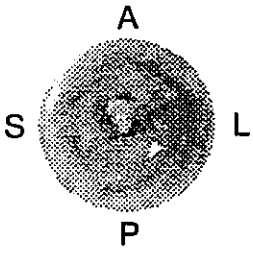

G. LV blood integrals

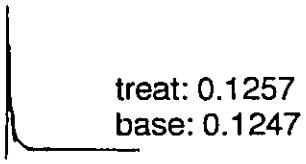

H. Ischemic Regions

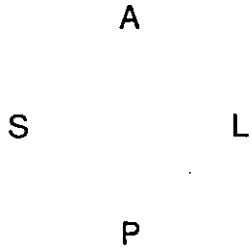

I. Largest Region

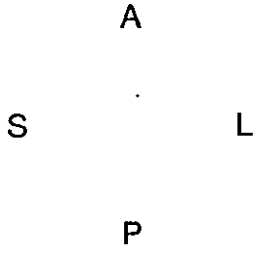

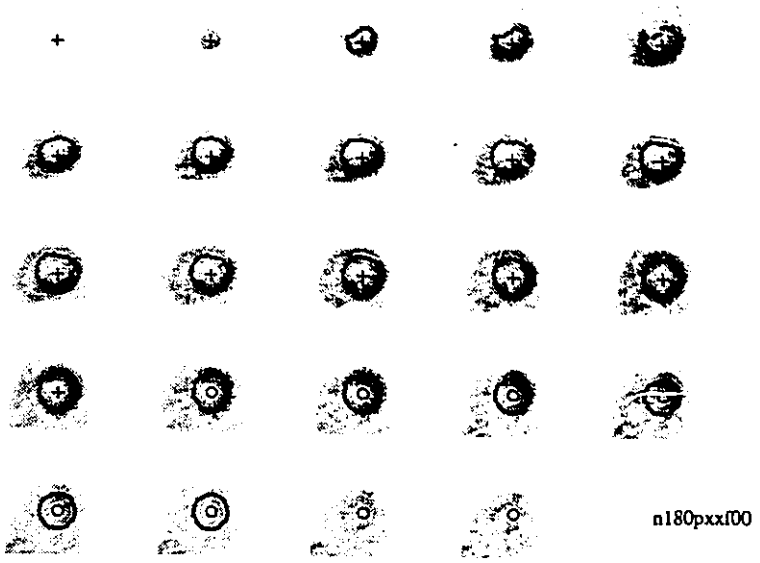
n180pxxf00
n181pxxf00
n182pxxf00

Axial distribution

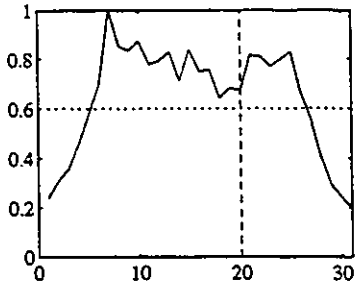

Transaxial Plane 20

Long Axis Section

Short Axis Section

Axial distribution

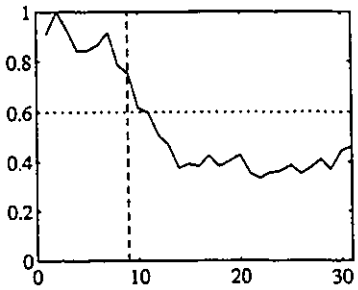

Transaxial Plane 9

Long Axis Section

Short Axis Section

Axial distribution

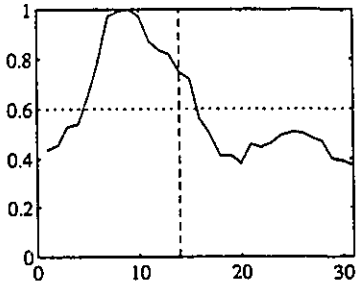

Transaxial Plane 14

Long Axis Section

Short Axis Section

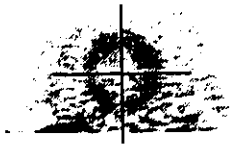

Quality Assurance: Subject Drug 7 (D7)

A. FDG

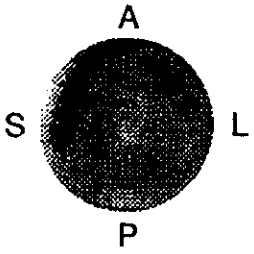

B. Base Flow

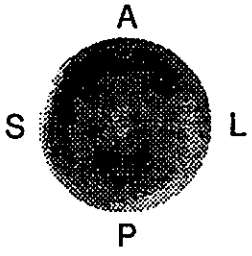

C. Treat Flow

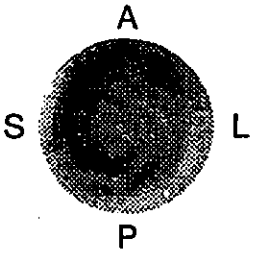

D. Treat/Base

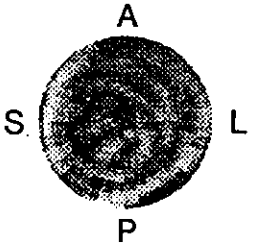

E. FDG/Base

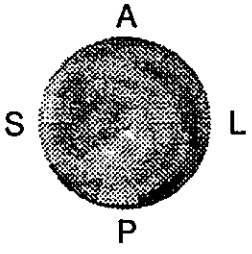

F. FDG/Treat

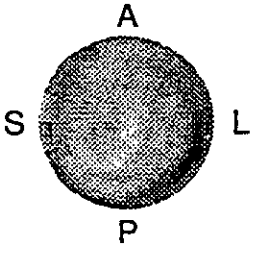

G. LV blood integrals

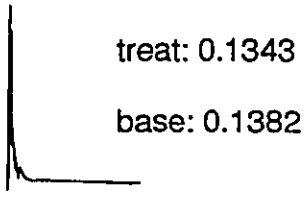

H. Ischemic Regions

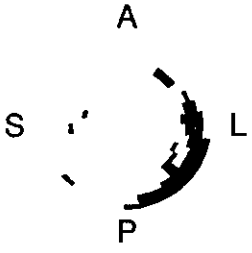

I. Largest Region

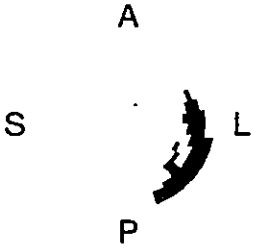

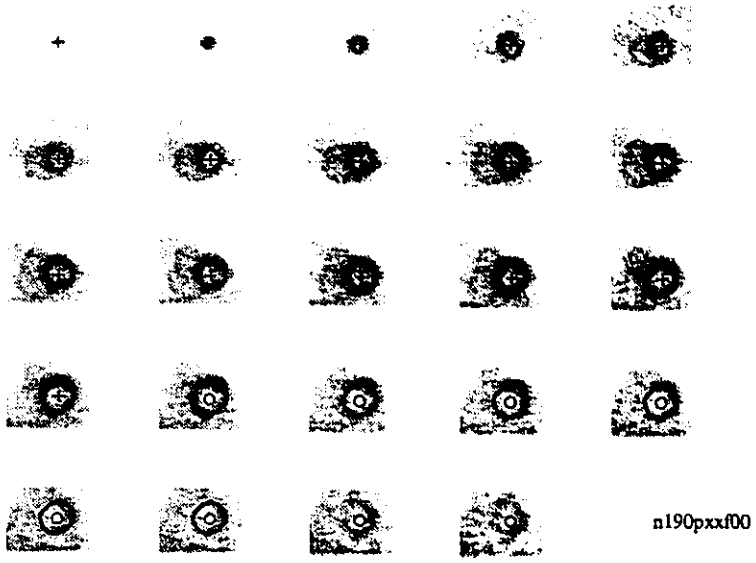

n190pxxf00

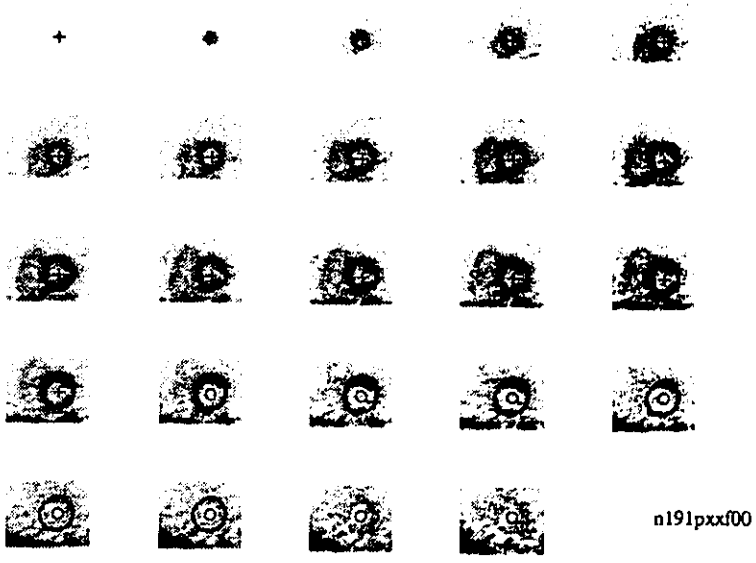

n191pxxf00

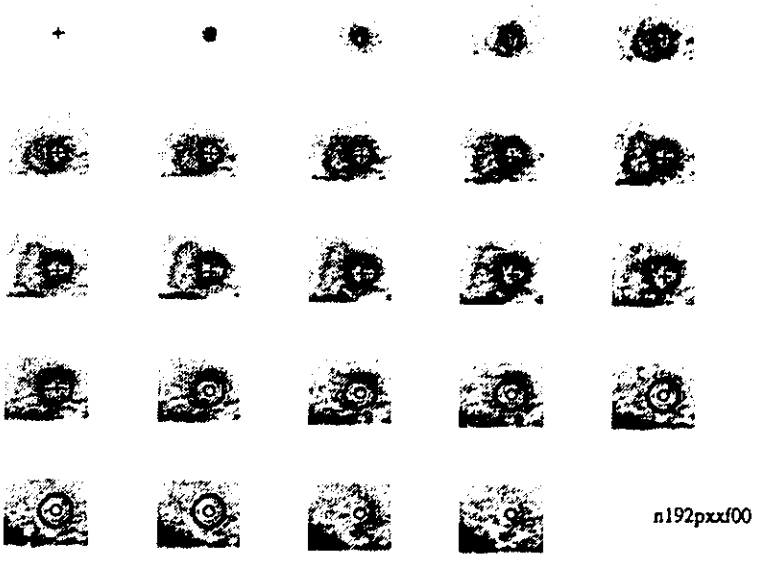

n192pxxf00

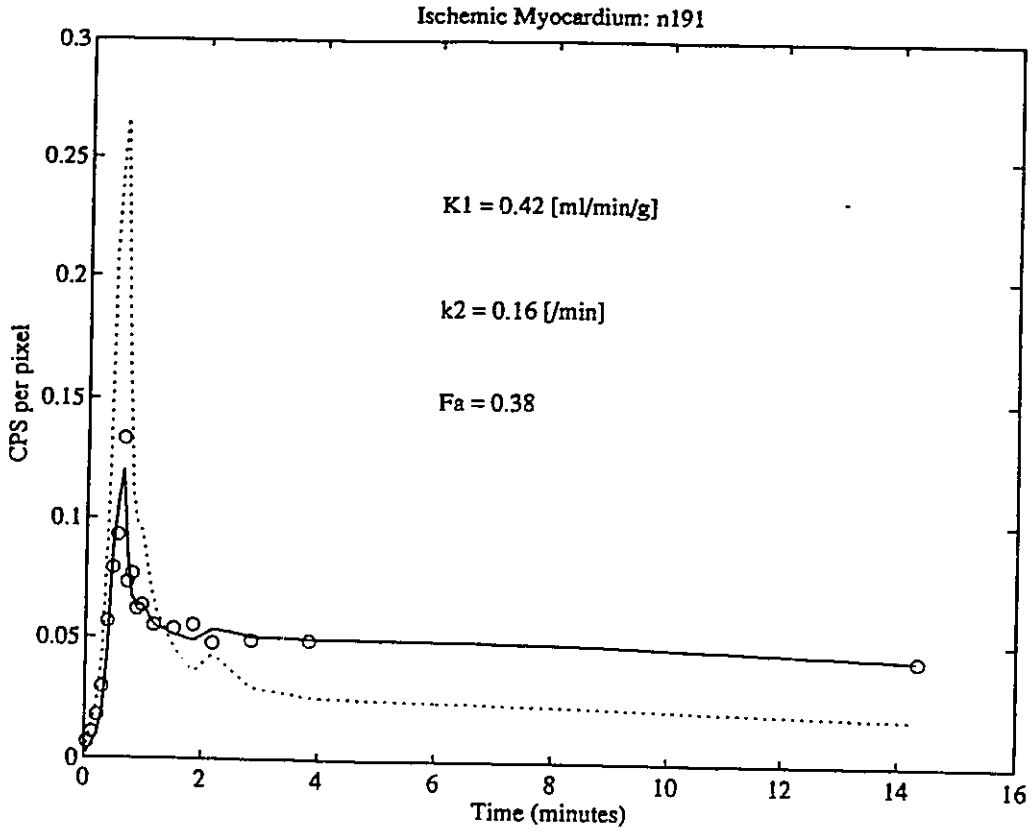
Ischemic Myocardium: n191
K1 = 0.42 [ml/min/g]
k2 = 0.16 [/min]
Fa = 0.38
CPS per pixel
Time (minutes)
0.3
0.25
0.2
0.15
0.1
0.05
0
0
2
4
6
8
10
12
14
16

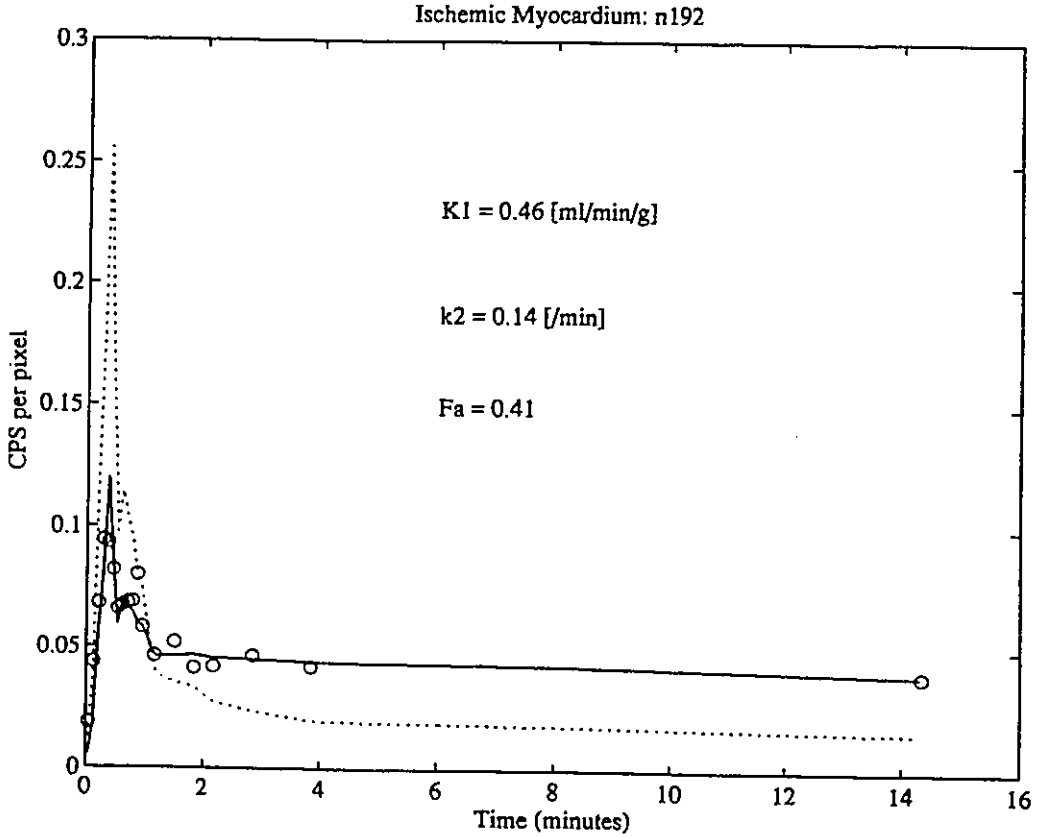
Ischemic Myocardium: n192
K1 = 0.46 [ml/min/g]
k2 = 0.14 [/min]
Fa = 0.41
CPS per pixel
Time (minutes)
0.3
0.25
0.2
0.15
0.1
0.05
0
0
2
4
6
8
10
12
14
16

Axial distribution

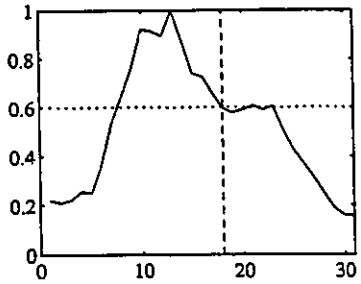

Transaxial Plane 18

Long Axis Section

Short Axis Section

Axial distribution

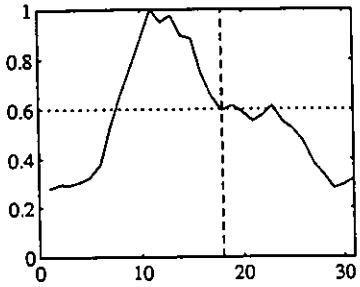

Transaxial Plane 18

Long Axis Section

Short Axis Section

Axial distribution

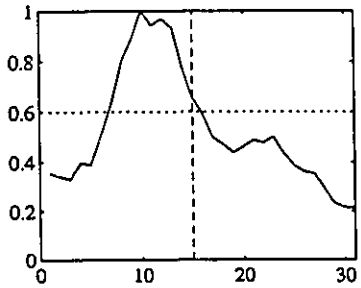

Transaxial Plane 15

Long Axis Section

Short Axis Section

Quality Assurance: Subject Placebo 7 (P7)

A. FDG

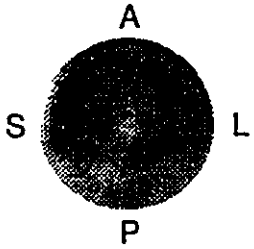

B. Base Flow

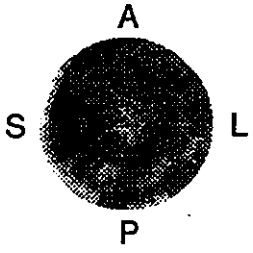

C. Treat Flow

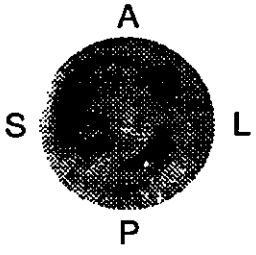

D. Treat/Base

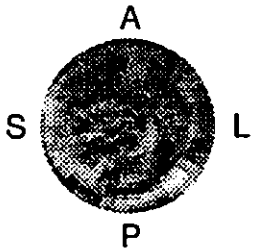

E. FDG/Base

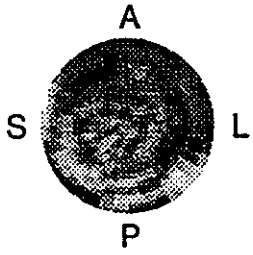

F. FDG/Treat

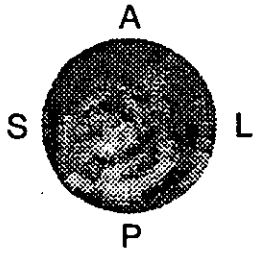

G. LV blood integrals

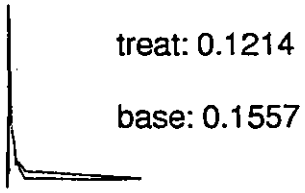

H. Ischemic Regions

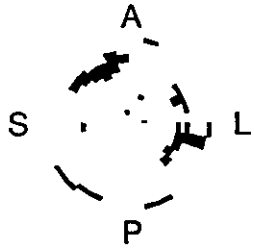

I. Largest Region

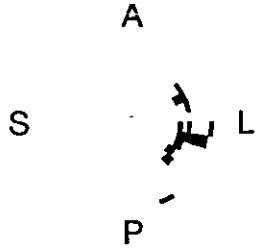

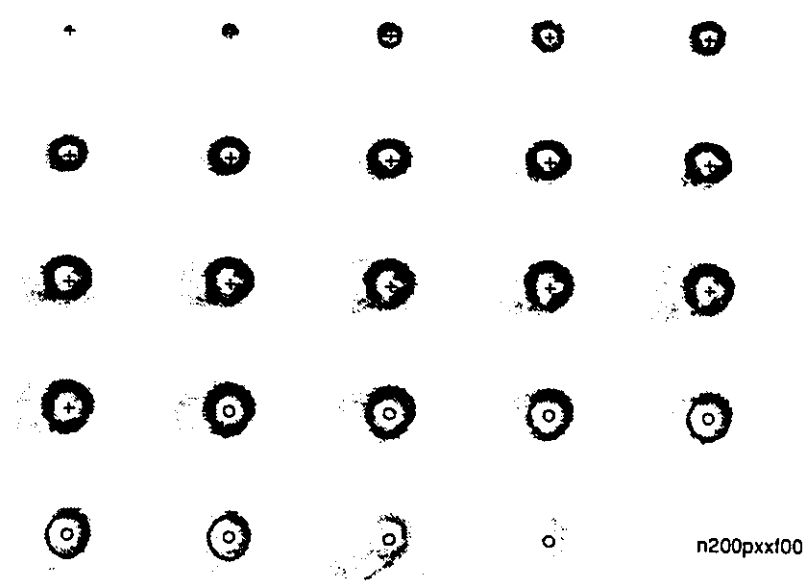
n200pxxf00

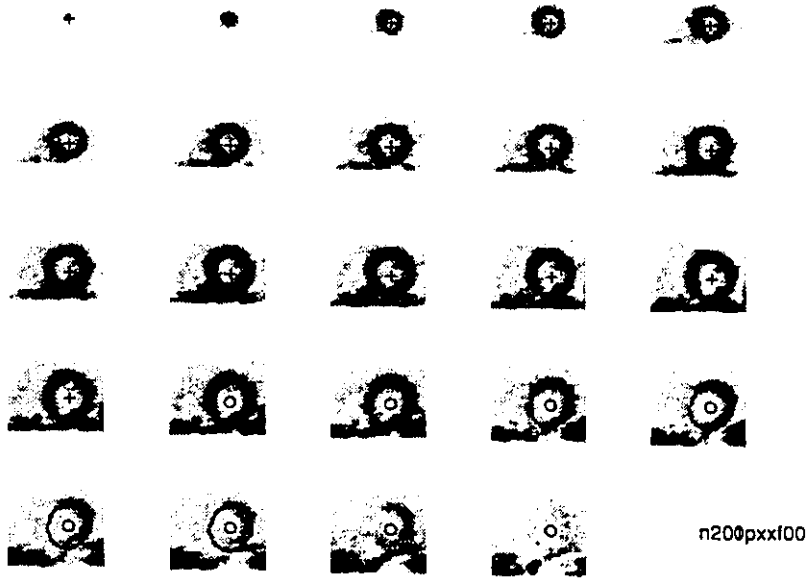
n200pxxf00

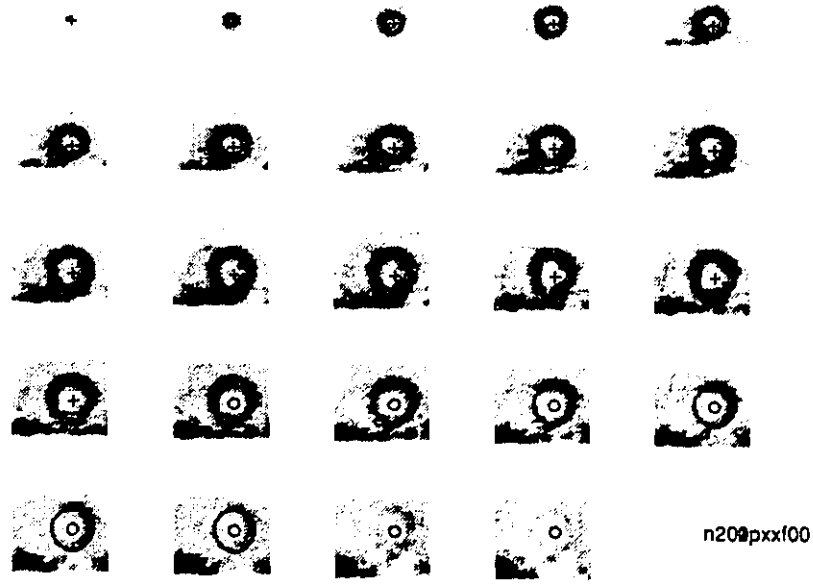
n200pxxf00

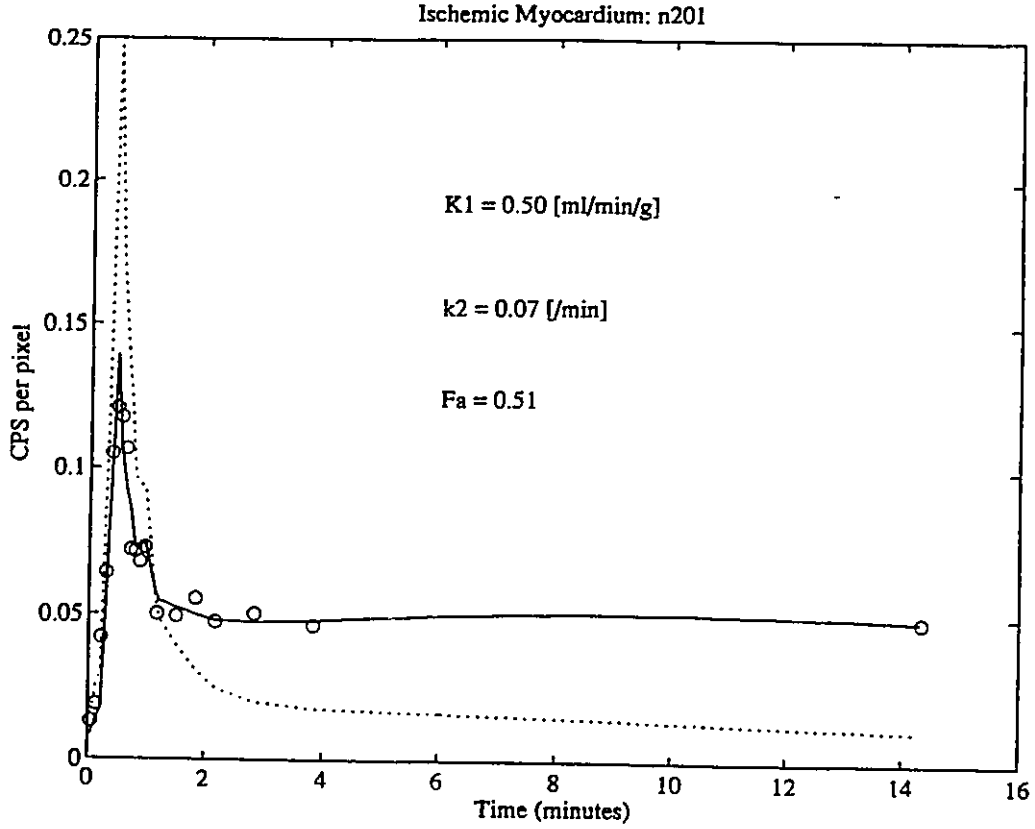
Ischemic Myocardium: n201
K1 = 0.50 [ml/min/g]
k2 = 0.07 [/min]
Fa = 0.51
CPS per pixel
Time (minutes)
0.25
0.2
0.15
0.1
0.05
0
0
2
4
6
8
10
12
14
16

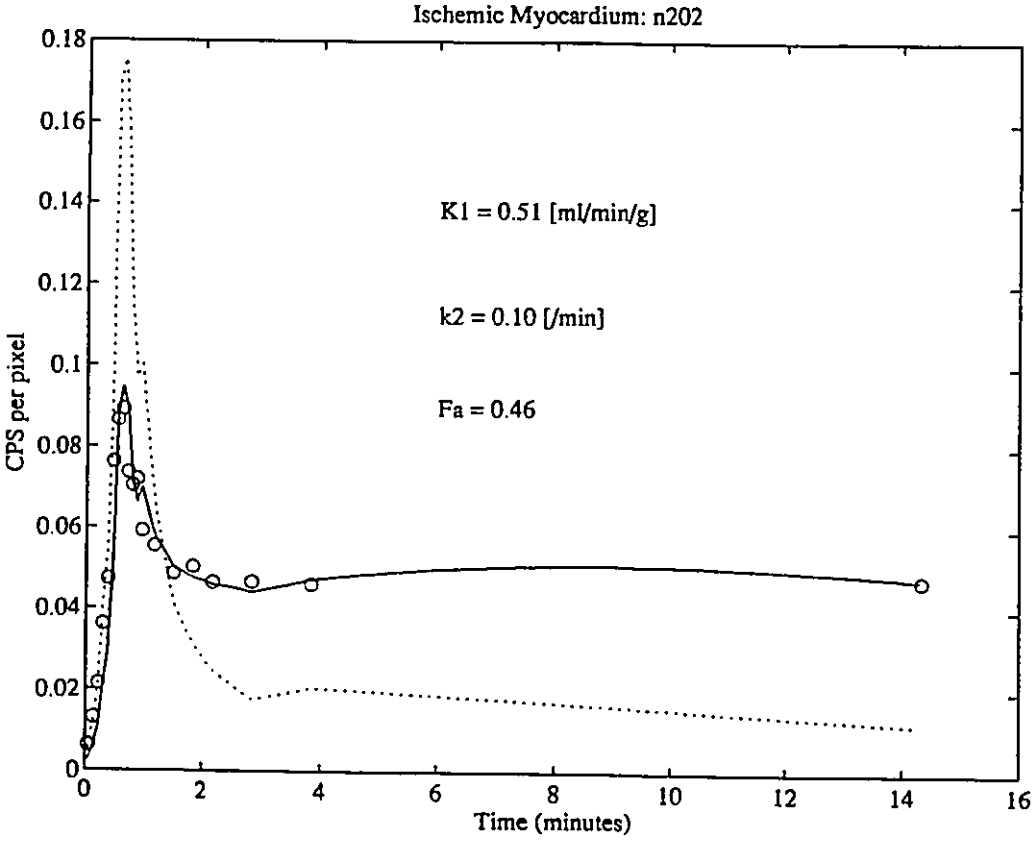
Ischemic Myocardium: n202
K1 = 0.51 [ml/min/g]
k2 = 0.10 [/min]
Fa = 0.46
CPS per pixel
Time (minutes)
0.18
0.16
0.14
0.12
0.1
0.08
0.06
0.04
0.02
0
0
2
4
6
8
10
12
14
16

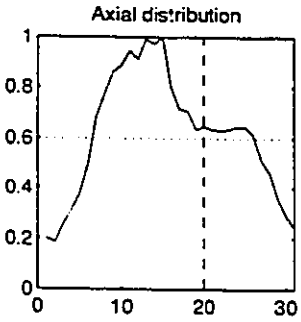

Transaxial Plane 20

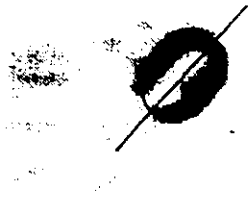

Long Axis Section

Short Axis Section

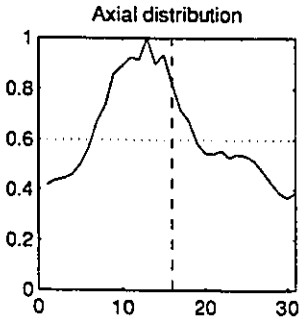

Transaxial Plane 16

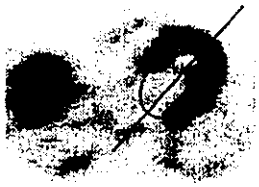

Long Axis Section

Short Axis Section

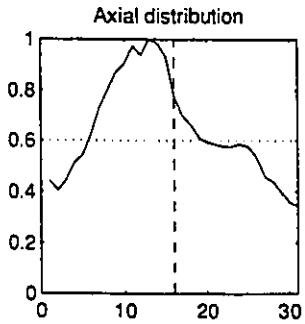

Transaxial Plane 16

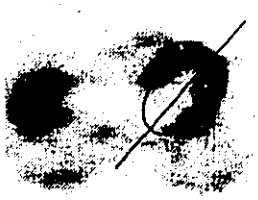

Long Axis Section

Short Axis Section

GLOSSARY

Anatomy and Physiology (Guyton 1992, Opie 1984)

ADP	Adenosine Diphosphate
AMP	Adenosine Monophosphate
ATP	Adenosine Triphosphate
AV	Atrioventricular node
CAD	Coronary Artery Disease
ECG	Electrocardiogram
EF	Ejection Fraction
FFA	Free Fatty Acid
HR	Heart Rate
LA	Left Atrium
LAD	Left Anterior Descending artery
LCx	Left Circumflex artery
LOR	Line of Response
LV	Left Ventricle
MBF	Myocardial Blood Flow
MI	Myocardial Infarction
$M\dot{V}O_2$	Myocardial rate of oxygen consumption
NE	Norepinephrine
PTCA	Percutaneous Transluminal Coronary Angioplasty
RA	Right Atrium
RCA	Right Coronary Artery
RV	Right Ventricle
SA	Sinoatrial node

Statistics (Campbell 1993)

ANCOVA	Analysis of Covariance
ANOVA	Analysis of Variance
CV	Coefficient of Variation
F	F statistic
Ho	Null Hypothesis
LVmap	Left Ventricular significance polar map
MSE	Mean Squared Error
SD	Standard Deviation
T	T statistic
Z	Z statistic

Tomography (Bacharach 1992)

BGO	Bismuth Germanate
Cu-PTSM	Copper(II)pyruvaldehyde bis-4-N-methylthiosemicarbazone
FDG	^{18}F-fluorodeoxyglucose
FOV	Field of View
FWHM	Full Width at Half Maximum
HED	Hydroxyephedrine
MRI	Magnetic Resonance Imaging
NEC	Noise Equivalent Counts
PET	Positron Emission Tomography
QA	Quality Assurance
ROI	Region of Interest
SNR	Signal-to-Noise Ratio
SPECT	Single Photon Emission Computed Tomography

Ammonia Compartmental Model (Hutchins 1990)

K1	Ammonia uptake rate [ml/min/g]
k2	Ammonia washout rate [1/min]
Fa	Fractional blood volume

Orientation

A	Anterior
P	Posterior
S	Septal
L	Lateral

REFERENCES

ACC/AHA/SNM Policy Statement, 1992. Standardization of Cardiac Tomographic Imaging: American Heart Association, American College of Cardiology, and the Society of Nuclear Medicine. J Nucl Med;33:1434-1435.

Alpert NM, Bradshaw JF, Kennedy D, Correia JA, 1990. The Principal Axes Transformation -A Method for Image Registration. J Nucl Med;31:1717-1722.

Bacharach SL, Douglas MA, Carson RE, et al, 1993. Three-Dimensional Registration of Cardiac Positron Emission Tomography Attenuation Scans. J Nucl Med;34:311-321.

Bacharach SL, 1992. The Physics of Positron Emission Tomography. In: Positron Emission Tomography of the Heart. Bergmann SR, Sobel BE (eds). Mount Kisko, NY, Futura Publishing Company, Inc.

Bellina CR, Parodi O, Camici P, et al, 1990. Simultaneous in Vitro and in Vivo Validation of Nitrogen-13-Ammonia for the Assessment of Regional Myocardial Blood Flow. J Nucl Med;31:1335-1343.

Bergstrom M, Eriksson L, Bohm C, et al, 1983. Correction for Scattered Radiation in a Ring Detector Positron Camera by Integral Transformation of the Projections. J Comput Assist Tomogr;7:42.

Bettinardi V, Gilardi MC, Lucignani G, et al, 1993. A procedure for Patient Repositioning and Compensation for Misalignment Between Transmission and Emission Data in PET Heart Studies. J Nucl Med;34:137-142.

Blockland JAK, Vossepoel AM, Bakker AR, Pauwels EKJ, 1987. Delineating Elliptical Objects with an Application to Cardiac Scintigrams. IEEE Trans Med Imaging;6:57-66.

Bonow R, Dilsizian V, Cuocolo A, Bacharach S, 1991. Identification of Viable Myocardium in Patients With Chronic Coronary Artery Disease and Left Ventricular Dysfunction. Comparison of Thallium Scintigraphy With Reinjection and PET Imaging With ^{18}F-Fluorodeoxyglucose. Circulation;83:26-37.

Camici P, Marraccini P, Gistri R, et al, 1991a. Alpha-1 Adrenergic Tone and Coronary Reserve in Patients With Syndrome X (abstract). Circulation;84:II-424.

Camici P, Chiriatti G, Lorenzoni R, et al, 1991b. Coronary Vasodilation Is Impaired in Both Hypertrophied and Nonhypertrophied Myocardium of Patients With Hypertrophic Cardiomyopathy: A Study With Nitrogen-13 Ammonia and Positron Emission Tomography. J Am Coll Cardiol;17:879-886.

Camici P, Araujo LI, Spinks T, et al, 1986. Increased Uptake of F-18 Fluorodeoxyglucose in Postischemic Myocardium of Patients with Exercise-Induced Angina. Circulation;74:81-88.

Campbell MJ, Machin D, 1993. Medical Statistics. A Commonsense Approach. West Sussex, John Wiley & Sons Ltd.

Carson RE, Yan Y, Daube-Witherspoon ME, et al, 1993. An Approximation Formula for the Variance of PET Region-of-Interest Values. IEEE Trans Med Imaging;12:240-250.

Cherry SR, Woods RP, Hoffman EJ, Mazziota JC, 1993. Improved Detection of Focal Cerebral Blood Flow Changes Using Three-Dimensional Positron Emission Tomography. J Cereb Blood Flow Metab;13:630-638.

Choi Y, Huang SC, Hawkins RA, et al, 1993. A Simplified Method for Quantification of Myocardial Blood Flow Using Nitrogen-13-Ammonia and Dynamic PET. J Nucl Med;34:488-497.

Dahlbom M, Hoffman EJ, 1987. Problems in Signal-to-Noise Ratio for Attenuation Correction in High Resolution PET. IEEE Trans Nucl Sci;34:288.

Delbeke D, Lorenz CH, Votaw J, et al, 1993. Estimation of Left Ventricular Mass and Infarct Size from Nitrogen-13-Ammonia PET Images Based on Pathological Examination of Explanted Human Hearts. J Nucl Med;34:826-833.

Digby WM, Hoffman EJ, 1989. An Investigation of Scatter in Attenuation Correction for PET. IEEE Trans Nucl Sci;36:1038-1042.

Evans RD, 1982. The Atomic Nucleus. New York, NY, McGraw-Hill Book Company, Inc.

Faber TL, Cooke CD, Peifer JW, et al 1995. Three-Dimensional Displays of Left Ventricular Epicardial Surface from Standard Cardiac SPECT Perfusion Quantification Techniques. J Nucl Med;36:697:703.

Faber TL, McColl RW, Opperman RN, et al 1991a. Spatial and Temporal Registration of Cardiac SPECT and MR Images: Methods and Evaluation. Radiology;179:857-861.

Faber TL, Stokely EM, Peshock RM, Corbett JR, 1991b. A Model-Based Four-Dimensional Left Ventricular Surface Detector. IEEE Trans Med Imaging;10:321-329.

Fallen EL, Nahmias C, Scheffel A, et al, 1995. Redistribution of Myocardial Blood Flow With Topical Nitroglycerin in Patients With Coronary Artery Disease. Circulation;91:1381-1388.

Ford I, 1986. Confounded Correlations: Statistical Limitations in the Analysis of Interregional Relationships of Cerebral Metabolic Activity. J Cereb Blood Flow Metab;6:385-388.

Fox PT, Mintun MA, Reiman EM, Raichle ME, 1988. Enhanced Detection of Focal Brain Responses using Intersubject Averaging and Change Distribution Analysis of Subtracted PET Images. J Cereb Blood Flow Metab;8:642-653.

Friston KJ, Frith CD, Liddle PF, Frackowiak RSJ, 1991a. Plastic Transformation of PET images. J Comput Assist Tomogr;15:634-639.

Friston KJ, Frith CD, Liddle PF, Frackowiak RSJ, 1991b. Comparing Functional (PET) Images: The Assessment of Significant Change. J Cereb Blood Flow Metab;11:690-699.

Friston KJ, Frith CD, Liddle PF, et al, 1990. The Relationship Between Global and Local Changes in PET Scans. J Cereb Blood Flow Metab;10:458-466.

Gambhir SS, Schwaiger M, Huang SC, et al, 1989. Simple Non-invasive Quantification Method for Measuring Myocardial Glucose Utilization in Humans Employing Positron Emission Tomography and Fluorine-18 Deoxyglucose. J Nucl Med;30:359-366.

Goldstein RA, Kirkeeide RL, Smalling RW, et al, 1987. Changes in Myocardial Perfusion Reserve after PTCA: Noninvasive Assessment with Positron Tomography. J Nucl Med;28:1262-1267.

Gould KL, Martucci JP, Goldberg DI, et al, 1994. Short-term Cholesterol Lowering Decreases Size and Severity of Perfusion Abnormalities by Positron Emission Tomography After Dipyridamole in Patients With Coronary Artery Disease. A Potential Noninvasive Marker of Healing Coronary Endothelium. Circulation;89:1530-1538.

Gropler RJ, Siegel BA, Lee KJ, et al, 1990. Nonuniformity in Myocardial Accumulation of Fluorine-18-Fluorodeoxyglucose in Normal Fasted Humans. J Nucl Med;31:1749-1760.

Guyton AC, 1992. Human Physiology and Mechanisms of Disease. Philadelphia, PA, W.B. Saunders Company.

He ZX, Maublant JC, Cauvin JC, Veyre A, 1991. Reorientation of the Left Ventricular Long-Axis on Myocardial Transaxial Tomograms by a Linear Fitting Method. J Nucl Med;32:1794-1800.

Henes CG, Bergmann SR, Perez JE, et al, 1990. The Time Course of Restoration of Nutritive Perfusion, Myocardial Oxygen Consumption, and Regional Function after Coronary Thrombolysis. Coronary Artery Disease;1:687-696.

Hicks K, Ganti G, Mullani N, Gould KL, 1989. Automated Quantitation of Three-Dimensional Cardiac Positron Emission Tomography for Routine Clinical Use. J Nucl Med;30:1787-1797.

Hiltz LG, McKee BTA, 1994. Scatter correction for three-dimensional PET based on an analytic model dependent on source and attenuating object. Phys Med Biol;39:2059-2071.

Hoh CK, Dahlbom M, Harris G, 1993. Automated Iterative Three-Dimensional Registration of Positron Emission Tomography Images. J Nucl Med;34:2009-2018.

Huesman RH, 1984. A new fast algorithm for the evaluation of regions of interest and statistical uncertainty in computed tomography. Phys Med Biol;29:543-552.

Hutchins GD, Caraher JM, Raylman RR, 1992. A Region of Interest Strategy for Minimizing Resolution Distortions in Quantitative Myocardial PET Studies. J Nucl Med;33:1243-1250.

Hutchins GD, Schwaiger M, Rosenspire KC, et al, 1990. Noninvasive Quantification of Regional Blood Flow in the Human Heart Using N-13 Ammonia and Dynamic Positron Emission Tomography. J Am Coll Cardiol;15:1032-1042.

Iida H, Rhodes CG, de Silva R, et al, 1992. Use of the Left Ventricular Time-Activity Curve as a Noninvasive Input Function in Dynamic Oxygen-15-Water Positron Emission Tomography. J Nucl Med;33:1669-1677.

Iida H, Kanno I, Takahashi A, et al, 1988. Measurement of Absolute Myocardial Blood Flow With $H_2{}^{15}O$ and Dynamic Positron-Emission Tomography. Strategy for Quantification in Relation to the Partial-Volume Effect. Circulation;78:104-115.

Junck L, Moen JG, Hutchins GD, et al, 1990. Correlation Methods for the Centering, Rotation, and Alignment of Functional Brain Images. J Nucl Med;31:1220-1226.

Knoll GF, 1989. Radiation Detection and Measurement. New York, NY, John Wiley & Sons.

Kotzerke J, Hicks RJ, Wolfe E, 1990. Three-Dimensional Assessment of Myocardial Oxidative Metabolism: A New Approach for Regional Determination of PET-Derived Carbon-11-Acetate Kinetics. J Nucl Med;31:1876-1883.

Krivokapich J, Smith GT, Huang SC, et al, 1989. ^{13}N Ammonia Myocardial Imaging at Rest and With Exercise in Normal Volunteers. Circulation;80:1328-1337.

Krivokapich J, Stevenson LW, Kobashigawa J, et al, 1991. Quantification of absolute myocardial perfusion at rest and during exercise with positron emission tomography after human cardiac transplantation. J Am Coll Cardiol;18:512-517.

Lammertsma AA, De Silva R, Araujo LI, Jones T, 1992. Measurement of regional myocardial blood flow using $C^{15}O_2$ and positron emission tomography: comparison of tracer models. Clin Phys Physiol Meas;13:1-20.

Landaw EM, DiStefano JJ III, 1984. Multiexponential, multicompartmental, and noncompartmental modeling. II. Data analysis and statistical considerations. Am J Physiol;246:R665-R677.

Laubenbacher C, Rothley J, Sitomer J, et al, 1993. An Automated Analysis Program for the Evaluation of Cardiac PET Studies: Initial Results in the Detection and Localization of Coronary Artery Disease Using Nitrogen-13-Ammonia. J Nucl Med;34:968-978.

Lercher MJ, Weinhard K, 1994. Scatter Correction in 3D PET. IEEE Trans Med Imaging;13:649-657.

Levy WC, Cerquiera MD, Matsuoka DT, et al, 1992. Four Radionuclide Methods for Left Ventricular Volume Determination: Comparison of a Manual and an Automated Technique. J Nucl Med;33:763-770.

Marshall RC, Tillisch JH, Phelps ME, et al, 1983. Identification and Differentiation of Resting Myocardial Ischemia and Infarction in Man With Positron Computed Tomography F-18 Labeled Fluorodeoxyglucose and N-13 Ammonia. Circulation;67:766-768.

MATLAB 1992. Natick, MA, The Mathworks Inc.

McCord ME, Bacharach SL, Bonow RO, et al, 1992. Misalignment between PET transmission and emission scans: its effect on myocardial imaging. J Nucl Med;33:1209-1214.

Meikle SR, Dahlbom M, Cherry SR, 1993. Attenuation Correction Using Count-Limited Transmission Data in Positron Emission Tomography. J Nucl Med;34:143-150.

Miller TR, Wallis JW, Landy BR, et al, 1994. Measurement of Global and Regional Left Ventricular Function by Cardiac PET. J Nucl Med;35:999-1006.

Miller TR, Starren JB, Grothe RA Jr, 1988. Three-Dimensional Display of Positron Emission Tomography of the Heart. J Nucl Med;29:530-537.

Moeller JR, Strother SC, Sidtis JJ, Rottenberg DA, 1987. Scaled Subprofile Model: A Statistical Approach to the Analysis of Functional Patterns in Positron Emission Tomographic Data. J Cereb Blood Flow Metab;7:649-658.

Muzik O, Beanlands R, Wolfe E, et al, 1993. Automated Region Definition for Cardiac Nitrogen-13-Ammonia PET Imaging. J Nucl Med;34:336-344.

Nahmias C, Kenyon DB, Kouris K, Garnett ES, 1980. Understanding Convolution Backprojection. In: Single Photon Emission Computed Tomography and Other Selected Computer Topics. New York, NY, SNM.

Neinaber CA, Ratib O, Gambhir SS, et al, 1991. A Quantitative Index of Regional Blood Flow in Canine Myocardium Derived Noninvasively With N-13 Ammonia and Dynamic Positron Emission Tomography. J Am Coll Cardiol;17:260-269.

Opie LH, 1984. The Heart Physiology, Metabolism, Pharmacology and Therapy. Orlando, FA, Grune & Stratton Inc.

Pelizzari CA, Chen CTY, Spelbring DR, et al, 1989. Accurate three-dimensional registration of CT, PET, and/or MRI images of the brain. J Comput Assist Tomogr;13:20-26.

Rusinek H, Tsui WH, Levy AV, et al, 1993. Principal Axes and Surface Fitting Methods for Three-Dimensional Image Registration. J Nucl Med;34:2019-2024.

Schlant RC, Sonnenblick EH, 1986. Normal Physiology of the Cardiovascular System. In: The Heart, Hurst JW (ed.), New York, NY, McGraw Hill.

Schwaiger M, Brunken R, Grover-McKay M, et al, 1986. Regional myocardial metabolism in patients with acute myocardial infarction assessed by positron emission tomography. J Am Coll Cardiol;8:800-808.

Schwaiger M, Hutchins GD, 1992. Evaluation of Coronary Artery Disease With Positron Emission Tomography. Seminars in Nucl Med;XXII:210-223.

Schwaiger M, 1994. Myocardial Perfusion Imaging with PET. J Nucl Med;35:693-698.

Silbersweig DA, Stern E, Frith CD, et al, 1993. Detection of Thirty-Second Cognitive Activations in Single Subjects with Positron Emission Tomography: A New Low-Dose $H_2{}^{15}O$ Regional Cerebral Blood Flow Three-Dimensional Imaging Technique. J Cereb Blood Flow Metab:13:617-629.

Strother SC, Casey ME, Hoffman EJ, 1990. Measuring PET Scanner Sensitivity: Relating Countrates to Image Signal-to-Noise Ratios using Noise Equivalent Counts. IEEE Trans Nucl Sci;37:783-788.

Tamaki N, Yonekura Y, Yamashita K, et al, 1989. Positron Emission Tomography Using Fluorine-18 Deoxyglucose in Evaluation of Coronary Artery Bypass Grafting. Am J Cardiol;64:860-865.

Tillisch J, Brunken F, Marshall R, et al, 1986. Reversibility of Cardiac Wall-Motion Abnormalities Predicted by Positron Tomography. N Engl J Med;314:884-888.

van Train KF, Berman DS, Garcia EV, et al, 1986. Quantitative Analysis of Stress Thallium-201 Myocardial Scintigrams: A Multicenter Trial. J Nucl Med;27:17-25.

Walsh M, Geltman E, Steele R, et al, 1990. Augmented myocardial perfusion reserve after coronary angioplasty quantified by positron emission tomography with $H_2{}^{15}O$. J Am Coll Cardiol;15:119-127.

Weinberg IN, Huang SC, Hoffman EJ, et al, 1988. Validation of PET-Acquired Input Functions for Cardiac Studies. J Nucl Med;29:241-247.

Wildt AR, Ahtola OT, 1978. Analysis of Covariance. Sage University Paper Series on Quantitative Applications in the Social Sciences, 07-012. Beverley Hills and London, Sage Publications.